The Institute of Paper Chemistry

Appleton, Wisconsin

Doctor's Dissertation

**Oriented Fiber Refining:
Application of Individual Modes of Mechanical
Action to Single Pulp Fibers**

James E. Biasca

February 16, 1989

ORIENTED FIBER REFINING:

Application of Individual Modes of Mechanical Action to Single Pulp Fibers

A thesis submitted by

James E. Biasca

B. S. 1981, University of Idaho

M.S. 1983, Lawrence University

in partial fulfillment of the requirements
of The Institute of Paper Chemistry
for the degree of Doctor of Philosophy
from Lawrence University,
Appleton, Wisconsin

February 16, 1989

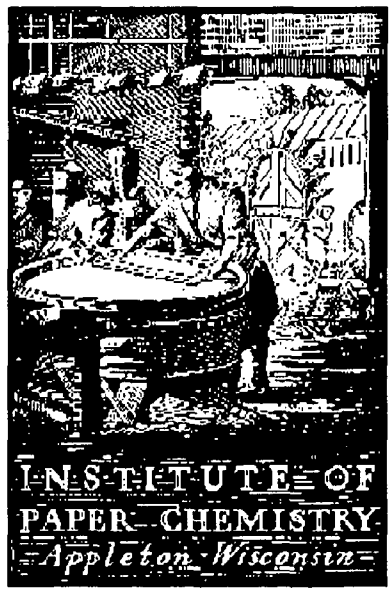

TABLE OF CONTENTS

ABSTRACT

Refining, or beating, is the application of mechanical stresses to pulp fibers in the presence of free water. Refining is an important part of the papermaking process, but a good understanding of this step is lacking. To increase this understanding, my approach is to subject fibers to mechanical stresses that are better defined than those occurring in a conventional stock refiner, form handsheets, and measure the properties of the paper. The paper properties reflect the effectiveness of the mechanical stresses.

The goal was to investigate the application of longitudinal mechanical stresses to pulp fibers. A special apparatus, the Bending Refiner, was developed to subject fibers to a bending action which produces the desired longitudinal stresses. The sheets were compared to sheets formed from fibers treated in a PFI mill and from fibers treated in another special apparatus. The second special apparatus, the Roll Refiner, developed by Hartman, subjects the fibers to repeated lateral compressions. The paper properties measured were density and the mass specific elastic stiffnesses (longitudinal and shear stiffness measured in and out of the plane of the sheet).

For the levels of stress applied, the results suggest that the Roll Refiner is more effective than the Bending Refiner, but not as effective as the PFI mill, in developing density and in-plane stiffnesses when compared at equal levels of treatment. The Roll Refiner develops the in-plane elastic stiffnesses to a level equal to the PFI mill when compared at equal densities and the Bending Refiner developed the in-plane stiffnesses to a slightly lower level. The addition of fines to Bending Refiner or Roll Refiner treated pulps has a more substantial effect on density and in-plane elastic stiffness than any additional mechanical treatment.

While the Bending Refiner does not affect density or the in-plane elastic stiffnesses, the out-of-plane stiffnesses substantially increase with treatment and with the addition of fines, reaching the level of PFI mill pulps at equivalent densities. Treatment in the Roll Refiner has little effect on the out-of-plane properties, even with the addition of fines. Both the Bending Refiner and PFI mill treatments decrease out-of-plane stiffness from the maximum at high treatment levels.

Fiber length measurements indicate little fiber cutting takes place in any of the apparatuses and, to some extent, low levels of treatment slightly increase average fiber length. In addition, no significant difference in fiber curl between differently treated samples is observed. The changes in the fiber length distribution, average fiber length, and fiber curl index are slight and these changes can not account for the observed changes in elastic properties.

The Bending Refiner subjects fibers to mostly in-plane stresses and is more effective at developing out-of-plane elastic properties. The Roll Refiner subjects fibers to mostly out-of-plane stresses and is more effective at developing in-plane properties. The Bending Refiner is more effective at developing out-of-plane elastic properties because the handsheets have a larger out-of-plane fiber orientation than the Roll Refiner handsheets. The Roll Refiner is more effective at developing in-plane properties because the fiber are mostly oriented in the plane of the handsheet and have higher levels of bonding compared to the Bending Refiner.

INTRODUCTION

Wood fibers which have been chemically pulped, but not additionally treated with mechanical stresses, produce a weak, bulky sheet. Fiber strength and fiber bonding are well below that achieved when the pulp is treated by mechanical action in the presence of water[1,2]. Beating or refining is the application of mechanical action to pulp slurries to develop paper strength properties. Beating develops various paper properties as illustrated in Fig. 1.

Refiners modify fibers by mechanically stressing them through mechanisms which are not fully understood. Agreement is lacking on the significance of the various changes in fiber morphology refining induces. A good understanding of how refiners modify fibers and which changes in fiber morphology are most significant for producing a high quality end-product would be extremely useful. This knowledge could lead to improvement of the current refining process and new methods for fiber modification.

OBJECTIVE

Additional knowledge of how mechanical stresses change fibers is necessary. Understanding these mechanisms can help us increase the potential of fibers for papermaking, increase the efficiency of the refining process, and decrease capital, operating, and raw material costs. To add to this knowledge, this thesis addresses the problem: "How do stresses applied either parallel to or transverse to the fiber longitudinal axis during refining affect the handsheet mechanical properties?"

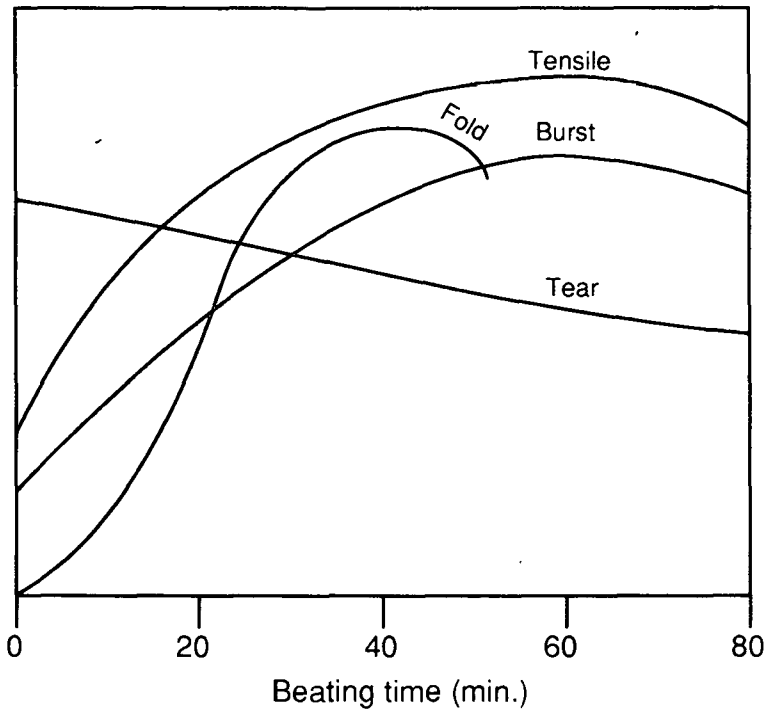

Figure 1. Development of paper properties on beating[2].

APPROACH

While many different mechanical actions play a role in the conventional refining process, this investigation concentrates on the stresses which are applied either parallel to or transverse to the fiber longitudinal axis during refining. The aim is not to measure or simulate the actual conditions inside a commercial refiner, but to apply stresses in a known manner and measure the effect on mechanical properties of handsheet made from the treated fibers. This will require many fibers which must be oriented and subjected to either uniform bending or transverse compression.

The approach was to make thin, highly oriented mats of wet fibers, enclose the mats between thin layers of polyester film (to help maintain the fiber orientations and keep the mats moist), and then treat the specimens in one of

two specialized apparatuses. This layered structure moved through one apparatus parallel to the major fiber orientation direction to provide primarily bending. The apparatus forced the layers to bend 160° around a small, semicircular radius (150 μm). This was repeated many times. The mat was then inverted and the fibers were subjected to bending in the opposite direction. The second apparatus subjects the fiber mats to repeated transverse compression by passing the mats through a roll nip with the fibers oriented parallel to the direction of travel. In both cases, the wet mats were disintegrated, the fibers formed into standard handsheets, and the handsheet mechanical properties were evaluated. Handsheets from pulp treated in a PFI mill were evaluated to provide a frame of reference to which handsheet from the specialized apparatuses could be compared.

BACKGROUND

FIBER MORPHOLOGY

The main structural component in wood species of economic importance is the axial system of fiber cells[3]. Wood tracheid (gymnosperms) or fiber (angiosperms) cells are slender tubular structures as depicted in Fig. 2. This axial system is transverse by a radial system of parenchyma cells. The spacing and cross-sectional shape of the tracheids vary to allow a very dense packing. The central cavities of cells, or lumina, are interconnected through thin areas of the cell walls called pits[4]. Pits are significant in governing the penetration of pulping liquors into the wood and in modifying the localized structural properties of the cell wall. In regions where tracheid cell walls are adjacent to parenchyma cells (ray crossings), the structural properties of the walls are influenced by the large number and size of pits associated with ray crossings. The distribution of pits is variable in other areas of the tracheid wall.

The tracheid and fiber cells are bonded together by the middle lamella[5]. The middle lamella is a thin layer of lignin and noncellulosic polysaccharides. Tracheid and fiber walls consist of multiple, concentric layers made up of fibrils. Fibrils are aggregates of cellulose chains surrounded by a matrix of amorphous hemicellulose and lignin material. As illustrated in Fig. 3, the fibrils are spirally wound in layers about the longitudinal axis of the tracheid at various angles in either an "*S*" (clockwise windings when viewed from the top) or "Z" (counterclockwise windings) orientation. The cell wall may be differentiated into layers based on variations in optical properties of the cell wall viewed in cross section. The changes in optical properties occur due to changes in the winding angle of the fibrils. The tracheid is normally described as having a two-part cell wall – a primary wall (*P*) and a secondary wall (*S*). The secondary wall is

further divided into three layers[3,6]. This organization is shown conceptually in Fig. 4. The designations, from exterior to interior layer, are P, S_1, S_2, and S_3. The primary layer varies from randomly oriented cellulose chains at the outer surface to more orderly windings of the cellulose chain at very high angle (as measured from the fiber longitudinal axis) in both directions at its inner surface. The outer layer of the secondary wall, S_1, has fibrils wound in both "S" and "Z" orientations at moderate angle. The middle layer, S_2, has fibrils wound mostly in a "Z" orientation and at a low angle. The inner layer, S_3, has fibrils wound in alternating "S" and "Z" orientations at moderate angle.

Krässig[7] divides the cellulosic structure of the cell wall into three levels: molecular, supermolecular, and morphological. At the molecular level, the chemical constitution, the steric conformation, the average molecular weight, the molecular weight distributions, and the intramolecular interactions define the structure. The structure of the supermolecular level is defined by the aggregation of the cellulose chains into elementary crystals and fibrils, the degree of order inside and around the these fibrils, and the perfection of their orientation with respect to the fiber axis. Finally, the morphological level is defined by the spatial arrangement of the fibrillar crystallite strands, the existence of cell wall layers, the presence of interfibrillar voids[8]. The relationship between these levels is illustrated in Fig. 5. In Fig. 5, parts *(a)*, *(b)*, and *(c)* are of the morphological level, parts *(d)*, *(e)*, and *(f)* are of the supermolecular level, and part *(g)* is of the molecular level.

At the molecular level, the cellulose molecule, 1,4–β–D-linked polyanhydro glucopryranose (see Fig. 6) is the basic unit[7]. Cellulose molecules have lengths of 1000 to 15,000 glucose units. Typical lengths in the primary wall are 2000–6000 units, compared to 14,000 units in the secondary wall[4]. Cellulose

molecules have the ability to form intra- and intermolecular hydrogen bonds (see Fig. 7) and cellulose molecules group together in a parallel manner to create the next level of organization[7].

At the supermolecular level, parallel aggregations of cellulose chains form micelles. Micelles are crystalline domains embedded in an amorphous matrix. The structures have dimension of 3 to 20 nm in cross dimension, and are about 25 nm in length[7]. More current terminology refers to micelles as elementary crystallites. The internal arrangement of the elementary crystallites is illustrated in Fig. 8. In Fig. 9, an example is given of the structure at the supermolecular level proposed by the fringed-fibrillar model of Hearle[9]. The model proposes that the fiber is built from a network of elementary fibrils (longer lines in Fig. 9) and their secondary aggregations (regions where short lines are perpendicular to the longer lines). The elementary fibrils are composed of consecutive elementary crystallites where internal cohesion is established by the transition of the long cellulose molecules from crystallite to crystallite (the small rectangles in the figure) in the elementary fibrils.

At the morphological level, the elementary fibril networks form microfibrils. The microfibrils are arranged in ribbon-like structures of 2 to 4 elementary fibrils bonded on their radial surfaces with their tangential surfaces co-planar and parallel to the middle lamella as shown in Fig. 10. Kerr and Goring[10] consider the elementary fibril dimensions to be 3.5 nm square or near the low end of the range given by Krässig[7]. The width of the microfibrils is then about 70 to 140 nm. Larger aggregations of microfibrils are referred to as macrofibrils.

A comparison of dimensions for the various structural units described is shown in Fig. 11. This figure illustrates the very large range of sizes involved in

fiber morphology and, thus, papermaking. The dimensions are for a typical thin-walled southern softwood. The dimensions in Fig. 11a are representative of those of the supermolecular level of Krässig. The distance between the two cellulose molecules represents the length of a hydrogen-bond. Also included is an example of the elementary fibril of Kerr and Goring. The dimensions associated with the morphological level are shown in Fig. 11b. Here, the lamellas and cell wall layers correspond to those described in Fig. 4. The cell wall thickness of the morphological level is associated with the macroscopic swollen fiber diameter and fiber length in Fig. 11b. Keeping in mind the scale factor of 1000 between Fig. 11a and Fig. 11c, compare the length of the hydrogen-bond in Fig. 11a to the wall thickness and fiber diameter of Fig. 11c. As discussed later, the bonding of fibers in paper requires the fiber surfaces to approach each other on the order of magnitude of the hydrogen-bond length.

The chemical composition of the cell wall is essentially three components: cellulose, hemicellulose, and lignin. The distribution of the components across the wood fiber cell wall is shown in Fig. 12. The two different structural relationships between the three components were proposed by Kerr and Goring[10] are shown in Fig. 13. In Fig. 13a, the hemicellulose are associated entirely with the cellulose microfibrils; in Fig. 13b, the hemicellulose are distributed throughout the 3-dimensional lignin network. Based on an approximate calculation by Kerr and Goring, the actual case probably lies between the two extremes with $\frac{1}{3}$ of the hemicellulose associated directly with the cellulose microfibrils and the rest distributed throughout the lignin network.

The major goal of pulping is the removal, by dissolution, of the middle lamella, and hence the freeing of the fibers. The majority of the lignin and hemicellulose, along with some cellulose, is also removed from the cell wall. In

pulping the wood to produce papermaking fibers, as much as 55% of the material may be removed. While pulping, and any subsequent bleaching, removes a large portion of the cell wall material, the integrity of the cell wall organization is retained[4]. Kerr and Goring[10] use a modification of the interrupted lamella model, made by Scallan[11], to illustrate the changes caused by delignification. Shown in Fig. 14 is the conversion of the uninterrupted cell wall into the delaminated structure normally associated with delignified fibers.

EFFECTS OF REFINING

The net effect of refining is a compromise between the desirable and the adverse results of refining on pulp fibers and sheet characteristics. Desirable results include higher flexibility and strength, removal of structural flaws, and removal of the primary wall. Adverse results include fiber shortening, and excessive external fibrillation and the formation of fines[12–14].

Fiber Morphology

Pulping of wood fibers does not disrupt the integrity of the cell wall and does little to improve the fibers papermaking potential without subsequent refining[15]. Wood fibers which have been chemically pulped, but not additionally treated with mechanical action, produce a weak, bulky sheet. Fiber strength and fiber bonding are well below that reached when the fibers are subjected to mechanical action in the presence of water[13–15].

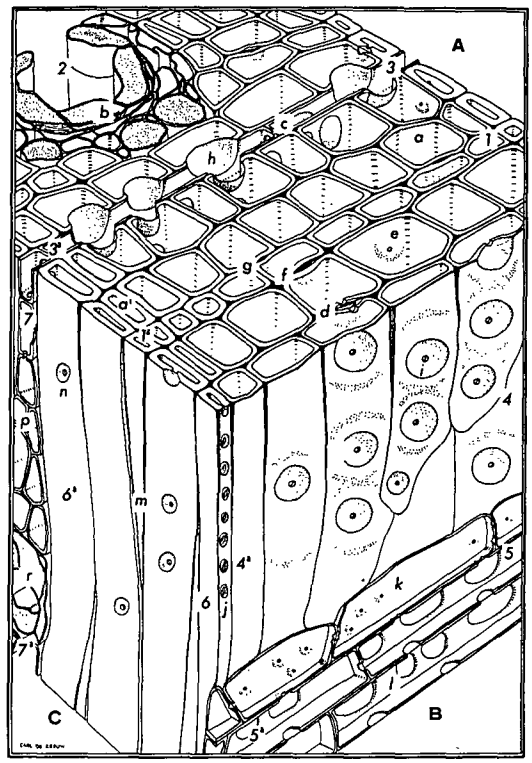

Figure 2. Schematic three-plane drawing of the wood of eastern white pine (*Pinus strobus* L.)[3]. Surface *A*. 1–1[a], portion of an annual ring; 2, resin canal; 3–3[a], wood ray; *a–a'*, longitudinal tracheids; *b*, epithelial cells; *c*, ray cells; *d*, pit pair in median sectional view; *e*, bordered pits in the back walls of longitudinal tracheids, in the surface view; *f*, pit pair in sectional view, showing the margin of the torus but so cut that the pit apertures are not included in the plane of section; *g*, pit pair in which neither the pit aperture nor the torus shows; *h*, window-like pit pairs between longitudinal tracheids and ray parenchyma. Surface *B*. 4–4[a], portions of longitudinal tracheids in radial aspect (the ends are blunt); 5–5[a], upper part of a uniseriate ray; *i*, bordered pits on the radial walls of longitudinal, earlywood tracheids (the base of the bit is towards the observer); *j*, small bordered pits on the radial walls of longitudinal late-wood tracheids, in the same view as in *i*; *k*, ray tracheids; *l*, cells of ray parenchyma. Surface *C*. 6–6[a], portions of longitudinal tracheids in tangential aspect; 7–7[a], portion of a xylary ray; *m*, tapering end of longitudinal tracheids in tangential aspect; 7–7[a], portion of a xylary ray; *m*, tapering ends of longitudinal tracheids; *n*, a small bordered pit on the tangential wall of longitudinal late-wood tracheid; *p*, cells of ray parenchyma; *r*, transverse resin canal.

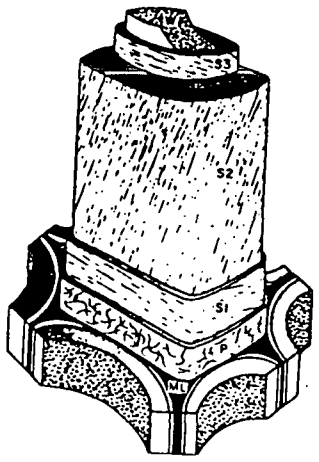

Figure 3. General depiction of the wood fiber cell wall structure showing the middle lamella (*ML*), primary (*P*) layer, and secondary (S_1, S_2, and S_3) layers[5].

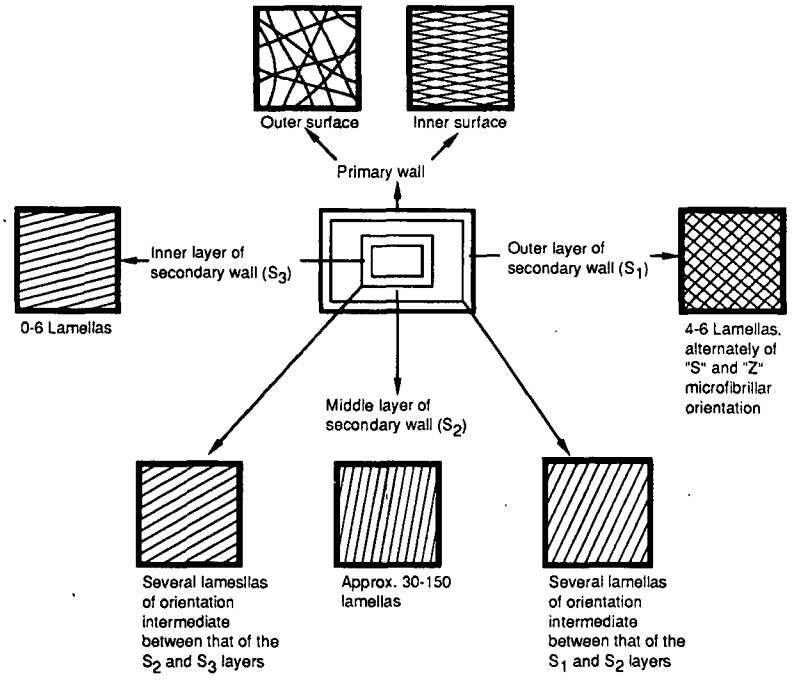

Figure 4. Diagrammatical representation of a typical mature wood fiber or tracheid showing the organization of the different cell wall layers. After Wardrop and Harada[6].

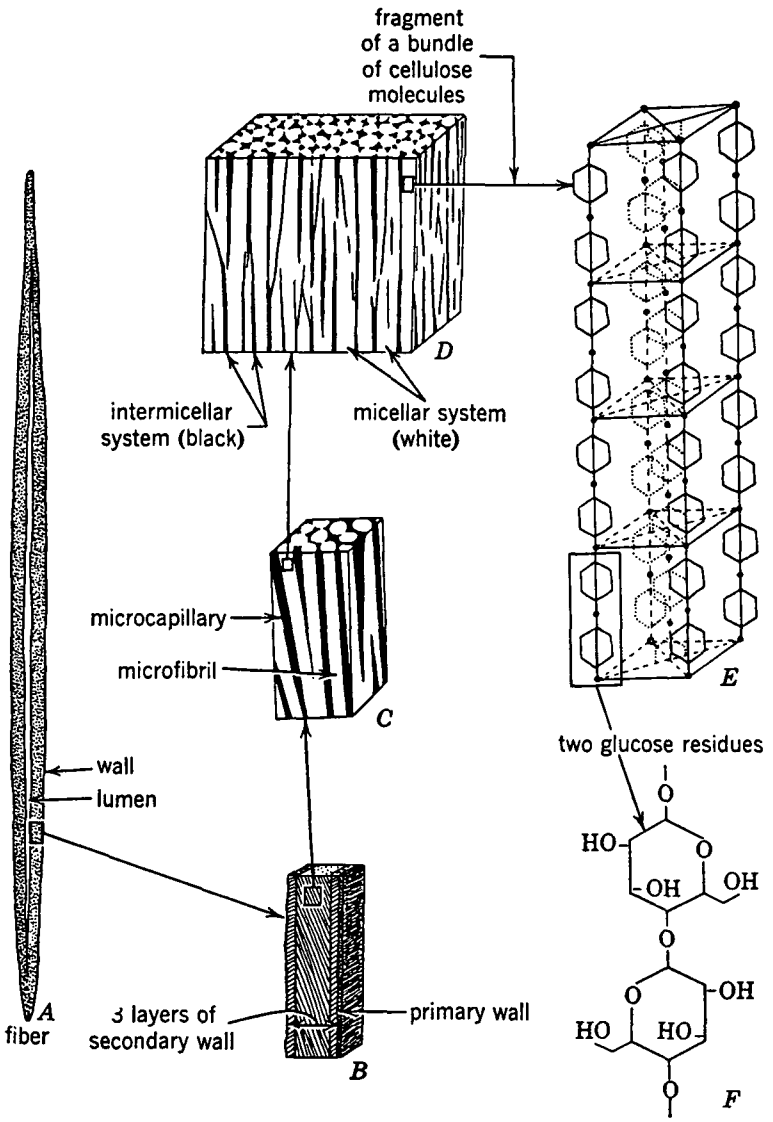

Figure 5. Detailed structure of the wood fiber cell wall[8]. *A*, strand of fiber cells. *B*, cross section of fiber cells showing gross layering – a layer of primary wall and three layers of secondary wall. *C*, fragment from middle layer of secondary wall showing macrofibrils (white) of cellulose and interfibrillar spaces (black), which are filled with noncellulosic materials. *D*, fragment of a macrofibril showing microfibrils (white). The spaces among microfibrils (black) are also filled with noncellulosic material. *E*, structure of microfibrils – chain-like molecules of cellulose, which in some parts of microfibrils are orderly arranged. These parts are the micelles. *F*, fragment of a micelle showing parts of chain-like cellulose molecules arranged in a space lattice. *G*, two glucose residues connected by a oxygen atom – a fragment of a cellulose molecule.

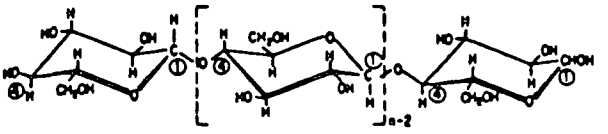

Figure 6. Constitution and conformation of the cellulose molecule[7].

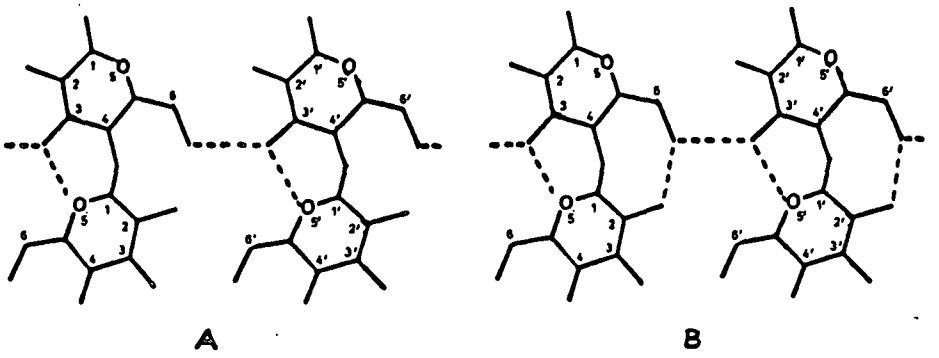

Figure 7. Intermolecular hydrogen bonds under the 002-lattice planes of cellulose-I[7].

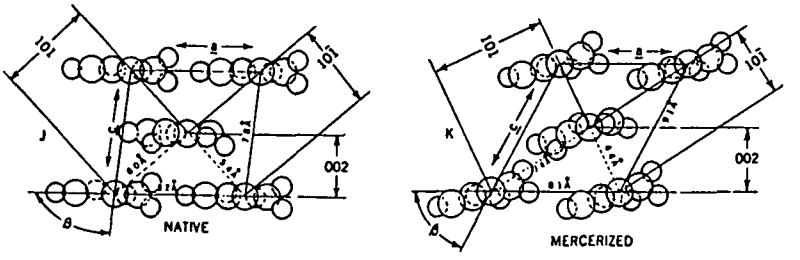

Figure 8. Unit cell structures of native cellulose-I and of mercerized cellulose-II[7].

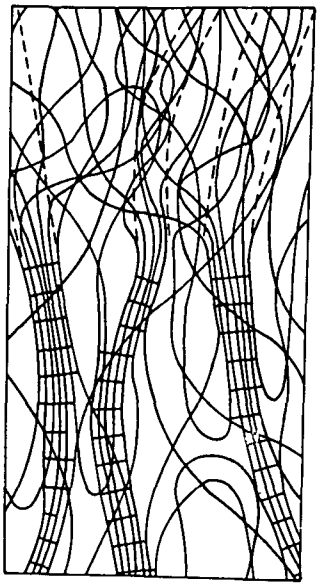

Figure 9. Formation of the fringed-fibril structure in the wood fiber cell wall[9].

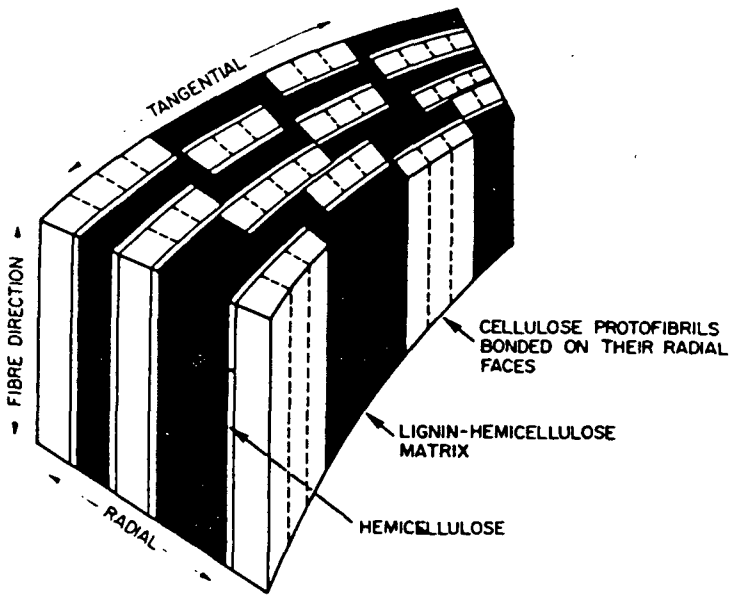

Figure 10. Pictorial representation of the proposed interrupted lamella model for the ultrastructural arrangement of lignin, cellulose and hemicelluloses in the wood fiber cell wall[10].

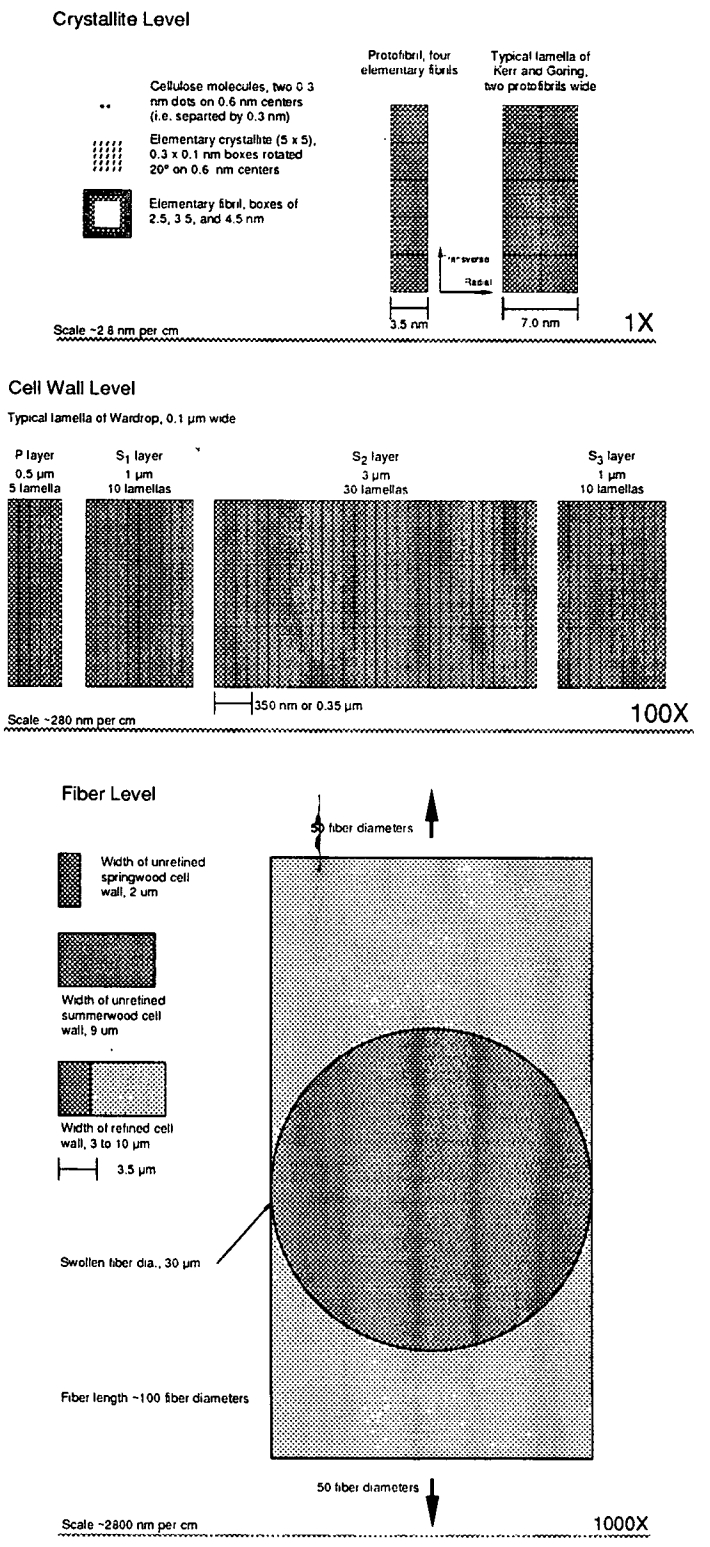

Figure 11. Comparison of dimensions for various structures in the wood fiber cell wall. (*a*) Crystallite level[7,10]. (*b*) Cell wall level[4]. (*c*) Fiber level[16].

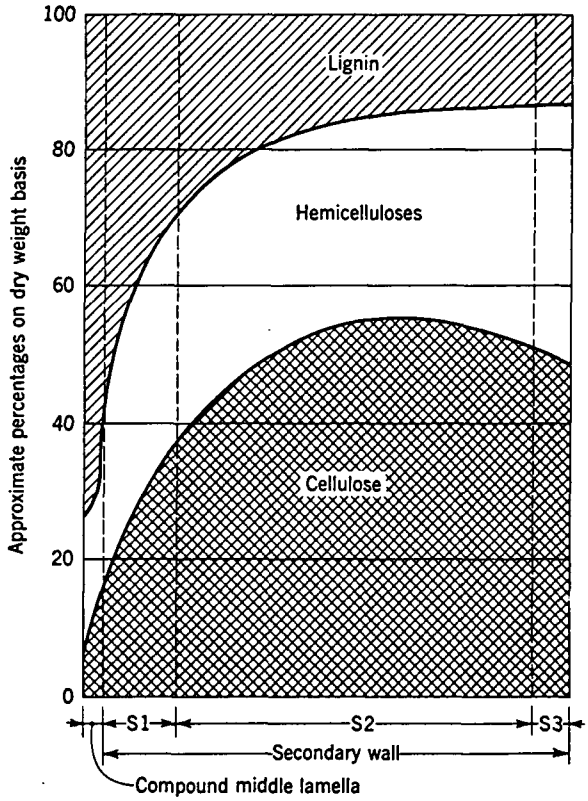

Figure 12. Distribution of the principal chemical constituents within the various layers of the wood fiber cell wall in conifers[3].

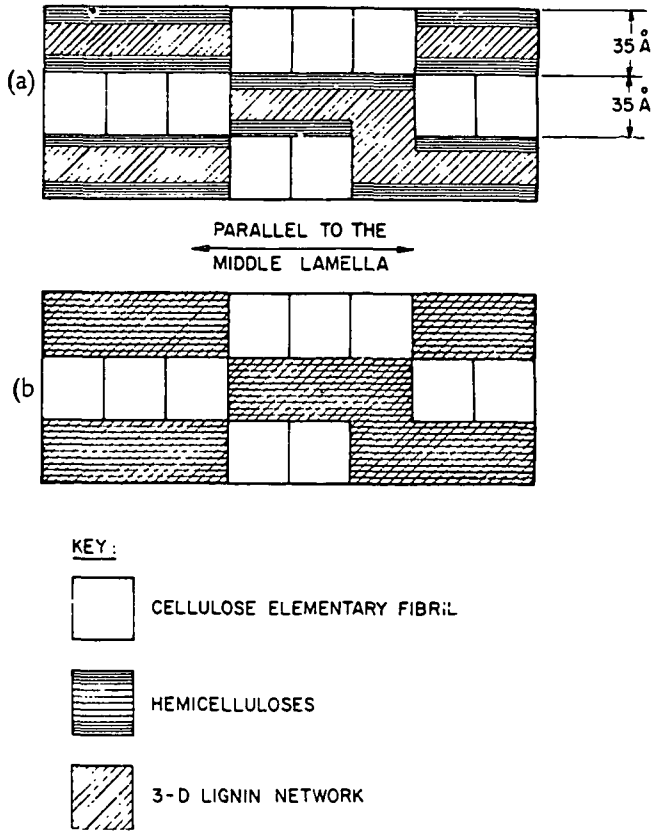

Figure 13. Two models for the ultrastructural arrangement of the wood fiber cell wall[10].

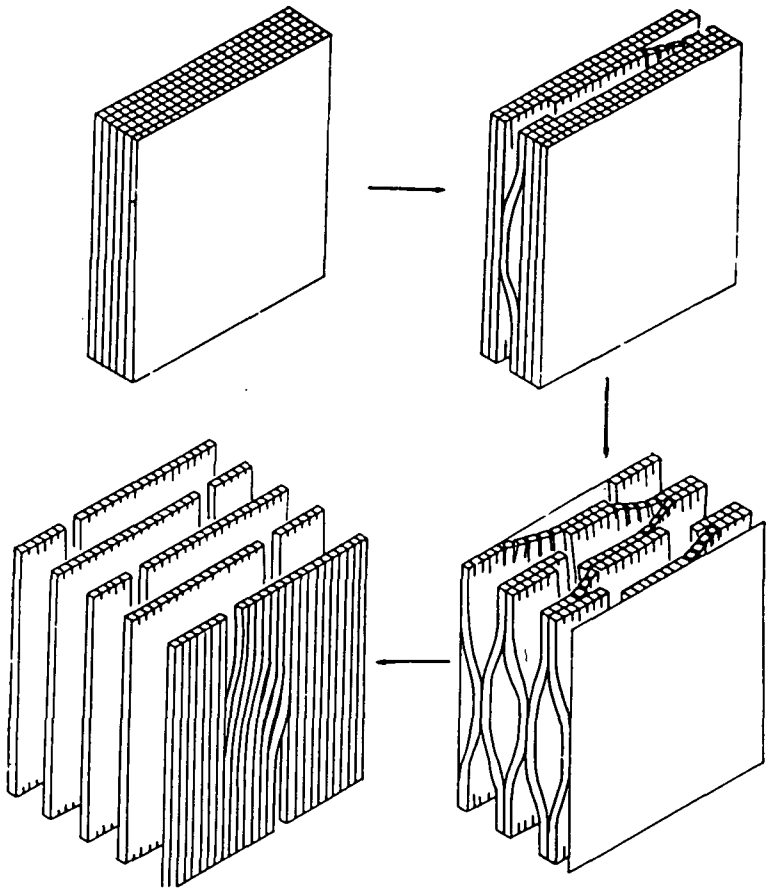

Figure 14. The internal fibrillation of the wood fiber cell wall[11]. The pattern of internal fibrillation of the wood fiber cell wall with progressive swelling, as might be expected from the preferential cleavage of tangentially-oriented bonds. The sketch is of a small section of a wall with zero fibril angle.

The primary effects of refining on fiber structure as proposed by several authors is presented in Table 1 taken from Ebeling[17]. Historically, refining was considered to cut and split the fibers as well as abrade the fiber surfaces. The desired effect was the "hydration" or swelling of the fiber. With time, these effects have become better defined and, currently, the description by Ebeling is the most comprehensive. Ebeling includes two additional effects, the local dislocation of the cell wall structure and dissolution of cell wall material. Both of these effect became apparent as new techniques for observing and measuring fibers were developed.

A very elegant approach is proposed by Fahey[18] which considers the primary effects of refining to be the breakage of either covalent or hydrogen bonds. While this reduces the effects to fundamental levels, the analytical methods are not available evaluate refining on this level.

The approach taken in this thesis is that of Ebeling[17,19]; the changes in the fiber produced by refining are divided into three categories: internal structural changes, external structural changes, and fiber shortening.

TABLE 1

PRIMARY BEATING EFFECTS (STRUCTURAL CONSIDERATIONS)

Historical	Fahey[18]	Higgins and de Yong[21]	Giertz[20]	Clark[13]	Ebeling[19]
Cutting/ splitting	Breaking of covalent bonds	Fiber shortening	Cutting and crushing	Shortening	Fiber Shortening
External fibrillation		External fibrillation	Successive cleavage of external layers of the cell wall and subsequent breaking away of these layers	External splitting	Successive cleavage of external layers of the cell wall and their subsequent breaking away[b]
Hydration	Intrafiber H-bond breaking	Intrafiber H-bond breaking	Intrafiber H-bond breaking	Internal splitting	Delamination of internal cell wall layers[b]
		Production of fines		(Production of debris)[a]	
			Creation of dislocations	(Longitudinal compression)[a]	Local dislocations of the cell wall structure
					Dissolution of the chemical components of the cell wall and simultaneous formation of colloidal carbohydrate solution on the surface affected

[a]Secondary effects
[b]See Ebeling[19]

Internal

The refining process results in a loosening of the concentric lamellae within the secondary wall and between the S_1-S_2 and S_2-S_3 layers. This is responsible for a subsequent increase in fiber flexibility[12,22,23]. Local dislocation zones (misalignment zones, slip planes, and kink bands) created by refining lower cell wall rigidity to compressive forces axially[24]. These dislocation zones are regions where the axes of the cellulose chains are radically altered. Both of these actions increase the surface area open to hydration. In addition, some chemical components of the cell wall partially dissolve into a colloidal carbohydrate solution[14,22,25,26]. This partial dissolution is referred to as molecular fibrillation and can also occur on external surfaces.

External

The partial detachment of lamellar and macrofibrillar material has been observed by many workers. Early descriptions of these changes were made by Steenberg and Sandgren[27] and Sandgren and Wahren[28]. McIntosh[12] indicates that the amount of fibrillation increases rapidly in the initial stages of beating and then levels off. This is most likely due to the complete detachment of material from the surface at a rate similar to the rate at which external fibrillation forms on the fiber surface. Giertz[29] reports that the primary layer is removed very early during beating. Giertz also reports that the amount of fiber surface free from primary wall can be correlated with paper tensile strength. The detached material includes the P layer, parts of the S_1 layer, and, if the pulp is heavily beaten, parts of the S_2 layer[4]. The detached material is referred to as fines or crill.

Shortening

Cottral[30] states that two types of mechanical effects of conventional refiners cause shortening of the fiber. The fiber may be cut by the direct shearing

force of the passing bars, or they may fail in tension when pulled from a fiber floc. In general, all conventional refining processes tend to reduce the fiber length distribution to a lower average. The degree to which this may happen is dependent on the type of refiner and the operating conditions.

Further study of refiner type, involving a statistical analysis, is presents by Corte and Agg[31]. They compared the results of beating a pulp with a predominantly cutting action (Rieth hollander) and with a mainly squashing action (Jokro mill). In addition to demonstrating that beating can reduce the average fiber length, they argue that change in mean fiber length does not sufficiently characterize the action of a beater. As an alternative, they introduce a parameter, called the fiber shortening rate, which is more useful in distinguishing between refiners and operating conditions which reduce fiber length by either cutting action or squashing action.

In some cases, refining can increase the length of specific fibers which are kinked or bent. A tensile force applied to a fiber which is sufficient to "straighten" the fiber without breaking it could increase the length. When fibers have been dried, kinks and crimps produced incidentally by previous mechanical actions are set into the fiber. Refining in this case, can help to remove the kinks and crimps and thus, increase the fiber length. This action also allows the fiber to transmit tensile load along the segments which were previously kinked or crimped and incapable of transmitting load[32].

Fiber Properties

Longitudinal Stiffness

Samuelsson[33] measured the bending stiffness of wet fibers in a cantilever configuration with a specialized apparatus. Measurements of bending stiffness, or the product of axial Young's modulus and the cross-sectional moment of

inertia, indicated that summerwood fibers (from a sulfite pulp) are more stiff than springwood fibers. In a second paper, Samuelsson[34] presented results for kraft pulped fibers showing that moderate refining in a PFI mill decreases the stiffness at least five-fold and short periods (< 300 seconds) of ultrasonic treatment decreased stiffness by about three-fold. Subjecting fibers to mechanical action by flexing them in the apparatus resulted in a 10% decrease in stiffness for earlywood kraft fibers. This increase required deflecting the fiber by 15% of the suspended fiber length only 100 times.

Leopold[35] in a study of pulping, bleaching, and refining effects on dry fiber tensile strength and axial modulus treated unbleached pine kraft pulp in a PFI mill. For both springwood and summerwood, the minimum tensile strength, average tensile strength, and axial modulus increased with beatings. The values at any level of beating were higher for summerwood than for springwood. The effect of beating on springwood was greater than on summerwood; for 8000 rev., the increase in springwood *vs.* summerwood for the minimum strength and average strength, and modulus was 69 *vs.* 25%, 37 *vs.* 23%, and 75 *vs.* 30% respectively.

Kallmes and Perez[36] studied the effect of drying restraint using a commercial never-dried, unbleached kraft pulp prepared from a 50/50 mixture of spruce and pine. Unbeaten fibers and fibers beaten in a Valley beater for 90 minutes were dried and tested under three different sets of conditions: 1) freely dried fibers which were mounted and tested wet, 2) freely dried fibers which were mounted and tested dry, and 3) fibers dried under restraint which were mounted and tested dry. The unbeaten fibers tested in the dry state had higher tensile strengths and axial moduli than the fibers tested wet. In the dry state, the freely dried fiber had the higher values than the restrained fibers. Beating the fibers

resulted in the wet fibers having the highest strengths and moduli followed by the fibers dried under restraint and the freely dried fibers. Beating increased the properties of the wet fibers and decreased the properties of the dry fibers.

McIntosh and Uhrig[37] measured the effect of refining on dry fiber tensile strength and axial modulus. The pulp used was an unbleached southern pine kraft pulp and refining was carried out using the PFI mill. For springwood fibers, the strength and modulus increased with with refining. The springwood values were very similar to the values obtained by Leopold[35]. However, refining of the summerwood fibers decreased the strength and modulus, a trend opposite that observed by Leopold.

Alexander and co-workers[38], with dried fibers, showed that tensile strength and axial modulus initially increased with refining and then decreased for both springwood and summerwood. Unfortunately, this trend was based on only three levels of refining. Alexander attributed the initial increase to decreases in the fibril angle which results from pulping and subsequent refining. The results also showed large differences in modulus for springwood (lower) and summerwood (higher) fibers at the same fibril angle.

Hardacker[39] studied the effect of beating on unbleached southern pine kraft pulp using a Valley beater. He recorded the load-elongation curve for dry, individual fibers placed in axial tension. The data showed beating rapidly increased the tensile strength and initial modulus during the early phases of refining after which there was a more moderate rate of increase. For 40 minutes of beating, the strength increased by 33% and the modulus almost doubled. The zero-span strength of 20 g/m^2 handsheets (and the individual fiber strengths, calculated from the zero-span measurements) showed similar increases.

Page[40] reported that fibers of equal fibril angle can have the same tensile strength regardless of whether they are springwood or summerwood. The strength of dried individual fibers was considered dependent on the fibril angle in the S_2 layer. Page and El-Hosseiny[41] later showed the slope of the stress-strain curve to increase with decreasing fibril angle.

Mohlin[42], in a study centered on bonding, presented results indicating that fiber conformability increased with refining (unrefined compared to 4000 rev. in a PFI mill). The conformability was determined by measuring the ability of the fiber to conform to a glass fiber (0.06 mm diameter) placed on a glass plate. The wet fiber was laid across the glass fiber and allowed to dry. The span length of the fiber not in contact with the plate was used as a measure of fiber conformability. The longer the free span, the less conformable the fiber. In addition, the breaking length of handsheets correlated with the single fiber-cellophane crossing bond strengths and the conformability values.

Tam Doo and Kerekes[43–45] have developed an apparatus for measuring the bending stiffness of wet fibers. The fiber is supported as a simple beam under uniform load in the apparatus and the deflection at known loads is measured. The results indicated that unrefined springwood fibers are more flexible than summerwood fibers. The relationship between handsheet breaking lengths of the long fiber fraction (R14) and fiber stiffnesses showed that the more flexible the fiber, the higher the breaking length. In this case, the differing fiber stiffnesses were from fibers of different species and different pulping processes. Unfortunately, breaking length data from pulps where fiber stiffness varies due to differing yields was not available. Over a wide range of yield in a sulfite pulping process, fiber stiffness was proportional to yield.

The relationship between refining (PFI mill) and fiber bending stiffness was also explored by Tam Doo and Kerekes[46]. Using their apparatus in a mode similar to that of Samuelsson[34], Tam Doo and Kerekes were able to superimpose a cyclic deflection of 1.5% of the span width up and down from on a mid-beam deflection of 2% (*i.e.*, cycle the fiber from 0.5 to 3.5% total deflection). The results showed a decrease in normalized stiffness (stiffness over initial stiffness) of 60–70% after 10^5 cycles. In this case, measurable decrease did not begin to take place until after the first 100 cycles. The contrast with Samuelsson data is most likely due to the difference in either strain amplitude or fiber configuration (cantilever *vs.* simply supported).

In order to compare the PFI mill data to the data from flexing the fibers in the apparatus, Tam Doo and Kerekes developed an estimate of the number of "bending" cycles per PFI mill revolution (see Appendix II). Comparisons were made on the basis of the number of "bending" cycles a fiber experienced. The initial decrease in fiber stiffness was greater for the apparatus than for the PFI mill. After about 17,500 cycles in the apparatus, the trend started to level off while the PFI mill continued to decrease stiffness. In general, the two trends are not different by more than a normalized stiffness of 0.1. After 25,000 cycles, the PFI mill treatment produced fibers with a normalized stiffness of 0.5 and the apparatus treatment produced fibers with a normalized stiffness of 0.6.

Luner[47] has measured wet fiber flexibility in another way from that of Samuelsson[33] or Tam Doo and Kerekes[43]. He placed very thin, wet fiber networks over a series of parallel stainless steel wires resting on top of a glass slide. The fibers are out of contact with the glass plate for a distance on both sides of each wire. This distance is measured and used as a relative indication of wet

fiber flexibility. Luner stated that his results were in the same range, but higher than the Tam Doo and Kerekes results without giving any explanation.

Luner reported a large difference in wet fiber flexibility (WFF) between springwood and summerwood fibers and attributed the differences to a relationship between the log of cell wall thickness and the WFF. The thicker the cell wall, the less flexible the fiber. This is expected since the thicker the cell wall, the higher the cross-sectional moment of inertia. Coarseness, the ratio of fiber length to weight, was directly related to fiber cell wall thickness and had a log-linear relationship to flexibility.

Beating the pulps increased the WFF by three to five-fold for treatments of 8000 rev. in a PFI mill. The effect of beating on WFF was larger in springwood-rich pulp fractions than in summerwood-rich fractions. For sheet density, the opposite trend was observed. The explanation given was that refining created a higher degree of fibrillation in the summerwood fibers which resulted in higher density values. Sheet properties were also related to wet fiber flexibility. Sheet density and tensile strength had linearly relationship WFF on either a constant fiber mass or number basis. The more flexible fibers had the higher densities and tensile strengths. The relative bonded area was strongly correlated to WFF, but additional factors needed to be considered in determining the sheet structure and tensile properties.

The following generalizations about the effect of refining on fiber axial properties can be made. Refining makes fibers more flexible and conformable (less stiff). The explanation put forth by Samuelsson[34] attributes the increase in wet flexibility to "modifications of the fibrillar structure in the fiber wall and due to changes of the molecular structure in the fiber material." The stiffness of dried fibers initially increases with refining and then remains constant or decreases.

Van den Akker, *et. al.*[48] attributed the increase in dry tensile strength and modulus to better stress distribution in the cell wall due to the loosening and rearrangement of the cellulose framework during refining. This could include a decrease in the S_2 fibril angle with decreasing pulp yield and increased refining as shown by Alexander, *et. al.*[38].

Transverse Stiffness

Harrington and co-workers[49–50] performed some of the early work in observing fibers in transverse compression. Their observations were limited to recording the stress-strain curves of the fibers to the point where the lumen was completely collapsed. The results indicated that wet fibers were less stiff than dry fibers, at least to the point of lumen collapse. The explanation stated that for the dried fiber, the lumen had partially collapsed into two sub-lumina, thus foreshortening that part of the stress-strain curve during which the lumen collapsed in the wet fiber. This resulted in the higher stiffness observed up to the point of complete collapse.

Kallmes and Perez[36] measured the elastic modulus of very highly oriented sheets. They estimated that 90% of the fibers were oriented within 10% of the machine direction. They argued that the ratio of sheet *MD–CD* modulus (~11:1) approximated the ratio of fiber axial-transverse modulus. While they justifiably resisted the temptation to use this ratio to give a value for fiber transverse modulus based on fiber axial modulus measurements, they stated that the transverse modulus was at least an order of magnitude less than the axial modulus.

Hartler and Nyrén[51–53] recorded load-deformation curves of wet and dry spruce kraft pulp fibers. The curves contained two phases, neither of which were elastic. The first phase related to the collapse of the lumen and the second phase

recorded compression of the cell wall. Their results were reported in terms of the force necessary to collapse the lumen and the "initial" slope of the second phase (termed transverse modulus). The collapse force and transverse modulus were lower in wet fibers than in dry fibers, lower in springwood fibers than in summerwood fibers, lower at lower pulp yields, and lower at higher refining levels (PFI mill) for wet or dry fibers. The modulus values for wet, kraft fibers of 50% yield ranges from 0.65 GPa for unrefined fiber down to 0.45 GPa for fiber subjected to 5000 rev. in a PFI mill. The collapse force for the same circumstances ranged from 350 N/m down to 150 N/m.

Berger[54] recorded force-deformation curves of dry pine kraft pulp fibers undergoing transverse deformation and obtained results similar to those of Hartler and Nyrén. Berger calculated transverse modulus values by measuring the slope of the curve after the lumen was assumed collapsed. Yield was reported as not having a significant effect on the modulus. The ratio of fiber thickness to width and the number of PFI mill rev. had a significant effect on modulus. As the ratio of thickness to width increased, the transverse modulus also increased. A generalized statement of this trend is that summerwood fibers have a higher modulus than springwood fibers. Refining decreased the transverse stiffness of fibers. This decrease was most prevalent when increasing the PFI mill rev. from 500 to 2000 (all fibers were subjected to at least 500 rev.). Further increases in refining resulted in smaller decreases in transverse modulus. The values reported range from 0.10 to 0.18 GPa or about 6 to 12 times lower than the dry transverse modulus results (0.48 to 1.25 GPa) reported Hartler and Nyrén.

In summary, transverse stiffness is lower in wet fibers, decreases as fiber thickness to width ratio decreases (or lower in springwood than in summerwood

fibers), and decreases with increasing refining. The transverse modulus is one or two orders of magnitude lower than the axial modulus.

Torsional Stiffness

Natio, *et. al.*[55–56], measured the torsion properties of pulp fibers dried from water and solvent-exchange dried from a nonpolar solvent. The relative torsional rigidity (rigidity over initial rigidity) decreased with increasing number or torsion cycles. Torques in the range of 3 to 10 nNm were applied at low frequency for up to 10^5 cycles. The rigidity decreased by 8 to 10% for dry fibers after 10^3 cycles and by 50 to 60% for wet fiber after 10^5 cycles. The rigidity decreased with pulp yield, while bleaching had little effect on the rigidity. The rigidity was significantly lower for the solvent-exchanged fibers than for the fibers dried from water. They considered this evidence that intrafiber bonding was occurring during drying of the fibers.

Measuring torsion properties using Naito's method, de Ruvo, *et. al.*[57] observed that the shear modulus of dried, latewood kraft and sulfite fibers were 1.2 and 1.5 GPa respectively.

Paper Properties

The relationships between fiber morphology and paper properties proposed by Giertz are illustrated in Fig. 15[58]. While Fig. 15 shows a slightly different view of the effect of refining on the fiber than described earlier, it is still useful in understanding the relationship between fiber properties and paper properties. The lines indicate effects of refining on the individual fibers. These changes in the fibers are then considered to affect web consolidation, fiber-fiber bonds, and fiber segments. Further, the relationship between these changes and

the dry sheet properties, such as density, strength, and optical properties, are illustrated.

For the purposes of this background section, the paper mechanical properties are of primary interest. To this end, the nature of the fiber network in paper can be described in terms of fiber and fiber-fiber bond characteristics. Fiber characteristics include fiber length, diameter, cell wall thickness, strength, presence of defects, and conformability. Bond characteristics include the number of bonds, area per bond, and the strength of the bond per unit area.

Density

The apparent density of the fiber network depends on the packing of the fibers. The development of intrafiber delaminations by beating increases fiber flexibility at the ultrastructural level and allows adjacent cell wall laminae and adjacent fibers to conform to one another during pressing and drying[59]. Thus, fiber flexibility influences the degree of web consolidation. Wet pressing will also conform fibers to one another, but refining has a much larger effect. A combination of the two is required to reach high sheet densities[13].

Campbell[60–62] first described the forces responsible for consolidating the web during the forming, pressing, and drying processes. His hypothesis is supported by the experimental work of Lyne and Gallay[63–65]. The hypothesis described the consolidating forces arising from the surface tension of water.

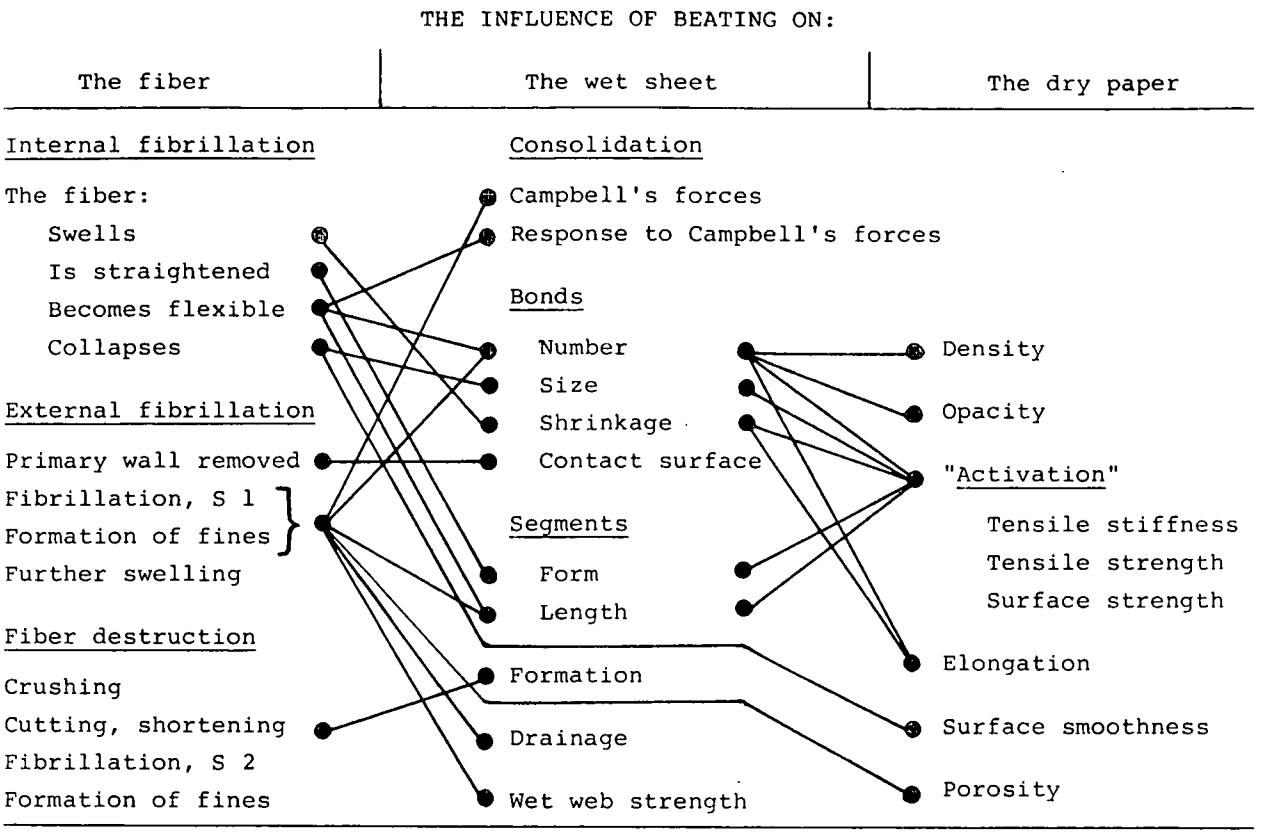

Figure 15. The cause-and-effect diagram of beating demonstrating the causal correlation between fiber treatment and paper properties[58].

During web consolidation, the removal of bulk water reaches a point, about 10% solids content, where meniscuses form between the surfaces of adjacent fibers. This is shown schematically in Fig. 16a taken from Swanson[66]. A force pulling the fibers toward one another arises from the surface tension of the water. If the radius of curvature of the meniscus is sufficiently large, the force, F, is approximately $F = \gamma L$ where γ is the surface tension of the water, and L is the length of line contact between air, water, and fiber. As more water is removed, a second meniscus can form opposite the first as shown in Fig. 16b. The force which results is equal to $2\gamma L$.

As the solid content reaches 20 to 25%, most of the bulk water has been removed and the liquid-water film is discontinuous as shown in Fig. 16c. The radius of curvature of the meniscuses is now sufficiently small to become important in determining the force pulling the fibers together. This situation may now be approximated by $\Delta P = 2\gamma/X$ where ΔP is the force per unit area pulling the surfaces together, γ is the surface tension of the water, and X is the thickness of the film. The pressure differential, ΔP, is inversely proportional to the film thickness X, the pressure difference can reach 100 to 200 atmospheres as the sheet approaches dryness. Campbell claims this effect is responsible for pulling fiber surfaces close enough together to allow hydrogen bonds to form. At any point during web consolidation, the forces described above are counter-balanced by the rigidity of the fibers. As refining creates more conformable fibers, more surface area is brought within the distance where hydrogen bonds may form producing a denser and stronger sheet.

The presents of fines can increase the effectiveness of Campbell forces in creating a dense, strong sheet. As explained by Giertz[67], unbeaten fibers form relatively few points of contact leading to a low density and low strength sheet. The Campbell forces are present, but ineffective in developing large areas of bonded surfaces. With refining, fibers become more flexible and the external surfaces become fibrillated. This allows partially dispersed fibrils from neighboring fibers to partly intermingle in a common solution or gel. The wet strength of this interface is much higher than the strength of a free water interface. As water is removed from the sheet, more bonded area is developed and a higher density and higher strength sheet results. Webs which contain fines have higher compacting forces since more meniscuses are present. These three cases are shown schematically in Fig. 17.

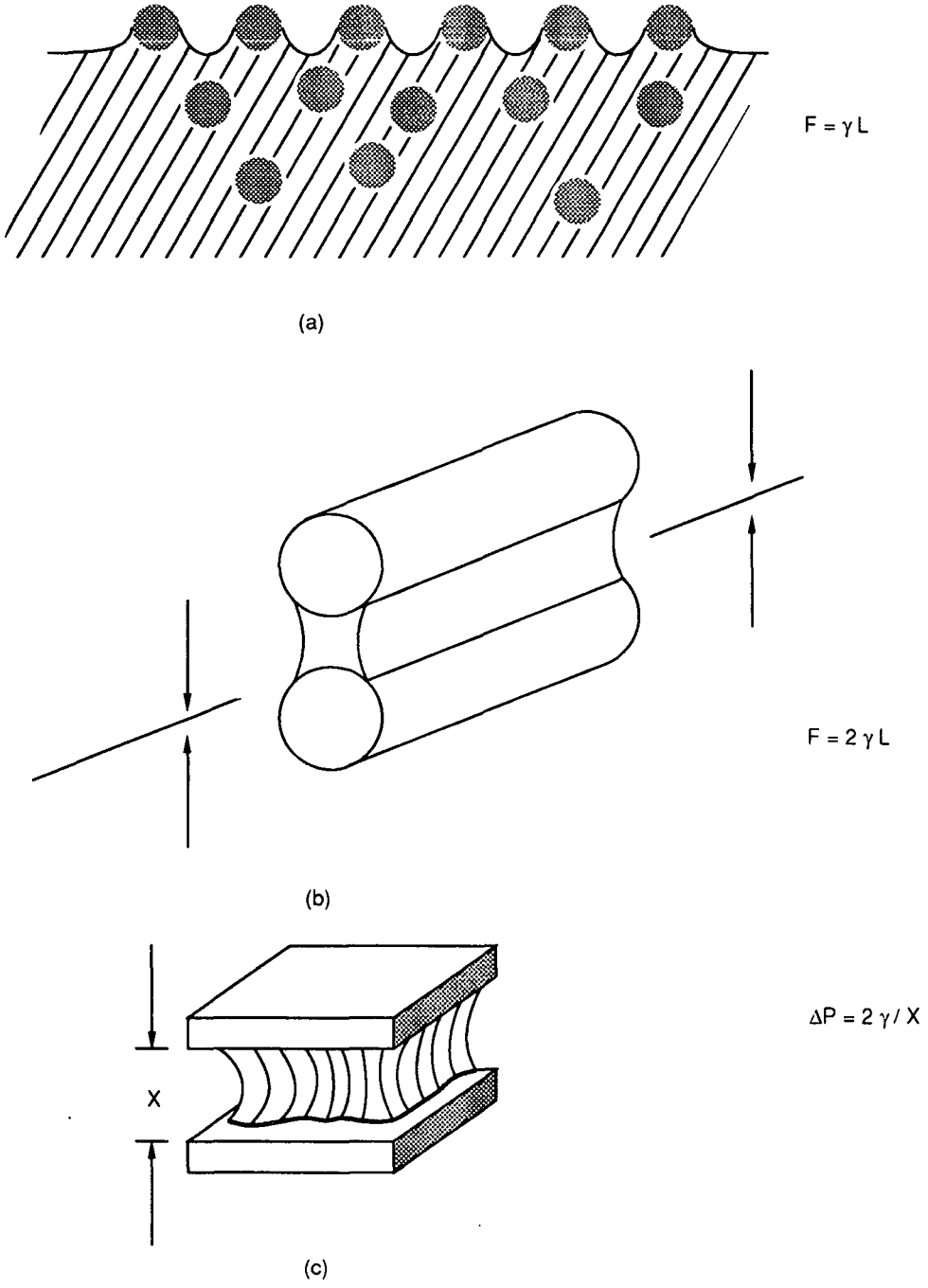

Figure 16. Action of surface tension forces when wet fiber webs are dried. After Swanson[66].

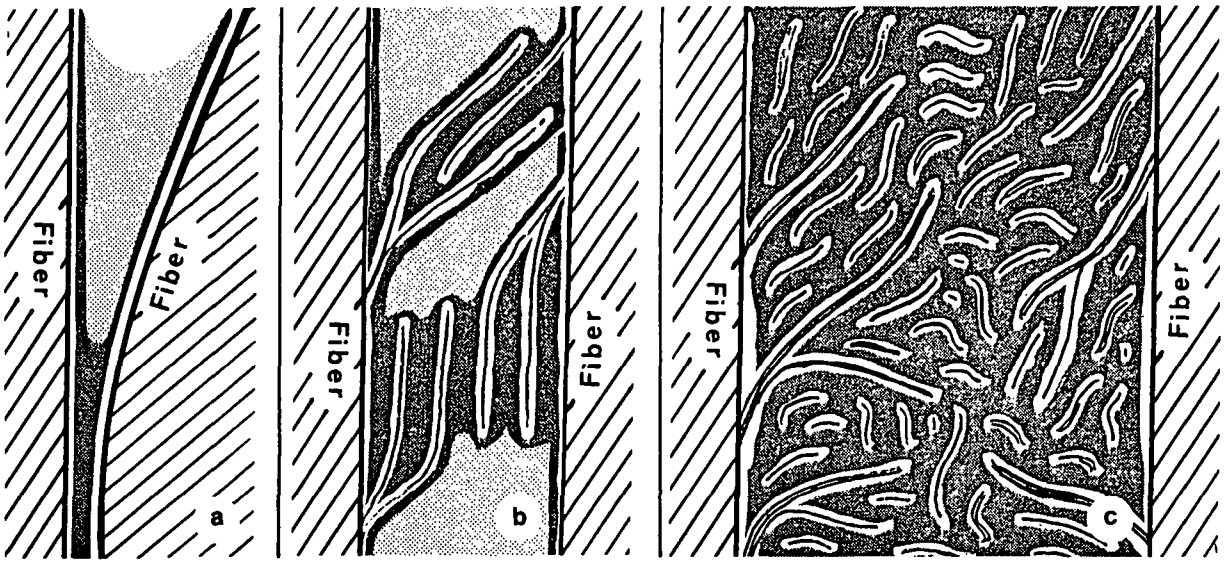

Figure 17. Schematic drawing of the interaction between two fibers with: a, no fibrils, b, only fibrils, and c, fibrils and fines present[67].

Strength

The relationship between refining and tensile strength can be approached using the Page model of tensile strength[68]. The theory considers tensile strength in the same manner as the network was considered above, in terms of fiber characteristics and bond characteristics. The theory results in the following equation describing paper tensile strength in terms of fiber and bond properties:

$$\frac{1}{T} = \frac{9}{8Z} + \frac{12\,A\,\rho\,g}{b\,P\,L\,(RBA)}$$

where T is the finite-span tensile strength of paper (expressed as a breaking length), Z is the zero-span tensile strength of paper (a measure of fiber tensile strength, expressed as a breaking length), A is the mean fiber cross-sectional area, ρ is the density of the fibrous material, g is the gravitational constant, b is the shear strength per unit area of the fiber-fiber bonds, P is the perimeter of the

average fiber cross section, L is the mean fiber length, and RBA is relative bonded area, the fraction of the fiber surface that is bonded in the sheet.

The equation developed by Page says that maintaining (or increasing) fiber strength and length, increasing the bond shear strength, and increasing the relative bonded area are all significant in increasing paper tensile strength. Provided that only a single furnish is involved, the fiber properties, A, ρ, and P, are not considered to significantly change during beating.

Refining can significantly decrease the average fiber length, which is detrimental to the development of tensile strength. Shown in Fig. 18, taken from Levlin[69], is the average fiber length plotted against the total amount of energy applied. Data is presented for a pine and a birch kraft pulp at several rates of energy input for refining conducted in a Escher-Wyss conical refiner. Depending on total amount of energy applied and the rate at which it is applied, refining can reduce the average fiber length of a pulp to half the original value. While very little reduction in average fiber length occurs for low energy input rates even at high total energy input, high rates of energy input can decrease the average fiber length by half at the same total energy input.

Refining can increase the average fiber tensile strength under mild conditions. Alexander and co-workers[38,70] in studying beating reported increases in single fiber tensile stress for both springwood and summerwood fibers refined 6000 rev. in a PFI mill. Their explanation for the initial increase was that a reduction in the fibril angle of the S_2 cell wall layer increased the ability of the fiber to support a tensile load. Subsequent refining may continue to decrease the fibril angle, but the number of defects added to the fiber reduces the tensile

strength. A some point the reduction in strength from defects is large enough to cancel the initial increases in strength.

The Page equation, given above, requires estimates of the specific shear strength of the fiber-fiber bonds and of the relative bonded area. Mohlin[42] studied fiber-fiber bonding using fiber-cellophane bonds. The experimental method emphasized measurement of the bond shear strength. The results presented indicate that refining has less influence on fiber-fiber bond shear strength than it does on the relative bonded area. Mohlin reported that beating actually caused a decrease in the bond strength of kraft pulps. The increase in fiber conformability and associated increase in the amount of bonded area was held responsible for the increase in tensile strength of paper with refining.

Skowronski and Bichard[71] studied fiber-fiber bond strength and the amount of bonded area using paper. As described by Skowronski and Bichard, "The technique is based on the controlled delamination of the sample using a specially designed free-rotating wheel to maintain the same geometry throughout the whole measurement under slow, quasistatic conditions." The technique is mostly a measurement of bond tensile strength. While the absolute value of these measurements is inappropriate for use in Page model, the trends observed by Skowronski for the bond tensile strength could likely apply for bond shear strength. The results indicated that refining and wet pressing increased total bond strength per unit area of specimen. However, neither had significant effect on the specific bond strength (bond strength per unit area bonded). In concurrence with Mohlin, it was concluded that the effect of refining on the bond strength is insignificant relative to the increase in bonded area.

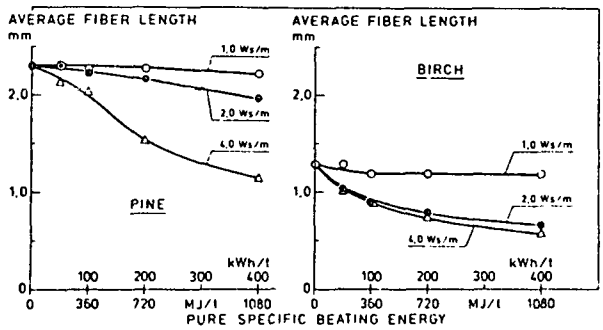

Figure 18. Average fiber length *vs.* pure specific beating energy for bleached pine and birch kraft pulps[69].

Elasticity

For an orthotropic material with three mutually perpendicular axes of reflectional symmetry, nine material parameters are required to describe the elastic response of the material[72]. Oriented papers are such a case with the axes of symmetry corresponding to the machine direction (*MD*), cross machine direction (*CD*), and thickness direction (*ZD*). The nine parameters are known as elastic stiffnesses or can be reported as three Young's moduli, three shear moduli, and three Poisson's ratios (three independent ratios out of six total). A fundamental understanding of the elastic properties of paper is crucial if prediction of the paper performance properties are to be developed. Without this information, performance properties must be measured directly using specialized test procedures or predicted from less fundamental properties.

Early work in determining paper elastic properties with ultrasonic velocity methods was contributed by Craver and Taylor[73,74]. These techniques are very useful because they are nondestructive and measure the mass specific elastic properties directly[73]. Further development of the measurement techniques by Mann, Baum, Habeger, and Wink[75,76] have allowed all nine elastic constants of orthotropic paper to be determined. Some individual paper elastic properties correlate well with strength properties. Craver and Taylor[73] reported correlation

between in-plane ultrasonic modulus and in-plane tensile strength and between ultrasonic and low frequency measurements of in-plane modulus. Results reported by Baum and co-workers[77] show correlation between properties along the different axes in oriented papers. Correlations were found between ultrasonic elastic moduli and tensile strength properties for the *MD*, *CD*, and *ZD*, and between ultrasonic and low frequency elastic moduli for the *MD* and *CD*. The use of the fundamental elastic properties in the prediction of paperboard compressive strength is illustrated by Habeger and Whitsitt[78]. They presented a correlation between the product of in-plane ultrasonic elastic stiffness and out-of-plane ultrasonic transverse stiffness with compressive strength in paperboard.

SPECIALIZED REFINING

Hartman and Higgins[79–82] developed two apparatuses to compare the effects internal delamination, external fibrillation, and fines addition on paper properties. The first apparatus emphasized the development of internal delaminations and the second emphasized the development of external fibrillation. The specimens were treated in each apparatus and some in both. Other treatments included the addition of fines from the same bleached spruce sulfite pulp.

The first apparatus, called the Roll Refiner (see Fig. 30 in the Experimental Program section), generated internal delaminations in the fiber cell wall without significant external fibrillation or shortening of the fiber. This was accomplished by sending fibers, in the form of a moist, oriented mat, through a roll nip. The oriented mats were formed in the Formette Dynamique. The nip was formed by a smooth roll (160 mm dia.) and a vented roll (60 mm dia., 0.8 mm bars on 2 mm centers). An end view of this nip is shown in Fig. 31 (Experimental Program section). The fiber mat was placed on the polished support roll where it

remained during the run held by surface tension forces. The machine direction of the mat was oriented parallel to the direction of travel through the nip. The nip load ranged from 2.8 to 13.3 kN/m (of bar width). The fiber mat was kept moist by blowing humidified air on the mat as it passed on the bottom of the support roll. Treatment of up to 4000 passes through the nip were applied. After treatment, the fiber mat was slurried, and formed into standard handsheets.

A second apparatus, called the Abrasion Refiner and shown in Fig. 19, caused fibrillation of the fiber surface without delaminating the cell wall. A pulp slurry of 3% consistency was placed between the fixed and rotating surfaces and the rotor turned at 1100 rpm. The disk surfaces were covered with an abrasive material which abraded the fibers. Carbide sandpaper was used as the abrasive material and the surface roughness ranged from the smooth disk surface (no sandpaper in place) to 60 grit. The distance between the two disks could be adjusted from 0 to 10 mm.

The results of the studies by Hartman and Higgins can be summarized by considering handsheet breaking length *vs.* apparent density plots for pulp samples treated in different manners. The effect of internal delamination with and without external fibrillation is illustrated in Fig. 20. Increases due to internal delamination, while increasing both density and breaking length, do not match the increases in the Valley beaten pulp. Subsequent external fibrillation increases the density, but has no effect on the breaking length. The treatments using the Abrasion Refiner are compared to a 12 inch disk refiner in Fig. 21. Abrasive refining alone increases the density for a untreated pulp, but does not match the increases in breaking length due to disk refining. The result of treatment in the roll refining and then the addition of fines is shown in Fig. 22.

The addition of fines increases both the density and the breaking length to combinations equivalent to the Valley beaten pulp.

The conclusions of Hartman and Higgins[80,81] are that repeated lateral compression of fibers achieves mostly internal delamination, that internal delamination is the single most important factor in making strong dense sheets, but that additional effects of refining (*i.e.*, addition of fines) are necessary to reach the highest strength potential of the pulp. They also remark that interfiber bonding is the central issue in understanding strength development in fiber networks and that the effects of refining are additive.

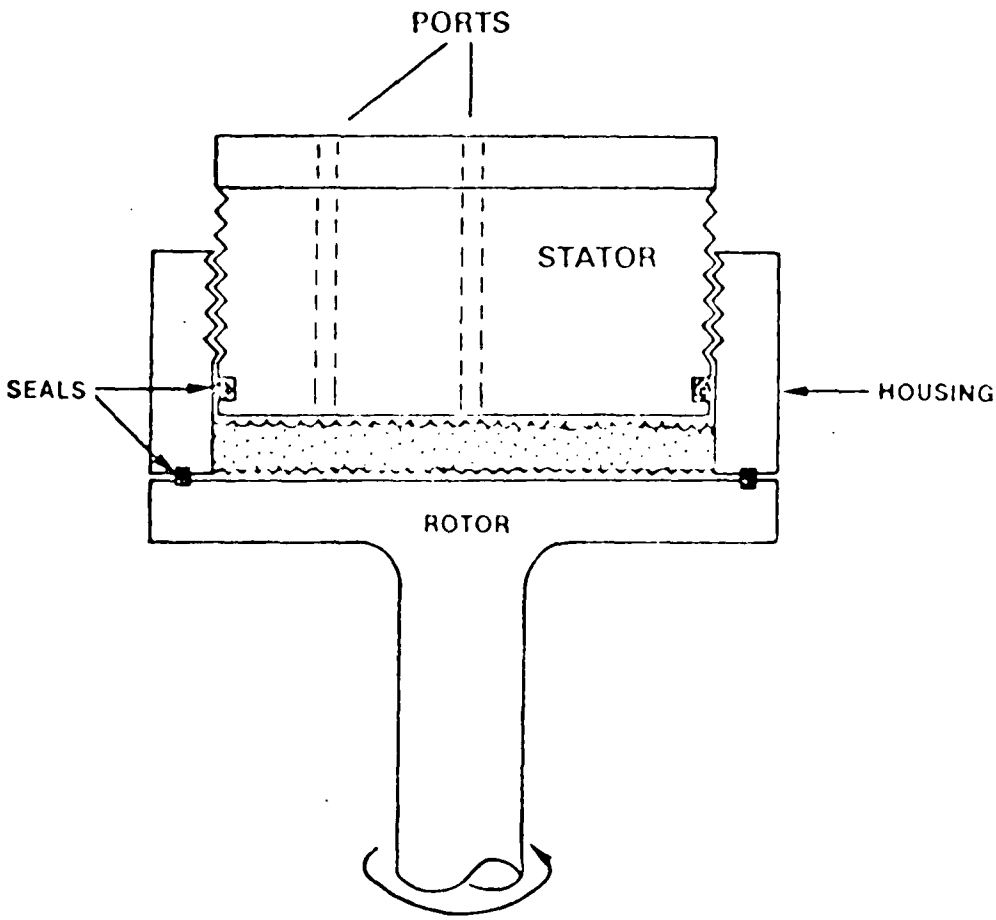

Figure 19. Abrasion refiner; schematic of the apparatus; stator diameter = 102 mm[79].

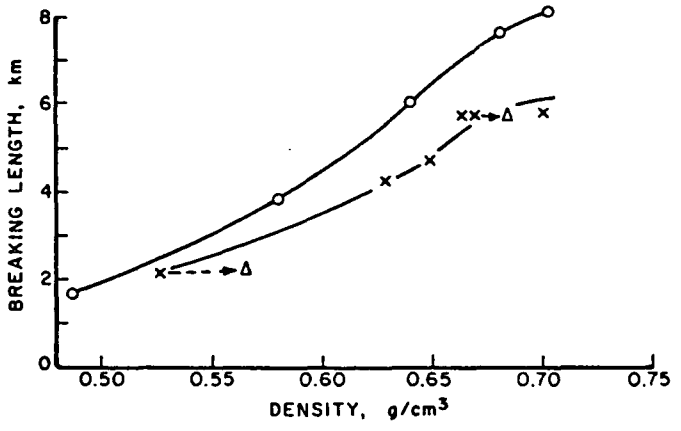

Figure 20. Breaking length *vs.* density[81]. x = roll refined, o = Valley beaten, Δ = effect of abrasion refining.

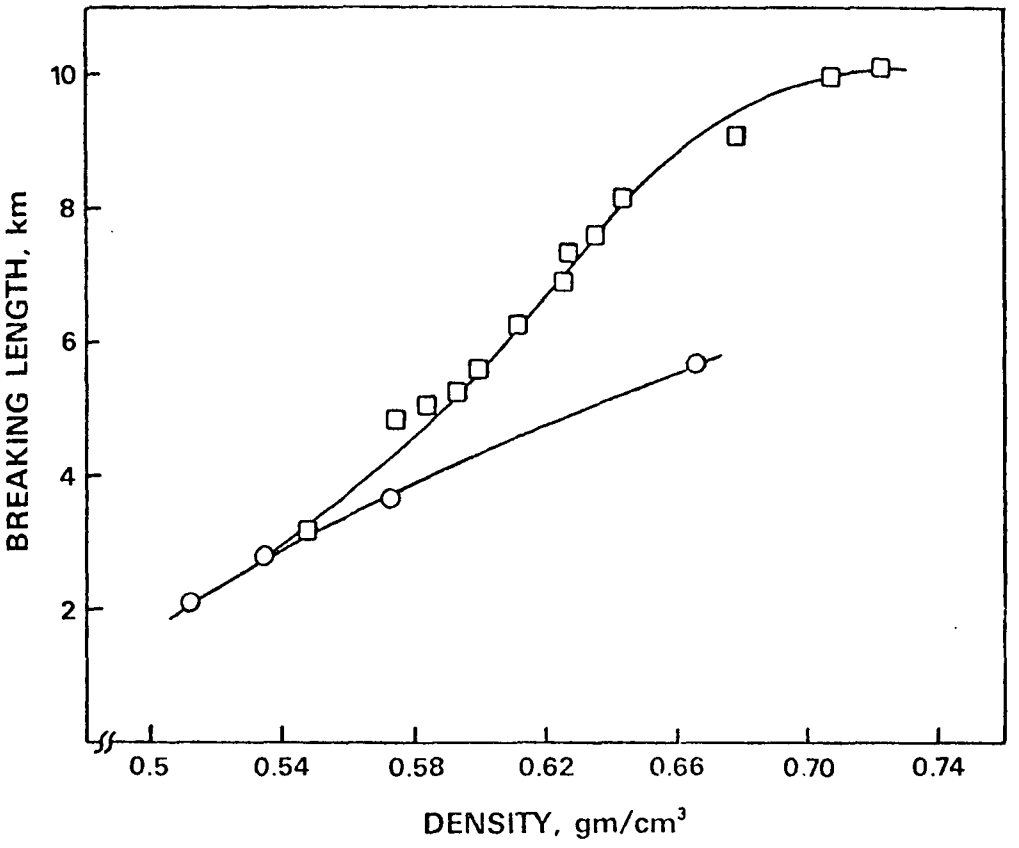

Figure 21. Breaking length development of bleached kraft softwood pulp with density[82]. o = abrasive wear, = disk refining.

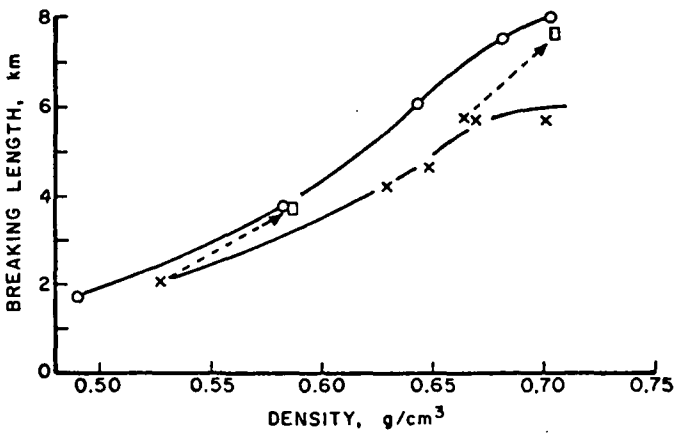

Figure 22. Breaking length *vs.* density[81]. x = roll refined, o = Valley beaten, = effect of fines addition.

EXPERIMENTAL PROGRAM

A bleached, softwood pulp was used in all experiments. This pulp was produced from loblolly pine chips by a laboratory kraft pulping process and a C_DEDED bleaching sequence. Pulp samples were refined in differing manners and then formed into standard handsheets. These handsheets were characterized with nondestructive and destructive test methods. The test results were used to measure the effect two different mechanical treatments have on paper properties.

The handsheets may be divided into four groups. The first group received no experimental treatments and is considered the control group. These specimens were used to measure the effect of the Formette Dynamique on untreated pulp. The second group were treated in the PFI mill. This group is used as a frame of reference to which the last two groups of specimens may be compared. The last two groups were treated in one of the two specialized apparatuses, the Bending Refiner or the Roll Refiner, which are described later. The two experimental variables within each treatment group were treatment level (the number of "stress cycles") and fines content (either normal or high). The control group included specimens with low, normal, and high fines contents.

The handsheet elastic properties were determined with ultrasonic wave propagation techniques and the performance properties were determined with conventional handsheet testing methods (tensile strength, tear factor, *etc.*). Other properties measured were apparent handsheet density and light scattering coefficient. The average fiber length and fines content were measured for several samples of untreated and treated fibers.

EXPERIMENTAL MATERIALS

Pulping

All pulp was produced from a kraft cook of loblolly pine (*Pinus taeda*) chips with a laboratory digester in which the circulating pulping liquor was indirectly heated with steam. The cook consisted of 8000 grams of chips on an oven-dry basis at a liquor-to-wood ratio of 3.8. The chemical charge for each cook was 17.5% effective alkali and 25% sulphidity. The cooking schedule was 9 min to 115°C, 60 min at 115°C, 20 min to 165°C, and 121 min at 165°C. This schedule results in an H-factor of 1276. The pulped chips were broken up in a Williams mixer. The pulp kappa number was 37.6 as determined by TAPPI Test Method T 236 cm-85 "Kappa Number of Pulp[83]."

The pulp was washed three times with hot (≈36°C) water over a 150 mesh flat screen. After the last washing, the pulp was screened through a 6 cut Koppers flat screen to remove shives. Next, the pulp was dewatered in a centrifuge to about a 70% moisture content and stored in sealed polyethylene bags in a cold room (4°C).

Bleaching

The bleaching sequence was C_DEDED. The C_D, D_1, and D_2 steps took place in a Pfaudler mixer. The extraction stages, E_1 and E_2, took place in a Hobart mixer. The bleaching conditions are summarized in Table 2.

Washing between each step used ambient temperature deionized water and a 150 mesh screen. After bleaching, the pulp was dewatered to a moisture content of about 65% and stored in sealed polyethylene bags in a cold room (4°C).

Table 2. Bleaching Conditions.

Stage	C_D	E_1	D_1	E_2	D_2
Consistency, %	3	10	7	10	7
Temperature, °C	25	70	70	70	70
Time, min.	45	60	180	60	180
Chemical, %[a]					
Cl_2	7.99	—	—	—	—
ClO_2	0.43	—	0.80	—	0.15
NaOH	—	4.70	0.40	0.50	0.015

[a]Percent of oven-dry pulp by weight.

Mat Forming

Lightweight oriented fiber mats (210 by 900 mm) were formed using the Formette Dynamique. This device is designed to simulate machine forming conditions by producing sheets with a nonrandom in-plane fiber orientation distribution and is described in the literature[84,85]. Operation consists basically of spraying pulp at low consistency through a nozzle onto the inner circumference of a rotating drum fitted with a forming fabric. The degree of fiber orientation can be varied by changing the ratio of stock flow pressure (spray velocity) to drum speed (fabric velocity). This ratio was held constant for all mat production.

Oriented mats were formed from stock at 0.1% consistency. The Formette wire speed was 1300 m/min and the nozzle pressure was 100 kPa. These conditions where chosen to produce a high fiber orientation in the machine direction (*MD*) based on the experience of the Formette Dynamique operator. As part of the routine procedure for determining the mat basis weight of the Formette Dynamique sheets, trial mats are dried under restraint. The machine direction and cross machine direction ultrasonic velocities of these dry sheets was measured with the Institute of Paper Chemistry in-plane velocity gage[75,86,87]. Since ultrasonic velocity squared is elastic stiffness divided by

apparent density (termed the specific elastic stiffness), the elastic stiffness anisotropy ratio could be calculated. The ratio of *MD* to *CD* mass specific longitudinal elastic stiffness was normally 3.5:1.

The mats were formed on a twill weave, 4-shed synthetic fabric (I.D. number 23) with a mesh of 100. The nozzle used to spray the stock onto the wire was a VEE JET H($\frac{1}{8}$) WV2504 type obtainable from Spraying Systems, Inc. The nozzle was positioned in a manner such that the stock jet traveled approximately 55 mm before impinging on the wall of the rotating drum at an angle of 25°. The nozzle had a circular opening, and the jet had a diameter of about 10 mm when it contacted the drum wall. The stock supply lines were filled with stock (as opposed to starting with water filled lines) and about 85 sweeps of the nozzle were used to form each mat. The resulting grammage was nominally 25 g/m^2. After forming, the solids content of the mats ranged from 20 to 35%. Each wet mat was couched from the wire onto a wet blotter, covered with another wet blotter, and then cut into half-length pieces. The half-length mats, stacked between moist blotters, were sealed in polyethylene bags, and stored in a cold room at 4°C.

EXPERIMENTAL APPARATUS

Bending Refiner

The Bending Refiner (*BR*) subjects a short length of stationary web by reciprocating a set of rolls and a working surface along the length of the web. The *BR* processes the web by bending the web around a small radius. In order to further describe the *BR*, it first necessary to describe the web which is treated in the *BR*.

Fabrication of Web

The web to be treated is composed of four layers and three different materials. The first of the two inner layers is the specimen. The specimen is a highly oriented, moist, lightweight fiber mat. The preparation of this fiber mat is described in the Mat Forming section above. The second inner layer is a thin, lightweight nonwoven polyester fabric. The outer layers are high strength polyester films.

The layer of nonwoven fabric is included to prevent disruption of the structure of the fiber mat as it is pulled over a fixed surface. As the web starts to move over a small radius, it is compressed and excess water is squeezed from the area under compression. Local flooding in the adjoining areas may suspend adjacent fibers not under compression allowing them to change their orientation. In light of this possibility, it was necessary to add the layer of nonwoven fabric to provide a pathway for any excess water to flow before accumulating and fluidizing the fiber mat. The material selected to do this was a thin, lightweight, nonwoven polyester fabric. The main requirements are that it be as thin as possible and as flexible as possible. The nonwoven should be thoroughly washed before use.

The outer layers of film provide the web with the integrity necessary to transport the fiber mat and nonwoven through the *BR*. The fiber mat and nonwoven fabric are enveloped in Mylar® (a register trademark of the E. I. Du Pont de Nemours & Company, Inc.) polyethylene terephthalate film (uncoated industrial type "A", 12.7 μm thick).

A cross-section and top view of the web is shown in Fig. 23. The following steps describe the fabrication of web. The fibers in the mat are oriented with their

long axis parallel to the long dimension of the web such that they will be bent along their long axis in the apparatus.

1. The lower layer of Mylar® film is cut to the proper dimensions (225 by 900 mm) and placed on a flat surface. The film is smoothed out and held in slight, uniform tension by taping the corners and edges to the surface with masking tape.

2. A 900 mm length of double-sided transfer tape (Scotch Brand No. 465, $\frac{1}{2}$ in. width) is carefully applied to each of the long edges of the film. The tape must be under minimal tension when applied. This minimizes distortion of the film when the tension on the tape is released. The tape backing is left in place, but at the mid-points on both of the long edge pieces, the backing is carefully cut in half without disturbing the underlying tape or film.

3. A 175 mm length of double-sided transfer tape (Scotch Brand No. 465, 1 in. width) is cut to span the gaps between the tape on the long sides and carefully applied to each of the short sides. The tape must be under minimal tension when applied. This minimizes distortion of the film when the tension on the tape is released.

4. The upper layer of film is cut to the same dimensions as the lower layer of film and positioned on top of the lower one. The second piece is smoothed out and held in position with masking tape in a similar manner to the first.

5. One half of tape backing is removed by working from the mid-point on one long edge towards the end, while keeping the upper film layer from contacting the exposed tape prematurely. After the tape backing is removed, the upper layer of film is gently pressed onto the exposed tape in a wrinkle and distortion free manner.

6. Repeat procedure in step 5 for the other length of tape on the same long edge.

7. The pieces of masking tape holding down the free edges of the top layer of film are removed and the top piece is folded back along the taped edge. A piece of damp nonwoven fabric, 215 mm wide and 150 mm in length, is placed at each end of the film such that when the fiber mat is positioned, the fiber mat will overlap the nonwoven fabric by 15 mm.

8. A blotter-mat sandwich is removed from its storage bag, the top blotter removed, and the remaining mat and blotter are placed mat-side down on the lower layer of film. The blotter is removed and the mat slightly misted with water. If necessary, the mat is then trimmed along the edges to fit the piece of film.

9. A piece of thin, flexible, moist nonwoven, 215 mm wide and 510 mm long, is placed over the mat.

10. Two additional pieces of damp nonwoven fabric, 215 mm wide and 150 mm in length, are placed directly above the identical one laid down in step 7.

11. The top piece of film is then placed carefully over the mat, smoothed, and taped back into position. The backing from the remaining piece of double backed tape is removed in the same manner as the first, and the second edge is pressed onto the lower layer of film.

12. The surfaces of the web holders (plastic bars) are cleaned with ethanol to remove any contaminants and tape adhesives. The large side of the web holders with the hole on the face is covered with two lengths of double-sided transfer tape (Scotch Brand No. 465, 1 in. width).

13. One web holders is placed, centered with the width of the web, at each end of the web. The tape backing is removed and the web holder is pressed onto the end of the web. The long sides of the web holder should be square with the long edges of the web, regardless of any misalignment with the short edges of the web ends.

The last two steps prepare the web for mounting in the apparatus. Each end of the web is attached to a plastic bar with double-sided tape; each bar is attached to the apparatus by springs. The plastic bars are known as *web holders*. The two web holders are 400 mm long (slightly wider that the web), 50 mm wide (the width of two pieces of 1 inch tape), and about 15 mm thick. Each web holder has a 5 mm hole drilled from the middle of one large surface, diagonally through the bar, to the middle of an adjoining long side. A line to apply vacuum to the inside of the web envelope will be inserted through this hole.

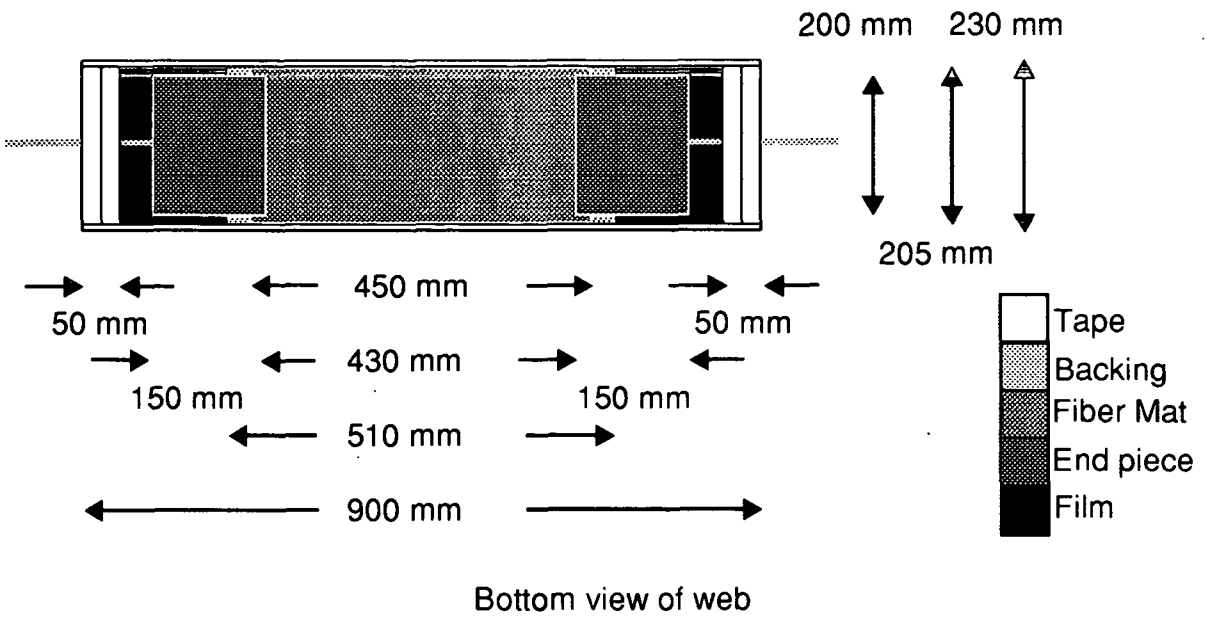

Figure 23. Schematic of Bending Refiner web construction. (a) Bottom view. (b) Side view.

Description of the Apparatus

The bending refiner is shown from the side in Fig. 24 with a web mounted and ready for treatment. The schematic in Fig. 25 identifies the major components of the apparatus which are italicized in the text.

The *carriage* and one end of the *web* are shown in Fig. 26. The clear plastic top of the carriage has been removed for the purpose of this photograph. Visible in the carriage are two outer rolls, the *bowd rolls*, and two inner rolls, the *guide rolls*. Between the guide rolls, the top portion of the *vane* is visible. The white portion of the web, right center in photo, are the *end pieces* of nonwoven fabric (see Fig. 23). A clear plastic *web holder* is to the right. The web holder is connected to the *attachment uprights* with *coil springs*.

The path of the web through the carriage is illustrated in Fig. 27. The web passes over the bowd rolls, under the guide rolls, and over the vane. The bowd

rolls are bowed by about 5° inwards towards the vane. When a bowd roll is the leading roll, it places the web in *CD* tension which is "set" by the (first) trailing guide roll. Placing the web in *CD* tension prevents lateral contraction, and the associated wrinkling, of the web during treatment. The trailing bowd roll has the opposite effect, contracting the web laterally as it leaves the carriage. However, since there is not an additional trailing guide roll to "set" the contracted state of the web, the web expands laterally back to the normal state. The web wraps about the guide roll and then the vane surface. The area where the web contacts the vane is termed the *working zone.* The vane is a 0.30 mm thick piece of spring steel shim stock. The top edge, which the web moves over, has been ground to a semicircular shape (with a radius of 0.15 mm). The web wraps 160° about the vane. The web leaves the vane, wraps the trailing guide roll and bowd roll before leaving the carriage.

Different aspects of the carriage are shown in Fig. 28. The partially opened carriage, with web mounted, is shown in Fig. 28a. This illustrates how the top part of the carriage is removed to allow either mounting or removal the web. In Fig. 28b, the carriage has been disassembled and the web removed. Note that the two rolls in the carriage are slightly bowed towards the vane. A profile view of the top portion of the vane is shown in Fig. 28c.

For the working zone to treat the stationary web, the *carriage* must reciprocate on the *guide rods* using *linear bearings*, a reversible *motor*, and a lightweight *chain drive. Magnetic proximity switches*, at each end of the rods, sense the presence of the carriage and reverse the rotation of the motor. The motor is a permanent magnet, DC type with a variable speed drive and a variable torque controller. The variable torque feature of the controller prevents full torque from being applied instantaneously when the direction of motor rotation

is reversed. This provides for a smooth change in the direction of travel of the carriage.

The outer pair of uprights at each end provide adjustable *attachment points* for the web. Using the perspective in Fig. 25, each attachment point may be moved left or right and up or down. Coil springs are used to attach the web to the uprights. The inner pair of uprights provide *stops* against which the web holders rests during the part of the cycle when the carriage is moving towards that upright. During this time, the web between the web holder and carriage is slack. The stops may be moved left or right and up or down as necessary. The distance between the *attachment upright* and the *stops upright* is adjusted to keep the springs in tension and the web holder pulled against the stop when it is free of tension from the web. The attachment uprights and stops upright are independently adjusted to ensure the web is distortion-free during the run.

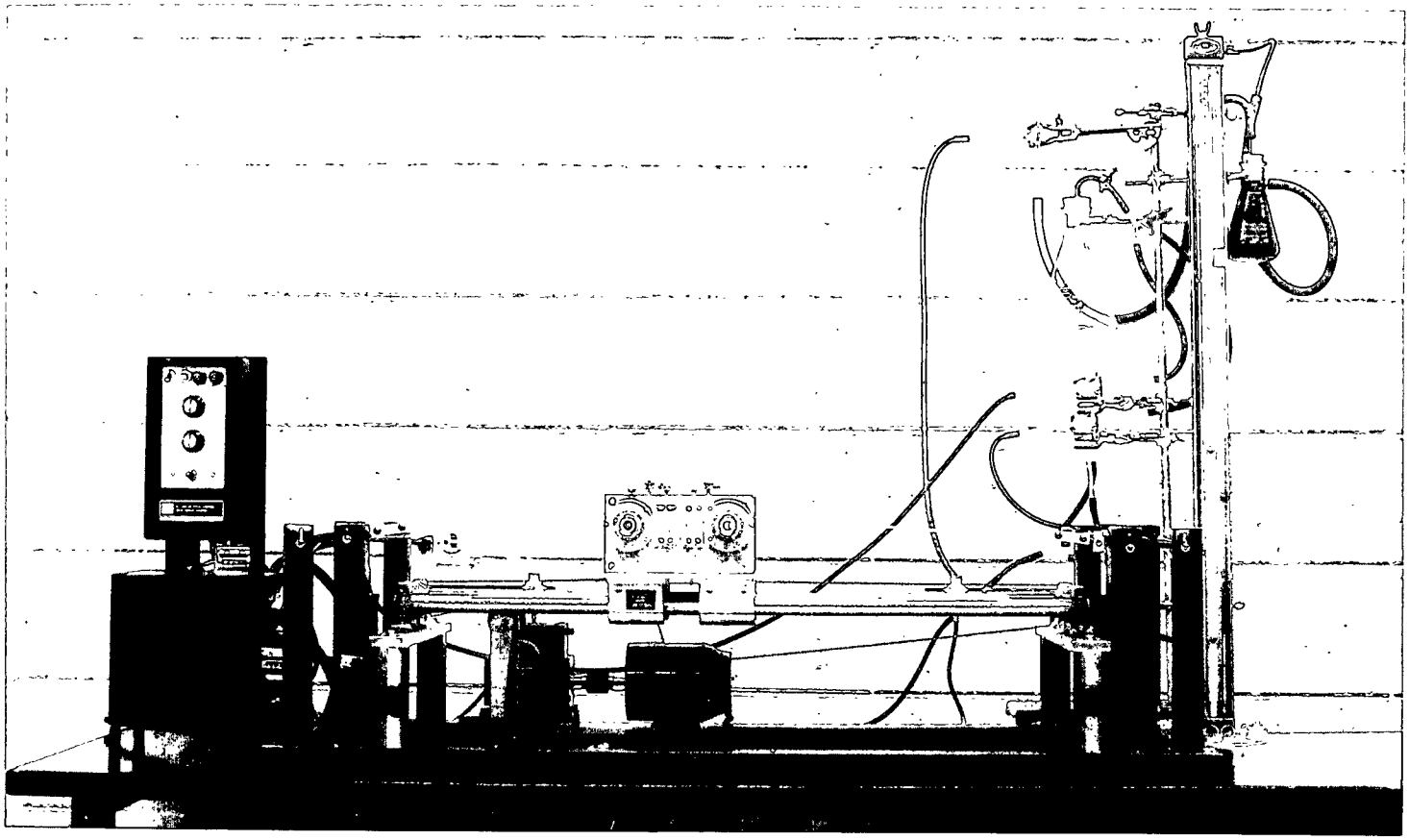

Figure 24. Bending Refiner (side view).

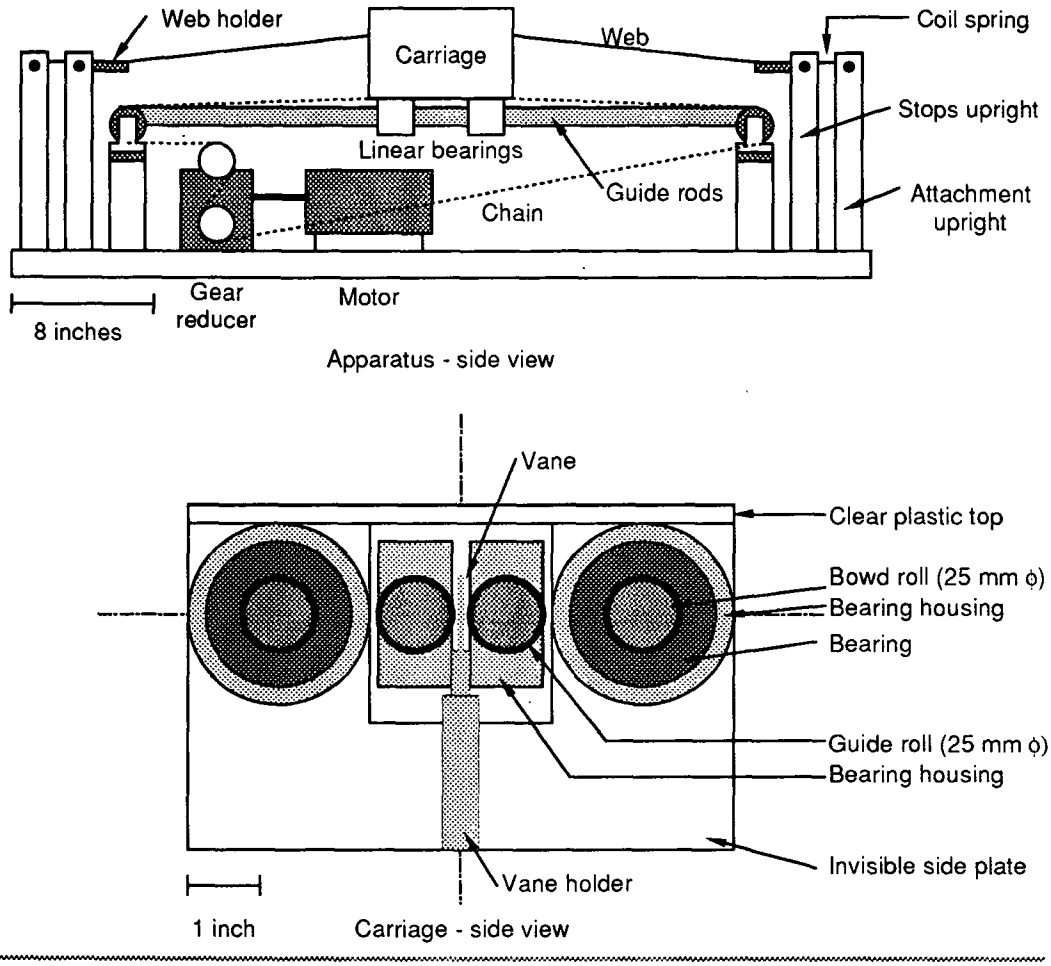

Figure 25. Schematic of Bending Refiner naming major components. (a) Apparatus – side view. (b) Carriage – side view.

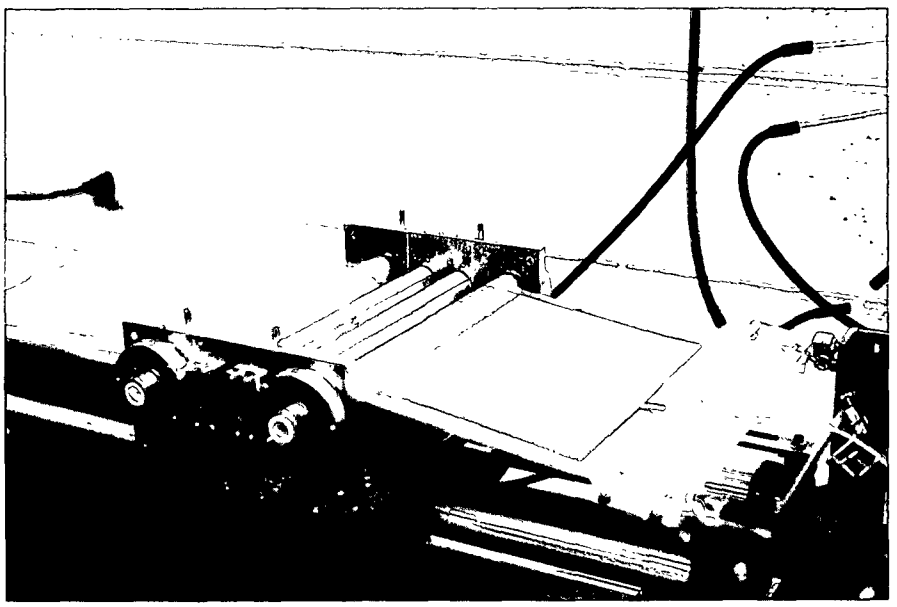

Figure 26. Bending Refiner carriage and web.

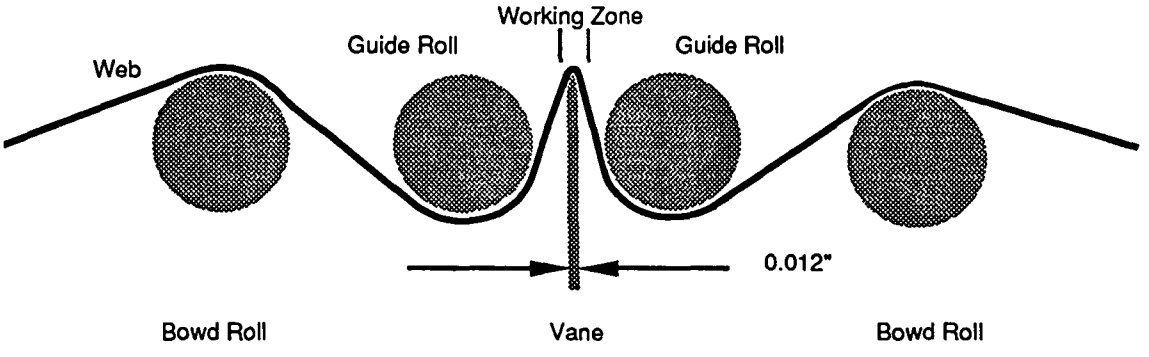

Figure 27. Schematic of web path through Bending Refiner carriage.

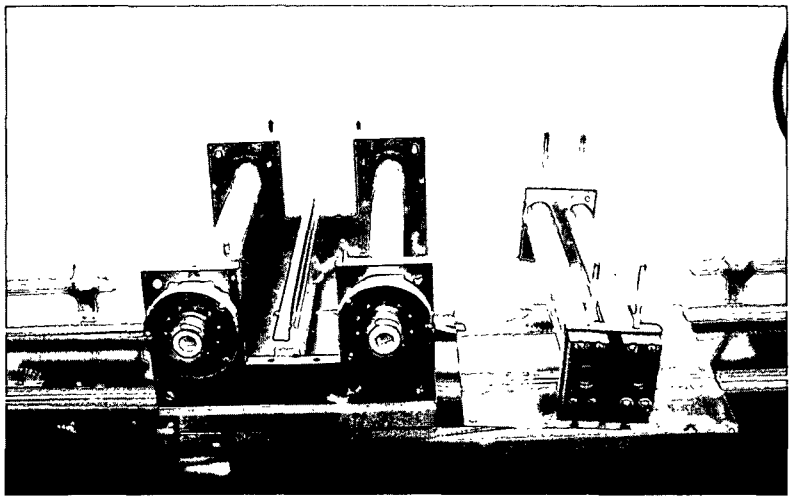

(a)

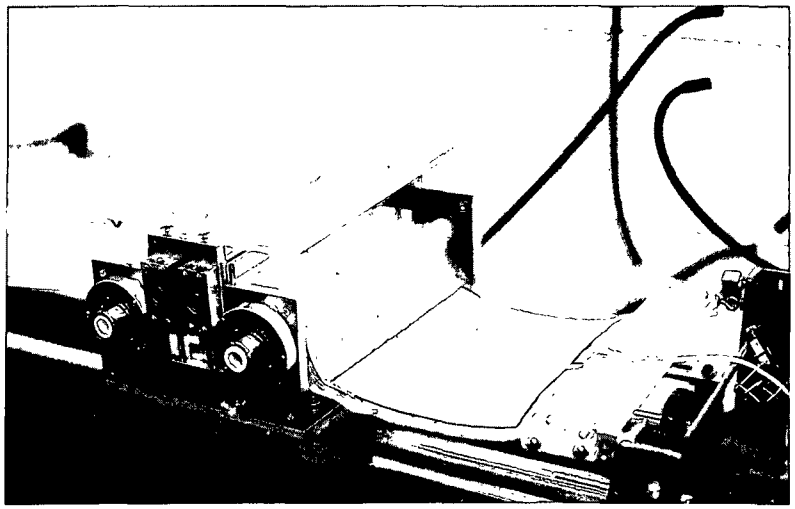

(b)

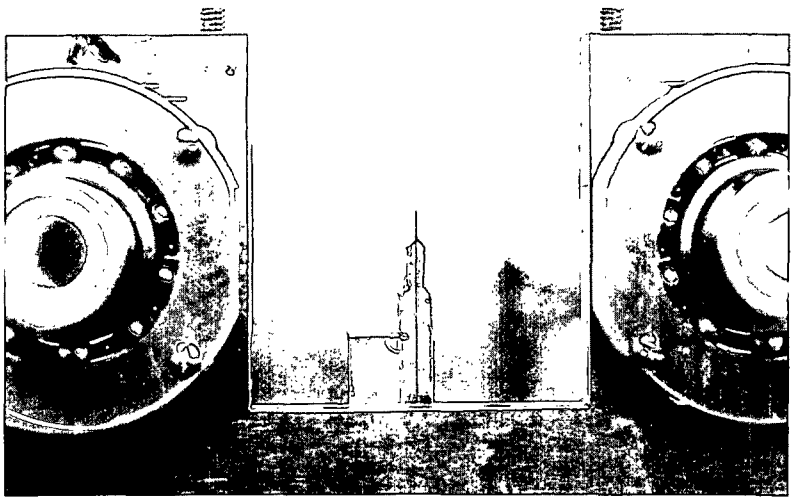

(c)

Figure 28. Bending Refiner carriage.

Treatment in the Bending Refiner

The web is initially mounted in the apparatus upside-down from the orientation depicted in Fig. 23 with the fiber mat between the vane and the nonwoven layer. Mounting the web for treatment in the apparatus begins by attaching the springs to the web holder and placing the web, temporarily, in a state of moderate tension by adjusting the attachment uprights. While in this state, the film layer facing the vane is lubricated with stopcock grease.

Next, a small hole is punched in the film covering the vacuum line holes on the web holders to allow insertion of the vacuum lines. This is accomplished using a scalpel. The two layers of film forming the web envelope are separated and the scalpel is carefully inserted without damaging the upper layer of film. The scalpel is pressed down into the hole and the film is punctured.

Vacuum lines (plastic tubes, $\frac{1}{8}$ in. OD and $\frac{1}{32}$ in. walls) are inserted through the holes in the web holders, and into the film envelope. The vacuum lines are extended to the end pieces of nonwoven and inserted between them. The hole is sealed with vacuum grease. The backing on the remaining pieces of tape are removed from between the two layers of film and the ends of the envelope are sealed. The vacuum is slowly applied to the envelope, and the web is straightened and smoothed as necessary. The level of vacuum applied is about 18 cm of Hg or 77 kPa absolute.

The final step is to adjust the uprights and assemble the carriage. The tension in the web is relieved by decreasing the distance between the uprights. Any obvious wrinkles or distortions in the web are remove by further adjustment of the uprights as necessary. The carriage is then assembled.

The apparatus is started and further adjustments made to the web made as necessary. The rate of treatment is about 500 passes of the carriage along the length of the web per hour. This is 3.5 to 4.5 m/min of linear velocity. The term "refining event" or *RE* is used to signify one pass of the carriage along the web. At the halfway point of a run (*i.e.*, one half the total treatment applied), the apparatus is stopped, the carriage is disassembled and the web is turned upside-down. The nonwoven layer is now between the fiber mat and the vane. Lubrication is applied to the film layer facing the working surface, the carriage is assembled, and the apparatus started. The fibers are now being bent in the opposite direction.

The average radius of curvature for the first half of the run is the radius of the vane plus the thickness of the film plus one half the thickness of the fiber mat. The average radius of curvature for the second half of the run includes the thickness of the nonwoven fabric. The radius of the vane is 0.1524 mm, the film caliper is 0.0127 mm, the mat caliper (dry) is about 0.085 mm, and the nonwoven caliper (dry) is about 0.085 mm. The vane radius and film calipers are nominal values supplied by the manufacturers and the mat (dry) and nonwoven (dry) calipers were measured using the IPC soft platen caliper gage[88]. The average radius of curvature without the nonwoven is 0.208 mm and 0.293 mm with the nonwoven. For the purposes of modeling the mechanics of the *BR*, a nominal radius of curvature is defined as 0.25 mm. While the mechanical action during the second half of the run could be less intense than the first half, all runs were subjected to the same two radiuses in equal proportions. Results are presented comparing the bending fibers in only one direction using the small radius with bending fibers in both directions using both radii.

Due to the opening of new surface areas in the fibers and the removal of water through the vacuum lines, the amount of free water decreases during the run. This makes it necessary to saturated the mat with water at 2000 RE (2 hr) intervals. This is accomplished by stopping the apparatus and disassembling the vane module (to allow unrestricted flow along the mat). Next, the web at the water inlet end is lowered to provide a spot for excess water to pool without affecting the fiber mat. The vacuum at one end is replaced with a water supply (hydraulic head of 500 mm of water). About 100 ml of water is allowed to slowly flow into the film envelope before the water supply is shut off. The water wicks along the length of the mat towards the opposite (higher) end which is still attached to a vacuum source. As the water reaches the far end, the second vacuum supply is attached, and the excess water is removed. The apparatus is then assembled and restarted. The time required to wet the mat is about 5 minutes.

At the end of the run, the carriage is opened and the web placed in tension. The vacuum is removed and the section of web containing the fiber mat is cut from the surrounding web. This section is turned upside-down and placed on a flat surface. One long edge of the web is removed and the top piece of film is folded back. The nonwoven is peeled from the mat. Along the lateral edges, the mat sticks to the nonwoven due to entanglement with loose synthetic fibers. This material is allowed to be removed with the nonwoven. The remaining fibers are gathered and weighed. Next the fibers are misted with water and placed in a polyethylene bag. About 5 ml of water is added to the bag. The bag is sealed and stored in a refrigerator.

Roll Refiner

The Roll Refiner (*RR*), developed by Hartman[79], is an apparatus which subjects a fiber mat to transverse compression by repeatedly sending it through a nip. The nip is formed between a smooth and vented roll. Hartman treated fiber mats without any enclosing envelope. The procedure described here is a major modification of his procedure. The method envelopes the mat in a film envelope which is similar in construction to the one described above for the Bending Refiner.

Fabrication of Web

The web treated in the apparatus consists of four layers of Mylar® film, a layer of thin nonwoven synthetic fabric, and the fiber mat. A cross-section view of the web is shown in Fig. 29. The following steps describe the fabrication of film-mat-nonwoven envelope (web). The major differences from the *BR* web construction are the size of the fiber mat (105 by 450 mm *vs.* 210 by 450 mm for the *BR*), the number of fiber mat layers (two), and number of film layers (four). Two extra layers of film are added to the top of the web to prevent the layer next to the mat from tearing.

1. The outer layer of film is cut to the proper dimensions (165 by 530 mm) and placed on a flat surface. The film is smoothed out and held in slight, uniform tension by taping the corners and edges to the surface with masking tape.

2. A 530 mm length of double-sided transfer tape (Scotch Brand No. 465, 1 in. width) is carefully applied to each of the long edges of the film. The tape must have the least tension possible when it is placed in position. This will prevent distortion of the film when the tension on the tape is released. The tape backing is left in place.

3. A second layer of film is cut to the same dimensions as the outer layer of film and positioned on top of the first. The second piece is smoothed out and taped into position with masking tape in a similar manner to the first.

4. One side of the top film layer is lifted from the bottom film layer and the exposed tape backing removed. The top film layer is then carefully returned to the original position and pressed onto the exposed tape.

5. The other side of the top film is then folded back along the taped edge to expose the bottom layer of film. The backing on the exposed piece of tape is removed and the top film is returned to its original position and pressed onto the exposed tape.

6. A length of tape is applied along the long sides as in step #2.

7. A third layer of film is prepared as in step #3.

8. The third layer of film is attached as in step #4.

9. The top film layer is then folded back along the taped edge to expose the second film layer.

10. A layer of nonwoven fabric (110 by 480 mm) is then placed on the second layer of film. The width allows it to fit between the taped edges. One narrow end is attached to the second layer of film with 2 inches of 1 inch wide double-sided tape. This end will become the end entering the *RR* nip first (*i.e.* the leading end).

11. The second tape backing is removed from the second layer of film and the third film layer is returned to the original position and pressed onto the exposed tape.

12. A length of tape is applied along the long sides of the topmost film layer as in step #2. Then additional lengths of tape are cut to span the gap between the tape along the long edges and applied along the short edges.

13. The fourth layer of film is prepared as in step #3.

14. The fourth layer of film is attached as in step #4. The fourth film layer is folded back along the taped edge to expose the third layer of film.

15. At this point, two holes are poked through the first three layers of film and the nonwoven fabric with a hot dissecting needle. The holes are made at the end opposite where the tape attaches the nonwoven fabric to the film (*i.e.* the trailing end).

16. A blotter-mat sandwich is removed from its storage bag and cut into half-width pieces. The top blotter is removed and the mat-lower blotter placed mat-side down on the third layer of film. The blotter is removed and the mat slightly misted with water.

17. Step #16 is repeated for the second piece of fiber mat. This piece is placed on top of the first piece.

18. The exposed backing of the three remaining sides of tape are removed and the fourth layer of film is put in place. The four edges of the fourth film layer are taped to allow eventual attachment to the support roll.

Note that the mat is enveloped in the film and no moisture can enter or leave except through the two small holes. Also, the nonwoven fabric is separated from the fiber mat by a layer of film.

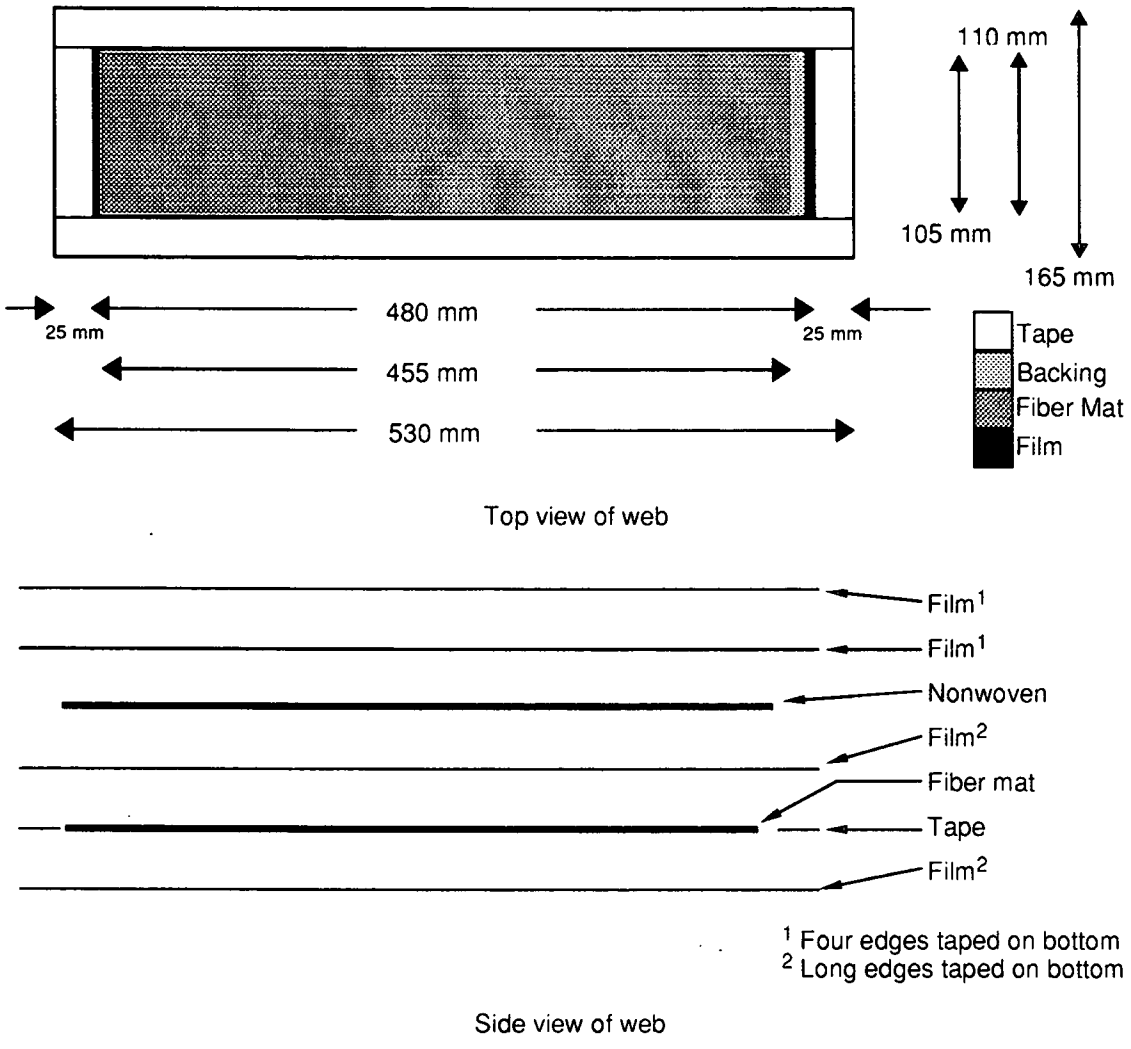

Figure 29. Schematic of Roll Refiner web construction. (a) Bottom view. (b) Side view.

Description

The Roll Refiner was originally conceived and developed by Hartman[79]. Description of the apparatus is included in the Background section. Two schematics of the *RR*, taken from Hartman, are shown in Fig. 30 and in Fig. 31. Two modifications to the apparatus were made for the work described here.

Hartman experienced limitations with the number of passes the fiber mat could make through the nip before the mat became disorganized. To increase

the number of passes, the first modification consisted of enclosing the fiber mat in a Mylar® film envelope, similar to that described for the *BR*, and attaching the envelope to the support roll with tape. This helped retain the fiber network integrity without effecting the action of the apparatus.

The second modification was necessary because of the first. Hartman used a humidifier to blow moist air on the fiber mat during treatment. Now that the mats are enveloped in film, this approach is not feasible. The change replaces the humidifier with a water bath. The water bath was arranged such that the bottom of the support roll just barely touches the surface of the water. Through several small openings in the web, water can wick into the envelope and keep the fibers moist.

The operating variables of the Roll Refiner are the velocity of web and the nip load. The linear velocity of the web was 16.5 cm/s. The nip loading was 107 N or 2.55 kN/m of bar width. This is the equivalent of the lowest nip loading used by Hartman.

Treatment in the Roll Refiner

The web is attached to the smooth support roll with the tape on the last layer of film. The envelope is mounted with the edge where the nonwoven is attached to the film leading into the nip. This allows excess water, if present, in the fiber mat to be expressed through the holes at the trailing edge as the web moves through the nip. Water may still be wicked into the mat as necessary to keep the fibers moist. After mounting the web, the grooved roll is set in place and adjusted. The support roll is started rotating and then the transverse motion of the grooved roll is started. The water bath is filled until water just touches the bottom of the support roll.

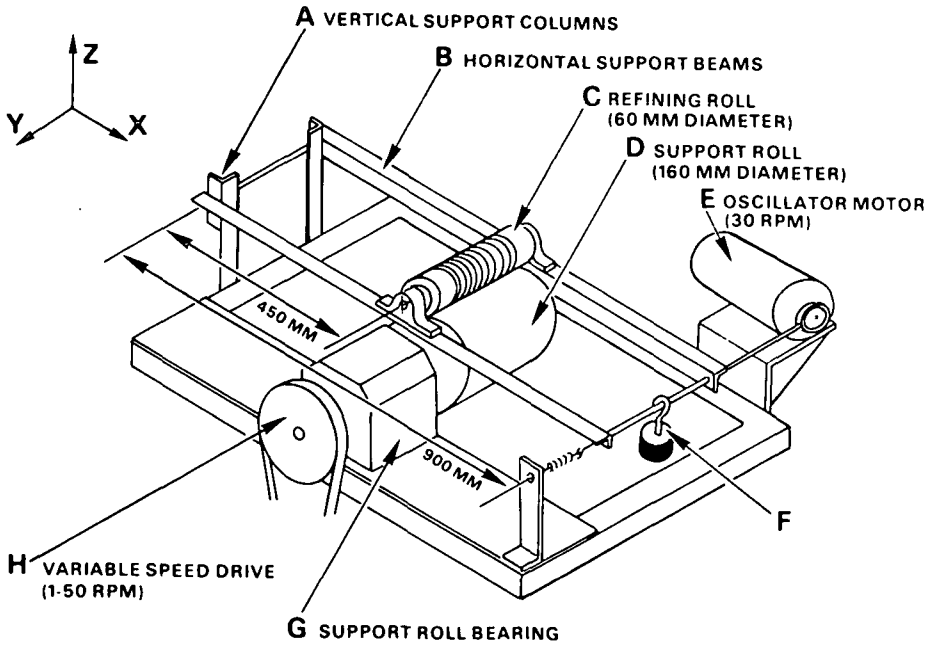

Figure 30. Schematic of Roll Refiner naming major components, overhead view[79].

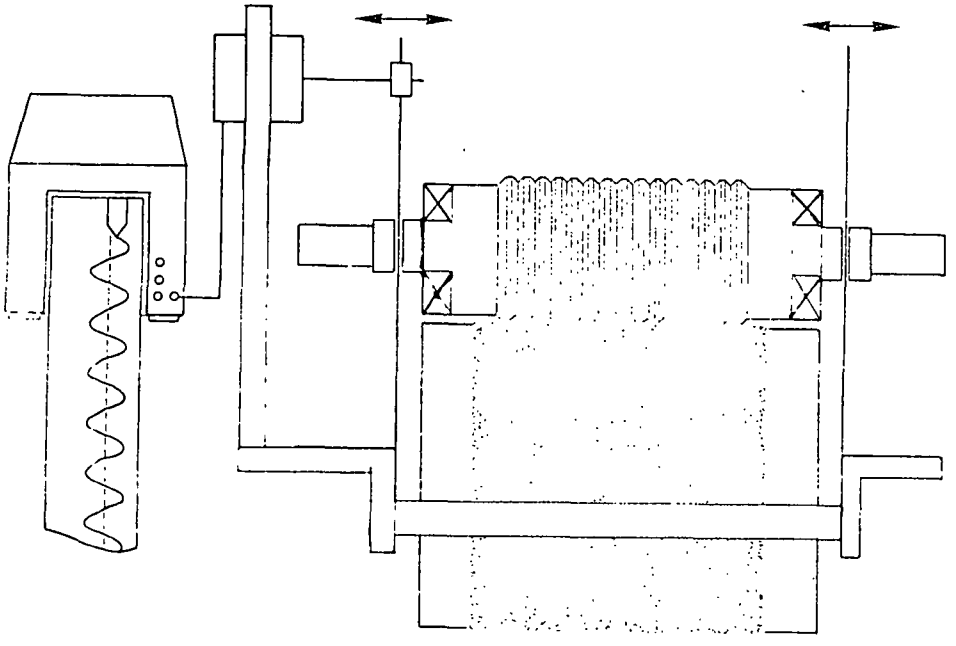

Figure 31. Schematic of Roll Refiner, end view[79].

At the end of the run, the transverse motion is stopped and then the support roll is stopped. The web is peeled from the support roll and the intact fiber mat is removed from the film envelope. The mat is compressed, but it has

good wet strength and contains free water. The fibers are gathered, placed in a polyethylene bag, and the bag is stored in a refrigerator.

PFI Mill

Description

The PFI mill (*PM*) is described in TAPPI Test Method T 248 cm-85 "Laboratory Beating of Pulp (PFI Mill Method)[83]."

Treatment in the PFI Mill

The detailed method for treatment of pulp in a PFI mill is described in the TAPPI method above. Basically, the pulp specimen, 24 oven-dry grams (o.d. g) at 10% consistency, is beaten between a roll with bars and a smooth-walled beater housing. The roll and housing rotate in the same direction, but at differing peripheral speeds. The fibers are forced against the beater housing by centrifugal forces. The beating action is applied to the fibers through a shearing action and through a compressive action between the bars and housing. The specimen is treated for a specified number of revolutions.

Two levels of compressive loads were used. In addition to the standard load, the loading for easily beaten furnishes was used. This requires a 9 kg bar loading, as opposed to the 17 kg loading for standard treatments. The minimum clearance allowed between the roll and housing was 0.20 mm. The TAPPI method states that zero clearance is possible; however, IPC operating procedure is to set the minimum to 0.20 mm to protect the roll and housing from damage by metal to metal contact. The gap maintained during the runs appeared to be greater than 0.20 mm. This statement is based on the observation of the clearance stop and base; the clearance stop was not in contact with the base.

After completing a run, the pulp is removed from the bowl and rotor by hand, placed in a polyethylene bag and the bag stored in a refrigerator. The roll and housing are allowed to cool to ambient temperature before starting the next run.

EXPERIMENTAL PROCEDURES

Sheetmaking

Pulp specimens from the different experimental treatments, described later, were formed into randomly oriented handsheets to allow paper properties to be measured. The procedures correspond those given in TAPPI Test Method T 205 om-81 "Forming Handsheets for Physical Tests of Pulp[83]." Two exceptions to the standard methods involved the disintegrating procedure and the final sheet weight. For the untreated and PFI mill treated specimens, the normal disintegrating and dilution procedures were used, except the pulp specimens were disintegrated for only 1500 revolutions (the standard specifies 15,000 to 50,000 revs.). For pulp specimens processed in the Formette, the disintegrating and dilution procedures were modified as described below. In both cases, the amount of disintegration was kept to a minimum to avoid "refining" of the fiber in the disintegrator. The target final sheet weight was 2.2 o.d. g. This higher sheet weight was necessary to allow measurement of the out-of-plane ultrasonic velocities.

Disintegrating

Disintegrating the untreated and PFI mill treated specimens begins by preparing 2000 ml of 0.4% with deionized water (the standard method specifies 1.2% consistency or 24 o.d. g in 2000 ml of water). The nonstandard consistency of 0.4% is the result of diluting only one third (or 8 o.d. g) of the untreated or PFI mill pulp specimen with 2000 ml of water. This slurry is disintegrated for 1500

revolutions in the standard disintegrator at 3000 rpms. After disintegration, the stock is diluted with deionized water to a total volume of 3500 ml or 0.30% consistency (the standard method specifies diluting to 7200 ml total volume or 0.30% consistency).

Disintegrating the Formette treated specimens begins by placing the pulp specimen (about 2.2 o.d. g) in a standard disintegrator jar and adding 2000 ml of deionized water (about 0.11% consistency). This slurry is disintegrated for 1500 revolutions in the standard disintegrator at 3000 rpms. The slurry is not diluted further and the entire pulp specimen is used to form one handsheet.

All of the specimens had fair to poor formation. The *RR* specimens had the poorest formation because the *RR* produced a more compacted fiber mat during treatment. The highly compacted mats did not disintegrate completely before handsheet were formed. The result was poor formation. The length of time the samples were disintegrated before the forming step, only 30 seconds, did not completely disintegrated all the fiber flocs.

Forming, Pressing, and Drying

The untreated and PFI mill treated handsheets use 770 ml of stock from the well-mixed slurry. This volume is the 733 ml, at 0.30% consistency, required for a 2.2 o.d. g sheet plus 37 ml of stock to compensate for the lost of fine material through the wire. The Formette treated specimens are added directly from the disintegrator jar to the sheet machine.

In both cases, the wire is prepared by scrubbing with a brush to remove any fibers and air pockets trapped in the wire. The cylinder is closed and filled in the standard way. The specimen is poured directly into the half filled sheet mold while the water supply to the cylinder is turned on. The specimen is poured

slowly in a way that avoids impinging fibers on the wire. The procedure given in the TAPPI method is used to form, couch, press, and dry the handsheet.

Conditioning

The dry sheets were cycled through a moist and dry state to help relieve any internal stresses. By relieving the internal stresses, the affect of slight variations in moisture content during testing are minimized. After drying the sheets at 23 ± 2°C and 50 ± 2% relative humidity, they were removed from the drying rings, placed in sealed polyethylene bags, and transported to a high humidity room. The conditions were 23°C and 85% or higher relative humidity. The sheets were removed from the bag, laid out in a single layer on an open mesh and left for 24 hours.

The sheet were then moved to a low humidity room for 24 hours. The conditions were 23°C and 10–35% relative humidity. Finally, the sheets were placed in the testing room environment of 23 ± 2°C and 50 ± 2% relative humidity for 24 hours before testing. If testing was to be delayed, the sheets were placed in sealed bags until 24 hours before actual testing, at which time they were opened to the atmosphere to allow adjustment to the room conditions.

This practice differs from the TAPPI standard (See TAPPI Test Method T 402 om-83 "Standard Conditioning and Testing Atmospheres for Paper, Board, Pulp Handsheets, and Related Products[83].") in that the sheets were subjected to high humidity without restraint before being brought to standard conditions from a low moisture state (per T 402 om-83). The normal TAPPI handsheet method (T 205 om-81) dries handsheets in an environment of 23 ± 2°C and 50 ± 2% relative humidity for 24 hours before testing without any additional conditioning.

Sheet Testing

The sheets were tested according to the TAPPI Test Methods[83] unless otherwise specified. Only three handsheets (as opposed to five as specified in the TAPPI method) were tested. See TAPPI Test Method T 220 om-83 "Physical Testing of Pulp Handsheets" for further details.

Grammage (Weight per Unit Area)

The weight per unit area measurements were made according to TAPPI Test Method T 410 om-83 "Grammage of Paper and Paperboard (Weight per Unit Area)." The sheets were individually weighed after being conditioned. The conditioned grammage, W, in g/m^2 was determined from the following formula based on the the handsheet weight, w, in grams and the handsheet area in m^2 (area of a 6 inch diameter circle, 0.01824 m^2):

$$W = \frac{w}{0.01824}$$

Thickness (Caliper)

The thickness of the handsheets was determined as part of the out-of-plane longitudinal velocity measurements. The longitudinal device uses a method similar to the Institute of Paper Chemistry soft platen caliper gage described by Wink and Baum[88]. The soft platen method normally results in caliper measurement lower than the hard platen method[88]. Hard platen method tends to measure the distance between the high spots on each surface of the sheet. Since the soft platens conform to the rough sheet surfaces, this method tends to measure the distance between average of the high and low spots on one side and average of the high and low spots on the other side of the sheet. The average of nine measurements per sheet are reported for the thickness results from the soft platen method in μm.

Apparent Density

The density values for soft platen thickness measurements, in g/cm^3, were calculated from the grammage, W, in g/m^2 and the soft platen thickness, t_s in μm as

$$\rho_s = \frac{W}{t_s}$$

The density values from the soft platen thickness measurements are higher than values based on hard platen thickness measurements due to the lower calipers measured by the soft platen method.

Elastic Stiffness Properties

Wave propagation techniques can be used to measure elastic stiffnesses of paper. These nondestructive tests enable elastic properties to be measured on a single sample which may then be tested for strength properties using destructive tests. Assuming that machine-made paper behaves as an orthotropic elastic material[72], three mutually perpendicular planes of symmetry are present. For paper, these planes of symmetry are taken to be perpendicular to the *MD* (x), *CD* (y), and *ZD* (z) axes. Paper is assumed to behave as a homogeneous orthotropic plate when describing in-plane propagation of elastic waves. When propagating waves through the out-of-plane direction, however, paper can be considered a bulk material. For machine-made papers, the stresses, τ_{ij}, can be expressed in terms of the strains, ε_{ij}, through use of the elastic stiffnesses[72], C_{ij}, as

$$\begin{aligned}
\tau_{11} &= C_{11}\varepsilon_{12} + C_{22}\varepsilon_{22} + C_{13}\varepsilon_{33} \\
\tau_{22} &= C_{12}\varepsilon_{22} + C_{22}\varepsilon_{22} + C_{23}\varepsilon_{33} \\
\tau_{33} &= C_{13}\varepsilon_{33} + C_{23}\varepsilon_{22} + C_{33}\varepsilon_{33} \\
\tau_{23} &= 2C_{44}\varepsilon_{23} \\
\tau_{13} &= 2C_{55}\varepsilon_{13} \\
\tau_{12} &= 2C_{66}\varepsilon_{12}
\end{aligned}$$

The nine C_{ij} are called elastic stiffnesses and have units of stress. Alternatively these stiffnesses can be expressed in terms of engineering elastic constants which include three Young's moduli, three shear moduli, and three Poisson's ratios.

The sheet elastic stiffness properties were measured using wave propagation techniques[72–76,87,89–91]. For this study, due to the random orientation of fibers in the sheets, only four of the nine elastic stiffnesses are independent and required to describe the elastic behavior of the material. Thus, only four wave velocities are required to calculate the elastic stiffness coefficients. Longitudinal and shear wave velocities were measured in both the in-plane (16 measurements per sheet for each in-plane velocity) and out-of-plane directions (9 measurements per sheet for each out-of-plane velocity). The frequency of the in-plane waves was 80 kHz and the out-of-plane waves was 1 MHz. The average wave velocities, V_k, in km/s, are

V_{Lxy} = in-plane longitudinal wave velocity
V_{Sxy} = in-plane shear wave velocity
V_{Lz} = out-of-plane longitudinal wave velocity
V_{Sz} = out-of-plane shear wave velocity

For sheet with random orientations, the elastic stiffnesses, C_{ii}, in GPa, are related to wave velocities, V_k, in km/s and soft platen apparent sheet density[75], ρ, in g/cm^3 by

$$C_{11} = C_{22} = \rho\,(V_{Lxy})^2$$
$$C_{33} = \rho\,(V_{Lz})^2$$
$$C_{44} = C_{55} = \rho\,(V_{Sz})^2$$
$$C_{66} = \rho\,(V_{Sxy})^2$$

Normally is preferable to express the elastic behavior of paper in terms of mass specific elastic stiffnesses since these are measured directly using sound wave propagation techniques[75].

Specific Scattering Coefficient

The specific scattering coefficient was calculated based on reflectance measurements made according to TAPPI Test Method T 425 om-86 "Opacity of Paper (15°/Diffuse Illuminant A, 89% Reflectance Backing and Paper Backing)." The Technidyne TB-1 Brightness Color Opacity meter was used to measure reflectance in each of the paper specimens. The single sheet reflectance, R_0 (with a black body backing), and the thick pad reflectance, R_∞, were found using 15°, diffuse illuminant A incandescent light source (wavelength of 572 nm). Two determinations of R_0 per sheet were made. The values from all sheet were used to calculate an average R_0. The value of R_∞ was determined from five measurements on a thick stack of several pieces from each group of sheets. The following formula was used to find the product of specific scattering coefficient, s, and grammage, W, in g/m^2:

$$sW = \frac{R_\infty}{1 - R_\infty^2} \ln\left(\frac{1 - \Omega R_\infty^2}{1 - \Omega}\right) \qquad \text{where } \Omega = \frac{R_0}{R_\infty}$$

Tensile Index

The tensile properties were determined according to TAPPI Test Method T 494 om-81 "Tensile Breaking Properties of Paper and Paperboard (Using Constant Rate of Elongation Apparatus)." Three measures per handsheet were made using an Instron Corporation, Series IX Automated Material Testing System (v2.51n). The test span was set at 4.0 inches and the testing speed was 0.5 in/min The specimens, 1.0 inch wide, were clamped, one at a time, in the tester and the load-elongation graph was obtained. The tensile index, T_i, was calculated in N·m/g, from the tensile strength, T_u, in kN/m and the grammage, W, in g/m^2 as

$$T_i = 1000 \frac{T_u}{W}$$

Zero-span Tensile Index

The zero-span tensile strength measurements were made according to TAPPI Test Method cm-85 "Zero-span Breaking Length of Pulp." The specimens were tested in an Instron Corporation, Series IX Automated Material Testing System (v2.51n) using the IPC Zero-span Breaking Length Attachment. The average of three determinations per handsheet of zero-span breaking strength were recorded. The zero-span tensile index, zT_i, was calculated in N·m/g, from the zero-span breaking strength, zT_u, in kN/m and the grammage, W, in g/m^2 as

$$zT_i = 1000 \frac{zT_u}{W}$$

In addition, the ratio of the tensile index, T_i, in N·m/g to the zero-span tensile index, zT_i, in N·m/g, is reported as the bonding index.

Short Span Compressive Strength

The short span (STFI) compressive strength measurements were made according to TAPPI Test Method T 826 pm-86 "Short Span Compressive Strength of Paperboard" using the STFI Compressive Strength Tester. Three measurements per handsheet were made on the undamaged ends of the tested tensile strips. The compressive strength index, C_i, in N·m/g is calculated from the compressive strength, C_u, in kN/m and the grammage, W, in g/m^2 as

$$C_i = 1000 \frac{C_u}{W}$$

Internal Tearing Resistance

The internal tearing resistance was determined using TAPPI Test Method T 414 om-82 "Internal Tearing Resistance of Paper" using an Elmendorf-type tearing tester. Three specimens were clamped together in the tester and three tear test made using the 1600 gram (15.7 N) pendulum. The average tear force, T_r, in mN/ply was calculated by multiplying the average instrument reading by 9.81 (conversion of gram force to mN) and 16 (standard number of plies), and dividing by 3 (actual number of plies). The average tear factor, T_f, in mN·m^2/g, was calculated from average tearing force, T_r, in mN/ply and grammage, W, in g/m^2 as

$$T_f = \frac{T_r}{W}$$

Fiber Measurement

Fiber Length

The Kajaani FS-100 was used to determine fiber length distributions and fines contents of the pulp samples according to procedures provided by Kajaani with the instrument. Fines are defined as any measurable particle less than 0.4 mm in length. One pulp specimen in addition to the number required to produce handsheets was treated and processed through the couching step during handsheet forming process. At this point the sample was peeled from the mold screen, sealed in a polyethylene bag and stored in a refrigerator. Several random samples of pulp (about 0.2 o.d. g total) were taken from this pad and diluted to 0.001% using tap water before being passed through the instrument. At least 5000 fibers were measured for each sample. The measurement range chosen for the instrument was 0 to 7 mm with a corresponding resolution of 0.20 mm. Ths instrument divided the fiber lengths into 24 classes. The first 12 (0 to 2.4 mm)

having widths of 0.20 mm and the second 12 (2.4 to 7 mm) having widths of 0.40 mm.

Measurement of a sample in the Kajaani results in the population distribution of the fiber lengths. From this data the following can be calculated: length weighted fiber length distribution, the arithmetic, the length weighted, and the weight weighted fiber length averages and the arithmetic and length weighted average fines contents.

Fiber Curl

The fiber curl index of selected samples were measured by the Pulp and Paper Research Institute of Canada in the manner described by Jordan[92]. The method uses dyed fibers that are sparsely deposited onto slides and viewed through a microscope by a video camera. A computer controls stepping motors on the microscope stage, so that the entire specimen is automatically scanned. The image generated by the camera is processed by a commercial image analyzer. The equipment is capable of distinguishing fiber contour length and longest projected dimension. These measurements are combined into a fiber curl index which is defined in Fig. 32.

Several selected samples were characterized. The samples were the 12,000 RE *BR*, 12,000 RE *RR*, 3000 RE and 12,000 RE *PM*, untreated, and unrefined samples; all with normal fines contents.

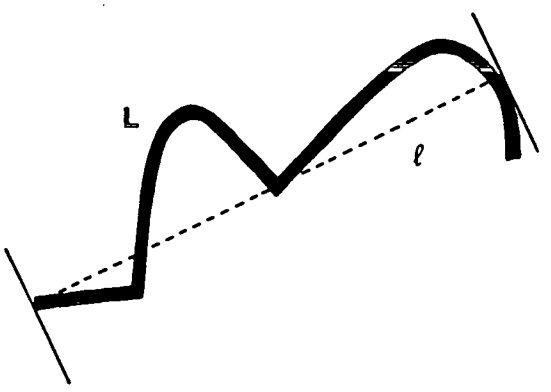

$$\text{Curl index} = \frac{L}{\ell} - 1$$

Figure 32. Definition of the curl index[92]. The fiber contour length *(L)* and the "longest dimension" *(l)* are measure with an image analyzer. Longest dimension is the distance between those points within the fiber which are furthest apart.

EXPERIMENTAL TREATMENTS

The treatments can be divided into three groups. The first group of treatments were used as a control group. Their purpose was to identify the effect of the procedures, other than the refining treatments, on the specimens. The second group of treatments used the specialized apparatuses, the Bending Refiner and the Roll Refiner, to beat fibers in nonconventional manners. These treatments established the effect of both apparatuses. The last group treated specimens in a conventional manner using the PFI mill. The purpose was to provide baseline data for comparison with the *BR* and *RR* experimental data. In all three groups, handsheets with low fines contents, with regular fines contents, and with high fines contents were formed.

The low fines content furnishes were produced by screening pulp using a method developed by Hawes[93] to separate the fines and fiber fraction. The method washed pulp specimens with cold tap water while on an operating

Sweeco Dynoscreen Separator to remove the fines. The Dynoscreen is composed of a circular mesh screen, a short, walled ring about the circumference to retain the material being screened, and an eccentric drive system which oscillates the screen in the plane of the mesh. The result is a rapid vibrating action. Hawes reports data showing the screen method to be equivalent to using a Bauer-McNett in retaining the long fiber fraction and let the fines fraction pass. The screen was 400 mesh and 2 liters of tap water per gram of oven-dry pulp were used to wash the fines through the screen.

The normal fines content specimens had no screening performed and were simply diluted with 2 liters of fines-free tap water.

A specimen which was to have a high fines content was first screened using the Dynoscreen method to remove any fines initially present. A high fines content specimen was achieved by diluting the screen specimen with fines-rich water. This served at the dilution step in preparation for sheet forming. This fines-rich water was the wash water produced by screening a *PM* pulp specimen subjected to 10,000 rev. The *PM* specimen had an oven-dry weight equivalent to the oven-dry weight of the specimens to be diluted and was washed with 2 liters of tap water per oven-dry gram. The dilution used 2 liters of fines-rich wash water per gram of oven-dry pulp. The sample nomenclature is given in Table 3.

Controls

The control group is composed of five types of specimens. The specimens are combinations of two types of treatments and three levels of fines contents. The specimen designations, the types of treatments, and fines contents are presented in Table 4.

Table 3. Specimen Designations.

Form of designation: A – L / F

A – Apparatus	L – Treatment[a]	F – Fines
C – Control	U – Untreated	L – Low content
B – Bending refiner	F – Formette	N – Normal content
R – Roll refiner	1 – 800 RE	H – High content
P – PFI mill	2 – 1600 RE	
	3 – 3000 RE	
	6 – 6000 RE	
	12 – 12000 RE	
	24 – 24000 RE	

[a] *BR* specimens subjected to one direction bending have an "S" appended to the treatment designation. *BR* specimens treated with the fiber perpendicular to the of plane of the radius of bending have a "P" appended to the treatment designation. *PM* specimens have either an "H" or an "L" appended to the treatment designation to indicate either high or low intensity of refining.

Table 4. Control Specimen Designations (C).

Fines	Untreated (U)	Formette (F)
Low (L)	C–U/L	—
Normal (N)	C–U/N	C–F/N
High (H)	C–U/H	C–F/H

Control specimens were either "untreated" or "Formette treated." The "untreated" designation means that raw pulp samples were handled only in the sheetmaking process, unless they were screened to remove fines as described below. The "Formette treated" designation means that raw pulp samples pulp were formed into Formette mats before the sheetmaking process.

Nonconventional Refining

Bending Refiner

Treatments using the Bending Refiner were conducted at three different levels with two different fines contents. The levels of treatment and the fines contents of these specimens along with the specimen designations are presented in Table 5. Treatment level are expressed in terms of refining events. For the *BR*, one RE is the same as one pass of the web through the working zone.

In addition, two special treatments were conducted to help define the action of the apparatus. Both are used to argue that the beating action taking place was a result of bending the fibers along the longitudinal axis as opposed to compressing the fiber cell wall in the radial direction. The radial compression can be described as compression of the fibers in the direction perpendicular to the plane of the fiber mat or as lateral compression. Normal treatments bent the fibers in one direction and then in the opposite direction. The first special treatment bent fibers in only one direction. The second special treatment had the *MD* of Formette mat parallel to vane over which the fiber were bent. The normal treatments were performed with the *MD* of the mat perpendicular to this plane.

In the first special experiment, the hypothesis was: if longitudinal bending is the action responsible for "refining" the fibers, then longitudinal bending of the fibers in two directions should produce a more beaten pulp than longitudinal bending of the fibers in only one direction (see Fig. 33a). The bending of a beam-shaped object subjects part of the material to elongation (positive strains) and the other part to compression (negative strains). The assumption in this experiment is that a more flexible fiber results when all regions of the fiber experience both longitudinal tension and compression. If the fiber is bent in only one direction, half of the fiber experiences only elongation, and half experiences only

compression. When the fiber is bent in the second, opposite direction the elongation and compression states are reversed and a more flexible fiber should result. Admittedly, the amount of material subjected to each type of strain during bending and the magnitude of these strains may not be equal due to lack of symmetry in fibers and the two differing radiuses of curvature described earlier.

Specimens were treated in the *BR* to 3000 and 6000 RE in one direction and to 3000 and 6000 RE in two directions. Treatment in two directions applied one half of the cycles before the fiber mat was turned upside-down and the run completed. The handsheet apparent density and specific elastic stiffnesses were used to compare the effectiveness of refining. These results are presented in Table I of Appendix I.

The treatment contrasts compared are one versus two direction bending at 3000 RE and 6000 RE. These two contrasts are orthogonal and, hence, uncorrelated. Another contrast of potential interest is one versus two direction bending for the combined 3000 and 6000 RE data. However, this contrast is nonorthogonal (correlated) with the previous two contrasts. The comparisons were made with an analysis of variance (ANOVA) method presented by Ostle and Mensing[94].

The analysis results are summarized in Table 6. At the 3000 RE level, bending in two directions was significantly different ($\alpha = 0.05$) from bending in one direction for all properties. At the 6000 RE level, a significant difference ($\alpha = 0.10$) existed only for the in-plane and out-of-plane shear stiffnesses. These results support the assertion that the bending of the fiber in the working zone is contributing more to the "refining" of the fiber than is the lateral compression. First, bending the fiber in two direction results in an increase in density and

elastic properties over bending in only one direction. This indicates that bending is the action at work in increasing these properties. If lateral compression (see Fig. 33b) was the mechanism responsible for the increase in the elastic stiffnesses, then the results should have shown no differences because the lateral compressive action should not depend on the "up" or "down" orientation of the fibers.

The hypothesis for the second experiment was: if longitudinal bending is the action responsible for "refining" the fibers, then a more beaten pulp should result from orienting most fibers perpendicular to the vane over which the fibers are bent as opposed to parallel. The assumption for this experiment was the same as before; a more flexible fiber results when all regions of the fiber experience both longitudinal tension and compression. In this case longitudinal bending was compared to tangential bending (see Fig. 33c). Note that the radial or lateral compressive action described above was again present.

The treatment contrasts compared are perpendicular versus parallel bending direction at normal and high fines contents. The handsheet apparent density and specific elastic stiffnesses are used to compare the effectiveness of refining. These results are given in Table II of Appendix I. The comparisons were made with the method described for the first experiment and the results are summarized in Table 7.

A statistically significant difference ($\alpha = 0.05$) exists only for the in-plane stiffnesses in the normal fines content specimens. No other differences are detected. The mixed results may indicate that the fiber mats are not sufficiently oriented or that the even when the mat is oriented parallel to the vane, a significant number of fibers are still oriented perpendicular to the vane. In the case of the high fines content specimens, the increase in properties due to adding the fines appears to overwhelm or mask any differences due to perpendicular *vs.*

parallel treatments. The conclusion drawn is that this experiment does not disprove the hypothesis and provide little support for the hypothesis.

Roll Refiner

Experimental treatments using the Roll Refiner were conducted at five different levels of treatment and two fines contents. The experimental conditions and their designations are presented in Table 8. Measurement of the amount of treatment was in refining events. For the *RR*, one refining event is one compression of the fiber. Since a given fiber may not be compressed during a revolution of the roll (*i.e.* the fiber passes under one of the grooves on the refining roll), conversion from roll revolution into refining events must take this into account. The number of revolutions of the top roll were recorded during a run by a mechanical counter. The conversion from refining roll revolutions into refining events is:

$$RE = N \frac{\phi_R}{\phi_S} \frac{W_b}{W_{b+g}} = 0.158\ N$$

where *RE* is the number of refining events, *N* is the number of refining roll revolutions, ϕ_S is the support roll diameter (160 mm), ϕ_R is the refining roll diameter (63 mm), W_{b+g} is the width of the bar plus the width of the groove (2 mm), and W_b is the width of the bar (0.8 mm).

Conventional Refining – PFI Mill

Experimental treatments using the PFI mill were conducted at four levels of treatment, two levels of intensity, and three fines contents. The experimental conditions and their designations are summarized in Table 9. Note that measurement of the amount of treatment is in refining events as opposed to the normal measurement of revolutions. A method to convert from PFI mill revolutions to refining events has been developed by Tam Doo and Kerekes[46]

(see Appendix II). Using this approach, the conversion factor is 2.5 RE per PFI mill revolution for the PFI mill operation conditions.

Table 5. Bending Refiner Specimen Designations (B).

	Treatment Level, RE		
Fines	3000 (3)	6000 (6)	12000 (12)
Normal (N)	B–3/N	B–6/N	B–12/N
Normal (N)[a]	B–3S/N	B–6S/N	—
High (H)	B–3/H	B–6/H	B–12/H

[a]Special specimens treated with only one out-of-plane direction of bending have an "S" appended to the treatment level designation.

Table 6. Comparison of One vs. Two Direction Bending.

	Handsheet properties which differ significantly[a]				
Group	Density (ρ)	C_{11}/ρ	C_{66}/ρ	C_{33}/ρ	C_{44}/ρ
3000 RE Level	✔✔[b]	✔✔	✔✔	✔✔	✔✔
6000 RE Level	✔[c]		✔✔	✔	✔✔

[a]See the Sheet Testing, Elastic Stiffness Properties section for definitions of C_{ij}.

[b]Significantly different at $\alpha = 0.05$

[c]Significantly different at $\alpha = 0.10$

Table 7. Comparison of Parallel vs. Perpendicular Orientations.

	Handsheet properties which differ significantly[a]				
Group	Density (ρ)	C_{11}/ρ	C_{66}/ρ	C_{33}/ρ	C_{44}/ρ
6000 RE, Norm		✔✔[b]	✔✔		
6000 RE, High					

[a]See the Sheet Testing, Elastic Stiffness Properties section for definitions of C_{ij}.

[b]Significantly different at $\alpha = 0.05$

Table 8. Roll Refiner Specimen Designations (R).

	Treatment Level, RE				
Fines	800 (1)	1600 (2)	3000 (3)	6000 (6)	12000 (12)
Normal (N)	R–1/N	R–2/N	R–3/N	R–6/N	R–12/N
High (H)	R–1/H	R–2/H	R–3/H	R–6/H	R–12/H

Table 9. PFI Mill Specimen Designations (P).

Hi Intensity	Treatment Level, RE			
Fines	3000 (3)	6000(6)	12000 (12)	24000(24)
Low (L)	P–3H/L	P–6H/L	P–12H/L	P–24H/L
Normal (N)	P–3H/N	P–6H/N	P–12H/N	P–24H/N
High (H)	P–3H/H	P–6H/H	P–12H/H	P–24H/H
Lo Intensity	**Treatment Level, RE**			
Fines	3000 (3)	6000(6)	12000 (12)	24000(24)
Low (L)	P–3L/L	P–6L/L	P–12L/L	P–24L/L
Normal (N)	P–3L/N	P–6L/N	P–12L/N	P–24L/N
High (H)	P–3L/H	P–6L/H	P–12L/H	P–24L/H

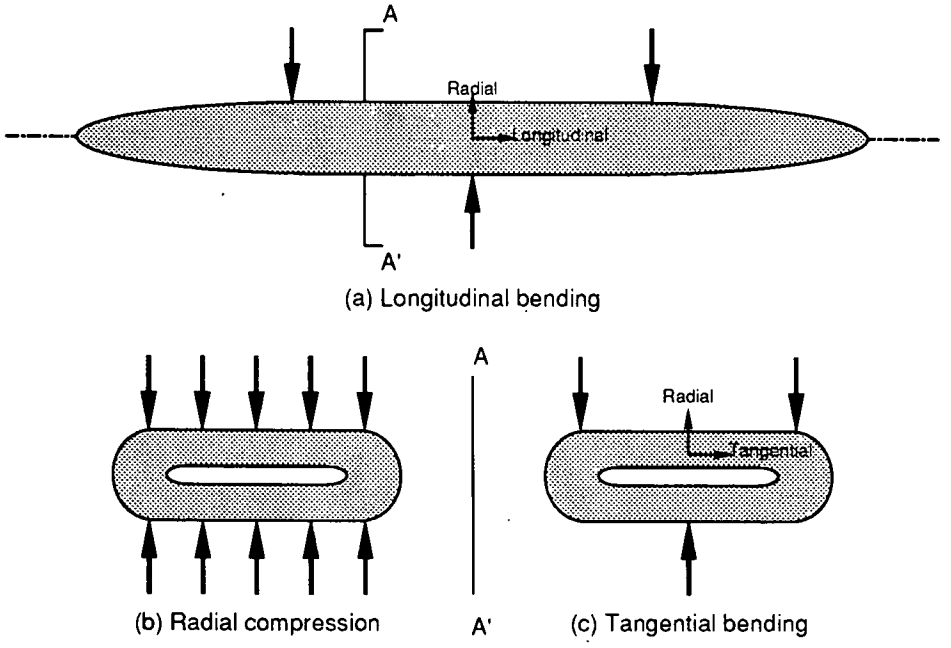

Figure 33. Schematic of forces acting on fibers in Bending Refiner.

THEORETICAL ANALYSIS

NOMENCLATURE

A, B, C, D, E	equation coefficients
A	area
BL	breaking length
F	transverse stress
G	shear elastic modulus
I	moment of inertia
M	moment
P	tensile force
P	vertical line load
R	radius
T	normal stress
U	energy
U	average energy
U	energy density
U	average energy density
V	shear stress
Z	compressive stress
b	nip width
m	mass
r	radius
t	thickness
w	width
y	distance from neutral axis
α, β	equation coefficients
ε	normal strain
γ	shear strain
λ	ρ/t
ν	Poisson's ratio
θ	angle
ρ	radius of curvature
σ	normal stress
τ	shear stress
ω	wrap angle

Subscripts

b	bending
eff	effective
min	minimum
max	maximum
r	radial dimension
z	longitudinal dimension
θ	theta dimension

Superscripts

*	simplified equation

OBJECTIVE

When stresses are applied to an elastic material, work is done on the material[95]. The amount of work done on (or energy stored in) an elastic material can be calculated from

$$U = \frac{1}{2}\int_V (\sigma_r\varepsilon_r + \sigma_\theta\varepsilon_\theta + \sigma_z\varepsilon_z + \tau_{r\theta}\gamma_{r\theta} + \tau_{\theta z}\gamma_{\theta z} + \tau_{rz}\gamma_{rz})\, dV \qquad (1)$$

The *BR* and *RR* subject fibers to different types of mechanical treatments (bending and transverse compression, respectively), but the types of stress which result are the same. The fibers are subjected to tensile or compressive stress along the fiber axis, compressive stress transverse to the fiber axis, and shear stress in the longitudinal-transverse plane. The magnitude of each stress differs from the other stresses in the same apparatus and from the same stress in the other apparatus. In order to speculate on how the two apparatuses modify fiber and sheet properties, it would be useful to know the relative magnitudes of the stresses and of the amount of work done on the fiber. This section derives equations which estimate the amount of work done on a fiber segment by stresses listed above for a fiber subjected to the *BR* and *RR*.

The main comparison is between the stresses and strains resulting from bending a fiber segment about a fixed radius and from compressing a fiber laterally. In the case of the *BR*, both situations are considered. Estimates are reported for longitudinal tensile, transverse compressive, and out-of-plane shear stresses (shear stress in the longitudinal-transverse plane). In the *RR*, only transverse compression is considered present and an estimate of the amount of work done on the fiber segment by the transverse compressive stresses is calculated. This value is compared to all three values calculated for the *BR*.

BENDING REFINER

The analysis is for a single, isolated fiber segment perfectly oriented in the direction of bending. The fiber segment is considered to be anisotropic and linearly elastic with axial elastic modulus E_θ, transverse elastic modulus E_r, and shear elastic modulus $G_{r\theta}$. The cross section is uniform and rectangular with fiber thickness t and unit width w. The segment is forced to conform to a surface of constant radius of curvature ρ for $2\theta_w$ radians as illustrated in Fig. 34. The

length of the fiber segment is sufficient to completely wrap the radius of the surface.

The major assumptions for the model are listed below. (1) Poisson's ratio effects are considered insignificant. (2) The friction forces between the fiber and the surface are considered to be very small because of the lubricating affect of water and the layer of Mylar which intervenes between the fibers and the surface of the radius. The presence of significant friction forces would increase the amount of shear stress since the surface of the radius could apply a force in the θ-direction on the surface of the fiber. (3) No transverse compressive stresses are applied to the outer surface of the fiber in this model. Any compressive forces applied by the film or mat to the fiber would increase the amount of work done the fiber in the out-of-plane direction. The effect of transverse compressive stresses can be included by increasing the tensile force on the ends of the fiber (see Fig. 35). (4) The tensile and shear forces, and the moment used to deformed

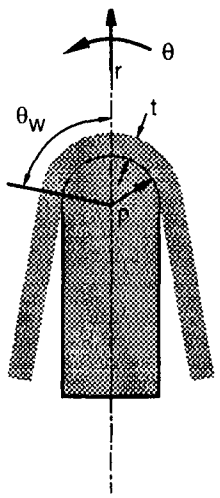

Figure 34. Schematic of fiber undergoing bending in Bending Refiner.

the fiber are concentrated at the point where the fiber comes in contact with the surface of the radius.

Two initial conditions will be necessary to solve the model and they represent additional assumptions. The initial conditions are two of the stresses specified at some point other than $\theta = 0$. The most logical location is the end of the fiber segment or $\theta = \theta_w$. One initial condition must specify the tensile stress and the other may specify either the shear stress or bending moment. Two cases are presented with Case 1 specifying an initial condition for the bending moment and Case 2 specifying the shear stress.

The first case assumes that the bending moment at the end of the fiber segment be zero. This assumption leads to a case which develops the maximum shear stress and minimum bending moment in the fiber segment. The second case assumes that the shear stress at the end of the fiber segment be zero. This assumption leads to a case which develops the maximum bending moment and the minimum shear stress in the fiber segment. Thus, Case 2 reduces to a case of pure bending with an applied tensile stress. In both cases, the tensile stress on the ends of the fiber segment is also assumed. The actual situation the fiber segment experiences is between the two extremes the cases presented.

Analysis of Differential Fiber Element

Force and Equilibrium Requirements

The fiber illustrated in Fig. 34 is being bent about a surface of known radius by the tensile force P. A differential element, ABC, as shown in Fig. 35, is defined to have a normal stress, $T(\theta)$, a shear stress, $V(\theta)$, a moment, $M_b(\theta)$, and a transverse stress (applied by the surface), $F(\theta)$, applied to it. No friction is assumed present where the fiber contacts the surface. The element is bent about radius ρ for $d\theta$ radians. The fiber height is t and the width is w (defined as the

unit width). The stresses T, V, and the moment M_b are per unit cross section area (width·height); the distributed stress F is per unit area (width·length).

Begin the analysis by summing the forces about point B in the radial direction

$$\sum F_r = - w\,t\,T\left(\theta+\frac{d\theta}{2}\right)\sin\left(\frac{d\theta}{2}\right) - w\,t\,T\left(\theta-\frac{d\theta}{2}\right)\sin\left(\frac{d\theta}{2}\right)$$

$$- w\,t\,V\left(\theta+\frac{d\theta}{2}\right)\cos\left(\frac{d\theta}{2}\right) + w\,t\,V\left(\theta-\frac{d\theta}{2}\right)\cos\left(\frac{d\theta}{2}\right)$$

$$+ w\,\rho\,d\theta\,F(\theta)$$

Express $sin(d\theta)$ and $cos(d\theta)$ as Taylor series expansions and take the limit as $d\theta \rightarrow 0$. Thus, $sin(d\theta) = 0$ and $cos(d\theta) = 1$. With these approximations, the above equation simplifies to

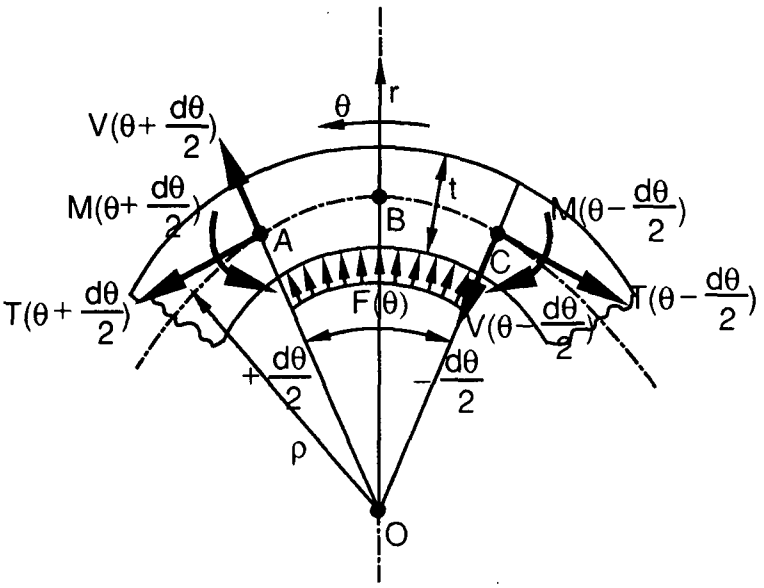

Figure 35. Differential element of fiber in bending.

$$\sum F_r = -w\,t\,T(\theta)\frac{d\theta}{2} - w\,t\,\frac{dT}{d\theta}\left(\frac{d\theta}{2}\right)^2 - w\,t\,T(\theta)\frac{d\theta}{2} + w\,t\,\frac{dT}{d\theta}\left(\frac{d\theta}{2}\right)^2$$

$$- w\,t\,V(\theta) - w\,t\,\frac{dV}{d\theta}\frac{d\theta}{2} + w\,t\,V(\theta) - w\,t\,\frac{dV}{d\theta}\frac{d\theta}{2}$$

$$+ w\,\rho\,d\theta\,F(\theta)$$

$$= -t\,T(\theta)\,d\theta - t\,\frac{dV}{d\theta}\,d\theta + \rho\,d\theta\,F(\theta)$$

$$\sum F_r = -T(\theta) - \frac{dV}{d\theta} + \frac{\rho}{t}F(\theta) = 0 \qquad (2)$$

Next, sum the forces about point *B* in the tangential direction

$$\sum F_\theta = w\,t\,T\left(\theta + \frac{d\theta}{2}\right)\cos\left(\frac{d\theta}{2}\right) - w\,t\,T\left(\theta - \frac{d\theta}{2}\right)\cos\left(\frac{d\theta}{2}\right)$$

$$- w\,t\,V\left(\theta + \frac{d\theta}{2}\right)\sin\left(\frac{d\theta}{2}\right) - w\,t\,V\left(\theta - \frac{d\theta}{2}\right)\sin\left(\frac{d\theta}{2}\right)$$

Note that $F(\theta)$ is symmetrical about OB, thus, there is no net force applied by $F(\theta)$ in the θ-direction at point B.

$$\sum F_\theta = T(\theta) + \frac{dT}{d\theta}\frac{d\theta}{2} - T(\theta) + \frac{dT}{d\theta}\frac{d\theta}{2}$$

$$- V(\theta)\frac{d\theta}{2} - \frac{dV}{d\theta}\left(\frac{d\theta}{2}\right)^2 - V(\theta)\frac{d\theta}{2} + \frac{dV}{d\theta}\left(\frac{d\theta}{2}\right)^2$$

$$= \frac{dT}{d\theta}\,d\theta - V(\theta)\,d\theta$$

$$\sum F_\theta = \frac{dT}{d\theta} - V(\theta) = 0 \qquad (3)$$

Finally, sum the moments about point *B*

$$\sum M = \; w\,t\,M_b\left(\theta + \frac{d\theta}{2}\right) - t\,M_b\left(\theta - \frac{d\theta}{2}\right)$$

$$+ \rho\,\frac{d\theta}{2}\cos\left(\frac{d\theta}{2}\right)\left(\; w\,t\,T\left(\theta + \frac{d\theta}{2}\right)\sin\left(\frac{d\theta}{2}\right) + w\,t\,V\left(\theta + \frac{d\theta}{2}\right)\cos\left(\frac{d\theta}{2}\right)\right)$$

$$+ \rho\,\frac{d\theta}{2}\sin\left(\frac{d\theta}{2}\right)\left(\; w\,t\,T\left(\theta + \frac{d\theta}{2}\right)\cos\left(\frac{d\theta}{2}\right) + w\,t\,V\left(\theta + \frac{d\theta}{2}\right)\sin\left(\frac{d\theta}{2}\right)\right)$$

$$+ \rho\,\frac{d\theta}{2}\cos\left(\frac{d\theta}{2}\right)\left(- w\,t\,T\left(\theta - \frac{d\theta}{2}\right)\sin\left(\frac{d\theta}{2}\right) + w\,t\,V\left(\theta - \frac{d\theta}{2}\right)\cos\left(\frac{d\theta}{2}\right)\right)$$

$$+ \rho\,\frac{d\theta}{2}\sin\left(\frac{d\theta}{2}\right)\left(- w\,t\,T\left(\theta - \frac{d\theta}{2}\right)\cos\left(\frac{d\theta}{2}\right) + w\,t\,V\left(\theta - \frac{d\theta}{2}\right)\sin\left(\frac{d\theta}{2}\right)\right)$$

Note that $F(\theta)$ is symmetrical about OB, thus there is no net moment applied by $F(\theta)$ at point B.

$$\sum M = \frac{dM_b}{d\theta}\,d\theta$$

$$+ \rho\,\frac{d\theta}{2}\left(\; T(\theta)\frac{d\theta}{2} + \frac{dT}{d\theta}\left(\frac{d\theta}{2}\right)^2 + V(\theta) + \frac{dV}{d\theta}\,\frac{d\theta}{2}\right)$$

$$+ \rho\,\frac{d\theta}{2}\left(- T(\theta)\frac{d\theta}{2} + \frac{dT}{d\theta}\left(\frac{d\theta}{2}\right)^2 + V(\theta) - \frac{dV}{d\theta}\,\frac{d\theta}{2}\right)$$

$$= \frac{dM_b}{d\theta}\,d\theta + \rho\,V(\theta)\,d\theta = 0$$

$$\sum M = \frac{dM_b}{d\theta} + \rho\,V(\theta) = 0 \qquad (4)$$

Deformations and Geometric Fit Requirements

This analysis requires the fiber segment to conform to a surface with a radius of curvature ρ. Given an infinitesimal element which conforms to the surface, the change in the angle of its sides due to the shear stress action plus the bending moment action must be equal to the change in angle of the surface or

$$\frac{1}{\rho} = \left(\frac{d\theta}{ds}\right)_{bending} + \left(\frac{d\theta}{ds}\right)_{shearing}$$

After substituting for the $d\theta/ds$ expression, the inverse of radius of curvature is

$$\frac{1}{\rho} = \frac{t\, M_b}{E_\theta\, I_{\theta\theta}} + \frac{1}{\rho\, G_{r\theta}} \frac{dV}{d\theta} \tag{5}$$

Application of Force-Deformation Relationships

Equations 2 through 5 represent four independent differential equations describing the stress-strain state of the deformed fiber. The boundary conditions for these equations come from symmetry considerations.

$$\begin{aligned} T(-\theta) &= T(\theta) \\ V(-\theta) &= -V(\theta) \\ M_b(-\theta) &= M_b(\theta) \\ F(-\theta) &= F(\theta) \end{aligned} \tag{6}$$

Case 1

Equations 2 through 5 can be solved assuming the initial conditions described for Case 1 which are

$$T(\theta = \theta_w) = T_w \tag{7}$$

$$M_b(\theta = \theta_w) = 0 \tag{8}$$

The tensile stress, T_w, is applied to the ends of the fiber and normal to the *rz*-plane. These assumptions will give the case with the maximum shear stresses. The solution for Case 1 begins by rearranging and differentiating Eq. 5

$$\frac{1}{\rho} = \frac{t\, M_b}{E_\theta\, I_{\theta\theta}} + \frac{1}{\rho\, G_{r\theta}} \frac{dV}{d\theta} \tag{5}$$

$$\frac{t\, M_b}{E_\theta\, I_{\theta\theta}} = \frac{1}{\rho} - \frac{1}{\rho\, G_{r\theta}} \frac{dV}{d\theta}$$

$$M_b = \frac{E_\theta\, I_{\theta\theta}}{t\,\rho} - \frac{E_\theta\, I_{\theta\theta}}{t\,\rho\, G_{r\theta}} \frac{dV}{d\theta}$$

$$\frac{dM_b}{d\theta} = -\frac{E_\theta\, I_{\theta\theta}}{t\,\rho\, G_{r\theta}} \frac{d^2V}{d\theta^2} \tag{9}$$

Substituting the result, Eq. 9, into Eq. 4 gives

$$-\frac{E_\theta\, I_{\theta\theta}}{t\,\rho\, G_{r\theta}} \frac{d^2V}{d\theta^2} + \rho\, V = 0$$

Defining α

$$\alpha = \left(\frac{t\,\rho^2\, G_{\rho\theta}}{E_\theta\, I_{\theta\theta}} \right)^{\frac{1}{2}} \tag{10}$$

and substituting α^2 into the above equation gives

$$\frac{d^2V}{d\theta^2} - \alpha^2\, V = 0 \tag{11}$$

The general solution to Eq. 11 is

$$V(\theta) = A\, e^{\alpha\theta} + B\, e^{-\alpha\theta} \tag{12}$$

The second of the boundary conditions, Eqs. 6, requires the solution to V be an odd function. Thus, Eq. 12 can be expressed as the odd function $sinh(\alpha\theta)$ and its derivative as the even function, $cosh(\alpha\theta)$

$$V(\theta) = D \sinh(\alpha\theta) \tag{13}$$

$$\frac{dV}{d\theta} = D\,\alpha \cosh(\alpha\theta) \tag{14}$$

Substitute Eq. 13 into Eq. 3.

$$\sum F_\theta = \frac{dT}{d\theta} - V(\theta) = 0 \tag{3}$$

$$\frac{dT}{d\theta} = D \sinh(\alpha\theta)$$

$$T = \frac{D}{\alpha} \cosh(\alpha\theta) + C \tag{15}$$

Note that this result satisfies the first boundary condition in Eqs. 6. Next, substitute Eqs. 15 and 14 into Eq. 2.

$$\sum F_r = -T(\theta) - \frac{dV}{d\theta} + \frac{\rho}{t} F(\theta) = 0 \tag{2}$$

$$0 = -\frac{D}{\alpha} \cosh(\alpha\theta) - C - D\,\alpha \cosh(\alpha\theta) + \frac{\rho}{t} F(\theta)$$

$$F = \frac{t}{\rho}\left(\frac{D}{\alpha} \cosh(\alpha\theta) + C + D\,\alpha \cosh(\alpha\theta)\right) \tag{16}$$

Since this result is an even function, the fourth boundary condition of Eqs. 6 is met. Equation 4 is rearranged,

$$\sum M_b = \frac{dM_b}{d\theta} + \rho\, V(\theta) = 0 \tag{4}$$

$$\frac{dM_b}{d\theta} = -\rho\, V(\theta)$$

and Eq. 13, is substituted, then the equation is integrated with respect to θ.

$$\frac{dM_b}{d\theta} = -\rho\, D \sinh(\alpha\theta)$$

$$M_b(\theta) = \int_\theta -\rho\, D \sinh(\alpha\theta)\, d\theta$$

$$M_b(\theta) = -\frac{\rho D}{\alpha}\cosh(\alpha\theta) + E \tag{17}$$

The initial condition of $M_b(\theta = \theta_w) = 0$ (Eq. 8) allows determination of E in Eq. 17

$$M_b \mid_{\theta=\theta_w} = -\frac{\rho D}{\alpha}\cosh(\alpha\theta_w) + E$$

$$E = \frac{\rho D}{\alpha}\cosh(\alpha\theta_w)$$

$$M_b(\theta) = \frac{\rho D}{\alpha}\left(-\cosh(\alpha\theta) + \cosh(\alpha\theta_w)\right) \tag{18}$$

Substitute Eq. 18 into Eq. 5 and rearrange

$$\frac{1}{\rho} = \frac{t\, M_b}{E_\theta\, I_{\theta\theta}} + \frac{1}{\rho\, G_{r\theta}}\frac{dV}{d\theta} \tag{5}$$

$$\frac{1}{\rho} = \frac{t\,\rho\, D}{E_\theta\, I_{\theta\theta}\,\alpha}\left(-\cosh(\alpha\theta) + \cosh(\alpha\theta_w)\right) + \frac{D\,\alpha}{\rho\, G_{r\theta}}\cosh(\alpha\theta)$$

$$G_{r\theta} = \frac{t\,\rho^2\, D\, G_{r\theta}}{E_\theta\, I_{\theta\theta}\,\alpha}\left(-\cosh(\alpha\theta) + \cosh(\alpha\theta_w)\right) + D\,\alpha\cosh(\alpha\theta)$$

Recall from Eq. 10,

$$\alpha = \left(\frac{t\,\rho^2\,G_{\rho\theta}}{E_\theta\,I_{\theta\theta}} \right)^{\frac{1}{2}} \tag{10}$$

After substituting α^2

$$G_{r\theta} = D\,\alpha\left(-\cosh(\alpha\theta) + \cosh(\alpha\theta_w)\right) + D\,\alpha\cosh(\alpha\theta)$$

$$G_{r\theta} = D\,\alpha\cosh(\alpha\theta_w)$$

$$D = \frac{G_{r\theta}}{\alpha\cosh(\alpha\theta_w)} \tag{19}$$

Finally, substitute Eq. 19 into the equations for $V(\theta)$ (Eq. 13), $T(\theta)$ (Eq. 15), $F(\theta)$ (Eq. 16), and $M_b(\theta)$ (Eq. 18), and simplify. The results are summarized below:

$$V(\theta) = \sqrt{\frac{E_\theta\,G_{r\theta}}{12}}\,\frac{t}{\rho}\,\frac{\sinh(\alpha\theta)}{\cosh(\alpha\theta_w)} \tag{20}$$

$$T(\theta) = \frac{E_\theta\,t^2}{12\,\rho^2}\,\frac{\cosh(\alpha\theta)}{\cosh(\alpha\theta_w)} + C \tag{21}$$

$$F(\theta) = \frac{E_\theta\,t^3}{12\,\rho^3}\,\frac{\cosh(\alpha\theta)}{\cosh(\alpha\theta_w)}\left(1+\alpha^2\right) + \frac{t}{\rho}C \tag{22}$$

$$M_b(\theta) = \frac{E_\theta\,t^2}{12\,\rho}\left(1 - \frac{\cosh(\alpha\theta)}{\cosh(\alpha\theta_w)}\right) \tag{23}$$

The constants α and C are

$$\alpha = \left(\frac{t\,\rho^2\,G_{\rho\theta}}{E_\theta\,I_{\theta\theta}} \right)^{\frac{1}{2}} \tag{10}$$

C = integration constant

$$I_{\theta\theta} = \frac{t^3}{12}$$

The value of the integration constant C is determined from the initial condition $T(\theta_w) = T_w$ below. The functions $V(\theta)$, $T(\theta)$, $F(\theta)$, and $M_b(\theta)$ for Case 1 are shown graphically in Fig. 36 plotted versus angle.

Case 2

The initial conditions for Case 2 are

$$T(\theta = \theta_w) = T_w \tag{24}$$

$$V(\theta = \theta_w) = 0 \tag{25}$$

Instead of selecting $M_b(\theta_w) = 0$ (Eq. 8) as an initial condition for Eq. 23, the initial condition of $V(\theta_w) = 0$ (Eq. 25) is selected for Eq. 20. This gives the case with the maximum bending moments. The initial condition of $V(\theta_w) = 0$ (Eq. 25) reduces the analysis to that of pure bending with an applied tensile load. The bending moment, M_b, is constant, the longitudinal stress, T, is constant, and the shear stress, V, is zero everywhere. The distributed load (F), which balances the tensile load, is constant and proportional to t/ρ. These results are summarized below:

$$V(\theta) = 0 \tag{26}$$

$$T(\theta) = C \tag{27}$$

$$F(\theta) = \frac{t}{\rho} C \tag{28}$$

$$M_b(\theta) = E \tag{29}$$

$$E = \frac{E_\theta t^2}{12 \rho} \tag{30}$$

The value of the integration constant C is determined from the initial condition $T(\theta_w) = T_w$ below.

Estimates for the Values of Integration Constants

Case 1

The value of C is unknown, but bounds on the values it may take on can be calculated for the first case where $M_b(\theta_w) = 0$. To keep the model appropriate, the fiber segment must remain in contact with the surface of the radius at all

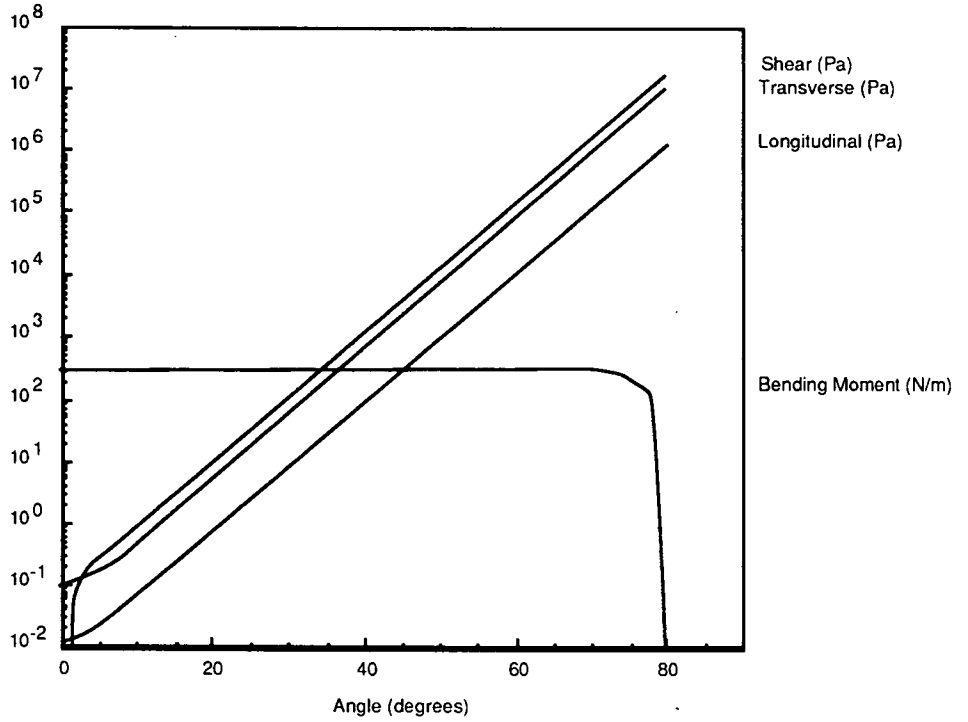

Figure 36. Stresses *vs.* angle in fiber segment for initial condition of $M_b(\theta_w) = 0$ using typical parameters. $E_\theta = 9$ GPa, $E_r = 0.045$ GPa, $G_{r\theta} = 0.64$, $t = 10$ μm, $\rho = 250$ μm, $\theta_w = 80°$, and $C = 0.0012$ GPa.

points between $-\theta_w$ and θ_w. Thus, the value of $F(\theta)$ must be greater than or equal to zero. The minimum C necessary to meet this restriction, $C(\theta)_{min}$ can be calculated from the equation for F by setting $F(\theta) = F(\theta)_{min} = 0$ (*i.e.*, no net radial forces present) and solving for $C(\theta)_{min}$.

$$F(\theta)_{min} = \frac{E_\theta t^3}{12 \rho^3} \frac{\cosh(\alpha\theta)}{\cosh(\alpha\theta_w)}(1 + \alpha^2) + \frac{t}{\rho} C_{min} = 0$$

$$C(\theta)_{min} = -\frac{E_\theta t^2}{12 \rho^2} \frac{\cosh(\alpha\theta)}{\cosh(\alpha\theta_w)}(1 + \alpha^2)$$

where θ_{min} is the angle where $F(\theta)$ is at a minimum or $\theta_{min} = 0$. (The function $F(\theta)$ is a minimum at $\theta = 0$ since $\cosh(\alpha\theta)$ is at its minimum of 1.) At θ_{min}, $C(\theta)_{min}$ reduces to

$$C(0)_{min} = -\frac{E_\theta t^2}{12 \rho^2} \frac{1}{\cosh(\alpha\theta_w)}(1 + \alpha^2) \tag{31}$$

The assumption is made that C must be equal to or greater than $C(0)_{min}$ in order to keep the fiber in contact with the surface.

Based on $C(0)_{min}$, several limiting values of T and F can be calculated. The minimum possible value of T, $T(\theta)_{min}$, at any angle is

$$T(\theta)_{min} = \frac{E_\theta t^2}{12 \rho^2} \frac{\cosh(\alpha\theta)}{\cosh(\alpha\theta_w)} + C(0)_{min}$$

$$T(\theta)_{min} = \frac{E_\theta t^2}{12 \rho^2} \frac{(\cosh(\alpha\theta) - 1 - \alpha^2)}{\cosh(\alpha\theta_w)} \tag{32}$$

The function $F(\theta)$ is minimized when $C = C(0)_{min}$

$$F(\theta)_{min} = \frac{E_\theta t^3}{12\,\rho^3}\frac{\cosh(\alpha\theta)}{\cosh(\alpha\theta_w)}(1+\alpha^2) + \frac{t}{\rho}C(0)_{min} = 0$$

$$F(\theta)_{min} = \frac{E_\theta t^3}{12\,\rho^3}\frac{1+\alpha^2}{\cosh(\alpha\theta_w)}\left(\cosh(\alpha\theta) - 1\right) \tag{33}$$

The value of $T(\theta_w)$ is the external tensile force applied to the ends of the fiber.

$$T(\theta_w) = \frac{E_\theta t^2}{12\,\rho^2} + C \tag{34}$$

The minimum value that $T(\theta_w)$ may assume, $T(\theta_w)_{min}$, is when $C(0)_{min}$ is substituted for C.

$$T(\theta_w)_{min} = \frac{E_\theta t^2}{12\,\rho^2} + C(0)_{min}$$

$$T(\theta_w)_{min} = \frac{E_\theta t^2}{12\,\rho^2}\left(1 - \frac{(1+\alpha^2)}{\cosh(\alpha\theta_w)}\right) \tag{35}$$

When $\cosh(\alpha\theta_w)$ is much larger than $1+\alpha^2$, $T(\theta_w)_{min}$ is approximately equal to $E_\theta t^2/12\rho^2$. This is true for all normal combination of E_θ, $G_{r\theta}$, t, and ρ which give α ($\alpha^2 = 12G_{r\theta}\rho^2/E_\theta t^2$) greater than 7. The value of alpha calculated using the nominal parameters is 14.2. The cases where α is less than 7 involve cases using the minimum ρ and the maximum t. Using E_θ = 1 GPa, t = 10 μm, and ρ = 250 μm (see Table 10), the minimum value of $T(\theta_w)_{min}$ is 1.3×10^{-4} GPa; using E_θ = 9 GPa gives $T(\theta_w)_{min}$ of 1.2×10^{-3} GPa.

The estimates of $C(0)_{min}$ are lower bounds on C. An estimate for the upper bound for C can be calculated by determining the maximum of $T(\theta_w)$ and solving for C. The maximum of $T(\theta_w)$ is calculated by assuming the sum of the external tensile forces applied to the end of the fibers are equal to the force on the whole web. This assumes that the polyester film carries no load and the fiber mat carries the full tensile load on the web in the region of the vane. A total tensile force on the web of 60 N (the force supported by the springs attached to the web holders) was measured during a typical run. For a mat 0.2 m wide with a thickness of 90×10^{-6} m, $T(\theta_w)_{max}$ is 0.0033 GPa. However, this assumes the force is evenly distributed over the total cross–sectional area. The force is actually distributed over the total *fiber* cross–sectional area. The total fiber cross-sectional area can be estimated by calculating an effective mat thickness, t_{eff}, in m from

$$t_{eff} = \frac{W}{\rho_{cw}}$$

where ρ_{cw} is the density of cell wall material in g/m^3 and W is the grammage of the mat in g/m^2. For ρ_{cw} equal to 1.5×10^6 g/m^3 and W equal to 25 g/m^2, t_{eff} is 16.7×10^{-6}m. Calculation of $T(\theta_w)_{max}$ based on $t_{eff} = 16.7 \times 10^{-6}$ m gives 0.018 GPa.

Other estimates of $T(\theta_w)_{max}$ may be based on the web breaking stresses for wet and dry webs. The transverse compression of the web in the experimental apparatus could increase the ability of the web to carry a load above that of uncompressed wet webs, however, for this analysis, it is assumed any increase in web web breaking stress is negligible. An estimate of the stresses on the fiber ends may be calculated from wet web breaking strengths reported by Seth and co-workers[96]. Typical wet web breaking lengths reported were 100 to 1000 m at 2 to 6% strain for both kraft and sulfite pulps. The conversion from breaking length in m, *BL*, to tensile stress in N/m^2 (or Pa), T_s, is

$$T_s = k \frac{BK\ W}{t_s}$$

where W is the grammage in g/m^2, t_s is the soft platen caliper in m, and k is the conversion constant from grams (force) to Newtons ($k = 0.0098\ N/g_f$). Using a basis weight of 25 g/m^2 and a caliper of 90×10^{-6} m, the resulting tensile stresses, T_s, for the breaking lengths of 100 and 1000 m are 0.00027 and 0.0027 GPa respectively. In order to estimate the tensile stress on the ends of the fibers, the effective caliper, t_{eff}, as described above should be used. Using $t_{eff} = 16.7 \times 10^{-6}$ m, the estimates of $T(\theta_w)$ (= T_s) for the 100 and 1000 m breaking lengths are 0.0015 and 0.015 GPa. These values can be compared to the dry web breaking length for the pulp used in the experiments. After 10,000 rev. in the PFI mill, the breaking length was 5000 m. The corresponding value of $T(\theta_w)$ is 0.073 GPa.

Since all the estimates of T are greater than T_{min}, the assumption that the fiber is in contact with the surface of the radius between $-\theta_w$ and θ_w is valid. In order to calculate values for T, V, M_b, and F, values for E_θ, E_r, $G_{r\theta}$, t, and ρ must be available. Given in Table 10, for each parameter, are estimates of its range and a typical value. These data are used in Table 11 to determine values of $T(\theta_w)$ and C. The values of $C(0)_{min}$ and $T(\theta_w)_{min}$ are calculated from Eq. 46 using appropriate minimum, nominal, and maximum values of E_θ, $G_{r\theta}$, t, and ρ. The other C values are determined from Eq. 39 based on the given $T(\theta_w)$ values and nominal values for E_θ, $G_{r\theta}$, t, and ρ.

Case 2

The minimum value of T, T_{min}, in Case 2 may be zero since no tensile force is require to keep the fiber in contact with the surface of the radius. The fiber is bent to the shape of the curved surface by the applied moments. Thus,

the minimum value of C, C_{min}, may also be zero. The estimates for the other values of T_w and C in Case 1 are valid for Case 2.

Table 10. Equation parameters.

Parameter	Units	Value	Range	Source
E_θ	GPa	9	1–14	36, 97
E_r	GPa	0.045	0.014–1	53, 54
$G_{r\theta}$	GPa	0.24	0.045–1.42	57, 98
t	μm	10.	5.–20.	12
ρ	μm	250	150–350	(see Experimental Program section)

Table 11. Estimates of C.

$T(\theta_w)$, GPa[a]	C, GPa	Basis
0.000017	0.0	Minimum C, a, $G_{r\theta}$
0.0012	-2.45E–09	Nominal C, a, $G_{r\theta}$
0.0015	0.0003	Low web breaking length
0.015	0.0138	High web breaking length
0.018	0.0168	Force on actual web
0.073	0.0718	Dry breaking stress

[a] $\theta_w = 80° = 1.4$ radians

Energy Calculations

The final step in this analysis is to calculate the work done on the fiber segment by the longitudinal, transverse, and shear stress. Assuming linear elastic behavior, the basic equation to calculate the total energy stored in the deformed fiber segment is

$$U = \frac{1}{2}\int_v (\sigma_r\varepsilon_r + \sigma_\theta\varepsilon_\theta + \sigma_z\varepsilon_z + \tau_{r\theta}\gamma_{r\theta} + \tau_{\theta z}\gamma_{\theta z} + \tau_{rz}\gamma_{rz})\,dV \qquad (1)$$

Since the fiber moves about the radius of curvature, the entire length of the fiber is assumed to be subjected to the maximum longitudinal, transverse, and shear stresses. Thus, the amount of work done on the fiber segment during one bending cycle for each component can be calculated using the appropriate term from the equation above and substituting the maximum stress and strain terms. Three terms are of interest in this analysis are the axial or longitudinal term ($\sigma_\theta \varepsilon_\theta$), the lateral or transverse term ($\sigma_r \varepsilon_r$), and the shear term in the $r\theta$ planes ($\tau_{r\theta} \gamma_{r\theta}$). Comparisons between these three terms will be made on an work per unit volume (energy density) basis.

Work Due to Longitudinal (θ) Stress

Case 1

The work due to the longitudinal stress for case with the initial condition of $M_b(\theta_w) = 0$ will be calculated first. The longitudinal stress (θ-direction) is the combination of stresses due to longitudinal tension (T) and due to bending. This requires knowing the longitudinal stress due to bending as a function of fiber thickness, $T_b(y,\theta)$. This may be calculated from the bending moment equation.

$$t\, M_b = \int_{-\frac{t}{2}}^{\frac{t}{2}} T_b(y,\theta)\, y\, dy \tag{36}$$

The distance from the neutral axis is represented by y. For cases of bending in linearly elastic materials, the stress is proportional to the distance from the neutral axis or $T_b(y,\theta) = \beta(\theta)y$. Substituting this into Eq. 36 gives

$$t\,M_b = \int_{-\frac{t}{2}}^{\frac{t}{2}} \beta(\theta)\, y^2\, dy$$

$$t\,M_b = \frac{\beta(\theta)\, t^3}{12} \tag{37}$$

Substitute Eqs. 10 and 23 into Eq. 37 and solve for β.

$$t\,\frac{\rho\, G_{r\theta}}{\alpha^2}\left(1 - \frac{\cosh(\alpha\theta)}{\cosh(\alpha\theta_w)}\right) = \frac{\beta\, t^3}{12}$$

$$\beta = \frac{\rho\, t\, G_{r\theta}}{\alpha^2\, I_{\theta\theta}}\left(1 - \frac{\cosh(\alpha\theta)}{\cosh(\alpha\theta_w)}\right)$$

$$\beta = \frac{E_\theta}{\rho}\left(1 - \frac{\cosh(\alpha\theta)}{\cosh(\alpha\theta_w)}\right)$$

Thus, $T_b(y,\theta)$ becomes

$$T_b(y,\theta) = \frac{E_\theta}{\rho}\left(1 - \frac{\cosh(\alpha\theta)}{\cosh(\alpha\theta_w)}\right) y \tag{38}$$

The longitudinal energy per unit width is

$$U_\theta = \frac{1}{2}\int_A \frac{\left(T_b(y,\theta) + T(\theta)\right)^2}{E_\theta}\, dA \tag{39}$$

where $dA = r \cdot d\theta \cdot dy = (\rho + y) \cdot d\theta \cdot dy$. Next substitute Eq. 38 and Eq. 21 into Eq. 39, integrate over y and evaluate from $-\frac{t}{2}$ to $\frac{t}{2}$. The result is the longitudinal work done as a function of angle.

$$U_\theta(\theta) = \frac{1}{2\,E_\theta}\left[\begin{array}{l} \dfrac{E_\theta^2\,t^3}{12\,\rho}\left(1-\dfrac{\cosh(\alpha\theta)}{\cosh(\alpha\theta_w)}\right)^2 + \rho\,t\left(\dfrac{G_{r\theta}}{\alpha^2}\dfrac{\cosh(\alpha\theta)}{\cosh(\alpha\theta_w)}+C\right)^2 \\ + \dfrac{E_\theta\,G_{r\theta}\,t^3}{6\,\rho\,\alpha^2}\left(\dfrac{\cosh(\alpha\theta)}{\cosh(\alpha\theta_w)}-\left(\dfrac{\cosh(\alpha\theta)}{\cosh(\alpha\theta_w)}\right)^2\right) + \dfrac{E_\theta\,C\,t^3}{6\,\rho}\left(1-\dfrac{\cosh(\alpha\theta)}{\cosh(\alpha\theta_w)}\right) \end{array}\right] \quad (40)$$

Since the entire length of fiber is subjected to the maximum energy input during a bending cycle, the total work done will be calculated as the maximum energy (a constant) integrated over the remaining direction, θ. The maximum and minimum values of Eq. 40 can be found by differentiating Eq. 40 with respect to θ and solving for the value of θ where $dU_\theta/d\theta = 0$. The first derivative may be written as

$$\frac{d\left(U_\theta(\theta)\right)}{d\theta} = \frac{G\,t^3}{12\,\rho}\left(1-\frac{12\,\rho^2}{t^2}\right)\left(1-\frac{\cosh(\alpha\theta)}{\cosh(\alpha\theta_w)}\right)\left(\frac{\sinh(\alpha\theta)}{\cosh(\alpha\theta_w)}\right) \quad (41)$$

The derivative is zero at either $\theta = 0$ or $\theta = \theta_w$. The sign of the second derivative of $U_\theta(\theta)$ evaluated at $\theta = 0$ or $\theta = \theta_w$ determines whether U_θ is at either a maximum or minimum at $\theta = 0$ or $\theta = \theta_w$. The energy input, $U_\theta(\theta)$, is a maximum when the second derivative, evaluated at $\theta = 0$ or $\theta = \theta_w$, is negative and a minimum when the second derivative is positive. The second derivative may be written as

$$\frac{d^2\left(U_\theta(\theta)\right)}{d\theta^2} = \frac{G\,t^3}{12\,\rho}\left(1-\frac{12\,\rho^2}{t^2}\right)\left[\begin{array}{l} \left(1-\dfrac{\cosh(\alpha\theta)}{\cosh(\alpha\theta_w)}\right)\left(\alpha\dfrac{\cosh(\alpha\theta)}{\cosh(\alpha\theta_w)}\right) \\ + \left(-\alpha\dfrac{\sinh(\alpha\theta)}{\cosh(\alpha\theta_w)}\right)\left(\dfrac{\sinh(\alpha\theta)}{\cosh(\alpha\theta_w)}\right) \end{array}\right] \quad (42)$$

The sign of Eq. 42 depends on the ratio of $12\rho^2/t^2$. When $12\rho^2/t^2 < 1$, $U_\theta(\theta_w)$ is a maximum and when $12\rho^2/t^2 > 1$, $U_\theta(0)$ is a maximum. If $12\rho^2/t^2 = 1$ (or $t^2 = 12\rho^2$), then U_θ is independent of θ. Only cases where $12\rho^2/t^2 > 1$ are considered here and for $\theta = 0$, $d^2U_\theta/d\theta^2 < 0$ and $U_\theta(0)$ is a maximum. Substituting $\theta = 0$ into Eq. 40, integrating with respect to θ and evaluating from $-\theta_w$ to θ_w results in the total work done on the fiber segment by the longitudinal stress during one bending cycle.

$$U_\theta = \frac{\theta_w}{E_\theta}\left[\begin{array}{c} \dfrac{E_\theta^2 t^3}{12\rho}\left(1 - \dfrac{1}{\cosh(\alpha\theta_w)}\right)^2 + \rho t\left(\dfrac{G_{r\theta}}{\alpha^2}\dfrac{1}{\cosh(\alpha\theta_w)} + C\right)^2 \\ + \dfrac{E_\theta G_{r\theta} t^3}{6\rho\alpha^2}\left(\dfrac{1}{\cosh(\alpha\theta_w)} - \dfrac{1}{\cosh^2(\alpha\theta_w)}\right) + \dfrac{E_\theta C t^3}{6\rho}\left(1 - \dfrac{1}{\cosh(\alpha\theta_w)}\right) \end{array}\right] \quad (43)$$

The maximum energy density due to longitudinal stress is

$$\hat{U}_\theta = \frac{U_\theta}{2\rho\theta_w t}$$

$$\hat{U}_\theta = \frac{1}{2\rho t E_\theta}\left[\begin{array}{c} \dfrac{E_\theta^2 t^3}{12\rho}\left(1 - \dfrac{1}{\cosh(\alpha\theta_w)}\right)^2 + \rho t\left(\dfrac{G_{r\theta}}{\alpha^2}\dfrac{1}{\cosh(\alpha\theta_w)} + C\right)^2 \\ + \dfrac{E_\theta G_{r\theta} t^3}{6\rho\alpha^2}\left(\dfrac{1}{\cosh(\alpha\theta_w)} - \dfrac{1}{\cosh^2(\alpha\theta_w)}\right) + \dfrac{E_\theta C t^3}{6\rho}\left(1 - \dfrac{1}{\cosh(\alpha\theta_w)}\right) \end{array}\right] \quad (44)$$

To calculate the average amount of work done on fiber segment due to longitudinal stress, $\overline{U}_\theta$, integrate Eq. 40 with respect to θ and evaluate from $-\theta_w$ to θ_w. After simplifying, $\overline{U}_\theta$ is

$$\overline{U_\theta} = \frac{1}{2E_\theta}\left[\begin{array}{c} \frac{E_\theta^2 t^3}{12\rho}\left(2\theta_w - \frac{4}{\alpha}\frac{\sinh(\alpha\theta_w)}{\cosh(\alpha\theta_w)} + \frac{1}{\alpha}\frac{\sinh(\alpha\theta_w)}{\cosh(\alpha\theta_w)}\right) + \frac{\theta_w}{\cosh^2(\alpha\theta_w)} \\ + \rho t\left(\frac{G_{r\theta}^2}{\alpha^4}\left(\frac{1}{\alpha}\frac{\sinh(\alpha\theta_w)}{\cosh(\alpha\theta_w)} + \frac{\theta_w}{\cosh^2(\alpha\theta_w)}\right) + \frac{2G_{r\theta}C}{\alpha^3}\frac{\sinh(\alpha\theta)}{\cosh(\alpha\theta_w)} + 2C^2\theta_w\right) \\ + \frac{E_\theta G_{r\theta} t^3}{6\rho\alpha^2}\left(\frac{2}{\alpha}\frac{\sinh(\alpha\theta_w)}{\cosh(\alpha\theta_w)} - \frac{1}{\alpha}\frac{\sinh(\alpha\theta_w)}{\cosh(\alpha\theta_w)} + \frac{\theta_w}{\cosh^2(\alpha\theta_w)}\right) \\ + \frac{E_\theta t^3 C}{6\rho}\left(2\theta_w - \frac{2}{\alpha}\frac{\sinh(\alpha\theta_w)}{\cosh(\alpha\theta_w)}\right) \end{array}\right] \tag{45}$$

The average energy density due to longitudinal stress is

$$\widehat{\overline{U_\theta}} = \frac{\overline{U_\theta}}{2\rho\theta_w t} \tag{46}$$

Case 2

For the initial condition of $V(\theta_w) = 0$, start with Eq. 36, substitute $M_b(\theta) = E$, and proceed as in the first case. The maximum energy density for the Case 2 is

$$\widehat{U}_\theta = \frac{E_\theta}{2\rho^2} + \frac{C}{\rho} + \frac{C^2}{2E_\theta} \tag{47}$$

The other parameters may be calculated in the manner presented for Case 1.

Work Due to Transverse (r) Stresses

Case 1

The work due to the transverse stress for case with the initial condition of $M_b(\theta_w) = 0$ will be calculated first. The transverse stress (r-direction) on the fiber segment is F at the inner fiber surface and zero at the outer fiber surface. Assuming F decreases proportionally with distance, the average stress can be

approximated by one half the value of F at the inner surface. The work done on the fiber segment due to transverse stress, is

$$U_r = \frac{1}{2}\int_A \frac{\left(\frac{F}{2}\right)^2}{E_r}\,dA \tag{48}$$

$$U_r = \frac{1}{8}\int_A \frac{F^2}{E_r}\,dA$$

$$= \frac{1}{8}\int_{-\frac{t}{2}}^{\frac{t}{2}} \int_{-\theta_w}^{\theta_w} \frac{F^2}{E_r}\,dy\,(\rho + y).d\theta$$

After substituting Eq. 22 and integrating over y from $-\frac{t}{2}$ to $\frac{t}{2}$, and simplifying, the work done on the fiber segment due to transverse stress as a function of angle is

$$U_r(\theta) = \frac{t^3}{8\,\rho\,E_r}\left[G_{r\theta}^2\left(\frac{1}{\alpha^2}+1\right)^2 \frac{\cosh^2(\alpha\theta)}{\cosh^2(\alpha\theta_w)} + 2\,G_{r\theta}\left(\frac{1}{\alpha^2}+1\right)C\,\frac{\cosh(\alpha\theta)}{\cosh(\alpha\theta_w)} + C^2\right] \tag{49}$$

By inspection, Eq. 49 is a maximum setting $\theta = \theta_w$. The total work done on the fiber segment due to transverse stress during one bending cycle is $U_r(\theta_w)$ integrated with respect to θ and evaluated from $-\theta_w$ to θ_w.

$$U_r = \frac{\theta_w\,t^3}{4\,\rho\,E_r}\left[G_{r\theta}\left(\frac{1}{\alpha^2}+1\right) + C\right]^2 \tag{50}$$

The maximum energy density due to transverse stress is

$$\widehat{U}_r = \frac{U_r}{2\,\rho\,\theta_w\,t}$$

$$\widehat{U}_r = \frac{t^2}{8\,\rho^2\,E_r}\left[G_{r\theta}\left(\frac{1}{\alpha^2}+1\right)+C\right]^2 \tag{51}$$

To calculate the average work done on the fiber segment due to transverse stress, $\overline{U}_r$, integrate Eq. 49 with respect to θ and evaluate from $-\theta_w$ to θ_w. After simplifying, $\overline{U}_r$ is

$$\overline{U}_r = \frac{t^3}{8\,\rho\,E_r}\left[G_{r\theta}^2\left(\frac{1}{\alpha^2}+1\right)^2\left(\frac{1}{\alpha}\frac{\sinh(\alpha\theta_w)}{\cosh(\alpha\theta_w)}+\frac{\theta_w}{\cosh^2(\alpha\theta_w)}\right)\right]$$

$$\left[\quad +\frac{2\,G_{r\theta}\,C}{\alpha}\left(\frac{1}{\alpha^2}+1\right)\frac{\sinh(\alpha\theta_w)}{\cosh(\alpha\theta_w)}+2\,C^2\,\theta_w\right] \tag{52}$$

The average energy density due to transverse stress is

$$\widehat{\overline{U}}_r = \frac{\overline{U}_r}{2\,\rho\,\theta_w\,t} \tag{53}$$

Case 2

The maximum energy density due to transverse stress can be calculated for Case 2 where $V(\theta_w) = 0$ as shown in Case 1. The maximum energy density is

$$\widehat{U}_r = \frac{C^2\,t^2}{2\,E_r\,\rho^2} \tag{54}$$

The other parameter may be calculated in the manner shown in Case 1.

Work Due to Shear ($r\theta$) Stresses

Case 1

The work due to the shear stress for case with the initial condition of $M_b(\theta_w) = 0$ will be calculated first. The work done on the fiber segment, per unit width, due to the shear stresses in the $r\theta$–plane is

$$U_{r\theta} = \frac{1}{2}\int_A \frac{V^2}{G_{r\theta}}\,dA \tag{55}$$

$$U_{r\theta} = \frac{1}{2}\int_{-\frac{t}{2}}^{\frac{t}{2}}\int_{-\theta_w}^{\theta_w} \frac{V^2}{G_{r\theta}}\,dy\,(\rho + y)\,d\theta$$

After substituting Eq. 20 and integrating over y from $-\frac{t}{2}$ to $\frac{t}{2}$ and simplifying, the work done on the fiber segment due to the shear stress as a function of angle is

$$U_{r\theta}(\theta) = \frac{\rho\, G_{r\theta}\, t}{2\,\alpha^2}\,\frac{\sinh^2(\alpha\theta_w)}{\cosh^2(\alpha\theta_w)} \tag{56}$$

By inspection, Eq. 56 is a maximum setting $\theta = \theta_w$. The total work done on the fiber segment due to shear stress during one bending cycle is $U_{r\theta}(\theta_w)$ integrated with respect to θ and evaluated from $-\theta_w$ to θ_w.

$$U_{r\theta} = \frac{\theta_w\, \rho\, t\, G_{r\theta}}{\alpha^2}\,\frac{\sinh^2(\alpha\theta_w)}{\cosh^2(\alpha\theta_w)} \tag{57}$$

The maximum energy density due to shear stress is

$$\widehat{U}_{r\theta} = \frac{U_{r\theta}}{2\,\rho\,\theta_w\,t}$$

$$\widehat{U}_{r\theta} = \frac{G_{r\theta}}{2\,\alpha^2}\frac{\sinh^2(\alpha\theta_w)}{\cosh^2(\alpha\theta_w)} \tag{58}$$

To calculate the average work done on the fiber segment due to shear stress, $\overline{U}_{r\theta}$, integrate Eq. 56 with respect to θ and evaluate from $-\theta_w$ to θ_w. After simplifying, $\overline{U}_{r\theta}$ is

$$\overline{U}_{r\theta} = \frac{\rho\,G_{r\theta}\,t}{2\,\alpha^2}\left[\frac{1}{\alpha}\frac{\sinh(\alpha\theta_w)}{\cosh(\alpha\,\theta_w)} + \frac{\theta_w}{\cosh^2(\alpha\theta_w)}\right] \tag{59}$$

The average energy density due to shear stress is

$$\widehat{\overline{U}}_{r\theta} = \frac{\overline{U}_{r\theta}}{2\,\rho\,\theta_w\,t} \tag{60}$$

Case 2

For the second case with the initial condition of $V(\theta_w) = 0$, the shear stress is zero on the interval of $-\theta_w$ to θ_w and, thus, the energy density due to shear stress is zero.

Application of Energy Calculations

The equations developed above may be used to compare the relative amounts of energy put into the fiber by the three different modes of mechanical action associated with the *BR*. At some point during the treatment, since the fiber moves about the entire radius, every point along the fiber segment will be subjected to the maximum stress level of each mode. Thus, the comparisons

will be made using the maximum energy density of each mode. For the purposes of comparison, the equations for the total work done on the fiber ($\hat{U}_\theta$, $\hat{U}_r$, and $\hat{U}_{r\theta}$) from Case 1, where $M_b(\theta) = 0$, may be simplified. For cases where $\alpha > 1.9$, $\rho > 6.9$, and $\gamma > 0.001$ (all are at or near the minimums for their respective ranges), the following simplified equations ($\hat{U}^*_\theta$, $\hat{U}^*_r$, and $\hat{U}^*_{r\theta}$) approximate the complete equations with less than 5% difference.

Longitudinal mode

Case 1

$$\hat{U}_\theta = \frac{1}{2\rho t E_\theta}\left[\frac{E_\theta^2 t^3}{12\rho}\left(1 - \frac{1}{\cosh(\alpha\theta_w)}\right)^2 + \rho t\left(\frac{G_{r\theta}}{\alpha^2}\frac{1}{\cosh(\alpha\theta_w)} + C\right)^2\right]$$

$$\left[+ \frac{E_\theta G_{r\theta} t^3}{6\rho\alpha^2}\left(\frac{1}{\cosh(\alpha\theta_w)} - \frac{1}{\cosh^2(\alpha\theta_w)}\right) + \frac{E_\theta C t^3}{6\rho}\left(1 - \frac{1}{\cosh(\alpha\theta_w)}\right)\right] \quad (44)$$

$$\hat{U}^*_\theta = \frac{E_\theta t^2}{24\rho^2} + \frac{C^2}{2E_\theta} + \frac{C t^2}{12\rho^2} \quad (61)$$

For typical values of the elastic and geometric parameters, the first term in Eq. 61 dominates in determining the energy density due to longitudinal stress.

Case 2

$$\hat{U}_\theta = \frac{E_\theta}{2\rho^2} + \frac{C}{\rho} + \frac{C^2}{2E_\theta} \quad (47)$$

Transverse mode

Case 1

$$\widehat{U}_r = \frac{t^2}{8\,\rho^2\,E_r}\left[G_{r\theta}\left(\frac{1}{\alpha^2}+1\right)+C\right]^2 \tag{51}$$

$$\widehat{U}_r^* = \frac{t^2}{8\,\rho^2\,E_r}\left[G_{r\theta}^2 + C^2 + 2\,G_{r\theta}\,C\right] \tag{62}$$

For typical values of the elastic and geometric parameters, the first term in Eq. 62 dominates in determining the energy density due to transverse stress in the first case.

Case 2

$$\widehat{U}_r = \frac{C^2\,t^2}{2\,E_r\,\rho^2} \tag{54}$$

Shear mode

Case 1

$$\widehat{U}_{r\theta} = \frac{G_{r\theta}}{2\,\alpha^2}\,\frac{\sinh^2(\alpha\theta_w)}{\cosh^2(\alpha\theta_w)} \tag{58}$$

$$\widehat{U}_{r\theta}^* = \frac{t^2}{24\,\rho^2}\,E_\theta \tag{63}$$

Case 2

The energy density due to shear stress in the second case is zero.

The maximum energy densities for Case 1 are shown in Figs. 37–39 for sets of parameters giving low, medium, and high energy densities respectively. The plots were constructed using the full equations to calculate the energy

densities. In order to simplify the plotting of the results, two dimensionless variables are introduced. The first is the dimensionless variable γ which is defined as E_θ/E_r and the second is the dimensionless variable λ which is defined as ρ/t. In addition, the shear modulus, $G_{r\theta}$, is calculated using an modification of the relationship between extensional and shear modulus in isotropic materials. For isotropic materials, the shear modulus may be calculated from the extensional modulus and Poisson's ratio as

$$G = \frac{E}{2(1 + \upsilon)}$$

For orthotropic materials, E and υ may be replaced by suitable averages of the modulus and Poisson's ratios in the plane of the shear modulus[99]. Using these averages, the above formula can be written, using geometric means, as

$$G_{ij} = \frac{\sqrt{E_i E_j}}{2(1 + \sqrt{\upsilon_i \upsilon_i})}$$

For the case discussed here, this formula can be simplified to

$$G_{r\theta} = a\sqrt{E_\theta E_r} = a\sqrt{\gamma}\, E_\theta$$

where

$$a^{-1} = 2(1 + \sqrt{\upsilon_\theta \upsilon_r})$$

This insures that the values of $G_{r\theta}$ are reasonable with respect to E_θ and E_r.

Over the wide range of γ shown in Figs. 37–39, the longitudinal and shear energy densities are approximately equal and constant. The transverse energy density is substantially less than either of the other energy densities, but still constant over the range of γ. The simplified equations illustrate these results

analytically by showing that $\hat{U}^*_\theta$, $\hat{U}^*_r$, and $\hat{U}^*_{r\theta}$ are all proportional to E_θ. (This assumes that only the square of the first term in Eq. 62 is significant.) Increasing the value of E_θ by one order of magnitude increases the resulting energy densities by one order of magnitude (compare Figs. 37 and 39). This may be seen by comparing energy densities for similar cases of λ between each of the figures.

The ratio of bending radius to fiber thickness ($\lambda = \rho/t$) has a substantial effect on energy density. Increasing this ratio by less than an order of magnitude reduces the energy density by over two orders of magnitude. This is apparent in the analytical expressions (Eqs. 56–58) since energy density is inversely proportional to λ^2.

The longitudinal load applied at the ends of the fibers (T_w)has little effect on the results since the energies are mostly independent of C (if C is small), and hence, T_w. The expected value of T_w is about 10^6 Pa. As shown in Fig. 40, only when T_w is increased from $1\text{x}10^6$ to $1\text{x}10^9$ Pa, does the longitudinal energy increase significantly from 10^6 to 10^8 J/m^3. The transverse energy density, when T_w equal $1\text{x}10^9$ Pa, can vary from 10^7 J/m^3 at low values of γ to 10^5 J/m^3 at high values of γ. The shear energy density remains the same.

Only the transverse energy density is sensitive to variation of $G_{r\theta}$ (*i.e.* changes in a; see Fig. 41) with respect to E_θ and E_r, but since the transverse energy density is small relative to the other two, no significant differences in the fraction of energy input by the transverse mode results. This is illustrated in Fig. 41 by plotting energy density for the different modes *vs.* γ at several levels of a. The curves for the longitudinal and shear modes collapse into a single line while the curves for the transverse mode increase with increasing a. However, even at

the highest level of a considered, the transverse energy density is still only a small portion of the total.

The relative contributions of the modes can be compared using the fraction of the total energy density a given mode contributes. For constant E_θ and T_w, the variation in the fractions is small as γ and λ are varied over several orders of magnitude. In general, the contribution to total energy density by the longitudinal and shear modes ranges from 40 to 50% each with the remainder contributed by the transverse mode (10–20%).

The relative contributions of the modes in Case 2 are very different at in Case 1. The shear mode contribution is zero as a result of the chosen initial condition and the transverse contribution is many orders of magnitude below the longitudinal contribution. The model in Case 2 predicts that almost all the work done on the fiber will be by the longitudinal stress as the conditions approach pure bending. This may be seen by examining the ratio of energy densities for the longitudinal (Eq. 47) and transverse (Eq. 54) stresses.

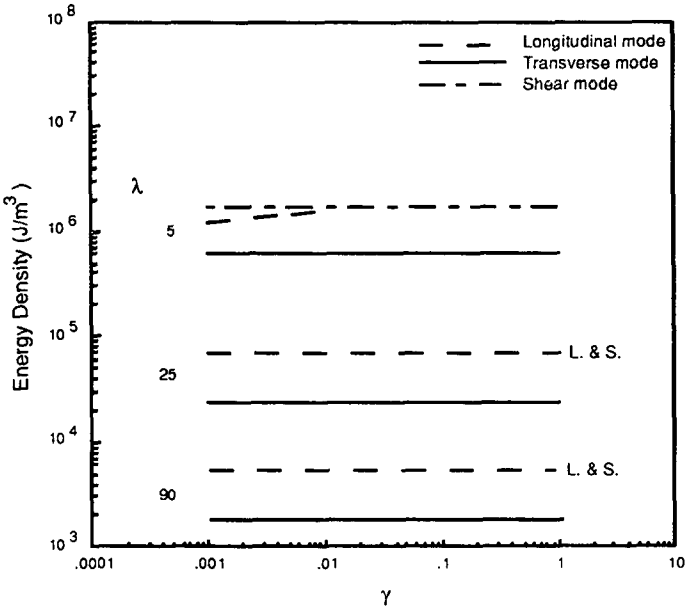

Figure 37. Energy density (Case 1) as a function of E_θ over E_r (γ) and of ρ over t (λ) for low energy density parameter set (E_θ = 1.0 GPa, T_w = 0.0 GPa).

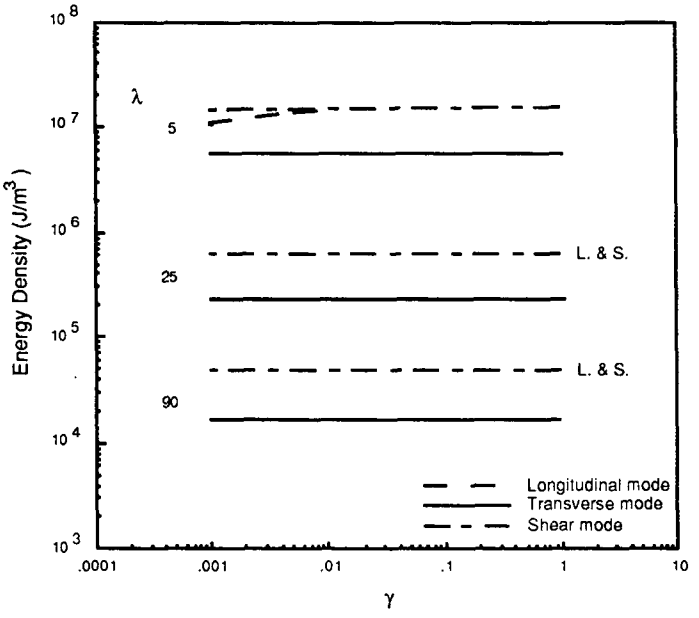

Figure 38. Energy density (Case 1) as a function of E_θ over E_r (γ) and of ρ over t (λ) for medium energy density parameter set (E_θ = 9.0 GPa, T_w = 0.0012 GPa).

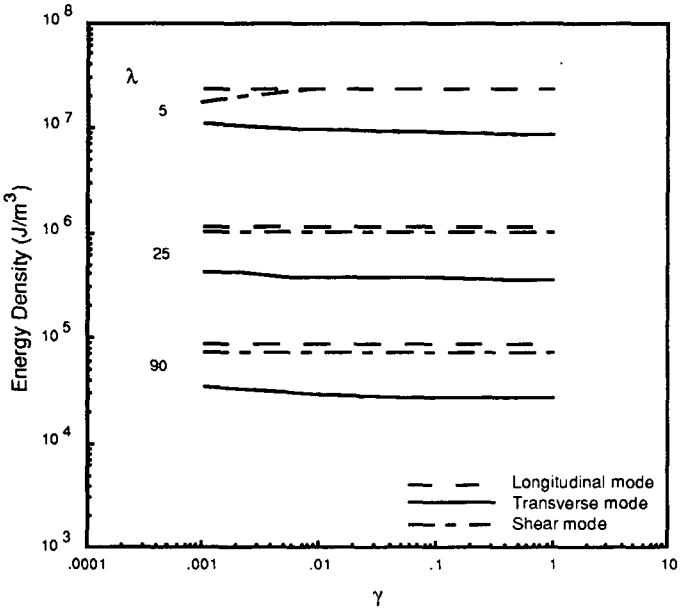

Figure 39. Energy density (Case 1) as a function of E_θ over E_r (γ) and of ρ over t (λ) for high energy density parameter set (E_θ = 14.0 GPa, T_w = 0.018 GPa).

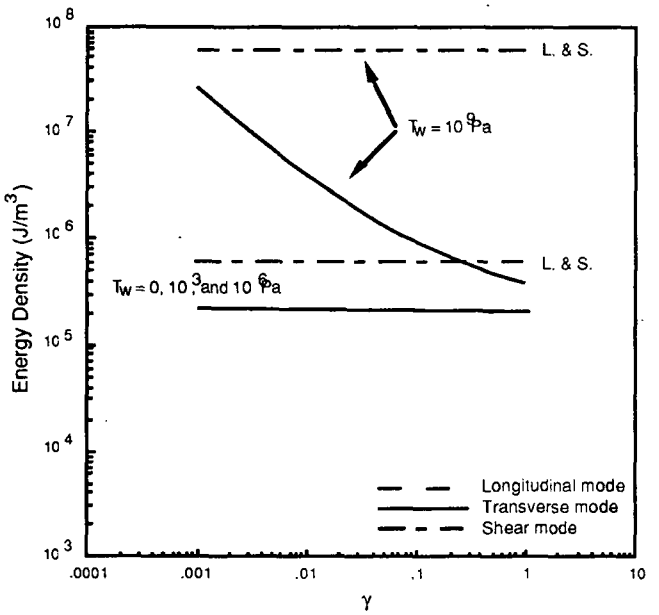

Figure 40. Energy density (Case 1) as a function of E_θ over E_r (γ) and of T_w for medium elastic parameter set (E_θ = 14.0 GPa).

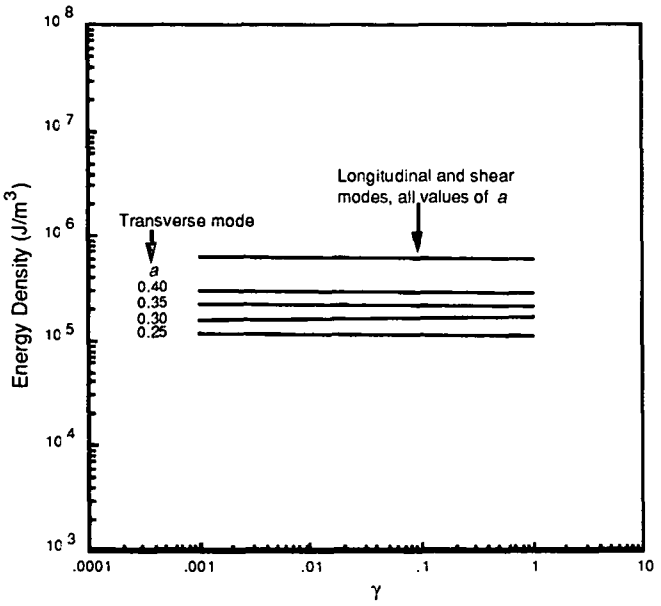

Figure 41. Energy density (Case 1) as a function of E_θ over E_r (γ) and of the coefficient a for medium energy density parameter set (E_θ = 9.0 GPa, T_w = 0.0012 GPa).

ROLL REFINER

During the treatment of pulp fibers in the Roll Refiner (*RR*), the fibers are subjected to the same in-plane and out-of-plane normal stresses and out-of-plane shear stresses in the refining zone as fibers in the Bending Refiner (*BR*). However, the magnitudes of these stresses and the work done on the fibers by the different modes are not the same. The purpose of this analysis is to estimate the amount of work done on the fibers by the out-of-plane compressive stress. In addition, the analysis developed by Hartman[79] to estimate the work done on the fiber will be reviewed and estimates for the conditions in these experiments made. The analysis is for a single, isolated fiber perfectly oriented in the direction of travel through the nip. The fiber is considered to be anisotropic with axial elastic modulus E_θ, transverse elastic modulus E_r, and shear elastic modulus $G_{r\theta}$. The cross section is uniform with fiber thickness t and unit width w.

Energy calculations

Elastic Theory Method

Th e calculation of the work due to the transverse stresses uses the maximum transverse stress the fiber encounters in the nip. An analysis of roll nips is presented by Peel and Hudson[100] for supercalender rolls. They treat the situation as a Hertz compression which assumes two stationary elastic cylinders are simply pressed together. As presented by Peel and Hudson, the Hertz compression equation relating the transverse stress, Z_z, in N/m^2 to the applied vertical line load, P, in N/m, the radius of the two rolls, R_1 and R_2, in m, and the distance from the nip center, y, in m is

$$Z_z = \frac{2P}{\pi b^2}\left(b_2 - y^2\right)^{\frac{1}{2}}$$

$$b^2 = \frac{4P}{\pi}\frac{R_1 R_2}{R_1 + R_2}\left(\frac{1-\nu_1^2}{E_1} + \frac{1-\nu_2^2}{E_2}\right) \qquad (64)$$

While is method does not account for the presence of a material in the nip formed by the two cylinders, it is still useful in estimating the maximum compressive stress to which a material in the nip could be subjected. The values of the various parameters of Eq. 81 and the calculated values of Z_z are shown in Table 12. Based on the maximum stress, Z_z, the work done on a length of fiber may be calculated from

$$U_r = \frac{1}{2}\int_V \frac{Z_z^2}{E_r}\,dV \qquad (65)$$

where the length is the same as in the BR calculation, $2\rho\theta_w$, The energy density, U_r/V, for several nip widths is shown in Table 13. The first entry, 33.0 MJ/m^3, is

the energy density based on the nip width and maximum stress calculated in the Hertz compression analysis. The other entries were calculated using arbitrarily wider nips and the average stress ($P/2b$) to estimate the effect of adding a material between the two rolls.

The energy density values of Table 13 plotted with the data of Fig. 38 are illustrated in Fig. 42. For the narrow and medium width nips, the energy density values are equal to or greater than the energy density values for *BR* calculations. Unless the actual nip width approaches 600 μm, the energy density for the transverse mode in the *RR* is equal to or greater than the longitudinal and shear mode energy densities in the *BR*.

Hartman's Method

Hartman[79] estimated the amount of work done on the fibers by considering the forces applied by the rolls and the distances traveled by the fiber mat. In general, the major contribution to total work was the net tangential force applied by the rolls on the fiber mat times the circumference of the roll times the number of revolutions. The oscillating motion of the top roll contributed a minor amount and this contribution is included in the calculation. The net tangential force was the difference between the horizontal force required to maintain the vertical alignment of the rolls with and without a fiber mat in the nip. His equation calculates energy per revolution put into the fiber mat in J/rev based on the tangential force, F_T, in kg_f.

$$U_l = \left[F_T \left(9.81 \frac{m}{sec^2} \right) \left(0.16\, \pi \frac{m}{rev} \right) \right] + \left(0.014 \frac{J}{rev} \right) \qquad (66)$$

To compare this result with the early estimates, the energy for 1 revolution is divide by the mass of fiber treated, m, in g, and multiplied by an assumed fiber density, ρ, equal to 1.5×10^6 g/m^3.

$$\widehat{U_l} = U_l \frac{\sigma}{m} \tag{67}$$

Due to the grooves in the top roll, only 40% of the fiber mat is treated on each revolution and thus the fiber mass is $m = f \cdot W \cdot w \cdot l$ where f is the fraction of the mat treated, 0.4, W is the basis weight, 50 g/m^2, w is the width of the mat, 0.105 m, and l is the length of the mat, 0.450 m. For the normal load applied to the roll, F_N = 12 kg$_f$, the tangential force, calculated from Hartman's calibration data, is F_T = 0.434 kg$_f$. The calculated energy density is 0.362 MJ/m^3.

SUMMARY

The analyses presented here for the *BR* and *RR* indicate that different modes of mechanical action predominate in the two refiners. For the *BR*, longitudinal tension and shearing in the longitudinal–radial plane contribute about 80% of the total energy input. The longitudinal and shear modes contribute 1.37 and 0.6 MJ/m^3 respectively. The *RR* energy density for the transverse mode is estimated to be 0.2 to 20 MJ/m^3 which is of the same magnitude or higher than the *BR* longitudinal and transverse energy densities.

This section derived equations which estimate the amount of energy put into à fiber segment by various stresses and strains in the Bending Refiner (*BR*) and Roll Refiner (*RR*). The results of this analysis support arguments made in the Results and Discussion section that the *BR* and *RR* produces fibers with different properties. The analysis presented here shows that the *BR* puts more energy into the longitudinal direction of the fiber than into the transverse

direction. Doing work mostly in the longitudinal direction is expected to modify the longitudinal properties of the fiber more that the transverse properties. The *RR* puts more energy into the transverse direction, through transverse compression, than into the longitudinal direction; the *RR* is expected to modify the transverse properties of the fiber more than the longitudinal properties.

Table 12. Results of Nip Width and Stress Calculations.

Roll Parameters	Brass	Steel
Radius	0.03 m	0.08 m
Stiffness	110 GPa	207 GPa
Poisson's Ratio	0.33	0.29
Nip load	2550 N/m	
Calculated Parameters		
Nip Width	60 μm	
Maximum Stress	0.0545 GPa	

Table 13. Results of Energy Density Calculations.
(E_r = 0.045 GPa, ρ_{cw} =1.5x10^6 g/cm^3)

Case	Nip Width (μm)	Stress (GPa)	Energy Density (MJ/m^3)
Max. Nip Stress	60	0.0545	33.0
Avg. Nip Stress	60	0.0428	20.1
	600	0.0043	0.201
	6000	0.0004	0.002
Hartman	n/a	n/a	0.362

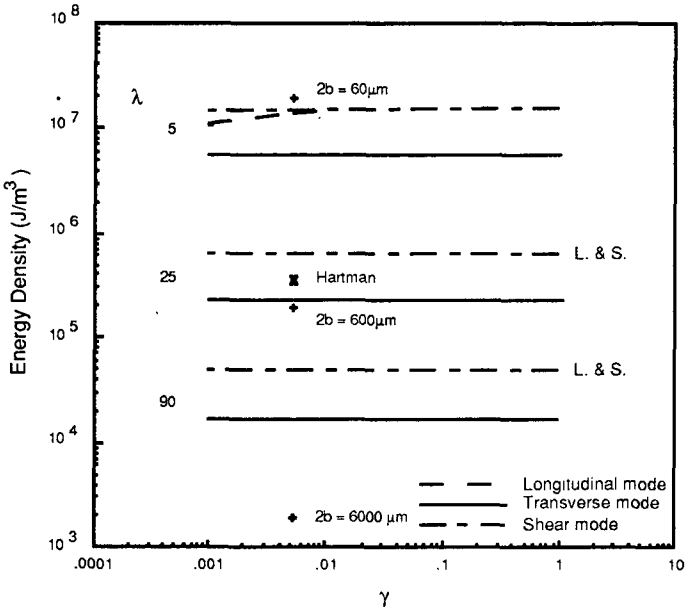

Figure 42. *BR* energy density (Case 1) as a function of E_θ over E_r (γ) and of ρ over t (λ) for medium energy density parameters (E_θ = 9.0 GPa, T_w = 0.0012 GPa) and *RR* energy density as a function of nip width (2b).

RESULTS AND DISCUSSION

This section describes the effects of the Bending Refiner and Roll Refiner on fiber length, fiber strength, fiber-fiber bonding, and handsheet elastic properties and presents possible explanations for the differences between the Bending Refiner and Roll Refiner. The specimen designation nomenclature is defined in Table III of the Experimental Program section and the experimental data are presented in tabular form in Appendices III through V for the physical, elastic, and fiber length data, respectively. The experimental data are presented in graphical form in Appendices VI and VII for the physical and elastic data, respectively.

EFFECT OF PREPARATION PROCEDURES

The preparation procedures included screening pulp samples to remove fines, adding fines to pulp samples, and forming fiber mats in the Formette Dynamique. However, the preparation procedures for the Bending Refiner (*BR*) and Roll Refiner (*RR*) specimens were different from those used for the PFI mill (*PM*) specimens. The *BR* and *RR* procedures included processing in the Formette Dynamique to form the oriented fiber mats, whereas, the *PM* specimens did not. The effect of this extra treatment was measured using a group of control specimens. The effect of screening and adding fines is also measured using specimens in the control group. The control specimens consisted of handsheets made from control pulp samples which were either untreated, screened, or formed into wet mats. In addition, control specimens were formed from screened or Formette treated control pulp samples to which PFI mill fines had been added.

The percentage change in the control handsheet properties and the control pulp fiber lengths and fines contents, relative to the pulp without the treatment,

are given in Table 14 for the screening and mat forming treatments. The first column represents the effect of screening and the second and third columns represent the effect of treatment in the Formette. The second and third columns are for normal and high fines contents, respectively.

Statistical analysis of the data on which Table 14 is based indicates that properties differing by more than 15% are significantly different (exceptions are tear factor and C_{66}/ρ). When the specimens were screened (Table 14, first column represents C–U/N *vs.* C–U/L), the only property affected was bonding index (and possibly tear factor and C_{66}/ρ). The changes in physical and elastic properties are the result of removing fines and agitating the fibers during the screening process. However, the effects of removing fines and agitating the fibers are small and, in general, screening does not significantly affect the length of individual fibers.

The comparison of untreated and Formette treated specimens (Table 14, second column represents C–U/N *vs.* C–F/N), shows significant differences for tensile index, bonding index, tear factor, in-plane stiffness, and out-of-plane shear stiffness (and possibly for compressive index and in-plane shear stiffness), and fines content. Note that no significant differences in densities or scattering coefficients exist and that treatment in the Formette removes fines from the untreated sample. The addition of fines to untreated and Formette treated specimens reduces the differences for all properties except scattering coefficient and fines content.

In this comparison, C–U/H *vs.* C–F/H, only the zero span tensile index, bonding index, tear factor, and fines content differ significantly. The difference in zero span tensile index is less than 13% and the difference in bonding index

and tear factor are much less than the differences between the normal fines content specimens. The higher level of fines in the Formette treated pulps could result from Formette treatment allowing more fines to be retained during handsheet formation. However, this is contradicted by a small decrease in density. The conclusion drawn from these comparisons is that treatment in the Formette has a small, but significant effect and this effect can be masked when fines are added.

The differences due to adding fines to untreated and Formette treated samples are shown in Table 15. The addition of fines significantly increases all properties except zero span tensile index, scattering coefficient, and fiber length. Since zero span tests mostly measure fiber strength, adding fines to samples would not be expected to increase fiber strength and, thus, not increase zero span tensile index. The increases in the other properties as the density increases is normally attributed to increases in bonding. However, the scattering coefficient does not increase and this indicates that bonded area is not increasing. The conclusion based on these comparisons is that adding fines to the untreated and Formette treated samples increases the physical and elastic properties by increasing the density and the strength of the fiber-fiber bonds without increasing the bonded area.

EFFECT ON FIBER LENGTH

In calculating the average fiber length of pulp samples, the average fiber length weighted by weight is used instead of either the arithmetic average fiber length or the average fiber length weighted by length. The arithmetic and length weighted averages are strongly influenced by the very short fibers which is inappropriate in this situation since the short fiber fraction and fines contents of the specimens can vary due to screening and adding fines. The weight weighted

average reduces the influence of the short fibers to an appropriate level. The weight weighted average fiber length is defined as

$$\text{Weight Weighted Average} = \frac{\sum_{i=n}^{n} n_i l_i^3}{\sum_{i=n}^{n} n_i l_i^2}$$

where n is the number of fibers in fiber length class i, and l is the average fiber length of class i. The control samples indicate that mild agitation of the fibers will slightly increase the average fiber length. This is the case when fines are either added or removed.

Table 14. Control Specimen Comparisons – Treatments.

	Percent Difference		
Property	Effect of Screening	Effect of Formette with Normal Level of Fines Content	Effect of Formette with High Level of Fines Content
Density	0.6	2.6	-0.4
Scattering Coeff.[b]	-4.5	-5.2	-10.6
Tensile Index	-11.3	29.6[a]	6.5
Z.S. Tensile Index	9.3	-14.3	-12.9[a]
Bonding Index	-24.5[a]	54.1[a]	21.8[a]
Compressive Index[b]	-13.1	27.6	1.2
Tear Factor	67.9	103.7[a]	31.8[a]
C_{11}/ρ	5.9	24.3[a]	1.9
C_{66}/ρ	-34.9	-22.8	1.7
C_{33}/ρ	-10.9	10.9	-0.8
C_{44}/ρ	1.1	17.8[a]	-6.1
Fiber Length[b]	4.6	6.7	2.1
Fines Content[b]	-35.1	-29.2	34.1

[a]Property which is significantly different (t-test, 95% confidence level).

[b]No statistical comparison made.

Table 15. Control Specimen Comparisons – Fines Contents.

Property	Percent Difference: Effect of Adding Fines to Untreated Pulp	Percent Difference: Effect of Adding Fines to Formette Treated Pulp
Density	36.6[a]	31.9[a]
Scattering Coeff.[b]	4.5	-1.5
Tensile Index	203.1[a]	140.8[a]
Z.S. Tensile Index	7.8	3.9
Bonding Index	178.1[a]	113.8[a]
Compressive Index[b]	159.7	107.2
Tear Factor	208.7[a]	93.2[a]
C_{11}/ρ	85.9[a]	288.2[a]
C_{66}/ρ	95.7[a]	59.6[a]
C_{33}/ρ	184.9[a]	154.9[a]
C_{44}/ρ	154.4[a]	102.8[a]
Fiber Length[b]	2.5	-2.0
Fines Content[b]	98.3	85.8

[a]Property which is significantly different (*t*–test, 95% confidence level).

[b]No statistical comparison made.

The *BR* and *PM* have a small effect on the average fiber length (see Fig. 45). The *RR* data does not show a trend. During early stages of treatment in the *PM*, the fibers lengthen. The initial increase in fiber length is due to the removal of curl and dislocations from the fiber[12,92]. At the higher levels of treatment, the average fiber length is decreased by either cutting fibers, curling fibers, or by increasing the amount of fines without necessarily reducing fiber length.

The *BR* creates few fines (see Fig. 46) and any decrease in the average fiber length with additional refining is probably due the increased fines. This is very likely in the specimens which had *PM* fines added (see discussion below). The *BR* and *RR* treatments probably remove kinks and dislocations from the fibers at low treatment levels and it is unlikely that further treatment would place either

back into the fibers. Any fiber cutting in the *BR* and *RR* would probably be due to the failure of the fiber at cell wall defects or ray crossings from repeated straining. The two mechanism may balance each other in affecting the average fiber length.

The creation of fines by the *PM* during treatment is illustrated in Fig. 46 and shows fines content to be proportional to the level of treatment.

The specimens with normal fines content (specimens which were neither screened nor had fines added) which were formed into mats using the Formette had fines contents lower than the untreated samples (see Fig. 46). This is due to a loss of fines during processing in the Formette. The *BR* and *RR* specimens with high fines contents had equal amounts of *PM* fines added, but did not retain similar amounts of fines. The explanation for this may be that the lower treatment levels in the *BR* or *RR* produce fibers that are less flexible producing a more open mat during the dewatering step which allows more fines to be removed from the mat. At the higher treatment levels, a more closed mat or fibers with external fibrillation retain more fines during dewatering. For whatever reason, the fines levels are different among the *BR* and *RR*, samples and these differences need to be considered when analyzing the handsheet properties.

The average fiber length is not significantly reduced by the *BR* or *PM*, and at low to medium levels of treatment, the average length may increase. Only the *PM* creates significant amounts of fines, which probably result from removal of the outer layers of the cell wall. Since the *BR* and *RR* create few fines, much of the outer cell wall layer (S_1) is probably intact.

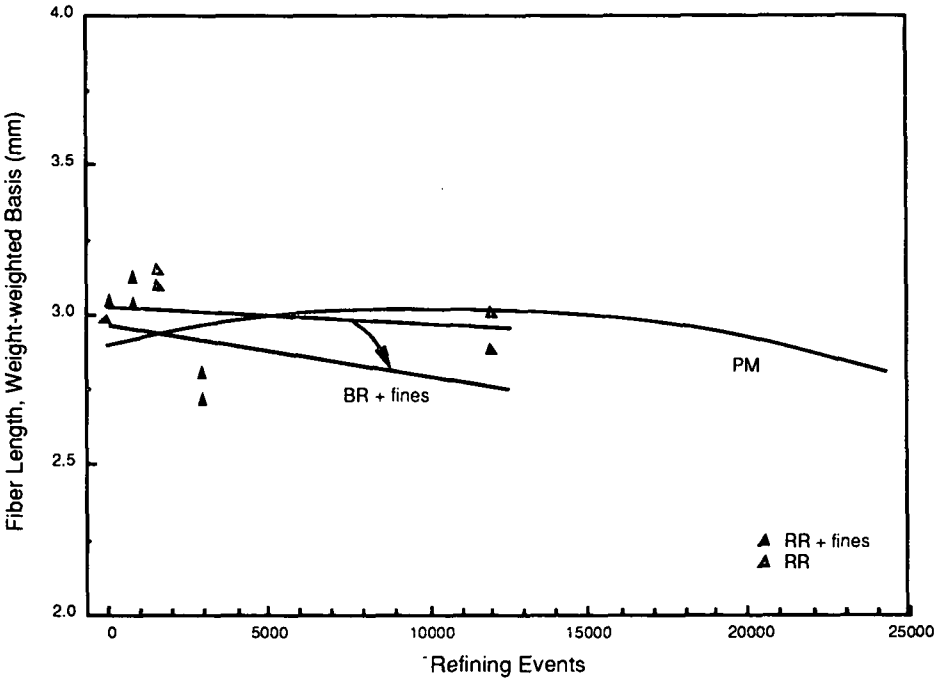

Figure 45. *BR*, *RR*, and *PM* weight weighted average fiber length *vs.* treatment level.

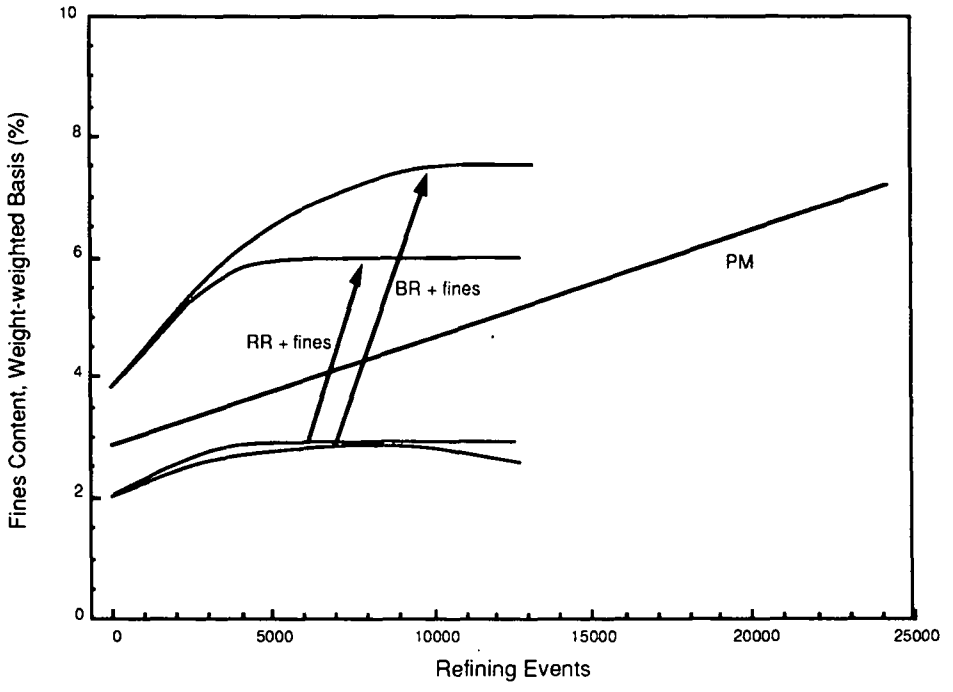

Figure 46. *BR*, *RR*, and *PM* weight weighted average fines content *vs.* treatment level.

EFFECT ON FIBER STRENGTH

The zero-span tensile index data for the specimens are illustrated in Figs. 47 and 48. The low amounts of disintegration used before handsheet forming did not completely remove all of the fiber flocs from the pulp samples which caused fair to poor handsheet formation. The *RR* specimens had very poor formation because the *RR* produced a more compacted fiber mat during treatment. The highly compacted mats did not disintegrate as completely as the *BR* or *PM* samples. The result was poor formation or large variations of the basis weight within a handsheet. The large variations in basis weight gave large variations in zero-span tensile index within a handsheet since the index is based on the average basis weight and not the local basis weight of the region were the measurement was made. The large variation within the handsheets leads to variations between handsheets because only a limited number of measurements could be made on each handsheet.

The zero span tensile index increases with refining and with decreasing fines content (see the *PM* results in Appendix III). Alexander and co-workers[38] provide evidence that refining increases the strength of the fibers by lowering the fibril angle of the S_2 cell wall layer, which would be expected to increase zero-span tensile index. Normally, zero span tensile measurements are considered to reflect fiber properties as opposed to network properties. However, to the extent that consolidation and bonding can make more fibers participate in load bearing, increased bonding can increase zero-span tensile index. The increase in zero-span tensile index as fines content decreases appears contradictory to the expectation that the zero-span tensile strength will increase with increased bonding. This contradiction is resolved by noting that when compared at equal grammage, sheets containing fewer fines contain more fibers. The larger

number of fibers increases zero-span tensile index more than the lack of fines decreases the bonding.

The maximum level of zero-span tensile index developed in the *BR*, 80 N·m/g, is at 6000 RE and normal fines content (*i.e.* few fines). The *BR* maximum is equivalent to the highest *PM* value (75 N·m/g at 24000 RE), but develops at a much lower level of treatment. Additional treatment in the *BR* (with normal fines content) decreases zero-span tensile index to a level below the *PM* at 12000 RE. The addition of fines to the *BR* specimens decreases the zero-span tensile index to the levels developed by the *PM* when compared at equal densities, but the *BR* values are still higher than the *PM* values when compared at equal treatment levels. The development of zero-span tensile index by the *BR* is likely the result of increased fiber strength since the *BR* does not develop bonding in the sheets (as shown later). The reason for the decrease in zero-span tensile index from the highest *BR* treatment level with additional treatment is unclear, but may be the result of fatigue.

The *RR* zero-span tensile index values are greater than the *PM* values when compared at equal treatment levels, but are the same or lower when compared at equal densities. The *RR* zero-span values are always lower than the *BR* zero-span tensile index. The maximum zero-span tensile index for the *RR* is the normal fines content specimen subjected to 6000 RE.

The *BR* develops zero-span tensile index to higher levels at lower amounts of treatment than the *RR* or *PM*. If in all three specimen groups, zero-span tensile index is a good indicator of fiber tensile strength, then the *BR* is better at developing fiber strength than the *RR* or *PM* when compare at equal treatment levels or sheet densities.

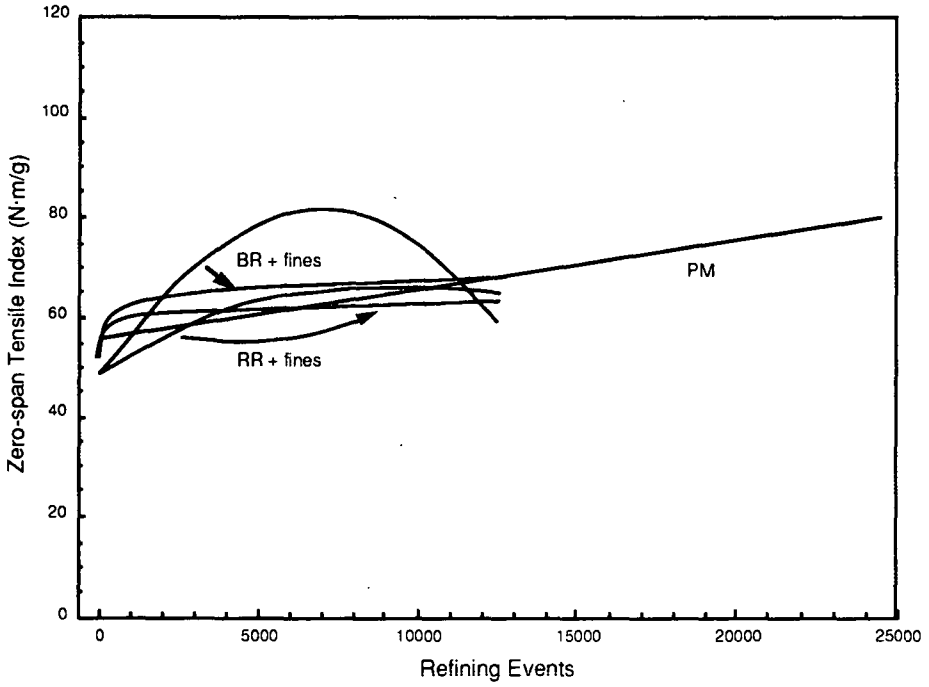

Figure 47. *BR*, *RR*, and *PM* zero span tensile index *vs.* treatment level.

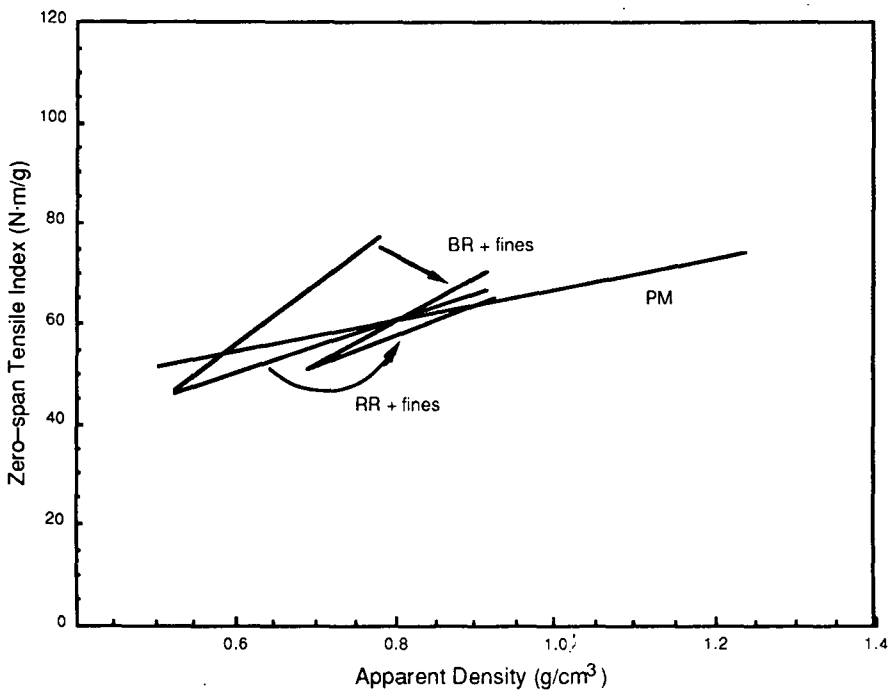

Figure 48. *BR*, *RR*, and *PM* zero span tensile index *vs.* handsheet density.

The compressive index results are shown in Figs. 49 and 50. The *PM* initially increases compressive index with refining and then levels off at higher levels of treatment or sheet density. The compressive index is higher at higher levels of fines and density. The leveling off of compressive index may indicate that the maximum compressive strength of the fibers is limiting since the network is well bonded at the higher levels of refining. Evidence of this is can be seen in Fig. 50 at the higher levels of density where increasing density produces no corresponding increase in compressive index.

The *BR* develops higher compressive index than the *RR* at equal treatment levels and densities. However, the *BR* developed the compressive index very early and fails to increase compressive index with increasing treatment. The *RR* appears to be slowly developing compressive index with increasing treatment, but since it starts at a very low level, the amount of treatment required to develop compressive index to the level of the *PM* is probably very high. The addition of fines to fibers subjected to either apparatus increases the compressive index by 50-100%. At equal densities, the *BR* develops compressive index to the same level as the *PM* or higher. The *RR* is capable of this only when fines are added.

A model of compressive strength in terms of elastic stiffnesses has been developed by Habeger and Whitsitt[78]. In general, the model predicts that the sheet compressive strength should correlate with the product of $C_{11}^{2/3}.C_{55}^{1/6}.C_{33}^{1/6}$. The experimental data are presented in this manner in Fig. 51 with compressive index plotted against the product of the mass specific stiffnesses. The *BR* and *PM* data are equivalent while the *RR* data does not develop equivalent compressive index at the same level of $C_{11}^{2/3}.C_{55}^{1/6}.C_{33}^{1/6}$.

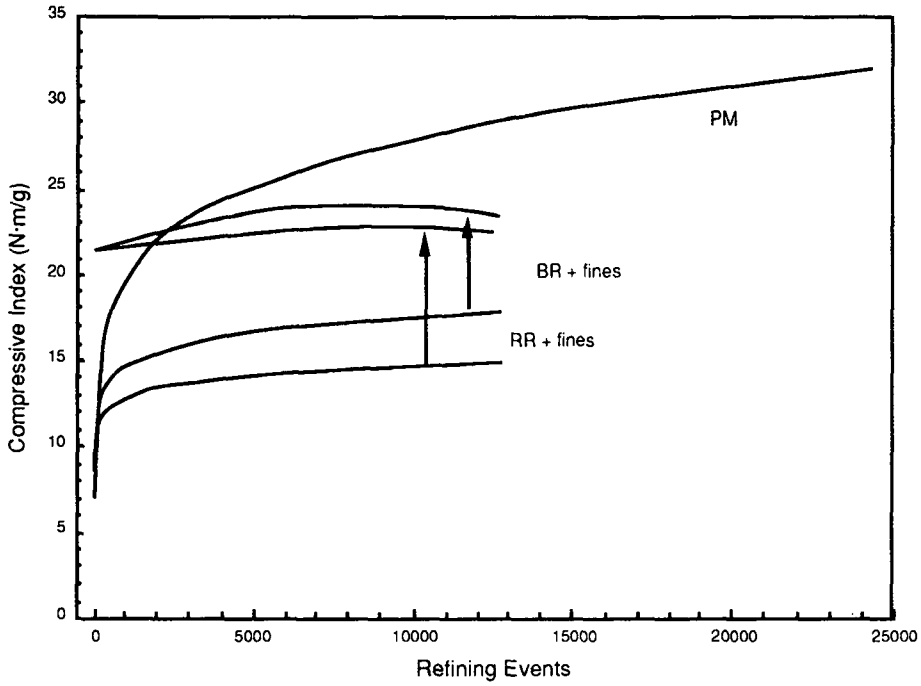

Figure 49. *BR*, *RR*, and *PM* compressive strength index *vs.* treatment level.

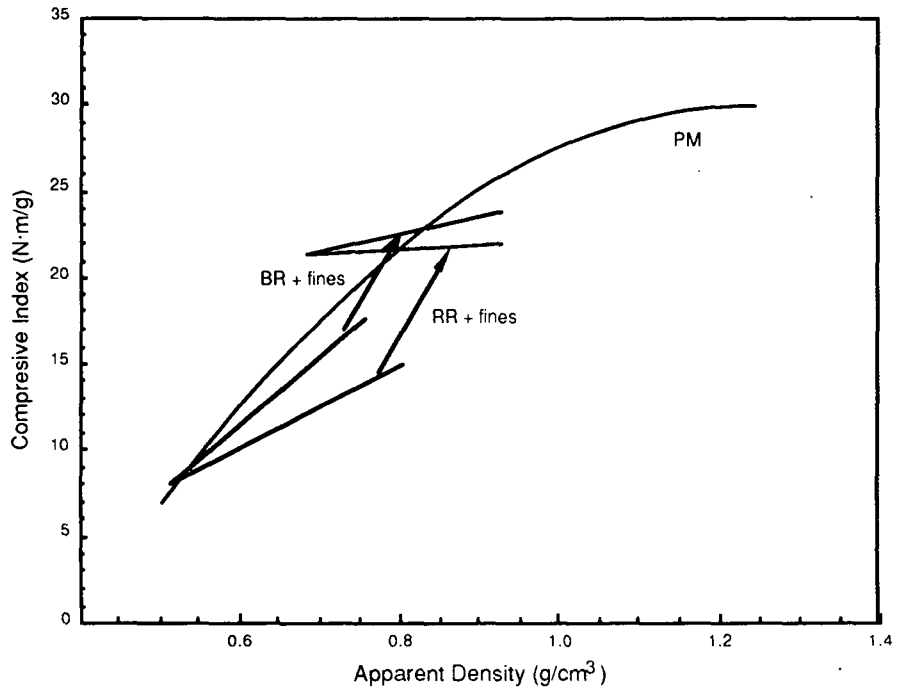

Figure 50. *BR*, *RR*, and *PM* compressive strength index *vs.* handsheet density.

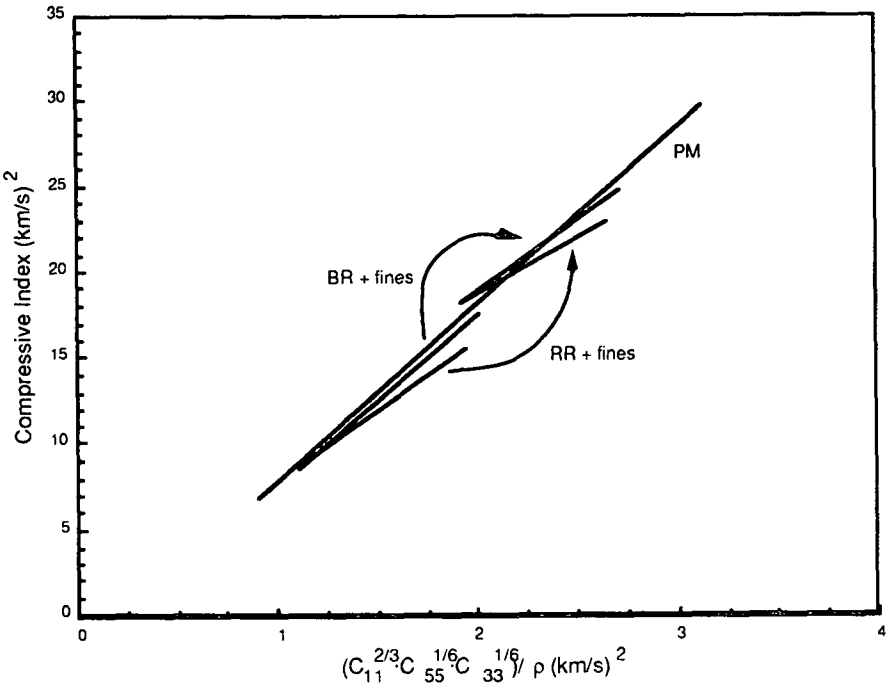

Figure 51. *BR*, *RR*, and *PM* compressive strength index *vs.* $C_{11}^{(2/3)} \cdot C_{55}^{(1/6)} \cdot C_{33}^{(1/6)}$.

EFFECT ON FIBER-FIBER BONDING

High densities and low scattering coefficients indicate sheets which are well bonded. Refining in the *PM* produces pulps with fibers which have more flexibility along their longitudinal axis[46], have more collapsed cross sections[101,102], and have higher fines contents and external fibrillation (see fines contents results above). These three effects combine to produce higher consolidation forces and larger bonded areas. The higher consolidation forces are partially a result of the increased fines content. The larger bonded areas come from the increase in fiber width which occurs as fiber cross sections collapse, and the higher flexibility in the axial direction (which allows fibers to better conform to or wrap about one another).

A second consequence of generating fines is the removal of the S_1 layer of the cell wall. During refining, the cell wall can become partially delaminated. A preferential plane of delamination is the S_1–S_2 boundary. This plane is weaker that the planes within either layer because of the change in fibril angle from high (in the S_1) to low (in the S_2). If the S_1 layer remained intact, this delamination could be a zone of weakness in the fiber after the sheet is formed. If refining generates fines by removing the S_1 layer, the zone of weakness would not be present and the fines would increase the consolidate forces. (Also note that mass specific fiber axial tensile strength will probably increase as the S_1 layer is removed since the S_1 layer has a lower mass specific tensile strength that the fiber average.)

The development of apparent density by the *BR* and *RR* is shown in Fig. 52. The response produced by the *PM* using the high bar loading with normal fines content is included for comparison. The *BR* and *RR* are equally effective in developing moderate levels of density. At low levels of treatment, the *BR* and *RR* increase density significantly over the control samples, but additional increases in density develop slowly with additional treatment. The addition of fines has a larger effect than additional treatment on the development of density. This is made apparent by comparing the normal fines content, high treatment level specimens with the high fines content control group specimen. The addition of fines to the *BR* and *RR* specimens increase density to the same level for both apparatuses when compared at equal treatment levels (see Fig. 52). The increase in density from the addition of fines is expected based on the explanation of Giertz[67] presented in the Background section. Giertz suggests that when more fines are present, more meniscuses will form during the sheet

consolidation processes. This leads to a higher compacting force which creates a higher relative bonded area, and, thus, higher sheet densities.

The development of scattering coefficient by the *BR* and *RR*, a good indicator of bonded area, is opposite to the response of density. As shown in Fig. 53, both the *BR* and *RR* develop the same level of scattering coefficient when compared at equal treatments level at either the normal or high fines contents. Both the *BR* and *RR* initially reduce scattering coefficient, but do not further decrease scattering coefficient with increasing treatment. The result of adding fines is to decrease scattering coefficient; however, the effect is not as large for scattering coefficient as it is for density.

While the develop of density and scattering coefficient by the *BR* and *RR* indicates that the level of bonding increases, the specimen do not become well bonded, even with high fines content. This can be seen in Fig. 54 where apparent density is plotted against scattering coefficient. The normal fines content specimen produce neither high densities nor low scattering coefficients (high bonded areas). For the high fines content specimens at a given level of density, the *BR* and *RR* produce sheets with higher scattering coefficients (and, thus, lower bonded area) than the *PM*. Assuming the *PM* produces well bonded sheets, the significantly lower bonded areas at the same densities indicated that the *BR* and *RR* sheets are poorly bonded.

The failure of the *BR* and *RR* to develop high densities indicates that some of the three effects (fiber flexibility, fiber collapse, and fines/external fibrillation) described above are small. The results of Tam Doo and Kerekes[46] show that longitudinal flexing, as in the *BR*, increases the fiber longitudinal flexibility. Further, they show that small amplitude flexing creates fibers which are more flexible than fibers subjected to an equivalent number of flexings in a

PM (see Background section and Appendix II). For the *BR*, the initial increase in density is attributed to an increase in the fiber flexibility. Further treatment and additional increase in fiber flexibility does not appear capable of developing density to the *PM* levels. The effect of the *RR* on fiber flexiblity is not known.

The large increase in density when fines are added to *BR* and *RR* pulp samples indicates that the apparatuses generate few fines. (This is supported by the results of the fiber length and fines content measurements presented above.) In addition, the apparatuses do not cause external fibrillation on the fiber surfaces. If this were the case, fines would be an expected "by-product" of external fibrillation. Since few fines are present in the pulp samples, significant external fibrillation is assumed not to occur.

This was confirmed by examining critical-point dried *BR* and *RR* fibers in the scanning electron microscope (*SEM*). Critical-point dried fibers do not experience the consolidation forces described above. Thus, the fibers do not have the lumen and cell wall delaminations collapse or have the external fibrillation collapse and bond to the fiber surface during drying. The critical-point dried state of the fiber is representative of wet state. The photomicrographs of critical-point dried fiber in Fig. 55 can be used to illustrate these points. In in Fig. 55a, the untreated and Formette treated fibers do not exhibit external fibrillation and the *BR* and *RR* fibers in Fig. 55b show very little. However, both the low and high intensity PFI mill treated fibers shown in Fig. 55c have substantial external fibrillation.

The fibers subjected to both the *BR* and *RR* are collapsed as they repeatedly pass over the radius of curvature or through the roll nip. In the Theoretical Analysis section, Eqs. 39 and 81 were developed to predict the transverse stress in the fiber during treatment in the *BR* and *RR*, respectively. The equations predict

maximum stresses on the order of 10^7–10^9 Pa. Measurement of the stress necessary to collapse fibers from a similar pulp were made by Berger[103] and are on the order to 10^6 Pa. During treatment in the *BR* or *RR*, the regions of the cell wall parallel to the direction of displacement are placed under significant shear stresses (see Fig. 56). In these regions, the fiber stiffness is probably reduced to a small value. These regions would then form "hinges" on opposite sides of the fiber. However, this does not assure that the fibers will be completely collapsed in the handsheet. Since the fiber mats are slurried before handsheet forming, and probably expand back to a circular cross sections, the "hinges" will not necessarily have the same orientation with respect to the *MD–CD* plane of the handsheet during sheet consolidation (see Fig. 56). Thus, the fibers may not collapse as easily or as completely as if the "hinges" maintained their original orientation.

The *SEM* photomicrographs of *BR* and *RR* handsheet cross sections in Fig. 57 provide some insight into the degree of fiber collapse. In general, the *BR* handsheets (Fig. 57a is typical) appeared to have more uncollapse lumens than the *RR* handsheets (Fig. 57b is typical). When the lumens were collapsed in the *BR* handsheets, a line delineating the boundary of the two S_3 layers was often still visible. In the *RR* handsheet, this delineation was not present as often. The conclusion drawn from these observations was that the fibers subjected to the *BR* do not collapse as completely as those subjected to the *RR*.

Hartman[81] was capable of developing the density of *RR* specimens to the levels produced by 40 min. of treatment in a Valley beater (see Fig. 22 in the Background section). He subjected mats to 500 revs. (200 RE) at a nip load of 6.1 kN/m (compared to 2.6 kN/m used in these experiments) and added fines (16% of final sheet weight on an oven dry basis). Thus, it appears Hartman, at least in

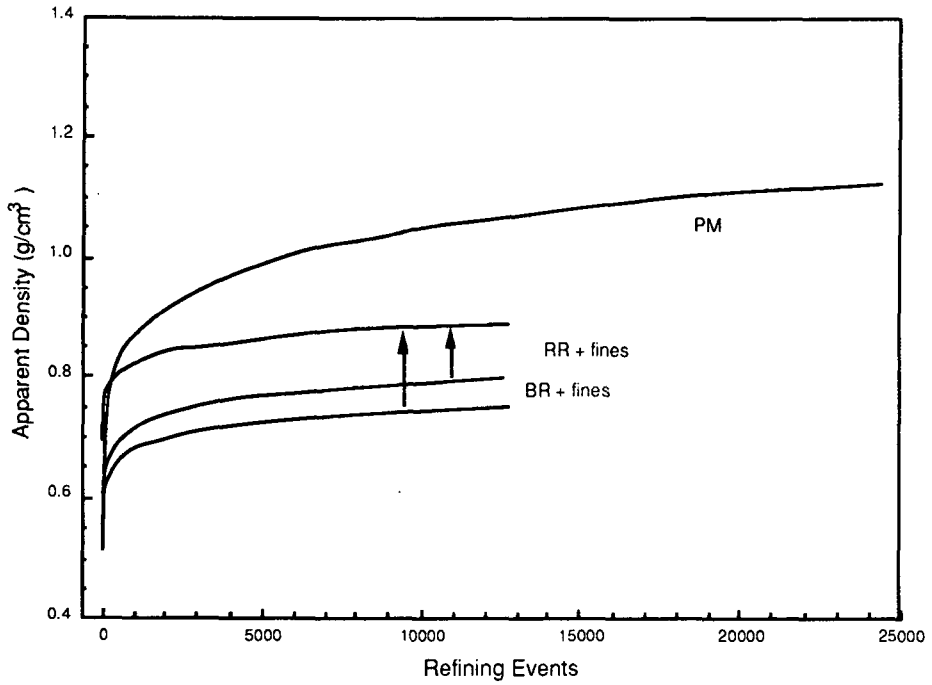

Figure 52. *PM*, *BR*, and *RR* apparent density *vs.* treatment level.

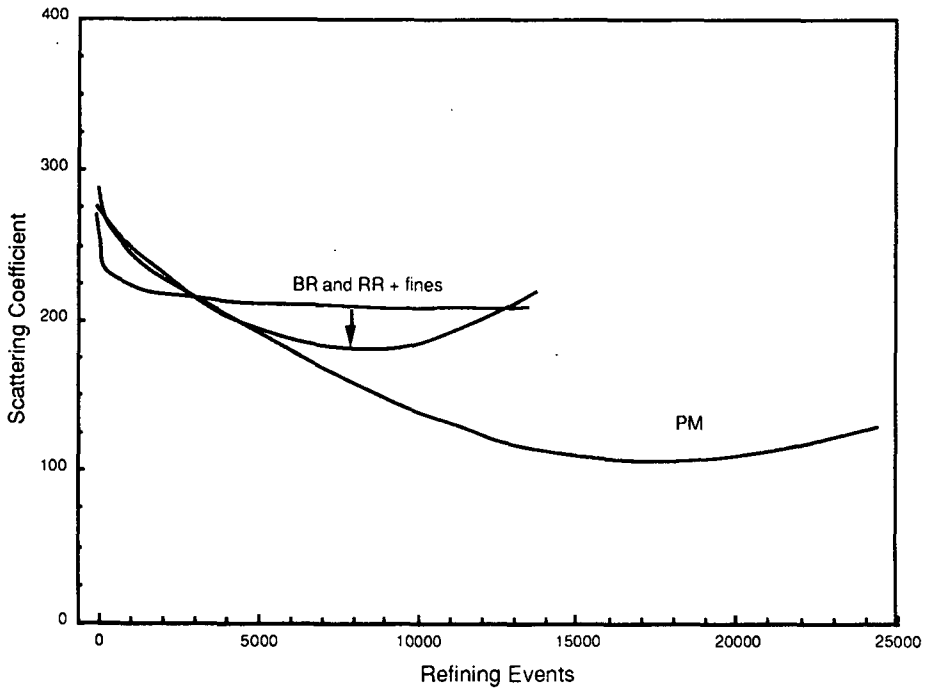

Figure 53. *PM*, *BR*, and *RR* scattering coefficient *vs.* treatment level.

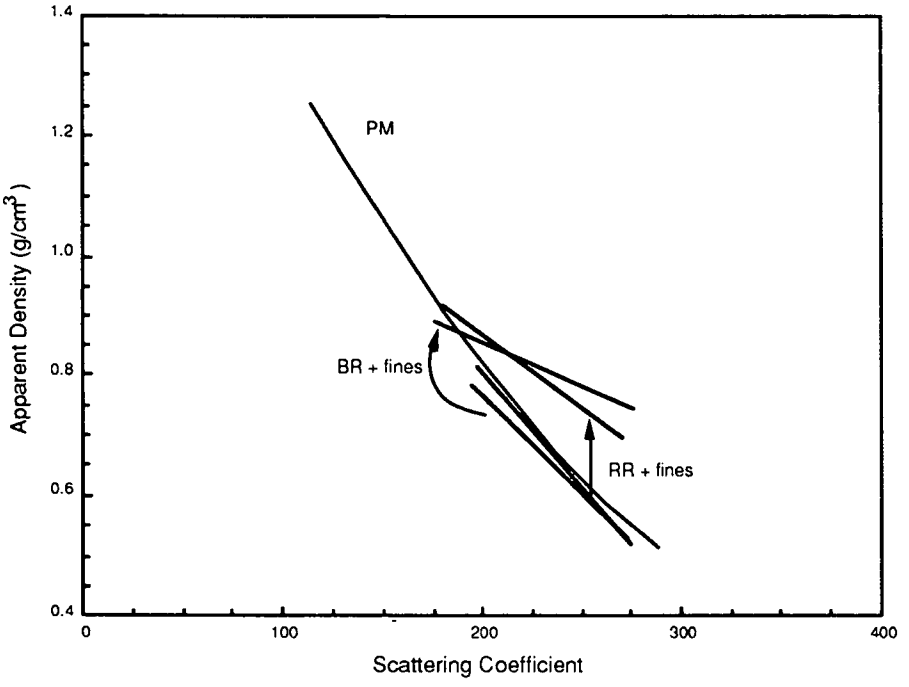

Figure 54. *PM*, *BR*, and *RR* scattering coefficient *vs.* apparent density.

this case, produce levels of fiber flexibility, fiber collaspe, and fines/external fibrillation to produce well bonded sheets using the *RR*.

The effects of treatment in the *BR* or *RR* on tensile index are shown in Figs. 58 and 59 and on bonding index in Figs. 60 and 61. These results are similar to apparent density and the same factors are responsible for the changes in tensile index and bonding index.

Bonding index is the ratio of tensile index to zero span tensile index. As its name implies, bonding index is a measure of how well a sheet is bonded. The concept of a bonding index is based on the premise that zero span tensile index is a measure of fiber strength and is independent of bonding, and that tensile index is sensitive to the degree of bonding. As bonding increases, the tensile index increases to the level of the żero-span tensile index indicating that bond strength

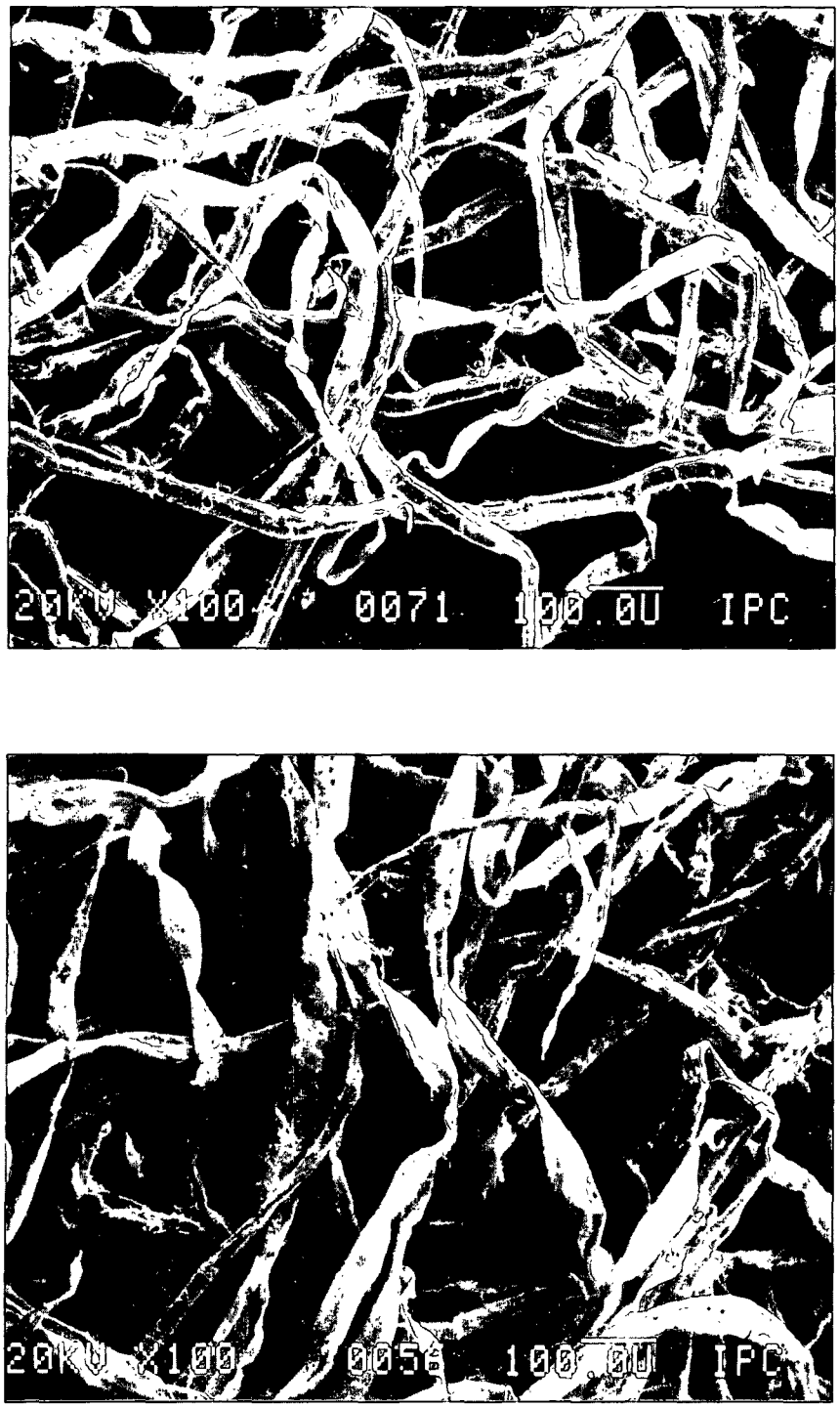

Figure 55a. *SEM* photomicrographs of *Untreated* (top) and *Formette Treated* (bottom) fibers.

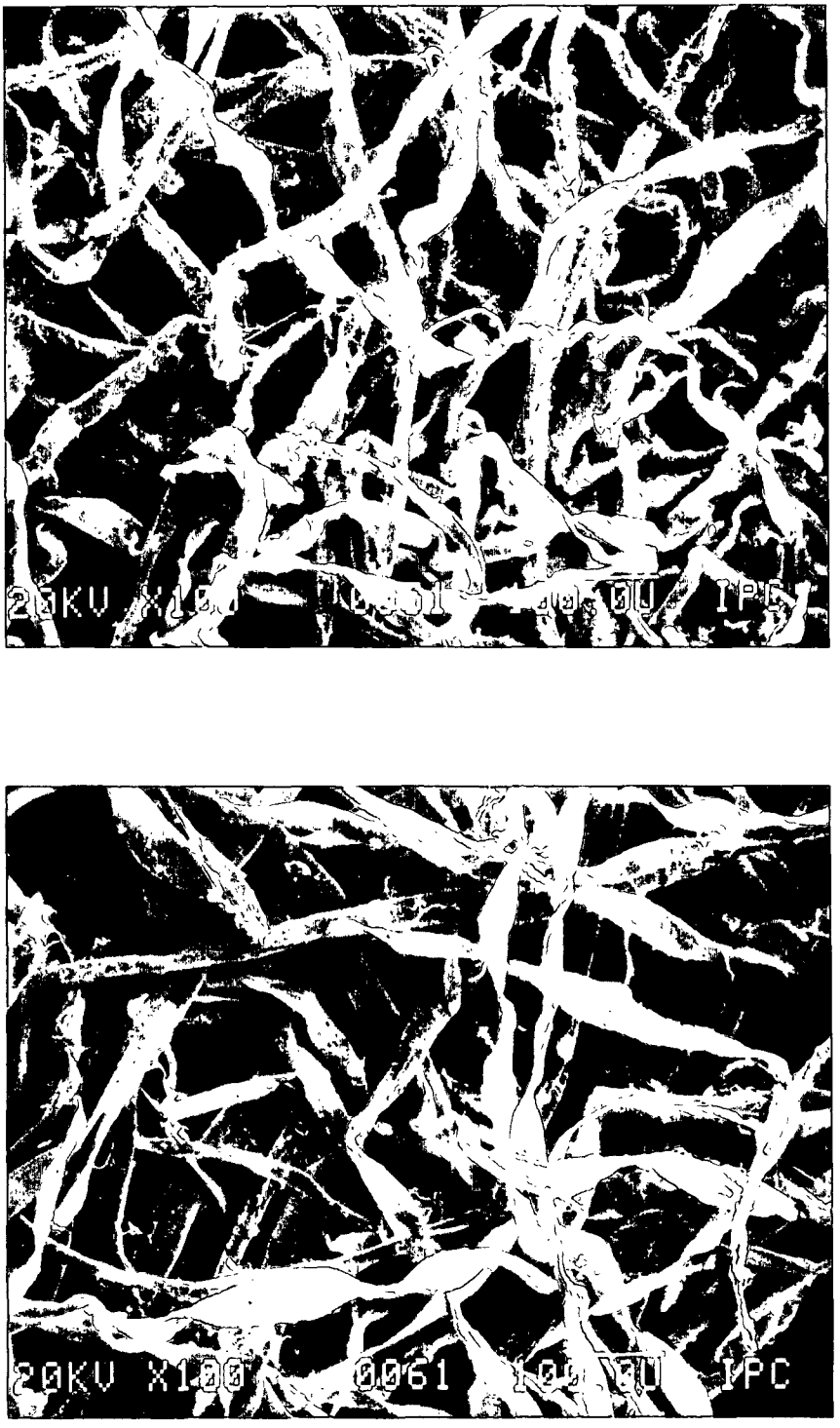

Figure 55b. *SEM* photomicrographs of *BR* (top) and *RR* (bottom) fibers subjected to 12000 RE.

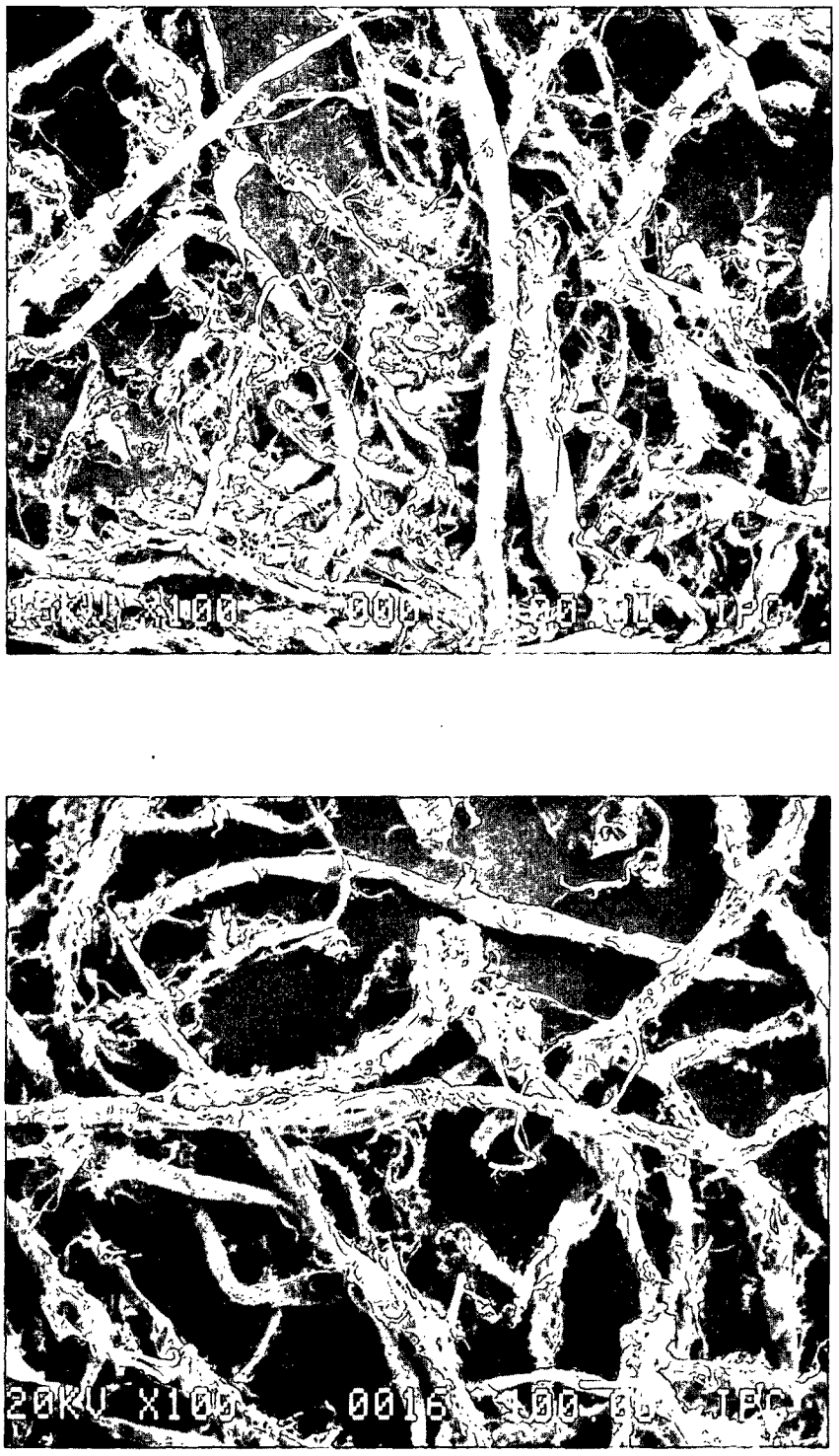

Figure 55c. *SEM* photomicrographs of *PM-Lo* (top) and *PM-Hi* (bottom) fibers subjected to 12000 RE.

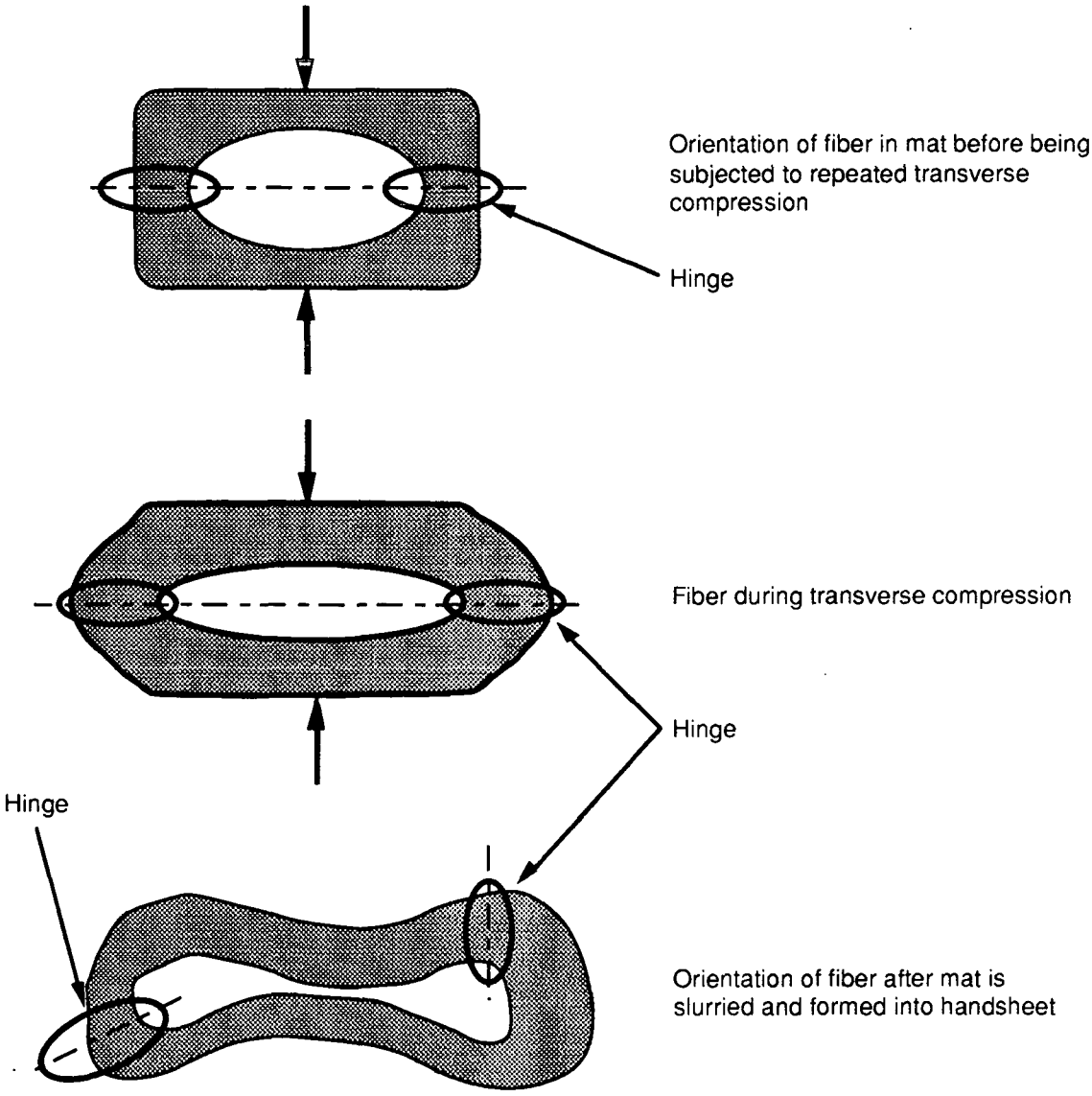

Figure 56. Schematic of fiber cross section before, during, and after treatment in *BR* and *RR*.

has approached the strength of the fibers. The decrease in bonding index for the normal fines content *RR* specimens is the result of the zero-span tensile index is increasing faster than the tensile index.

The internal tear resistance is plotted against treatment level and apparent density in Figs. 62 and 63. Internal tear resistance is a measure of the work

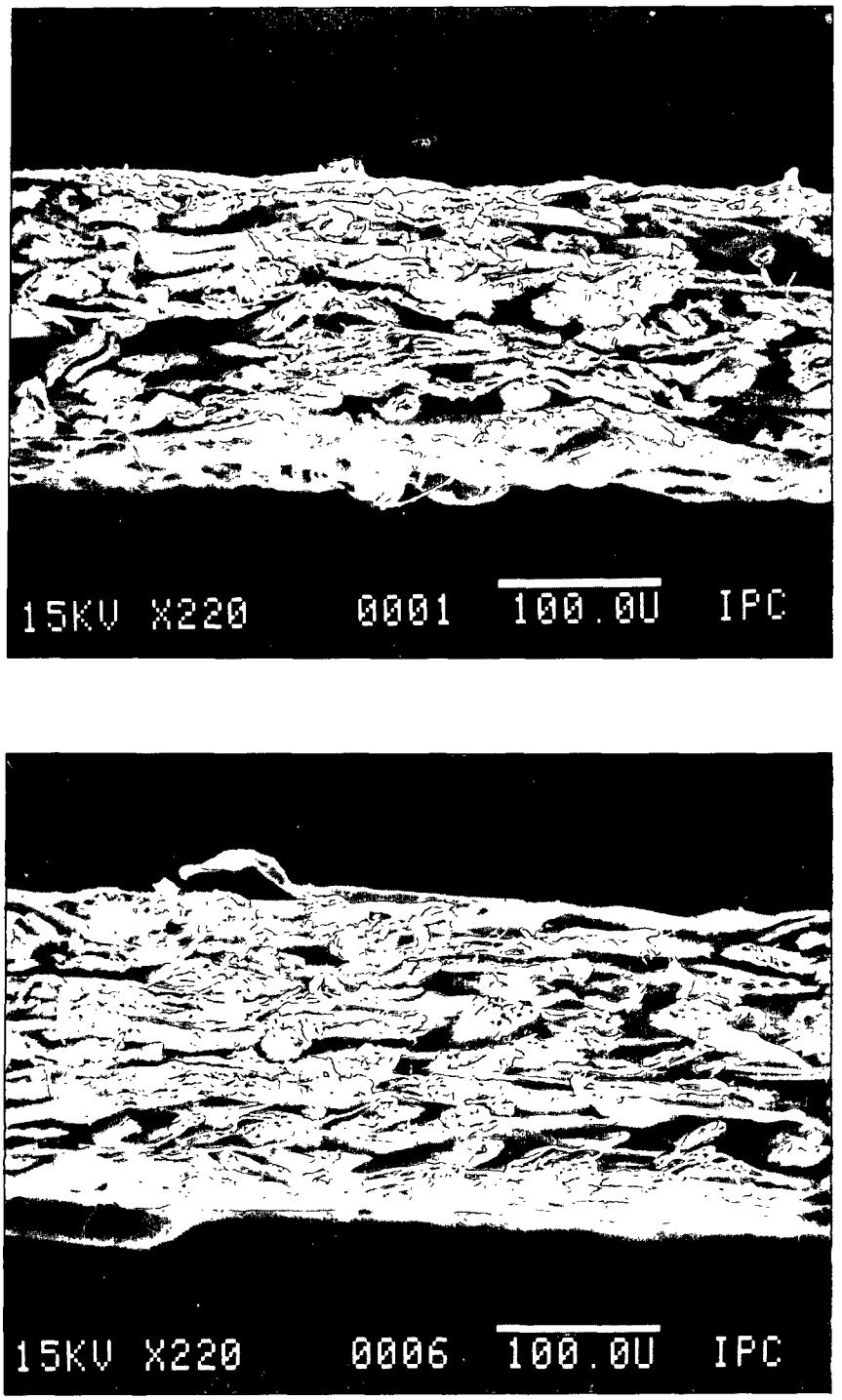

Figure 57. *SEM* photomicrographs of handsheet cross sections. (a) Fibers subjected to 12,000 RE in the *BR*, and (b) Fibers subjected to 12000 RE in the *RR*.

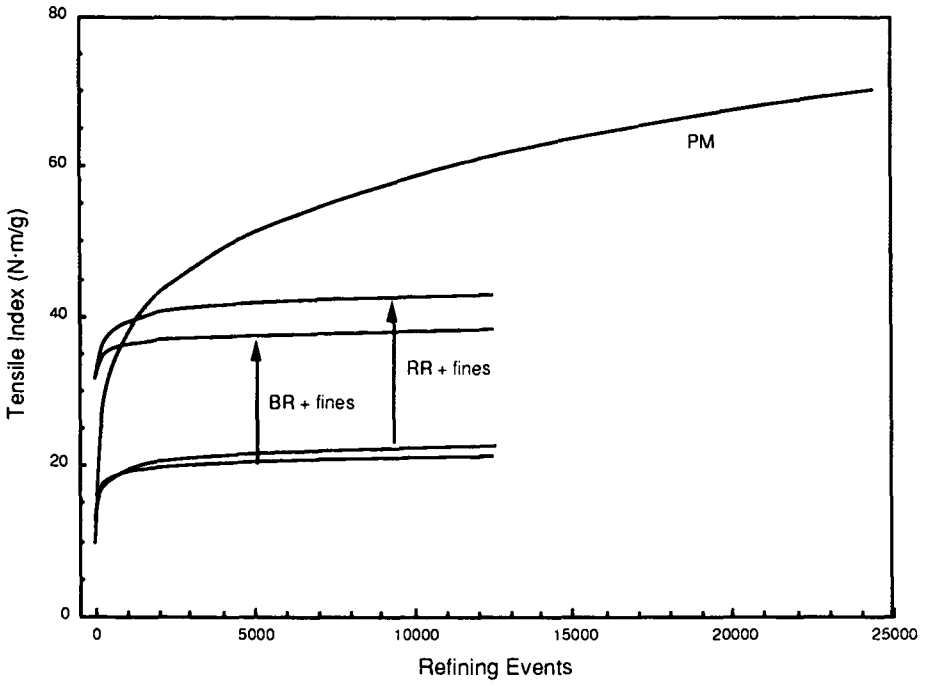

Figure 58. *BR*, *RR*, and *PM* tensile index *vs.* treatment level.

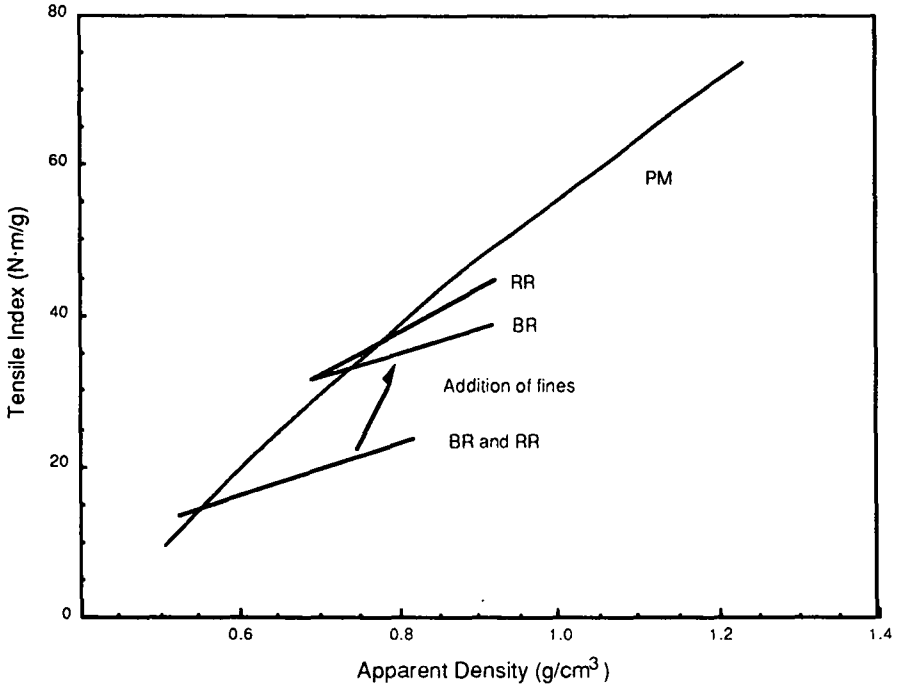

Figure 59. *BR*, *RR*, and *PM* tensile index *vs.* handsheet density.

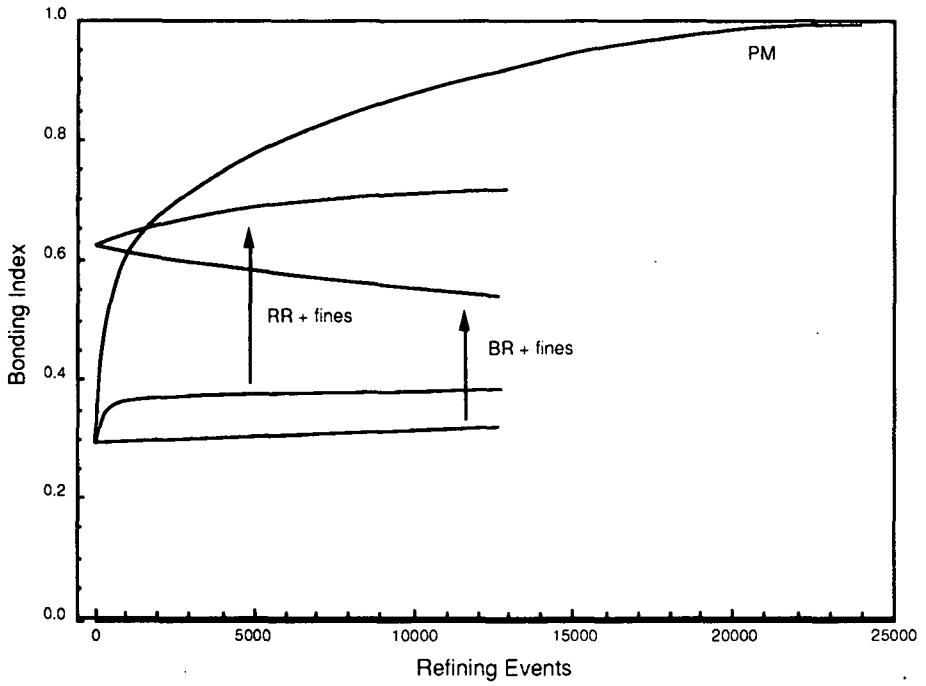

Figure 60. *BR*, *RR*, and *PM* bonding index *vs.* treatment level.

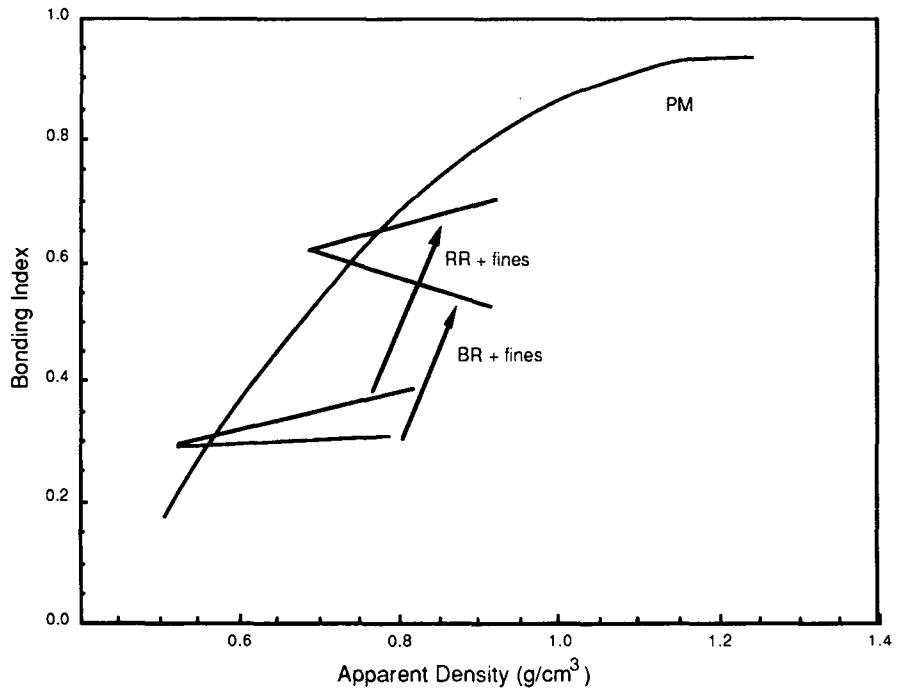

Figure 61. *BR*, *RR*, and *PM* bonding index *vs.* handsheet density.

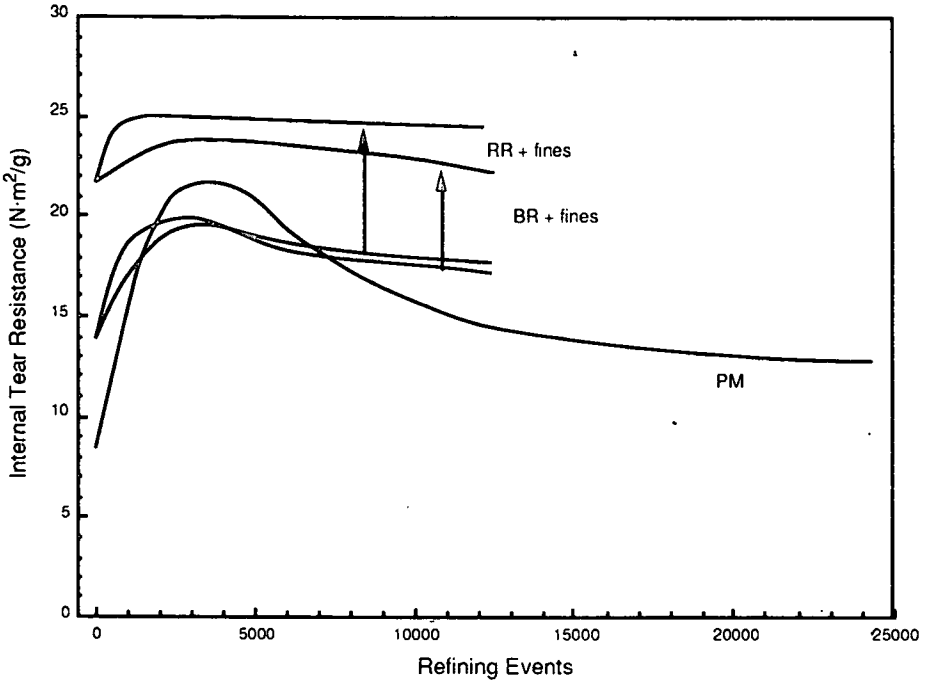

Figure 62. *BR*, *RR*, and *PM* internal tear resistance *vs.* treatment level.

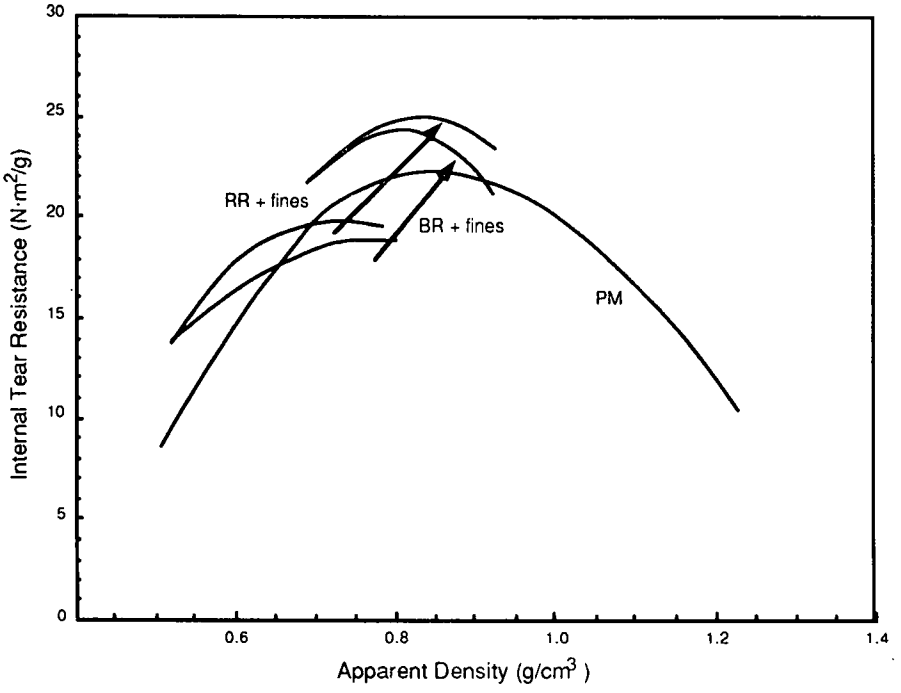

Figure 63. *BR*, *RR*, and *PM* internal tear resistance *vs.* handsheet density.

required to tear the sheet. The fibers along the tear may either be pulled from the surrounding paper or broken. At low levels of sheet consolidation, the fibers are pulled from the sheet before they can be broken. As refining increases the consolidation of the sheet, the tear resistance increases because additional work is required to pull the fibers from the sheet. In a well bonded sheet, the fibers are more likey to be broken than to be pulled out. Since breaking the fibers requires less energy that pulling fibers from the surrounding sheet, the tear resistance decreases with increased bonding. The internal tear resistance data indicates that the *BR* and *RR* sheets do not become well bonded since tear resistance does not significantly decrease at the higher levels of treatment or density as it does in the *PM*.

EFFECT ON HANDSHEET ELASTIC PROPERTIES

The development of in-plane mass specific longitudinal elastic stiffness, C_{11}/ρ, by the *BR* and *RR* with increasing treatment level and apparent density is depicted in Figs. 64 and 65, respectively. The in-plane mass specific shear elastic stiffness, C_{66}/ρ, is plotted against treatment level and apparent density in Figs. 66 and 67. The results are very similar to the apparent density and tensile index results. Since the in-plane stiffnesses have been show to correlate with in-plane properties such as density and tensile index[77], this result was expected.

However, the correlation of the *BR* and *RR* in-plane stiffness values to tensile index was different than that of the *PM* values. Tensile index is plotted against C_{11}/ρ in Fig. 68. For both the *BR* and *RR*, the tensile index increases at a slower rate than for the *PM*, even when fines are added to the *BR* and *RR* specimens. The explanation of this difference may be related to the present of the S_1 layer in the *BR* and *RR* fibers. The lower portion of the *PM* curve may represent fibers with the S_1 layer still intact and the upper portion of the curve

may represent fibers with the S_1 layer partially or completely removed. The *BR* and *RR* curves have slopes similar to the lower portion of the *PM* curve even when the density, stiffnesses, and tensile index are increased by adding fines. This may indicate that in order to reach high levels of strength and stiffness, the S_1 layer has to be removed.

The results of treatment in the *BR* and *RR* are shown for out-of-plane mass specific longitudinal stiffness, C_{33}/ρ, in Figs. 69 and 70 and for out-of-plane mass specific shear stiffness, C_{44}/ρ, in Figs. 71 and 72. The *BR* and *PM* specimens show a maximum in C_{33}/ρ and C_{44}/ρ at an intermediate level of treatment and density. The *RR* did little to develop either C_{33}/ρ or C_{44}/ρ. Response similar to the *BR* and *RR* results has been reported by Berger[54] for a range of PFI mill refining levels when the wet pressing is over 50 psi. In addition, at high refining levels, 8000 and 16000 revs., the same response was observed as wet pressing increased from 0 to 150 psi. Berger explained the decrease in terms of fiber cell wall disruption. At combinations of high refining and wet pressing levels, the sheet is very dense with most internal and external fiber surfaces in contact with other surfaces. At some point, additional pressing pressure begins to disrupt the cell wall structure as fibers are forced to deform plastically. The decrease in cell wall organization results in decreased stiffness. Disruption of the cell wall could be expected to decrease both the in-plane and out-of-plane stiffnesses. In these results, no decrease in the in-plane stiffness was observed; however, Berger did observe decreases for his specimens at high wet press pressures and refining levels.

For the in-plane stiffnesses, the *RR* produced slightly higher stiffnesses than the *BR*; however, for the out-of-plane stiffnesses, the *BR* produced values higher than the *RR*. In the case of C_{33}/ρ, the high fines content *BR* specimens were 80–90% of the *PM* specimens at equal treatment levels and for C_{44}/ρ the

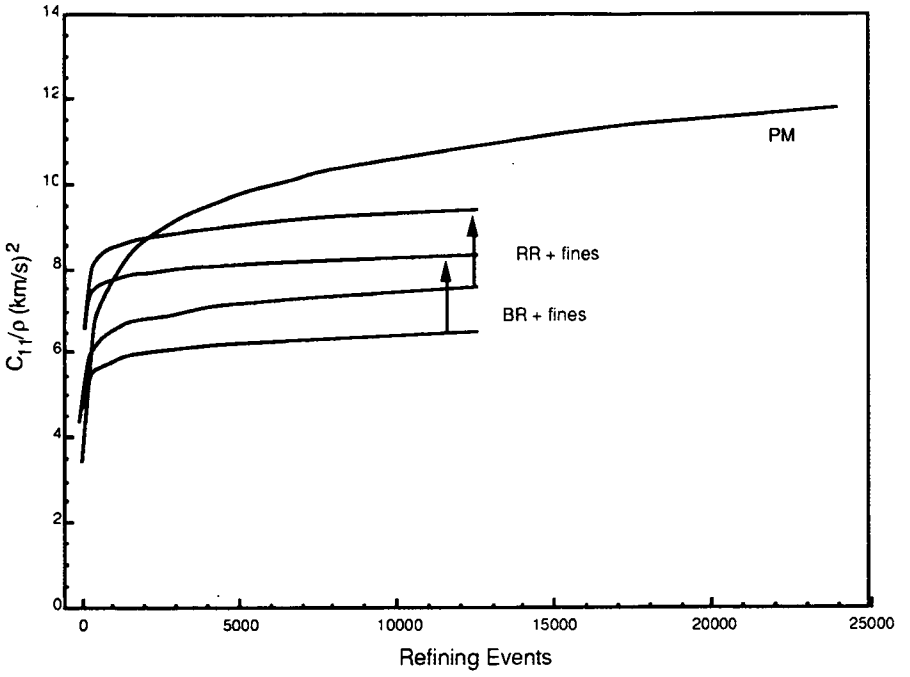

Figure 64. *BR*, *RR*, and *PM* in-plane mass specific longitudinal elastic stiffness *vs.* treatment level.

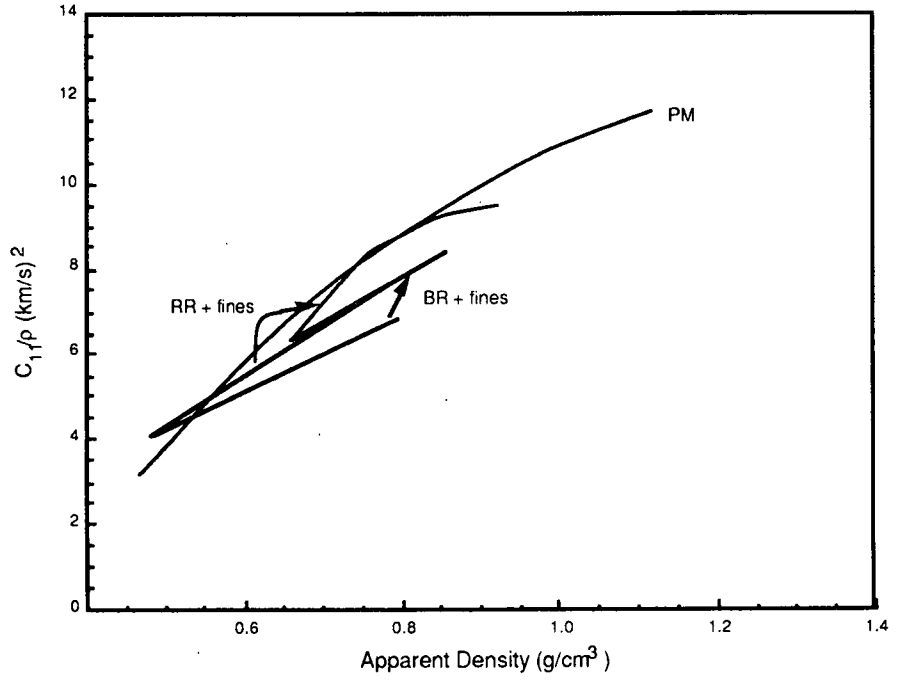

Figure 65. *BR*, *RR*, and *PM* in-plane mass specific longitudinal elastic stiffness *vs.* apparent density.

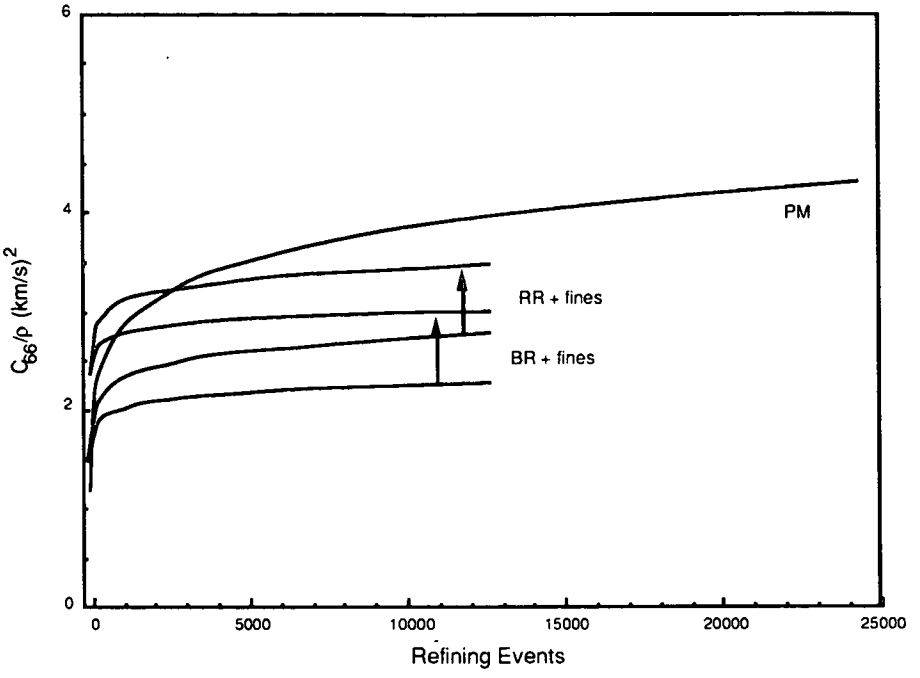

Figure 66. *BR*, *RR*, and *PM* in-plane mass specific shear elastic stiffness *vs.* treatment level.

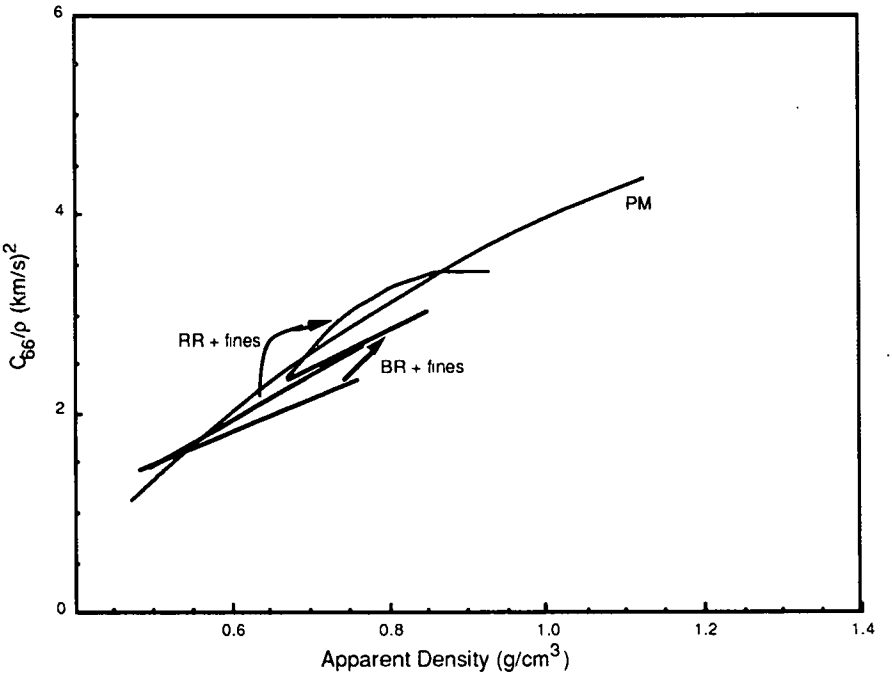

Figure 67. *BR*, *RR*, and *PM* in-plane mass specific shear elastic stiffness *vs.* apparent density.

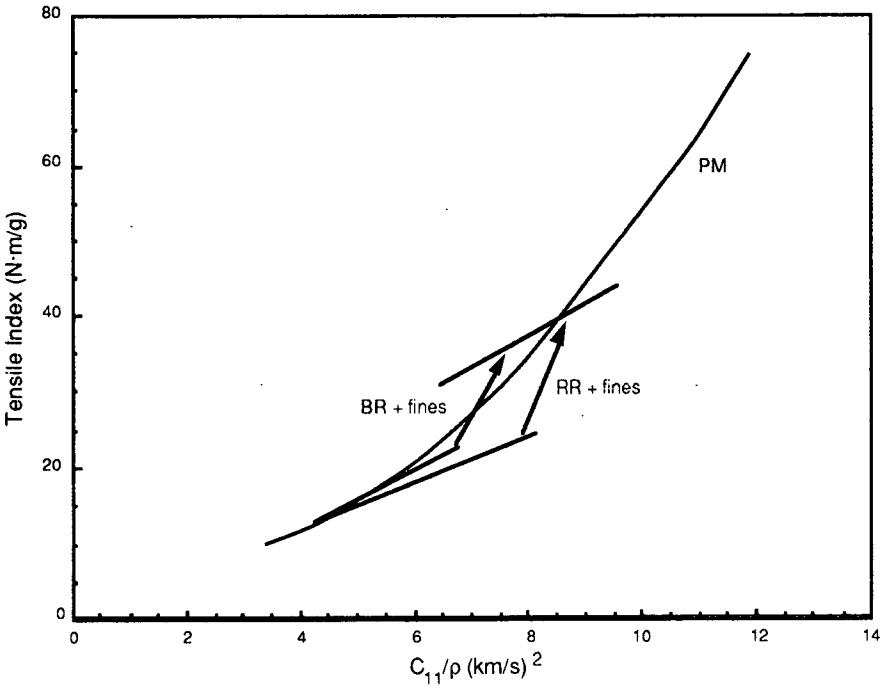

Figure 68. *BR*, *RR*, and *PM* tensile index *vs.* in-plane mass specific longitudinal elastic stiffness.

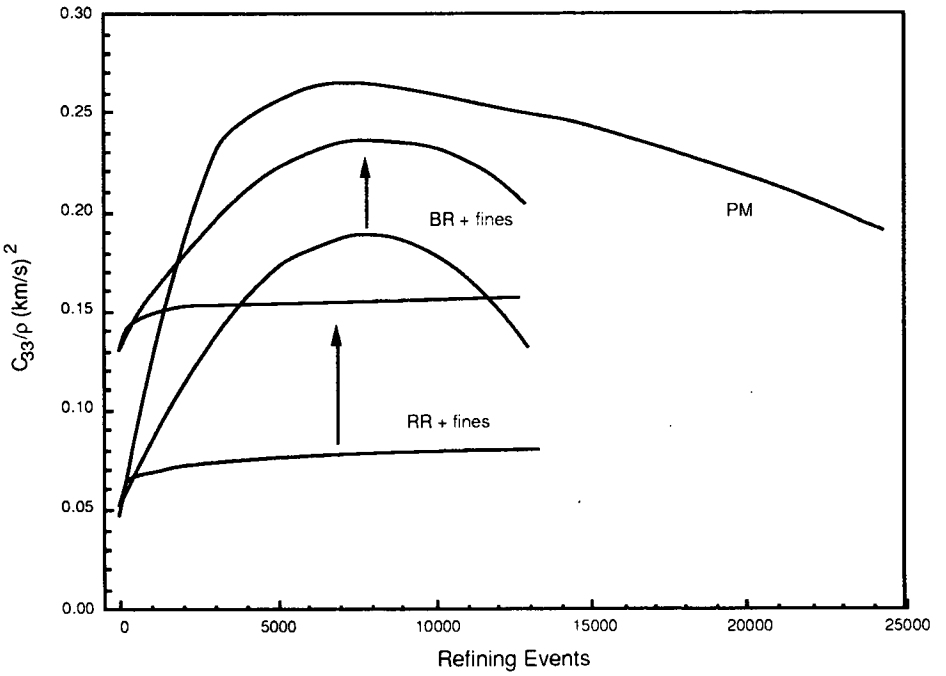

Figure 69. *BR*, *RR*, and *PM* out-of-plane mass specific longitudinal elastic stiffness *vs.* treatment level.

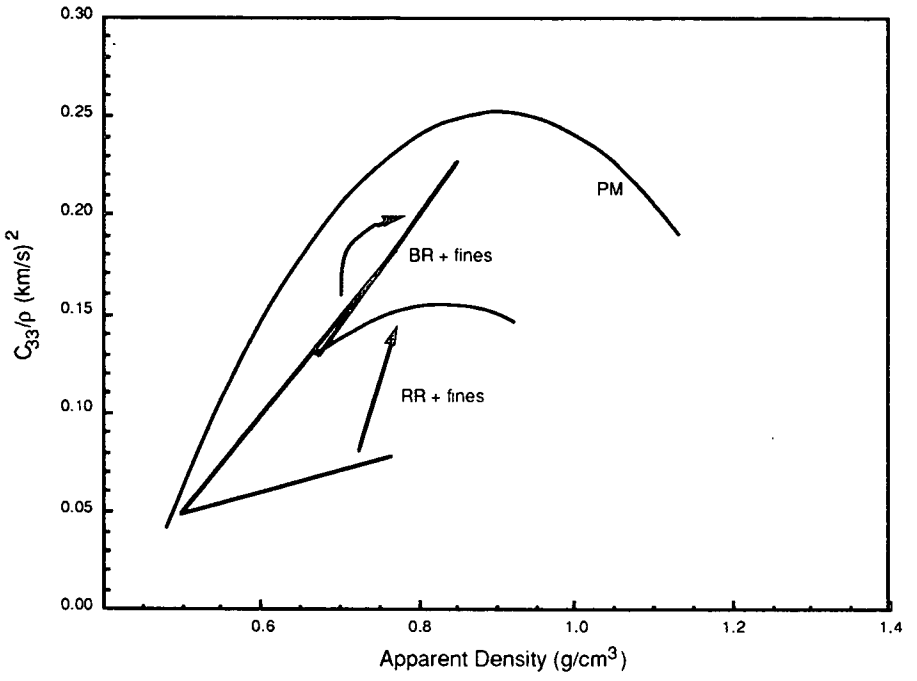

Figure 70. *BR*, *RR*,and *PM* out-of-plane mass specific longitudinal elastic stiffness *vs.* apparent density.

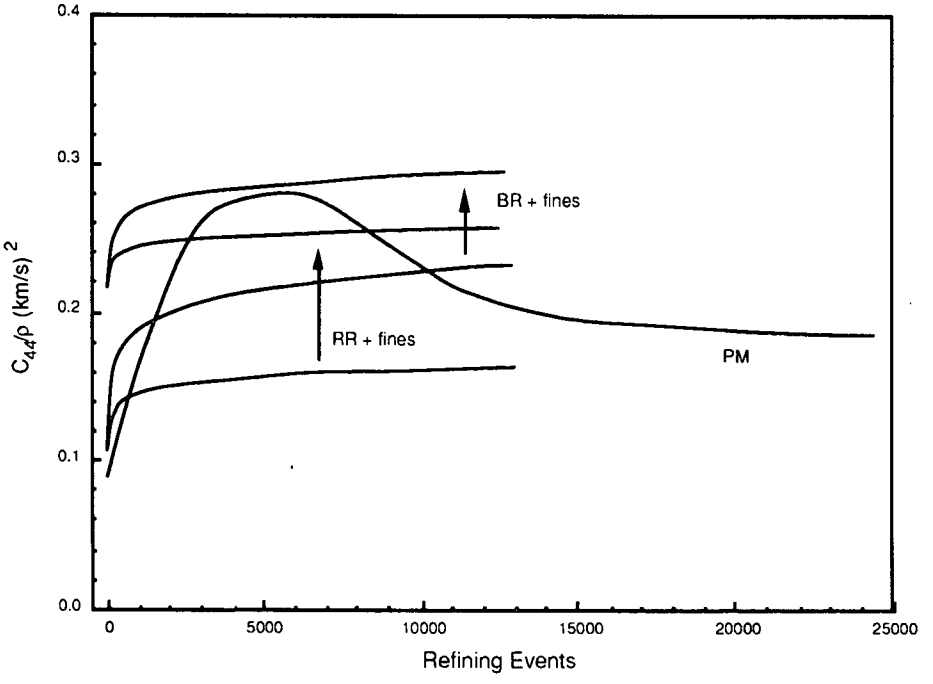

Figure 71. *BR*, *RR*, and *PM* out-of-plane mass specific shear elastic stiffness *vs.* treatment level.

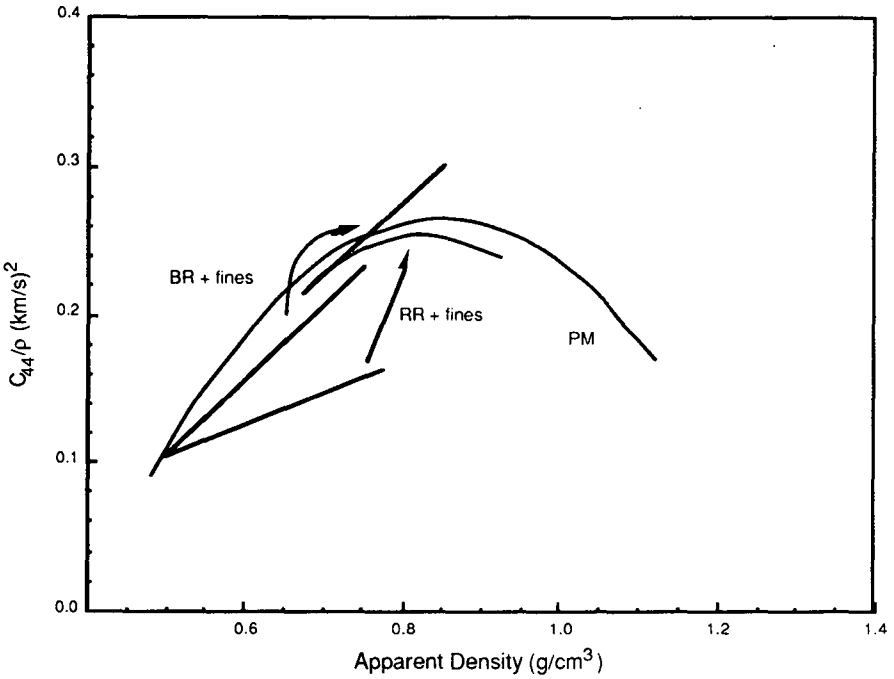

Figure 72. *BR*, *RR*, and *PM* out-of-plane mass specific shear elastic stiffness *vs.* apparent density.

specimens exceed the *PM* specimens. The *BR* is capable of developing the out-of-plane sheet properties, but not the in-plane sheet properties

EFFECT ON FIBER NETWORK GEOMETRY

For the in-plane stiffnesses, the development of sheet stiffness can result from producing a well-bonded sheet from undamaged, flexible, collapsed fibers[54]. The *BR* results indicate out-of-plane stiffnesses can be developed without fulfilling all of the conditions listed above. The density, scattering coefficient, and in-plane stiffness results show that the *BR* did not produce a well bonded sheet. But the *BR* still was capable of producing high out-of-plane stiffnesses which approached those of the *PM*. Two possible explanation are presented below.

The first explanation is based on an idea put forth by Berger[54] to explain decreases in transverse cell wall stiffness with refining. Berger pointed out that for a fiber undergoing transverse compression, the fibril angle of the S_1 layer would be low relative to the direction of compression (see Fig. 73). Thus, parts of the S_1 layer could make significant contributions to the transverse stiffness of the fiber. As refining removes the S_1 layer, the transverse stiffness of the fiber would decrease since no fibrils are oriented at a low angle relative to the transverse direction.

The initial increases in out-of-plane stiffness in the *BR* and *PM* are the result of increasing density by removing the voids between fibers and collapsing the fiber lumens. Once the sheet is moderately compacted, the stiffness of the fiber become the important. The presence of the S_1 layer would give the fibers a high transverse stiffness as described by Berger. When further refining removes the S_1 layer, as in the PFI mill, the fiber transverse stiffness, and, hence, the sheet transverse stiffness would decrease. While this mechanism may explain the *PM* results, it does not explain the decrease in the *BR* out-of-plane stiffnesses nor the low stiffness of the *RR* specimens, both of which are assumed to retain the S_1 layer. In the case of the *RR*, it is possible that the S_1 layer could become significantly damaged at low levels of treatment due to the high transverse stresses placed on the fiber as it passes through the nip. The damaged S_1 layer would remain attached, but would not contribute to the transverse stiffness of the fiber. The same could happen in the *BR*, but at higher levels of treatment.

A second explanation is presented in the schematics of three possible sheet cross sections illustrated in Fig. 74. A well bonded network of collapsed, flexible fibers is shown in Fig. 74a. This represents the type of network formed from fibers subject to the *PM*. Depicted in the second illustration, Fig. 74b, is a poorly

bonded network of uncollapsed, flexible fibers. The results produced by the *BR* will be explained using this model. The third possible network is represented in Fig. 74c. This network is composed of collapsed, but stiff fibers which are a poorly bonded.

The collapsed, flexible fibers shown in Fig. 74a produce high bonding, in-plane stiffness, and out-of-plane stiffness. The collapse of the fiber cross section leads to larger bonded areas by producing "wider" fiber crossings. The highly flexible fibers wrap about adjacent fibers to increase the bonded area by producing "longer" fiber crossings. The larger bonded area increases the sheet in-plane stiffness. The collapsed fibers increase the out-of-plane stiffness by eliminating voids in the fiber which would reduce fiber transverse stiffness. The increase in transverse fiber stiffness results in increased out-of-plane sheet stiffness. The *PM*, by producing fibers similar to those described here, develops high levels of density, in-plane stiffness, and out-of-plane stiffness.

Explanation of the *BR* results may be related to the degree of fiber collapse in the *BR* specimens. Although the fibers were made flexible[46] and sufficient fines were added, the density and in-plane stiffnesses remained low. Uncollapsed fibers could prevent the in-plane stiffness from developing (by preventing the sheet from becoming well bonded), yet allow the development of out-of-plane stiffness, if the *BR* subjected fibers formed a network as shown in Fig. 74b. The network would not be well bonded since the bonds at the fiber crossings would be narrow due to the uncollapsed fibers. The uncollapsed fibers would produce high out-of-plane stiffness due to a large number of fiber segments oriented out-of-plane. Since the stiffness along the fiber axis is much higher than in the transverse direction[36,53,54,97], the fiber segments aligned in the out-of-plane direction increase the average sheet out-of-plane stiffness. Due

to the high ratio of fiber axial stiffness to transverse stiffness, the number of fiber segments aligned in the out-of-plane direction would not have to be large in order for a large effect to be present. An alternative would be that more fiber segments could be aligned at a lower angle out of the plane of the sheet.

The results of the *RR* specimens could be explained by the network in Fig. 74c where collapsed fibers and less longitudinal fiber flexibility reduces the out-of-plane fiber orientation. The in-plane stiffness would benefit from the fiber being well aligned in the plane, but low bonded area, wide, but short fiber crossings, would limit in-plane stiffness development to moderate levels. The out-of-plane stiffness would benefit from the collapsed fiber cross-sections, but the bonded area would be insufficient to produce a stiff sheet.

The analysis of the mechanics involved in the *BR* and *RR* support these ideas. For the *BR*, most of the energy is consumed by flexing along the fiber axis. The result is the breaking of bonds and delaminating of the cell wall (especially at the S_1–S_2 and S_2–S_3 boundaries and within the S_2 layer) in a manner which increases the fiber longitudinal flexibility. The ability of the fiber to collapse is not greatly increased due to the low amount of work in the transverse direction.

The *RR* does the most work in the transverse direction of the fiber. The sides of the fiber parallel to the direction of compression would be significantly damaged. The S_1 layer could be delaminated from the S_2 on the sides of the fiber. The result is a fiber in which large regions which could act a "hinges" and make the fiber collapse quite readily. The longitudinal flexibility probably is not increased by this action, but the transverse stiffness could be significantly reduced.

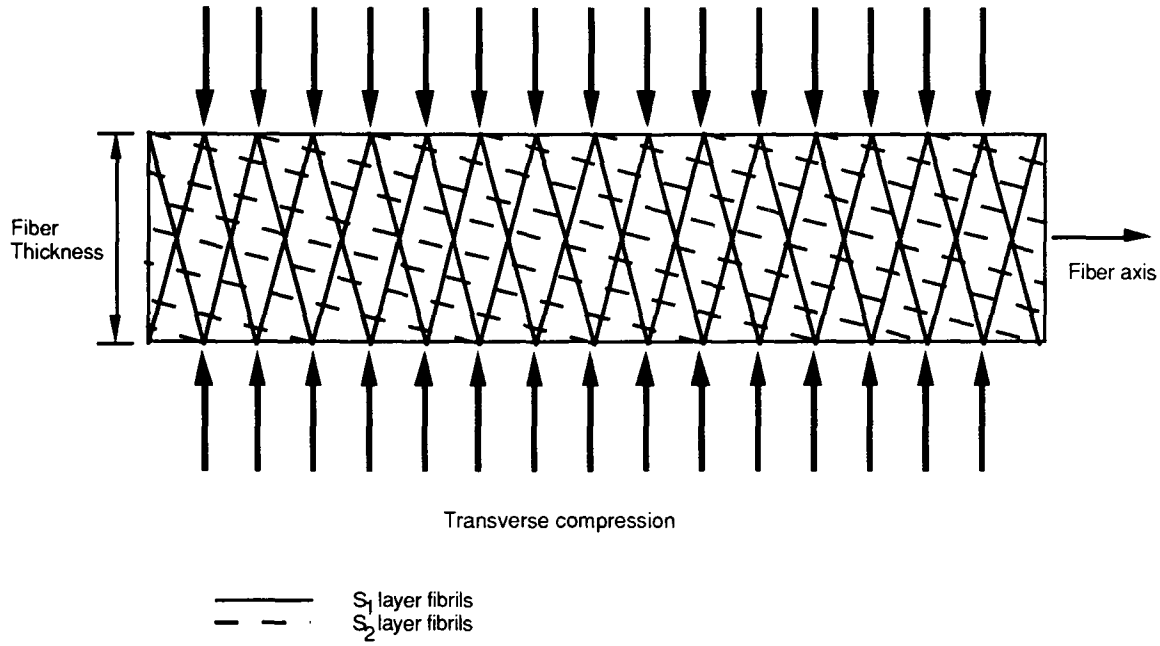

Figure 73. Side view of fiber segment showing fibril angle of S_1 and S_2 layers relative to the fiber axis.

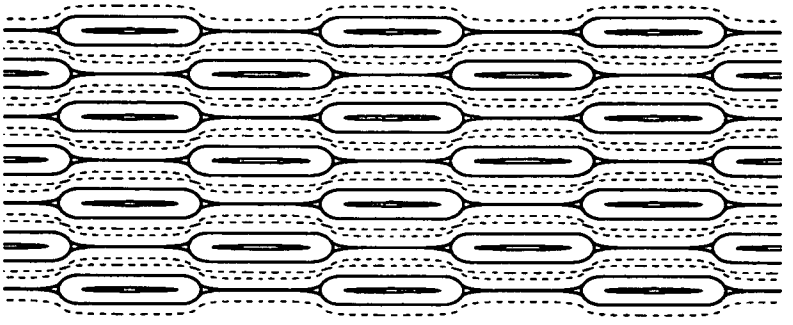

(a) PFI mill

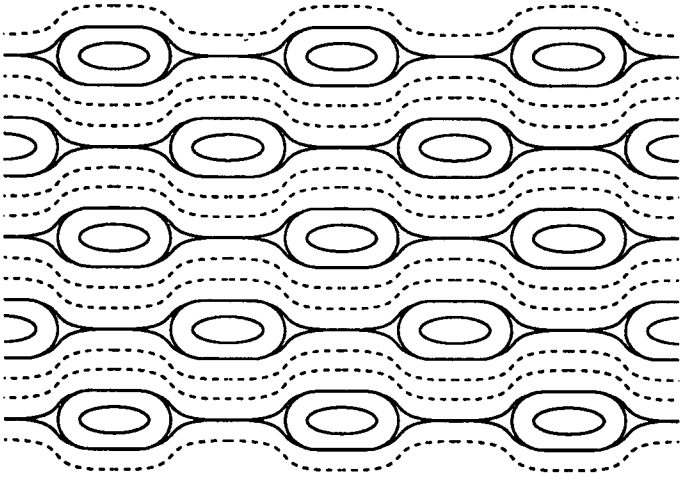

(b) Bending Refiner

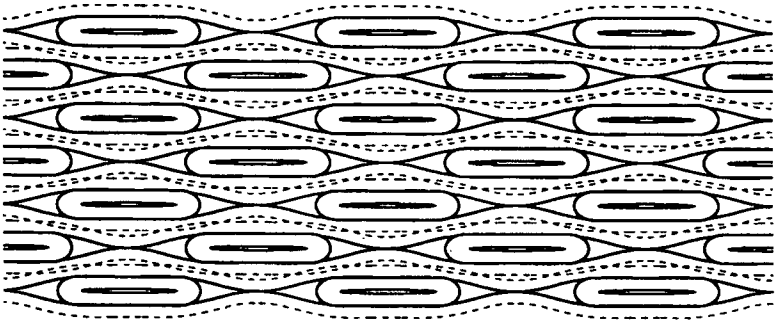

(c) Roll Refiner

Figure 74. Schematics of networks from fiber subjected to (a) PFI mill, (b) Bending Refiner, and (c) Roll Refiner.

CONCLUSIONS

1. The Bending Refiner primarily stresses fibers parallel to the direction of the fiber axis without reducing the average fiber length or generating significant amounts of fines. The result is a fiber that is flexible along its longitudinal axis, but in not easily collapsed during sheet consolidation.

2. The Roll Refiner treats primarily stresses fibers to the direction of the fiber axis without reducing the average fiber length or generating a significant amounts of fines. The result is a fiber that is readily collapsed during sheet consolidation, but has low flexibility along the fiber axis.

3. The Bending Refiner is effective in developing in-plane elastic and strength properties, but only up to low levels as compared to a PFI mill. This is probably due to low levels of bonding and density. The low amount of bonded area is a result of the small fiber crossing areas which are formed by the narrow uncollapsed fibers.

4. The Bending Refiner is very effective in developing out-of-plane elastic. This is interpreted as orientation of fiber segments in the out-of-plane direction. Fiber segments are oriented in the out-of-plane direction as the fiber, which is flexible along the fiber axis, wraps about an uncollapsed fiber. In this way, the high axial stiffness of the out-of-plane fibers segments contribute greatly to the out-of-plane sheet stiffness.

5. The Roll Refiner is effective in developing in-plane elastic and strength properties. For the nip load levels used here, only marginal increases in in-plane properties resulted, but, as demonstrated by Hartman, at higher levels of nip load and fines contents, the Roll Refiner can produce in-plane properties (density and breaking length) equivalent to those produced by a Valley beater. This results from the Roll Refiner producing fibers which readily collapse during sheet consolidation and are not flexible along their lengths. To develop in-plane properties, large amount of fines must be present during sheet consolidation to produce strong consolidation forces capable of overcoming the fiber stiffness.

6. The Roll Refiner is ineffective at producing out-of-plane properties. This is likely due to an inability to produce fiber flexible along the fiber axis. If the conditions described above were met, in-plane and out-of-plane properties similar to those produce by convention refiners could result.

LITERATURE CITED

1. Clark, J. d'A. Pulp Technology and Treatment for Paper. San Francisco, Miller Freeman, 1978.

2. Emerton, H. W. Preparation of pulp fibers for papermaking. *In* Handbook of Paper Science. Vol. 1.: The Raw Materials and Processing of Papermaking. p. 138–164. Rance, H. F., ed., Amsterdam, Elsevier Scientific Publishing Co., 1980.

3. Panshin, A. J.; de Zeeuw, C. Textbook of Wood Technology. 3rd ed. p. 91, 118. New York, McGraw-Hill Book Company, 1980.

4. Wardrop, A. B. Fiber morphology and papermaking. *Tappi* 52(3): 396–408 (March, 1969).

5. Côté, W. A. Ultrastructure – Critical domain for wood behavior. *Wood Sci. Technol.* 15: 1–29 (1981).

6. Wardrop, A. B.; Harada, H. *J. Exptl. Botany* 16: 356 (1965).

7. Krässig, H. Structure of cellulose and its relation to properties of cellulose fibers. *In* Cellulose and Its Derivatives: Chemistry, Biochemistry and Applications. p. 1–25. Kennedy, J. F.; Phillips, G. O.; Wedlock, D. J.; Williams, P. A., eds., Chichester, West Sussex, England, Ellis Horwood Ltd, 1985.

8. Esau, K. Anatomy of Seed Plants. p. 51. New York, John Wiley & Sons, Inc., 1960.

9. Hearle, J. W. S. The development of ideas of fine structure. *In* Fiber Structure. p. 209–234. Hearle, J. W. S.; Peters, R. H., eds., Manchester and London, The Textile Institute and Butterworths, 1963.

10. Kerr, A. J.; Goring, D. A. I. The ultrastructural arrangement of the wood cell wall. *Cellulose Chem. Technol.* 9: 563–573 (Nov.-Dec., 1975).

11. Scallan, A. M. The structure of the cell wall – a consequence of anisotropic inter-microfibrillar bonding? *Wood Sci.* 6(3): 266–271 (Jan., 1974).

12. Clark, J. d'A. Pulp Technology and Treatment for Paper. San Francisco, Miller Freeman, 1978.

13. Emerton, H. W. Preparation of pulp fibers for papermaking. *In* Handbook of Paper Science. Vol. 1.: The Raw Materials and Processing of Papermaking. p. 138–164. Rance, H. F., ed., Amsterdam, Elsevier Scientific Publishing Co., 1980.

14. Corte, H. Cellulose-water interactions. *In* Handbook of Paper Science. Vol. 1: The Raw Materials and Processing of Papermaking. p. 1–89. Rance, H. F., ed., Amsterdam, Elsevier Scientific Publishing Co., 1980.

15. Mohlin, U.-B. Cellulose fiber bonding. Part 5. Conformability of pulp fibers. *Svensk Papperstidning* 78(11): 412–416 (1975).

16. McIntosh, D. C. The effect of refining of the structure of the fiber wall. *Tappi* 50(10): 482–488 (Oct., 1967).

17. Ebeling, K. A critical review of current theories of the refining of chemical pulps. International Symposium on: Fundam. Concepts of Refining. Appleton, Wisconsin, The Institute of Paper Chemistry, Sept. 16–18, 1980.

18. Fahey, M. D. Mechanical treatment of chemical pulps. *Tappi* 53(11): 2050–2064 (Nov., 1970).

19. Ebeling, K. Effect of refining on fibers. *In* Paperin Valmistus. p. B2, 1–28. Ryti, N., ed., Finnish Paper Eng. Assocn., 1969.

20. Giertz, H. W. Ännett sätt att se på malningsprocessen. *Norsk Skogindustri* 18(7): 239–248 (July, 1964).

21. Higgins, H. G.; de Yong, J. The beating process. Primary effects and their influence on pulp and paper properties. *In* Formation and Structure of Paper. Trans. of the Symposium held at Oxford, Sept. 1961. Vol. 2. p. 651–695. Bolam, F., ed., London, Tech. Sect., Brit. Paper and Board Makers' Assocn., 1962.

22. Emerton, H. W. The outer secondary wall. Part 2. Its possible papermaking significance. *In* Fundam. of Papermaking Fibers. Trans. of the Symp. held at Cambridge, Sept., 1957. p. 431–434. Bolam, F., ed., Kenley, Surrey, England, Tech. Sect., Brit. Paper and Board Makers' Assocn., 1958.

23. Page, D. H.; De Grâce, J. H. The delamination of fiber walls by beating and refining. *Tappi* 50(10): 489–495 (Oct., 1967).

24. Page, D. H. The axial compression of fibers – a newly discovered beating action. *Pulp and Paper Mag. of Canada* 67(1): T2–T12 (Jan., 1966).

25. Levlin, J.-E.; Nordman, L. Material losses during defibration and beating of high-yield pulps. *In* Fiber-Water Interactions in Papermaking. Trans. of the Symp. held at Oxford, Sept., 1977. Vol. 1. p. 299–304. London, Fundam. Research Comm., Brit. Paper and Board Ind. Fed., 1978.

26. Clark, J. d'A. Fibrillation, free water, and fiber bonding. *Tappi* 52(2): 335–340 (Feb., 1969).

27. Steenberg, B.; Sandgren, B.; Wahren, D. Studies on pulp crill. Part 1. Suspended fibrils in paper pulp fines. *Svensk Papperstidning* 63(12): 395–397 (1960).

28. Sandgren, B.; Wahren, D. Studies on pulp crill. Part 3. Influence on some properties of pulp and paper. *Svensk Papperstidning* 63(24): 879–883 (1960).

29. Giertz, H. W. The effect of beating on individual fibers. *In* Fundam. of Papermaking Fibers. Trans. of the Symp. held at Cambridge, Sept., 1957. p. 389–409. Bolam, F., ed., Kenley, Surrey, England, Tech. Sect., Brit. Paper and Board Makers' Assocn., 1958.

30. Cottral, L. G. Proc. of Tech. Sect., Paper Makers' Assocn. 14(2): 241 (1934).

31. Corte, H.; Agg, S. On the shortening of pulp fibers during beating. p. 149–157. International Symposium on: Fundam. Concepts of Refining. Appleton, Wisconsin, The Institute of Paper Chemistry, Sept. 16–18, 1980.

32. Page, D. H. The mechanism of strength of development of dried pulps by beating. *Svensk Papperstidning* 88(3): R30–R35 (1985).

33. Samuelsson, L.-G. Measurement of the stiffness of fibers. *Svensk Papperstidning* 66(15): 541–546 (1963).

34. Samuelsson, L.-G. Measurement of the stiffness of fibers. Part 2. The effect of mechanical treatment. *Svensk Papperstidning* 67(23): 943–948 (1964).

35. Leopold, B. Effect of pulp processing on individual fiber strength. *Tappi* 49(7): 315 (July, 1966).

36. Kallmes, O. J.; Perez, M. Load-elongation properties of fibers. Consolidation of the paper web. *In* Consolidation of the Paper Web. Trans. of the Symposium held at Cambridge, Sept., 1965. Vol. 1. p. 507–528. Bolam, F., ed., Tech. Sect., Brit. Paper and Board Makers' Assocn., 1966.

37. McIntosh, D. C.; Uhrig, L. O. Effect of refining on load-elongation characteristics of loblolly pine, holocellulose and unbleached kraft fibers. *Tappi* 51(5): 268–273 (May, 1968).

38. Alexander, S. D.; Marton, R.; McGovern, S. D. Effect of beating and wet pressing on fiber and sheet properties. Part 1. Individual fiber properties. *Tappi* 51(6): 277–283 (June, 1968).

39. Hardacker, K. W. Effects of loading rate, span, and beating on individual wood fiber tensile properties. *In* The Physics and Chemistry of Wood Pulp Fibers (Special Technical Association Publication No. 8). p. 201–211. Page, D. H., ed., New York, Tappi, 1970.

40. Page, D. H.; El-Hosseiny, F.; Winkler, K.; Bain, R. The mechanical properties of single wood-pulp fibers. Part 1. A new approach. *Pulp and Paper Mag. of Canada* 73(8): T198–T203 (Aug., 1972).

41. Page, D. H.; El-Hosseiny, F. The mechanical properties of single wood pulp fibers. Part 6. Fibril angle and the shape of the stress-strain curve. *J. of Pulp and Paper Sci.* 9(4): TR99–TR100 (Sept., 1983).

42. Mohlin, U.-B. Cellulose fiber bonding. Part 3. The effect of beating and drying on interfiber bonding. *Svensk Papperstidning* 78(9): 338–341 (1975).

43. Tam Doo, P. A.; Kerekes, R. J. A method to measure wet fiber flexibility. *Tappi* 64(3): 113–116 (March, 1981).

44. Tam Doo, P. A.; Kerekes, R. J. The flexibility of wet pulp fibers. *Pulp and Paper Canada* 83(2): T37–T41 (Feb., 1982).

45. Kerekes, R. J.; Tam Doo, P. A. Wet fiber flexibility of some major softwood species pulped by various processes. Proc. of the 71st Annual Meeting, Tech. Sect., CPPA held at Montreal, Quebec, Jan. 29–30, 1985. Preprints A. p. A45–A46. Montreal, Quebec, CPPA, 1985.

46. Tam Doo, P. A.; Kerekes, R. J. The effect of beating and low amplitude flexing on pulp fiber flexibility. To be published, *J. Pulp and Paper Sci.*

47. Luner, P. Wet fiber flexibility as an index of pulp and paper properties. Advances in Refining Technology. Proc. of the International Conf. on New Technologies in Refining held at Birmingham, England, Dec. 9–11, 1986. Vol 1. Paper 3. Birmingham, England, PIRA, 1986.

48. Van den Akker, J. A.; Lathrop, A. L.; Voelker, M. H.; Dearth, L. R. *Tappi* 41(8): 416 (1958).

49. Balodis, W.; McKenzie, A. W.; Harrington, K. J.; Higgins, H. G. Effects of hydrophilic colloids and other non-fibrous materials on fiber flocculation and network consolidation. *In* Consolidation of the Paper Web. Trans. of the Symposium held at Cambridge, Sept., 1965. Vol. 2. p. 639–686. Bolam, F., ed., Tech. Sect., Brit. Paper and Board Makers' Assocn., 1966.

50. Harrington, K. J. Measurement of the lateral compression of single wood pulp fibers. *Appita* 23(5): 365–367 (March, 1970).

51. Hartler, N.; Nyrén, J. Transverse compressibility of pulp fibers. Part 2. Influence of cooking method, yield, beating and drying. *Tappi* 53(3): 820–823 (May, 1970).

52. Nyrén, J. Transverse compressibility of pulp fibers. *Pulp Paper Mag. Canada* 72(10): T321–T323 (Oct., 1971).

53. Hartler, N.; Nyrén, J. Influence of pulp type and posttreatments on the compressive force required for collapse. *In* The Physics and Chemistry of Wood Pulp Fibers (Special Technical Association Publication No. 8). p. 265–278. Page, D. H., ed., New York, Tappi, 1970.

54. Berger, B. F. The Effects of Yield and Refining on the Z-direction Elastic Properties of Paper. Doctoral Dissertation. Appleton, Wisconsin, The Institute of Paper Chemistry, 1988. 132 p.

55. Natio, T.; Usuda, M.; Kadoya, T. Torsional properties of single pulp fibers. *Tappi* 63(7): 115–118 (July, 1980).

56. Natio, T.; Usuda, M.; Kadoya, T. Fatigue phenomena of single pulp fibers under repeated torsional stress. *J. Soc. Fiber Technol. Japan (Sen-I Gakkaishi)* 39(1): T8–T13 (Jan., 1983).

57. de Ruvo, A.; Lundberg, R.; Martin-Löf, S.; Söremark, C. Influence of temperature and humidity on the elastic and expansional properties of paper and the constituent fiber. *In* Fundam. Properties of Paper Related to Uses. Trans. of the Symposium held at Cambridge, Sept., 1973. Vol. 2. p. 785–806. Bolam, F., ed., London, Tech. Sect., Brit. Paper and Board Makers' Assocn., 1976.

58. Giertz, H. W. The influence of beating on individual fibers and the causal effects on paper properties. International Symposium on: Fundam. Concepts of Refining. p. 87–92. Appleton, Wisconsin, The Institute of Paper Chemistry, Sept. 16–18, 1980.

59. Kibblewhite, R. P. Effects of beating on wet web behaviour. *Appita* 26(5): 341–347 (March, 1973).

60. Campbell, W. B. *Paper Trade J.* 95(8): 29–32 (Aug. 25, 1932).

61. Campbell, W. B. Canada Dept. Interior, Forest Service Bull. No. 84 (1933).

62. Campbell, W. B. *Ind. Eng. Chem.* 26(2): 218–219 (1934).

63. Lyne, L. M.; Gallay, W. Fiber Properties and fiber-water relationships in relation to the strength and rheology of wet webs. *Tappi* 37(11): 581–596 (Nov., 1954).

64. Lyne, L. M.; Gallay, W. Measurement of wet web strength. *Tappi* 37(12): 694–698 (Dec., 1954).

65. Lyne, L. M.; Gallay, W. Studies in the fundamentals of wet web strength. *Tappi* 37(12): 698–704 (Dec., 1954).

66. Swanson, J. W. Colloid Chemistry of Papermaking Materials (unpublished text), The Institute of Paper Chemistry, 1966.

67. Giertz, H. W. Understanding the role of fines. International Symposium on: Fundam. Concepts of Refining. Addendum, p. 324–326. Appleton, Wisconsin, The Institute of Paper Chemistry, Sept. 16–18, 1980.

68. Page, D. H. A theory for the tensile strength of paper. *Tappi* 57(4): 674–681 (April, 1969).

69. Levlin, J.-E. Some differences in the beating behaviour of softwood and hardwood pulps. International Symposium on: Fundam. Concepts of Refining. p. 51–60. Appleton, Wisconsin, The Institute of Paper Chemistry, Sept. 16–18, 1980.

70. Alexander, S. D.; Marton, R. Effect of beating and wet pressing on fiber and sheet properties. Part 2. Sheet properties. *Tappi* 51(6): 283–288 (June, 1968).

71. Skowronski, J.; Bichard, W. Fiber-to-fiber bonds in paper. Part 1. Measurement of bond strength and specific bond strength. *J. Pulp and Paper Sci.* 13(5): J165–J169 (Sept., 1987).

72. Habeger, C. C.; Mann, R. W.; Baum, G. A. Ultrasonic plate waves in paper. *Ultrasonics* 17(2): 57–62 (March, 1979).

73. Craver, J. K.; Taylor, D. L. Nondestructive sonic measurement of paper elasticity. *Tappi* 48(3): 142–147 (March, 1965).

74. Taylor, D. L.; Craver, J. K. Anisotropic elasticity of paper from sonic velocity measurements. *In* Consolidation of the Paper Web. Trans. of the Symposium held at Cambridge, Sept., 1965. Vol. 1. p. 852–872. Bolam, F., ed., Tech. Sect., Brit. Paper and Board Makers' Assocn., 1966.

75. Mann, R. W.; Baum, G. A.; Habeger, C. C. Determination of all nine orthotropic elastic constants for machine-made paper. *Tappi* 63(2): 163–166 (Feb., 1980).

76. Habeger, C. C.; Wink, W. A. Ultrasonic velocity measurements in the thickness direction of paper. *J. Appl. Polymer Sci.* 32(4): 4503–4540 (Sept., 1986).

77. Baum, G. A.; Habeger, C. C.; Fleischman, E. H. Measurement of the orthotropic elastic constants of paper. *In* Role of Fundam. Res. in Pmkg. Trans. BPBIF Symposium held at Cambridge, 1981. p. 453-478. Brander, J., ed., London, Mech. Eng. Publ. Ltd., 1983.

78. Habeger, C. C.; Whitsitt, W. J. A mathematical model of compressive strength in paperboard. *Fiber Science Technol.* 19(1): 1–25 (1983).

79. Hartman, R. R. Mechanical Treatment of Pulp Fibers for Property Development. Doctoral Dissertation. Appleton, Wisconsin, The Institute of Paper Chemistry, 1981. 127 p.

80. Hartman, R. R.; Higgins, B. G. Mechanical treatment of pulp fibers for sheet property development. Proc. of the TAPPI 1983 International Paper Physics Conf. held at Harwichport, Massachusetts, Sept. 18–22, 1983. p. 41–50. Atlanta, Georgia, TAPPI Press, 1983.

81. Hartman, R. R. Mechanical treatment of pulp fibers for paper property development. *In* Papermaking Raw Materials. Trans. of Fundam. Research Symposium held at Oxford, 1985. p. 413–442. Punton, V., ed., London, Mech. Eng. Publ. Ltd., 1985.

82. Higgins, B. G. Refining by Abrasive Wear of Pulp Fibers in Shear Flow, Project 3384, Report 4. Appleton, Wisconsin, The Institute of Paper Chemistry, 1981.

83. TAPPI Test Methods 1988. Atlanta, Georgia, TAPPI, 1987.

84. Sauret, G. *ATIP Bulletin* 16(6): 446–454 (1962).

85. Centre Technique de l'Industrie des Papiers, Cartons, et Celluloses, French pat. 2,030,715 (Nov. 13, 1970).

86. Baum, G. A.; Brennan, D. C.; Habeger, C. C. Orthotropic elastic constants of paper. *Tappi* 64(8): 97–101 (Aug., 1981).

87. Van Zummeren, M.; Young, D.; Habeger, C. C.; Baum, G. A.; Treleven, R. Automatic Determination of Ultrasound Velocities in Planar Materials. IPC Tech. Paper Ser. no. 181: 27 p. (June 1986).

88. Wink, W. A.; Baum, G. A. Rubber platen caliper gage: a new concept in measuring paper thickness. *Tappi J.* 66(9): 131–133 (Sept., 1983).

89. Johnson, J. N. Shock propagation produced by planar impact in linearly elastic anisotropic media. *J. Appl. Phys.* 42(13): 5522–5530 (Dec., 1971).

90. Baum, G. A.; Bornhoeft, L. R. Estimating Poisson ratios in paper using ultrasonic techniques. *Tappi* 62(5): 87–90 (May, 1979).

91. Mann, R. W.; Baum, G. A.; Habeger, C. C. Elastic wave propagation in paper. *Tappi* 62(8): 115–118 (Aug., 1979).

92. Jordan, B. D.; Page, D. H. Proc. of the TAPPI 1979 International Paper Physics Conf. held at Harrison Hot Springs, British Columbia, 1979. p. 105. Atlanta, Georgia, TAPPI Press, 1979.

93. Hawes, J. M. Characterizations of the fines fraction of papermaking pulps. Independent Study. Appleton, Wisconsin, The Institute of Paper Chemistry, 1984. 78 p.

94. Ostle, B; Mensing, R. W. Statistics in Research. 3rd ed. p. 317–322. Ames, Iowa, The Iowa State University Press, 1975.

95. Crandall, S. H.; Dahl, N. C.; Lardner, T. J. An Introduction to the Mechanics of Solids. 2nd ed. p. 416–510. New York, McGraw-Hill Book Company, 1978.

96. Seth, R. S.; Page, D. H.; Barbe, M. C.; Jordan, B. D. The mechanism of the strength and extensibility of wet webs. Proc. of the TAPPI 1983 International Paper Physics Conf. held at Harwichport, Massachusetts, Sept. 18–22, 1983. p. 73–82. Atlanta, Georgia, TAPPI Press, 1983.

97. Ehrnrooth, E. M.; Kolseth, P. The tensile testing of single wood pulp fibers in air and in water. *Wood and Fiber Sci.* 16(4): 549–566 (1984).

98. Page, D. H.; El-Hosseiny, F.; Winkler, K.; Lancaster, A. P. S. Elastic modulus of single wood pulp fibers. *Tappi* 60(4): 144–117 (Apr., 1977).

99. Berger, B. F.; Baum, G. A. Z–direction properties: the effects of yield and refining. *In* Papermaking Raw Materials. Trans. of Fundam. Research Symposium held at Oxford, 1985. p. 339–362. Punton, V., ed., London, Mech. Eng. Publ. Ltd., 1985.

100. Peel, J. D., Hudson, F. L. Application of elastic theory to a supercalender nip. *Paper Technology*, 7(5): 460–470 (T164–T174) (1967).

101. Page, D. H. The collapse behavior of pulp fibers. *Tappi* 50(9): 449–455 (Sept., 1967).

102. Kibblewhite, R. P.; Brookes, D. Dimension and collapse behavior of kraft and bisulphite fibers in wet pulps and 'in situ' in handsheets. *Appita* 31(2): 111–118 (Sept., 1977).

103. Berger, B. F. Unpublished work. Appleton, Wisconsin, The Institute of Paper Chemistry, 1988.

APPENDIX I

RESULTS AND ANALYSIS OF BENDING REFINER SPECIAL EXPERIMENTS

Two special experiments were conducted to determine the mechanism by which the fiber are refined in the Bending Refiner. The experiments are presented as 2^2 factorials. The first experiment compared the effect of bending the fibers in only one direction to the effect of bending the fibers in two directions. The experiment had factors of "number of bending directions" (with levels 1 and 2) and "number of refining events" (with levels 3000 and 6000 RE). The second experiment compared the effect of aligning the main direction of fiber orientation perpendicular to the vane, around which the fibers are bent, to the effect of aligning the main direction of fiber orientation parallel to the vane. The experiment had factors of "orientation direction" (with levels of "perpendicular" and "parallel") and fines content (with levels "normal" and "high" as described in the Experimental Program section).

The results were analyzed with an ANOVA technique presented by Ostle and Mensing[94]. The results of a conventional ANOVA can be used to test a hypothesis that the effect of the individual treatments equals zero (H: $\tau_i = 0$ ($i = 1,...,t$)) using an *F*-test. However, this test can only determine if one or more treatment effects is nonzero. The modified ANOVA technique used here allowed identification of the nonzero effects by comparing the contrasts listed in the tables below. The data, contrasts, ANOVA table, and test parameters are given in Table I for the one *vs.* two directions of bending and in Table II for the perpendicular *vs.* parallel bending experiments. The analyses are discussed and summarized in the Experimental Program section.

Table I. Analysis of One *vs.* Two Directions of Bending.

Apparent Density, g/cm^3

Data	One Dir. 3000 RE Norm. Fines 1	One Dir. 6000 RE Norm. Fines 2	Two Dir. 3000 RE Norm. Fines 3	Two Dir. 6000RE Norm. Fines 4
	0.696	0.695	0.731	0.737
	0.699	0.763	0.742	0.757
	0.681	0.726	0.766	0.831
Number	3	3	3	3
Total	2.076	2.184	2.239	2.325
Mean	0.692	0.728	0.746	0.775
Contrast coefficient				
C_1: 1 *vs.* 3	1	0	-1	0
C_2: 2 *vs.* 4	0	1	0	-1
C_3: 1&2 *vs.* 3&4	1	1	-1	-1

ANOVA Source of Variance	Degrees of Freedom	Sum of Squares	Mean Squares	F Ratio[a]
Mean	1	6.489	6.489	...
Bending Direction	3	0.011	0.004	3.604
C_1: 1 *vs.* 3	1	0.004	0.004	4.401
C_2: 2 *vs.* 4	1	0.003	0.003	3.293
C_3: 1&2 *vs.* 3&4	1	0.008	0.008	7.655
Experimental Error	8	0.008	0.001	...
Total	12	6.508	...	...

Scheffé Method	C_j[b]	$\hat{V}(C_j)$	$A \cdot \sqrt{\hat{V}(C_j)}$[c]
C_1: 1 *vs.* 3	-0.163	0.000	0.071
C_2: 2 *vs.* 4	-0.141	0.004	0.210
C_3: 1&2 *vs.* 3&4	-0.304	0.004	0.222

[a] $F_{(.95)(3,8)} = 4.07$

[b] Contrast differs significantly from 0 if $|C_j| > A \cdot \sqrt{\hat{V}(C_j)}$

[c] $A = \sqrt{(t-1) \cdot F_{(.95)(3,8)}}$

Table I, continued. Analysis of One *vs.* Two Directions of Bending.

C_{11}/ρ, km^2/s^2

Data	One Dir. 3000 RE Norm. Fines 1	One Dir. 6000 RE Norm. Fines 2	Two Dir. 3000 RE Norm. Fines 3	Two Dir. 6000RE Norm. Fines 4
	5.84	5.78	6.61	5.82
	6.01	6.13	6.21	6.69
	5.43	5.98	6.45	6.72
Number	3	3	3	3
Total	17.280	17.890	19.270	19.230
Mean	5.760	5.963	6.423	6.410
Contrast coefficient				
C_1: 1 *vs.* 3	1	0	-1	0
C_2: 2 *vs.* 4	0	1	0	-1
C_3: 1&2 *vs.* 3&4	1	1	-1	-1

ANOVA Source of Variance	Degrees of Freedom	Sum of Squares	Mean Squares	F Ratio[a]
Mean	1	452.272	452.272	...
Bending Direction	3	0.986	0.329	3.120
C_1: 1 *vs.* 3	1	0.660	0.660	6.263
C_2: 2 *vs.* 4	1	0.299	0.299	2.840
C_3: 1&2 *vs.* 3&4	1	0.924	0.924	8.768
Experimental Error	8	0.843	0.105	...
Total	12	454.102	...	...

Scheffé Method	C_j[b]	$\hat{V}(C_j)$	$A\cdot\sqrt{\hat{V}(C_j)}$[c]
C_1: 1 *vs.* 3	-1.990	0.129	1.257
C_2: 2 *vs.* 4	-1.340	0.292	1.889
C_3: 1&2 *vs.* 3&4	-3.330	0.422	2.269

[a] $F_{(.95)(3,8)} = 4.07$

[b] Contrast differs significantly from 0 if $|C_j| > A\cdot\sqrt{\hat{V}(C_j)}$

[c] $A = \sqrt{(t-1)\cdot F_{(.95)(3,8)}}$

Table I, continued. Analysis of One *vs.* Two Directions of Bending.

C_{66}/ρ, km^2/s^2

Data	One Dir. 3000 RE Norm. Fines 1	One Dir. 6000 RE Norm. Fines 2	Two Dir. 3000 RE Norm. Fines 3	Two Dir. 6000RE Norm. Fines 4
	2.09	2.05	2.45	2.14
	2.13	2.24	2.26	2.49
	1.97	2.13	2.32	2.49
Number	3	3	3	3
Total	6.190	6.420	7.030	7.120
Mean	2.063	2.140	2.343	2.373
Contrast coefficient				
C_1: 1 *vs.* 3	1	0	-1	0
C_2: 2 *vs.* 4	0	1	0	-1
C_3: 1&2 *vs.* 3&4	1	1	-1	-1

ANOVA Source of Variance	Degrees of Freedom	Sum of Squares	Mean Squares	F Ratio[a]
Mean	1	59.675	59.675	...
Bending Direction	3	0.208	0.069	4.179
C_1: 1 *vs.* 3	1	0.118	0.118	7.095
C_2: 2 *vs.* 4	1	0.082	0.082	4.927
C_3: 1&2 *vs.* 3&4	1	0.198	0.198	11.924
Experimental Error	8	0.133	0.017	...
Total	12	60.015	...	...

Scheffé Method	C_j[b]	$\hat{V}(C_j)$	$A \cdot \sqrt{\hat{V}(C_j)}$[c]
C_1: 1 *vs.* 3	-0.840	0.016	0.447
C_2: 2 *vs.* 4	-0.700	0.050	0.781
C_3: 1&2 *vs.* 3&4	-1.540	0.066	0.900

[a] $F_{(.95)(3,8)} = 4.07$

[b] Contrast differs significantly from 0 if $|C_j| > A \cdot \sqrt{\hat{V}(C_j)}$

[c] $A = \sqrt{(t-1) \cdot F_{(.95)(3,8)}}$

Table I, continued. Analysis of One *vs.* Two Directions of Bending.

C_{33}/ρ, km^2/s^2

Data	One Dir. 3000 RE Norm. Fines 1	One Dir. 6000 RE Norm. Fines 2	Two Dir. 3000 RE Norm. Fines 3	Two Dir. 6000RE Norm. Fines 4
	0.143	0.129	0.157	0.155
	0.125	0.169	0.150	0.177
	0.117	0.156	0.169	0.205
Number	3	3	3	3
Total	0.385	0.454	0.476	0.537
Mean	0.128	0.151	0.159	0.179
Contrast coefficient				
C_1: 1 *vs.* 3	1	0	-1	0
C_2: 2 *vs.* 4	0	1	0	-1
C_3: 1&2 *vs.* 3&4	1	1	-1	-1

ANOVA Source of Variance	Degrees of Freedom	Sum of Squares	Mean Squares	F Ratio[a]
Mean	1	0.286	0.286	...
Bending Direction	3	0.004	0.001	3.995
C_1: 1 *vs.* 3	1	0.001	0.001	4.201
C_2: 2 *vs.* 4	1	0.001	0.001	3.495
C_3: 1&2 *vs.* 3&4	1	0.003	0.003	7.680
Experimental Error	8	0.003	0.000	...
Total	12	0.292	...	...

Scheffé Method	C_j[b]	$\hat{V}(C_j)$	$A \cdot \sqrt{\hat{V}(C_j)}$[c]
C_1: 1 *vs.* 3	-0.091	0.000	0.057
C_2: 2 *vs.* 4	-0.083	0.001	0.113
C_3: 1&2 *vs.* 3&4	-0.174	0.001	0.127

[a] $F_{(.95)(3,8)} = 4.07$

[b] Contrast differs significantly from 0 if $|C_j| > A \cdot \sqrt{\hat{V}(C_j)}$

[c] $A = \sqrt{(t-1) \cdot F_{(.95)(3,8)}}$

Table I, continued. Analysis of One *vs.* Two Directions of Bending.

C_{44}/ρ, km^2/s^2

Data	One Dir. 3000 RE Norm. Fines 1	One Dir. 6000 RE Norm. Fines 2	Two Dir. 3000 RE Norm. Fines 3	Two Dir. 6000RE Norm. Fines 4
	0.190	0.182	0.227	0.224
	0.188	0.200	0.216	0.234
	0.186	0.232	0.211	0.267
Number	3	3	3	3
Total	0.564	0.614	0.654	0.725
Mean	0.188	0.205	0.218	0.242
Contrast coefficient				
C_1: 1 *vs.* 3	1	0	-1	0
C_2: 2 *vs.* 4	0	1	0	-1
C_3: 1&2 *vs.* 3&4	1	1	-1	-1

ANOVA Source of Variance	Degrees of Freedom	Sum of Squares	Mean Squares	F Ratio[a]
Mean	1	0.545	0.545	
Bending Direction	3	0.005	0.002	5.059
C_1: 1 *vs.* 3	1	0.001	0.001	4.431
C_2: 2 *vs.* 4	1	0.002	0.002	6.740
C_3: 1&2 *vs.* 3&4	1	0.003	0.003	11.051
Experimental Error	8	0.002	0.000	...
Total	12	0.552	...	...

Scheffé Method	C_j[b]	$\hat{V}(C_j)$	$A \cdot \sqrt{\hat{V}(C_j)}$[c]
C_1: 1 *vs.* 3	-0.090	0.000	0.029
C_2: 2 *vs.* 4	-0.111	0.001	0.118
C_3: 1&2 *vs.* 3&4	-0.201	0.001	0.122

[a] $F_{(.95)(3,8)} = 4.07$

[b] Contrast differs significantly from 0 if $|C_j| > A \cdot \sqrt{\hat{V}(C_j)}$

[c] $A = \sqrt{(t-1) \cdot F_{(.95)(3,8)}}$

Table II. Analysis of perpendicular *vs.* parallel fiber orientation.

Apparent Density, g/cm^3

Data	One Dir. 3000 RE Norm. Fines 1	One Dir. 6000 RE Norm. Fines 2	Two Dir. 3000 RE Norm. Fines 3	Two Dir. 6000RE Norm. Fines 4
	0.713	0.845	0.750	0.851
	0.740	0.844	0.742	0.870
	0.788	0.848	0.713	0.863
	0.731	0.818		
	0.700	0.822		
	0.765	0.829		
Number	6	6	3	3
Total	4.437	5.006	2.205	2.584
Mean	0.740	0.834	0.735	0.861
Contrast coefficient				
C_1: 1 *vs.* 3	1	0	-2	0
C_2: 2 *vs.* 4	0	1	0	-2
C_3: 1&2 *vs.* 3&4	1	1	-2	-2

ANOVA Source of Variance	Degrees of Freedom	Sum of Squares	Mean Squares	F Ratio[a]
Mean	1	11.253	11.253	...
Bending Direction	3	0.051	0.017	33.699
C_1: 1 *vs.* 3	1	0.000	0.000	0.080
C_2: 2 *vs.* 4	1	0.001	0.001	2.866
C_3: 1&2 *vs.* 3&4	1	0.001	0.001	0.995
Experimental Error	14	0.007	0.001	...
Total	18	11.311	...	...

Scheffé Method	C_j[b]	$\hat{V}(C_j)$	$A \cdot \sqrt{\hat{V}(C_j)}$[c]
C_1: 1 *vs.* 3	0.027	0.003	0.178
C_2: 2 *vs.* 4	-0.162	0.001	0.081
C_3: 1&2 *vs.* 3&4	-0.135	0.003	0.195

[a] $F_{(.95)(3,8)} = 4.07$

[b] Contrast differs significantly from 0 if $|C_j| > A \cdot \sqrt{\hat{V}(C_j)}$

[c] $A = \sqrt{(t-1) \cdot F_{(.95)(3,8)}}$

Table II, continued. Analysis of perpendicular *vs.* parallel fiber orientation.

C_{11}/ρ, km^2/s^2

Data	One Dir. 3000 RE Norm. Fines 1	One Dir. 6000 RE Norm. Fines 2	Two Dir. 3000 RE Norm. Fines 3	Two Dir. 6000RE Norm. Fines 4
	5.60	8.44	5.82	8.22
	6.48	8.21	5.71	8.24
	6.61	8.29	5.81	8.37
	6.35	8.36		
	6.25	7.91		
	6.73	8.07		
Number	6	6	3	3
Total	38.020	49.280	17.340	24.830
Mean	6.337	8.213	5.780	8.277
Contrast coefficient				
C_1: 1 *vs.* 3	1	0	-2	0
C_2: 2 *vs.* 4	0	1	0	-2
C_3: 1&2 *vs.* 3&4	1	1	-2	-2

ANOVA Source of Variance	Degrees of Freedom	Sum of Squares	Mean Squares	F Ratio[a]
Mean	1	931.249	931.249	...
Bending Direction	3	20.159	6.720	92.929
C_1: 1 *vs.* 3	1	0.620	0.620	8.571
C_2: 2 *vs.* 4	1	0.008	0.008	0.111
C_3: 1&2 *vs.* 3&4	1	0.243	0.243	3.366
Experimental Error	14	1.012	0.072	...
Total	18	952.420	...	...

Scheffé Method	C_j[b]	$\hat{V}(C_j)$	$A\cdot\sqrt{\hat{V}(C_j)}$[c]
C_1: 1 *vs.* 3	3.340	0.175	1.461
C_2: 2 *vs.* 4	-0.380	0.065	0.889
C_3: 1&2 *vs.* 3&4	2.960	0.240	1.711

[a] $F_{(.95)(3,8)} = 4.07$

[b] Contrast differs significantly from 0 if $|C_j| > A\cdot\sqrt{\hat{V}(C_j)}$

[c] $A = \sqrt{(t-1)\cdot F_{(.95)(3,8)}}$

Table II, continued. Analysis of perpendicular *vs.* parallel fiber orientation.

C_{66}/ρ, km^2/s^2

Data	One Dir. 3000 RE Norm. Fines 1	One Dir. 6000 RE Norm. Fines 2	Two Dir. 3000 RE Norm. Fines 3	Two Dir. 6000RE Norm. Fines 4
	1.98	3.02	2.03	3.01
	2.30	2.98	2.05	3.00
	2.31	2.97	2.08	3.04
	2.24	3.01		
	2.15	2.91		
	2.34	2.98		
Number	6	6	3	3
Total	13.320	17.870	6.160	9.050
Mean	2.220	2.978	2.053	3.017
Contrast coefficient				
C_1: 1 *vs.* 3	1	0	-2	0
C_2: 2 *vs.* 4	0	1	0	-2
C_3: 1&2 *vs.* 3&4	1	1	-2	-2

ANOVA Source of Variance	Degrees of Freedom	Sum of Squares	Mean Squares	F Ratio[a]
Mean	1	119.609	119.609	...
Bending Direction	3	3.134	1.045	144.196
C_1: 1 *vs.* 3	1	0.056	0.056	7.669
C_2: 2 *vs.* 4	1	0.003	0.003	0.406
C_3: 1&2 *vs.* 3&4	1	0.016	0.016	2.274
Experimental Error	14	0.101	0.007	...
Total	18	122.844	...	...

Scheffé Method	C_i[b]	$\hat{V}(C_i)$	$A \cdot \sqrt{\hat{V}(C_i)}$[c]
C_1: 1 *vs.* 3	1.000	0.021	0.505
C_2: 2 *vs.* 4	-0.230	0.003	0.199
C_3: 1&2 *vs.* 3&4	0.770	0.024	0.543

[a] $F_{(.95)(3,8)} = 4.07$

[b] Contrast differs significantly from 0 if $|C_j| > A \cdot \sqrt{\hat{V}(C_j)}$

[c] $A = \sqrt{(t-1) \cdot F_{(.95)(3,8)}}$

Table II, continued. Analysis of perpendicular *vs.* parallel fiber orientation.

C_{33}/ρ, km^2/s^2

Data	One Dir. 3000 RE Norm. Fines 1	One Dir. 6000 RE Norm. Fines 2	Two Dir. 3000 RE Norm. Fines 3	Two Dir. 6000RE Norm. Fines 4
	0.145	0.224	0.146	0.231
	0.179	0.248	0.136	0.226
	0.213	0.243	0.165	0.208
	0.154	0.206		
	0.134	0.202		
	0.223	0.212		
Number	6	6	3	3
Total	1.048	1.335	0.447	0.665
Mean	0.175	0.223	0.149	0.222
Contrast coefficient				
C_1: 1 *vs.* 3	1	0	-2	0
C_2: 2 *vs.* 4	0	1	0	-2
C_3: 1&2 *vs.* 3&4	1	1	-2	-2

ANOVA Source of Variance	Degrees of Freedom	Sum of Squares	Mean Squares	F Ratio[a]
Mean	1	0.679	0.679	...
Bending Direction	3	0.015	0.005	7.699
C_1: 1 vs. 3	1	0.001	0.001	1.965
C_2: 2 vs. 4	1	0.000	0.000	0.002
C_3: 1&2 vs. 3&4	1	0.001	0.001	1.047
Experimental Error	14	0.009	0.001	...
Total	18	0.703	...	...

Scheffé Method	C_j[b]	$\hat{V}(C_j)$	$A \cdot \sqrt{\hat{V}(C_j)}$[c]
C_1: 1 vs. 3	0.154	0.002	0.165
C_2: 2 vs. 4	0.005	0.001	0.108
C_3: 1&2 vs. 3&4	0.159	0.003	0.197

[a] $F_{(.95)(3,8)} = 4.07$

[b] Contrast differs significantly from 0 if $|C_j| > A \cdot \sqrt{\hat{V}(C_j)}$

[c] $A = \sqrt{(t-1) \cdot F_{(.95)(3,8)}}$

Table II, continued. Analysis of perpendicular *vs.* parallel fiber orientation.

C_{44}/ρ, km^2/s^2

Data	One Dir. 3000 RE Norm. Fines 1	One Dir. 6000 RE Norm. Fines 2	Two Dir. 3000 RE Norm. Fines 3	Two Dir. 6000RE Norm. Fines 4
	0.196	0.238	0.184	0.306
	0.222	0.297	0.155	0.270
	0.239	0.289	0.175	0.293
	0.242	0.310		
	0.193	0.321		
	0.139	0.314		
Number	6	6	3	3
Total	1.231	1.769	0.514	0.869
Mean	0.205	0.295	0.171	0.290
Contrast coefficient				
C_1: 1 *vs.* 3	1	0	-2	0
C_2: 2 *vs.* 4	0	1	0	-2
C_3: 1&2 *vs.* 3&4	1	1	-2	-2

ANOVA Source of Variance	Degrees of Freedom	Sum of Squares	Mean Squares	F Ratio[a]
Mean	1	1.067	1.067	...
Bending Direction	3	0.047	0.016	16.679
C_1: 1 vs. 3	1	0.002	0.002	2.456
C_2: 2 vs. 4	1	0.000	0.000	0.057
C_3: 1&2 vs. 3&4	1	0.002	0.002	1.632
Experimental Error	14	0.013	0.001	...
Total	18	1.127	...	...

Scheffé Method	C_i[b]	$\hat{V}(C_i)$	$A \cdot \sqrt{\hat{V}(C_i)}$[c]
C_1: 1 vs. 3	0.203	0.002	0.170
C_2: 2 vs. 4	0.031	0.002	0.165
C_3: 1&2 vs. 3&4	0.234	0.005	0.237

[a] $F_{(.95)(3,8)} = 4.07$

[b] Contrast differs significantly from 0 if $|C_i| > A \cdot \sqrt{\hat{V}(C_i)}$

[c] $A = \sqrt{(t-1) \cdot F_{(.95)(3,8)}}$

APPENDIX II

ESTIMATE OF THE NUMBER OF REFINING EVENTS IMPOSED ON FIBERS IN A PFI MILL

(After Tam Doo and Kerekes[46])

Based on an analysis of the geometry and operating conditions of the PFI mill, Tam Doo and Kerekes have proposed a method to estimate the number of times fibers, on the average, are subjected to a "bending cycle." This analysis has been used in this work to estimate the number of refining events (RE), which are equivalent to bending cycles.

Consider the cross section of a PFI mill bedplate and roll shown in Fig. I. The bedplate, with diameter $2R_B$, turns with rotational velocity Ω_B in the counterclockwise direction. The roll, with diameter $2R_R$, turns with rotational velocity Ω_R in the counterclockwise direction. The number of times a point on the bedplate will be contacted by a bar on the roll is the product of the rate at which bars contact the bedplate, the fraction of time the point can be contacted by a bar, and the total time. The following discussion illustrates how to estimate this value.

The linear velocities at R_B and R_R are V_B and V_R respectively. The difference between the two velocities is $V_{R/B}$. Note that the axis which the bedplate and roll rotate about are not the same. This means that the difference in the velocities of V_B and V_R is not the simple scalar difference. However, since the angle between the two is small, the velocity difference can be approximated by the scalar difference between V_B and V_R. Using the specifications from the

Table III. PFI Mill Specifications.

Bedplate	Rotor
Ω_B = 710 rpm	Ω_R = 1460 rpm
$2R_B$ = 0.250 m	$2R_R$ = 0.200 m
$V_B = \pi \Omega_B 2R_B / 60$	$V_R = \pi \Omega_R 2R_R / 60$
= 9.3 m/sec	= 15.3 m/sec

$V_{R/B}$ = 6.0 m/sec

TAPPI Test Method T 248 cm-85 "Laboratory Beating of Pulp (PFI Mill Method)[83]" shown in Table III, the velocity difference can be calculated.

The value of $V_{R/B}$ in Table III, 6.0 m/sec., is given in the TAPPI method; the value given by Tam Doo and Kerekes for $V_{R/B}$ is 1.8π or 5.65 m/sec. Since Tam Doo and Kerekes do not list all of the values used in the calculation, the source of this difference is unknown.

Using point *B* on the bedplate as the frame of reference, begin by calculating the rate of pulses applied to point *B* by the bars on the roll. This is simply the velocity of the roll relative to the bedplate over the spacing of the bars. The spacing of the bars, *S*, in m, is $2\pi R_R/33$ or 0.019 m. The rate of pulses is

$$p = \frac{V_{r/b}}{S} \approx 315 \frac{\text{pulses}}{\text{sec}} \qquad \text{(I)}$$

where *p* is the rate of bar pulses in pulses/sec, $V_{R/B}$ is the roll to bedplate velocity difference in m/sec, and *S* is the spacing of the bars in m. Using Eq. I, *p* is estimated to be 315 pulses/sec. (Tam Doo and Kerekes obtain 297 pulses/sec.).

Next, use the rate of bar pulses to calculate the total number of pulses during a PFI mill run at point *B*. This is simply the product of the rate of pulses, *p*, in pulses/sec, the fraction of time point *B* can be in contact with a bar, *k*, and the total time, *t*, in sec. The fraction of time point *B* can be in contact with a bar is

the length of the refining zone, s, in m, over the circumference of the bedplate, π d_B, in m. The total number of pulses is

$$P \approx p\ k\ t \qquad \text{(II)}$$

where P is the total number of pulses, k is the fraction of time in the refining zone in seconds, and t is the total time in seconds. The total time is 60 N_r / Ω_r where N_r is the total number of revolutions and Ω_r is the angular velocity of the roll in rpms.

Tam Doo and Kerekes have based their estimate of the length of the refining zone on the following assumptions:

1. "refining action begins when the refiner bars first come into contact with the fiber mat,"

2. "the fiber mate is evenly distributed around the periphery of the bedplate,"

3. "the minimum clearance between the bedplate and rotor is zero in the PFI mill."

To estimate the length of the refining zone, the height of the pulp mat must be estimated. Accomplish this by expressing the number of fibers in a PFI mill specimen as the weight of the sample over the weight of an individual fiber. Then, the average number of fiber per m^2, n_f, can be estimated, for a 24 oven-dry gram sample, as

$$n_f \approx 24 \ / \ (w\ \pi\ 2R_B\ h) \qquad \text{(III)}$$

where n_f is the number of fibers per m^2 in m^{-2}, w is the average weight of an individual fiber in g, $2R_B$ is the diameter of the bedplate in m, and h is the height of refining zone (*i.e.* the height of the rotor) which is 0.050 m.

If the fiber mat is initially at 10% consistency, the number density of the fibers, G in fibers per m^3, is the consistency, in grams per m^3, $1x10^5$ g/m^3, over the average weight of an individual fiber, w, in g.

$$G \approx 1x10^5 / w \qquad \text{(IV)}$$

where G is the number density of fibers per m^3 in m^{-3} and w is the average weight of an individual fiber in g.

The thickness of the mat, d, in m, may be calculated as the number of fibers per m^2 over the number of fibers per m^3.

$$\delta = \frac{n_f}{G} \qquad \text{(V)}$$

$$\delta = \frac{\frac{24}{w \pi 2R_R d}}{\frac{1x10^5}{w}} \qquad \text{(VI)}$$

After canceling the average weight of the individual fiber, w, out of the numerator and denominator, and substituting the appropriate values into Eq. VI, δ is calculated to be 6.1 mm.

The length of the refining zone is twice the distance from point B to the point where the roll would either contact or separate from the fiber mat. This point is the intersection of the circle described by radius of the the roll (center at

(0, 0.025) m and radius of 0.1 m) and the circle described by the radius of the bedplate minus the height of the mat (center at (0, 0) m and radius of 0.1189 m). Solving for this point and then calculating the arc length to point *B* gives a distance of 0.08 m. Thus, the refining zone is 0.16 m in length.

Finally, substituting the values into Eq. II (and using Tam Doo and Kerekes' value of 297 pulses/sec.) and solving in terms of N_r gives an expression to convert the number of PFI mill revolutions to refining events. The resulting value is is 2.5 RE/N_r.

$$P \approx 2.5\ N_r \text{ or } RE = 2.5\ N_r \qquad \text{(VII)}$$

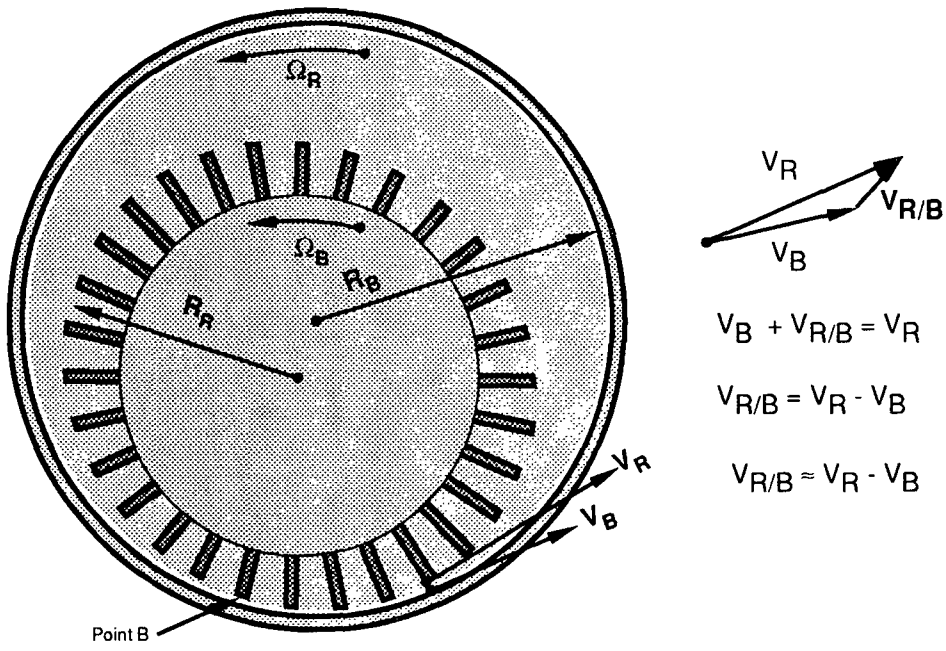

Figure I. PFI mill geometry – top view of rotor and bedplate.

APPENDIX III

HANDSHEET PHYSICAL PROPERTIES

ID	Caliper	Grammage	Apparent Density	SC	Tensile Index	Z.S. Tensile Index	Bonding Index	Compressive Index	Int. Tear Resistance
	µm	g/m^2	g/cm^3		Nm/g	Nm/g	%	Nm/g	mNm^2/g
C-U/L	230	123.1	0.535		9.9	56.6	17.4		
	224	121.4	0.542		10.3	57.9	17.7		
	214	118.1	0.552		10.1	60.5	16.7		
	206	103.1	0.500		6.6	68.2	9.7		
	220	115.1	0.523		8.1	51.5	15.6		
	271	123.8	0.457		7.7	55.3	13.9		
	270	125.9	0.466		7.7	61.2	12.6		
Avg.	234	118.6	0.511	276	8.6	58.8	14.8	6.0	10.03
S.D.	26	7.8	0.037		1.4	5.3	2.9	1.28	
C.I.	20	5.7	0.028		1.1	3.9	2.2	1.02	
C-U/N	235	127.1	0.541		8.4	43.9	19.1		
	227	127.0	0.559		9.9	43.9	22.5		
	230	118.1	0.513		9.8	59.8	16.4		
	248	119.4	0.481		9.3	62.3	14.9		
	245	117.7	0.480		9.6	54.4	17.7		
	240	118.3	0.493		12.1	57.4	21.1		
	255	124.2	0.487		8.9	55.2	16.2		
Avg.	240	121.7	0.508	289	9.7	53.8	18.3	6.9	8.46
S.D.	10	4.3	0.031		1.2	7.3	2.8	1.64	
C.I.	7	3.2	0.023		0.9	5.4	2.0	1.31	

ID	Caliper	Grammage	Apparent Density	SC	Tensile Index	Z.S. Tensile Index	Bonding Index	Compressive Index	Int. Tear Resistance
	µm	g/m^2	g/cm^3		Nm/g	Nm/g	%	Nm/g	mNm^2/g
C-F/N	267	141.3	0.529		13.8	53.1	26.1		
	264	139.0	0.527		12.2	55.3	22.0		
	322	161.8	0.502		11.6				
	295	160.1	0.543		15.4	51.9	20.0		
	315	161.4	0.512		13.1	58.4	22.5		
	315	166.5	0.529		11.1	46.8	23.7		
	353	168.3	0.477		10.4	50.9	20.4		
	306	166.4	0.544		11.9	33.0	36.0		
	290	153.9	0.531		13.6	33.7	40.4		
	321	173.3	0.540		15.9	32.2	49.4		
	280	149.0	0.532		14.1	71.1	19.9		
Avg.	303	158.3	0.524	274	13.0	48.6	29.0	8.5	13.77
S.D.	27	11.2	0.020		1.8	12.6	9.9	1.99	
C.I.	16	6.6	0.012		1.0	7.8	6.1	1.59	
C-U/H	178	126.9	0.713		27.8	52.3	53.2		
	176	129.8	0.738		29.2	52.5	55.6		
	180	126.0	0.700		27.1	56.5	47.9		
	195	134.4	0.689		32.9	64.0	51.4		
	217	144.4	0.665		28.6	59.1	48.3		
	209	142.4	0.681		30.1	55.6	54.1		
	156	104.8	0.672		29.9	65.6	45.6		
Avg.	187	129.8	0.694	302	29.4	58.0	50.9	17.9	26.12
S.D.	21	13.2	0.025		1.9	5.3	3.7		4.36
C.I.	16	9.8	0.019		1.4	3.9	2.7		3.82
C-F/H	254	173.7	0.684		28.9	45.4	63.6		
	265	179.5	0.677		30.2	46.9	64.3		
	226	163.2	0.722		31.6	53.1	59.6		
	236	158.5	0.672		31.7	50.9	62.3		
	240	168.1	0.700		34.0	56.5	60.2		
Avg.	244	168.6	0.691	270	31.3	50.5	62.0	21.5	21.64
S.D.	15	8.3	0.020		1.9	4.5	2.1		2.92
C.I.	13	7.3	0.018		1.7	3.9	1.8		2.86

ID	Caliper	Grammage	Apparent Density	SC	Tensile Index	Z.S. Tensile Index	Bonding Index	Compressive Index	Int. Tear Resistance
	µm	g/m^2	g/cm^3		Nm/g	Nm/g	%	Nm/g	mNm^2/g
B-3/N	191	129.4	0.677		19.6	79.1	24.8		
	201	144.0	0.716		20.6	73.7	28.0		
	207	141.0	0.681		21.9	74.0	29.6		
	186	130.2	0.700		21.4	54.2	39.5		
	204	135.2	0.663		22.3	59.0	37.8		
	186	127.3	0.684		20.0	40.1	50.0		
Avg.	196	134.5	0.687	209	21.0	63.3	34.9	17.1	19.90
S.D.	9	6.8	0.019		1.1	14.9	9.3		2.78
C.I.	7	5.4	0.015		0.9	11.9	7.5		2.23
B-6/N	146	111.7	0.765		17.9	92.1	19.5		
	152	116.1	0.764		19.5	94.0	20.7		
	158	117.5	0.744		23.1	81.5	28.3		
	163	127.2	0.780		24.9	56.9	43.8		
	166	122.1	0.736		22.1	69.0	32.0		
	84	67.1	0.799		22.8	119.8	19.0		
Avg.	145	110.3	0.765	206	21.7	85.5	27.2	16.6	18.58
S.D.	31	21.8	0.023		2.6	21.9	9.7		1.84
C.I.	25	17.5	0.019		2.0	17.5	7.7		1.47
B-12/N	123	97.8	0.795		21.2	81.3	26.1		
	168	117.6	0.700		18.9	70.1	27.0		
	146	111.4	0.763		20.7	58.8	35.2		
	180	122.5	0.681		20.3	55.2	36.7		
	176	134.0	0.761		21.0	53.8	39.0		
	180	128.7	0.715		17.5	54.6	32.1		
Avg.	162	118.7	0.736	221	19.9	62.3	32.7	16.9	17.56
S.D.	23	13.0	0.044		1.4	11.1	5.2		4.39
C.I.	18	10.4	0.035		1.1	8.9	4.2		3.51

ID	Caliper	Grammage	Apparent Density	SC	Tensile Index	Z.S. Tensile Index	Bonding Index	Compressive Index	Int. Tear Resistance
	µm	g/m^2	g/cm^3		Nm/g	Nm/g	%	Nm/g	mNm^2/g
B-3/H	197	160.3	0.814			62.5			
	185	147.9	0.799		33.6	66.4	50.6		
	146	135.2	0.926		40.2	73.9	54.4		
	156	126.5	0.811		39.7	55.1	72.1		
	171	143.7	0.840		39.5	65.0	60.8		
	173	146.7	0.848		39.9	60.2	66.2		
Avg.	171	143.4	0.840	218	38.6	63.9	50.7	22.1	23.78
S.D.	19	11.6	0.046		2.8	6.3	26.0		2.20
C.I.	15	9.3	0.037		2.5	5.1	20.8		1.76
B-6/H	136	122.3	0.899		42.7	70.6	60.6		
	164	137.5	0.838		43.9	70.7	62.1		
	165	141.0	0.855		35.8	69.6	51.5		
	151	128.4	0.850		36.2	67.4	53.7		
	160	145.7	0.911		35.9	58.8	61.0		
	163	146.1	0.896		36.2	55.6	65.2		
Avg.	157	136.8	0.875	187	38.5	65.5	59.0	24.3	23.48
S.D.	11	9.6	0.031		3.8	6.6	5.3		1.36
C.I.	9	7.7	0.024		3.0	5.3	4.2		1.09
B-12/H	170	131.2	0.772		36.6	62.8	58.2		
	165	146.1	0.885		35.9	67.2	53.5		
	152	136.6	0.899		33.2	69.7	47.6		
	146	131.2	0.899		40.5	68.9	58.8		
	144	139.4	0.968		38.6	65.1	59.3		
	137	125.5	0.916		33.0	77.5	42.5		
Avg.	152	135.0	0.890	198	36.3	68.5	53.3	23.4	22.25
S.D.	13	7.3	0.065		3.0	5.1	6.9		1.03
C.I.	10	5.8	0.052		2.4	4.0	5.5		0.82

ID	Caliper	Grammage	Apparent Density	SC	Tensile Index	Z.S. Tensile Index	Bonding Index	Compressive Index	Int. Tear Resistance
	µm	g/m^2	g/cm^3		Nm/g	Nm/g	%	Nm/g	mNm^2/g
R-1/N	178	139.1	0.781		20.5	49.0	41.7		
	219	155.4	0.710		19.1	33.8	56.4		
	238	151.6	0.637		14.9	52.0	28.7		
	236	162.7	0.689		16.7	39.4	42.5		
	203	142.0	0.700		19.5	54.7	35.6		
	214	146.6	0.685		19.2	49.0	39.2		
Avg.	215	149.6	0.700	231	18.3	46.3	40.7	11.8	18.51
S.D.	22	8.8	0.047		2.1	8.0	9.2		3.55
C.I.	18	7.0	0.038		1.6	6.4	7.4		2.84
R-2/N	165	130.5	0.791		22.2	49.8	44.6		
	181	147.1	0.813		25.0	49.0	51.0		
	194	146.3	0.754		22.1	51.7	42.8		
	238	151.0	0.634		15.6	56.2	27.7		
	207	139.9	0.676		19.6	71.6	27.3		
	217	151.6	0.699		18.7	64.0	29.2		
Avg.	200	144.4	0.728	211	20.5	57.0	37.1	13.2	19.20
S.D.	26	8.0	0.069		3.3	9.0	10.3		3.18
C.I.	21	6.4	0.056		2.6	7.2	8.2		2.54
R-3/N	154	127.0	0.825		28.0	53.7	52.1		
	142	116.8	0.823		26.2	68.0	38.5		
	161	114.7	0.712		19.1	58.4	32.7		
	163	133.3	0.818		26.6	52.9	50.3		
	188	140.6	0.748		21.3	62.0	34.4		
	175	135.5	0.774		20.5	64.6	31.7		
	173	140.8	0.814		20.2	56.2	36.0		
Avg.	165	129.8	0.788	201	23.1	59.4	39.4	14.7	20.05
S.D.	15	10.7	0.044		3.6	5.7	8.4		3.16
C.I.	11	7.9	0.033		2.7	4.2	6.2		2.53
R-6/N	190	145.8	0.767		19.5	56.1	34.7		
	190	145.6	0.766		22.8	64.0	35.6		
	186	139.8	0.752	217	17.3	74.0	23.3		
Avg.	189	143.7	0.762	217	19.8	64.7	31.2	14.0	17.65
S.D.	2	3.4	0.009		2.8	9.0	6.8		1.01
C.I.	3	3.9	0.010		3.1	10.2	7.8		1.15

ID	Caliper	Grammage	Apparent Density	SC	Tensile Index	Z.S. Tensile Index	Bonding Index	Compressive Index	Int. Tear Resistance
	µm	g/m^2	g/cm^3		Nm/g	Nm/g	%	Nm/g	mNm^2/g
R-12/N	185	147.3	0.796		19.4	66.6	29.1		
	203	154.2	0.760		27.6	69.2	39.9		
	212	144.5	0.682		23.5	56.0	41.9		
	186	147.0	0.790		26.3	57.5	45.8		
	148	121.8	0.823		20.6	73.5	28.0		
	176	141.0	0.801		20.0	46.3	43.3		
Avg.	185	142.6	0.775	214	22.9	61.5	38.0	14.9	18.22
S.D.	22	11.1	0.050		3.5	10.1	7.6		3.37
C.I.	18	8.9	0.040		2.8	8.1	6.1		2.70
R-1/H	214	170.3	0.796		37.4	58.7	63.8		
	189	161.5	0.854		37.9	58.9	64.4		
	185	163.0	0.881		39.1	65.5	59.7		
	156	137.0	0.878		43.6	59.7	73.0		
	160	139.6	0.873		45.4	59.9	75.9		
	188	157.3	0.837		37.0	62.4	59.3		
Avg.	182	154.8	0.853	254	40.1	60.9	66.0	21.0	25.63
S.D.	21	13.5	0.033		3.6	2.6	6.9		4.12
C.I.	17	10.8	0.026		2.9	2.1	5.5		3.30
R-2/H	197	159.9	0.812		35.4	55.3	64.1		
	207	158.1	0.764		36.0	66.8	53.9		
	190	158.2	0.833		41.2	69.0	59.8		
	186	152.6	0.820		45.4	73.7	61.7		
	168	142.2	0.846		45.6	67.6	67.5		
	199	159.7	0.803		38.1	55.0	69.3		
Avg.	191	155.1	0.813	211	40.3	64.5	62.7	21.5	24.51
S.D.	13	6.9	0.029		4.5	7.7	5.6		3.02
C.I.	11	5.5	0.023		3.6	6.1	4.5		2.42

ID	Caliper	Grammage	Apparent Density	SC	Tensile Index	Z.S. Tensile Index	Bonding Index	Compressive Index	Int. Tear Resistance
	µm	g/m^2	g/cm^3		Nm/g	Nm/g	%	Nm/g	mNm^2/g
R-3/H	172	153.4	0.892		42.6	63.6	66.9		
	193	161.2	0.835		37.1	65.7	56.5		
	209	163.7	0.783		36.8	68.3	53.9		
	192	158.1	0.823		38.9	58.1	66.9		
	177	145.5	0.822		41.5	58.9	70.4		
	176	149.4	0.849		40.3	48.4	83.1		
Avg.	187	155.2	0.834	221	39.5	60.5	66.3	21.2	25.06
S.D.	14	7.0	0.036		2.3	7.1	10.5		2.44
C.I.	11	5.6	0.029		1.9	5.7	8.4		1.95
R-6/H	166	154.2	0.929		48.8	68.1	71.7		
	187	156.9	0.839		41.0	60.7	67.6		
	200	156.9	0.785		41.2	61.4	67.0		
Avg.	184	156.0	0.851	186	43.7	63.4	68.8	23.0	24.48
S.D.	17	1.6	0.073		4.5	4.1	2.6		1.21
C.I.	19	1.8	0.083		5.1	4.6	2.9		1.37
R-12/H	184	160.4	0.872		36.9	58.1	63.5		
	176	154.6	0.878		45.3	60.6	74.7		
	183	167.9	0.917		42.8	58.3	73.5		
	170	148.1	0.871		39.7	61.5	64.6		
	168	151.2	0.900		42.4	62.2	68.3		
	172	155.7	0.905		41.9	51.8	81.0		
Avg.	176	156.3	0.891	197	41.5	58.7	70.9	22.4	24.04
S.D.	7	7.0	0.020		2.9	3.8	6.7		2.47
C.I.	5	5.6	0.016		2.3	3.0	5.4		1.98
P-3H/L	137	117.3	0.856		37.7	66.0	57.2		
	130	111.9	0.861		34.1	91.7	37.1		
	125	117.3	0.938		40.8	48.3	84.6		
Avg.	131	115.5	0.885	188	37.5	68.7	59.6	22.9	23.25
S.D.	6	3.1	0.046		3.4	21.8	23.8		2.49
C.I.	7	3.5	0.052		3.8	24.7	26.9		2.82

ID	Caliper	Grammage	Apparent Density	SC	Tensile Index	Z.S. Tensile Index	Bonding Index	Compressive Index	Int. Tear Resistance
	µm	g/m^2	g/cm^3		Nm/g	Nm/g	%	Nm/g	mNm^2/g
P-6H/L	130	119.8	0.922		45.3	81.4	55.6		
	126	116.9	0.928		51.5	77.6	66.3		
	126	117.8	0.935		54.2	73.0	74.2		
Avg.	127	118.2	0.928	153	50.3	77.4	65.4	25.7	19.92
S.D.	2	1.5	0.007		4.6	4.2	9.3		1.11
C.I.	3	1.7	0.008		5.2	4.8	10.6		1.25
P-12H/L	122	114.3	0.937		54.4	76.8	70.8		
	113	108.1	0.957		56.1	87.0	64.5		
	109	109.5	1.005		62.2	90.5	68.7		
Avg.	115	110.6	0.966	142	57.6	84.7	68.0	26.7	17.02
S.D.	7	3.3	0.035		4.1	7.1	3.2		0.63
C.I.	8	3.7	0.039		4.6	8.0	3.6		0.71
P-24H/L	109	106.8	0.980		53.9	68.0	79.3		
	97	101.5	1.046		55.8	75.4	74.0		
	103	108.1	1.050		52.9	77.4	68.4		
Avg.	103	105.5	1.025	145	54.2	73.6	73.9	26.3	15.87
S.D.	6	3.5	0.039		1.4	4.9	5.4		1.14
C.I.	7	4.0	0.045		1.6	5.6	6.1		1.29
P-3H/N	144	126.5	0.878		44.1	57.0	77.4		
	141	117.1	0.830		43.3	62.3	69.5		
	147	125.1	0.851		45.6	62.3	73.1		
Avg.	144	122.9	0.853	190	44.3	60.5	73.3	23.6	22.92
S.D.	3	5.1	0.024		1.2	3.1	4.0		0.86
C.I.	3	5.7	0.027		1.3	3.5	4.5		0.97
P-6H/N	122	123.3	1.011		48.1	65.9	73.0		
	140	127.5	0.911		56.0	64.7	86.6		
	115	118.1	1.027		54.3	61.8	87.9		
Avg.	126	123.0	0.983	168	52.8	64.1	82.5	26.6	19.29
S.D.	13	4.7	0.063		4.1	2.1	8.2		0.68
C.I.	15	5.3	0.071		4.7	2.4	9.3		0.77

ID	Caliper	Grammage	Apparent Density	SC	Tensile Index	Z.S. Tensile Index	Bonding Index	Compressive Index	Int. Tear Resistance
	µm	g/m^2	g/cm^3		Nm/g	Nm/g	%	Nm/g	mNm^2/g
P-12H/N	107	119.8	1.120		60.2	67.6	89.1		
	111	120.7	1.087		61.9	53.1	116.6		
	110	116.0	1.055		61.1	71.6	85.3		
Avg.	109	118.8	1.087	143	61.1	64.1	97.0	29.5	14.97
S.D.	2	2.5	0.033		0.8	9.7	17.0		0.44
C.I.	2	2.8	0.037		0.9	11.0	19.3		0.50
P-24H/N	95	112.7	1.186		72.2	78.7	91.8		
	95	117.1	1.233		75.5	84.1	89.8		
	95	116.1	1.222		70.2	78.4	89.5		
Avg.	95	115.3	1.214	122	72.7	80.4	90.4	29.7	12.71
S.D.	0	2.3	0.024		2.7	3.2	1.2		0.68
C.I.	0	2.6	0.027		3.0	3.6	1.4		0.77
P-3H/H	140	127.8	0.913		58.9	66.6	88.5		
	122	122.2	1.002		59.8	71.3	83.8		
	120	126.5	1.054		58.3	60.2	96.8		
Avg.	127	125.5	0.990	168	59.0	66.1	89.7	27.3	18.34
S.D.	11	2.9	0.071		0.7	5.6	6.6		0.21
C.I.	12	3.3	0.081		0.8	6.3	7.5		0.24
P-6H/H	102	118.7	1.164		69.7	74.4	93.7		
	106	119.6	1.128		65.2	79.3	82.1		
	111	120.6	1.086		72.2	78.4	92.1		
Avg.	106	119.6	1.126	137	69.0	77.4	89.3	31.0	13.34
S.D.	5	1.0	0.039		3.6	2.6	6.2		0.95
C.I.	5	1.1	0.044		4.0	2.9	7.1		1.08
P-12H/H	105	121.3	1.155		72.2	77.7	92.9		
	105	122.5	1.167		71.5	77.0	92.9		
	95	120.3	1.266		67.4	62.9	107.3		
Avg.	102	121.4	1.196	129	70.4	72.5	97.7	30.3	12.36
S.D.	6	1.1	0.061		2.6	8.4	8.3		0.33
C.I.	7	1.2	0.069		2.9	9.5	9.4		0.37

ID	Caliper	Grammage	Apparent Density	SC	Tensile Index	Z.S. Tensile Index	Bonding Index	Compressive Index	Int. Tear Resistance
	µm	g/m^2	g/cm^3		Nm/g	Nm/g	%	Nm/g	mNm^2/g
P-24H/H	91	114.6	1.259		75.0	63.7	117.8		
	89	116.4	1.308		71.1	72.4	98.3		
	84	110.8	1.319		72.0	76.0	94.7		
Avg.	88	113.9	1.295	113	72.7	70.7	103.6	29.4	11.94
S.D.	4	2.9	0.032		2.0	6.3	12.4		0.23
C.I.	4	3.2	0.036		2.3	7.2	14.0		0.26
P-3L/L	152	119.2	0.784		31.3	54.7	57.2		
	152	120.8	0.795		29.8	62.8	47.3		
	149	117.5	0.789		32.1	80.0	40.2		
Avg.	151	119.2	0.789	178	31.1	65.9	48.2	20.2	27.07
S.D.	2	1.7	0.005		1.2	12.9	8.6		2.25
C.I.	2	1.9	0.006		1.4	14.6	9.7		2.55
P-6L/L	149	128.8	0.864		44.5	65.2	68.3		
	141	126.0	0.894		44.4	72.0	61.7		
	148	123.6	0.835		44.6	77.7	57.4		
Avg.	146	126.1	0.864	173	44.5	71.6	62.5	24.1	21.71
S.D.	4	2.6	0.029		0.1	6.3	5.5		0.24
C.I.	5	2.9	0.033		0.1	7.1	6.2		0.27
P-12L/L	129	117.0	0.907		56.6	70.2	80.7		
	130	119.9	0.922		58.4	65.8	88.8		
	127	118.9	0.936		54.1	54.4	99.4		
Avg.	129	118.6	0.922	158	56.4	63.5	89.6	25.2	17.28
S.D.	2	1.5	0.015		2.2	8.2	9.4		1.40
C.I.	2	1.7	0.017		2.5	9.2	10.6		1.59
P-24L/L	104	105.1	1.011		64.9	63.5	102.3		
	102	105.0	1.029		62.6	58.5	107.1		
	98	105.8	1.080		57.1	71.2	80.1		
Avg.	101	105.3	1.040	145	61.5	64.4	96.5	26.9	17.14
S.D.	3	0.4	0.036		4.0	6.4	14.4		1.29
C.I.	3	0.5	0.040		4.6	7.3	16.3		1.46

ID	Caliper	Grammage	Apparent Density	SC	Tensile Index	Z.S. Tensile Index	Bonding Index	Compressive Index	Int. Tear Resistance
	µm	g/m^2	g/cm^3		Nm/g	Nm/g	%	Nm/g	mNm^2/g
P-3L/N	159	122.5	0.770		37.3	71.2	52.3		
	142	121.1	0.853		35.3	66.4	53.1		
	146	126.4	0.866		35.0	64.8	54.1		
Avg.	149	123.3	0.830	198	35.8	67.4	53.2	20.5	23.69
S.D.	9	2.7	0.052		1.2	3.3	0.9		1.41
C.I.	10	3.1	0.059		1.4	3.8	1.0		1.60
P-6L/N	128	114.6	0.895		50.5	76.9	65.7		
	121	114.9	0.950		52.6	74.6	70.5		
	120	114.4	0.953		54.2	57.0	95.0		
Avg.	123	114.6	0.933	171	52.4	69.5	77.1	24.4	19.78
S.D.	4	0.3	0.032		1.9	10.9	15.7		0.57
C.I.	5	0.3	0.037		2.1	12.3	17.8		0.65
							0.0		
P-12L/N	116	115.4	0.995		57.9	73.5			
	118	116.5	0.987		60.3	57.0	105.7		
	117	115.4	0.986		63.8	50.1	127.3		
Avg.	117	115.8	0.989	149	60.7	60.2	104.0	27.0	15.97
S.D.	1	0.6	0.005		2.9	12.0	24.3		0.57
C.I.	1	0.7	0.005		3.3	13.6	27.5		0.64
P-24L/N	107	123.4	1.153		70.9	81.2	87.3		
	103	122.9	1.193		65.9	69.0	95.5		
	104	127.1	1.222		67.0	71.2	94.2		
Avg.	105	124.5	1.190	133	67.9	73.8	92.3	28.6	14.43
S.D.	2	2.3	0.035		2.6	6.5	4.4		0.64
C.I.	2	2.6	0.039		3.0	7.4	5.0		0.73
P-3L/H	129	122.5	0.950		53.4	62.5	85.5		
	126	123.1	0.977		51.8	68.4	75.7		
	138	129.6	0.939		51.3	66.8	76.7		
Avg.	131	125.1	0.955	184	52.1	65.9	79.3	25.2	19.94
S.D.	6	3.9	0.020		1.1	3.1	5.4		1.23
C.I.	7	4.5	0.022		1.2	3.5	6.1		1.39

ID	Caliper	Grammage	Apparent Density	SC	Tensile Index	Z.S. Tensile Index	Bonding Index	Compressive Index	Int. Tear Resistance
	µm	g/m^2	g/cm^3		Nm/g	Nm/g	%	Nm/g	mNm^2/g
P-6L/H	120	122.7	1.023		66.3	68.4	96.9		
	115	123.2	1.071		64.1	73.7	87.0		
	114	121.6	1.067		65.2	88.3	73.9		
Avg.	116	122.5	1.053	154	65.2	76.8	86.0	27.5	14.45
S.D.	3	0.8	0.027		1.1	10.3	11.5		1.21
C.I.	4	0.9	0.030		1.2	11.7	13.1		1.37
P-12L/H	109	117.4	1.077		71.3	76.0	93.8		
	110	122.2	1.111		72.2	79.6	90.7		
	112	121.8	1.088		72.7	83.8	86.9		
Avg.	110	120.5	1.092	141	72.1	79.8	90.5	28.6	14.40
S.D.	2	2.7	0.017		0.7	3.9	3.5		1.07
C.I.	2	3.0	0.020		0.8	4.4	4.0		1.21
P-24L/H	102	120.9	1.185		71.9	80.7	89.1		
	109	124.5	1.142		70.6	87.2	81.0		
	102	122.8	1.204		71.9	74.9	96.1		
Avg.	104	122.7	1.177	125	71.5	80.9	88.7	29.9	14.00
S.D.	4	1.8	0.032		0.8	6.2	7.6		0.44
C.I.	5	2.0	0.036		0.9	7.0	8.6		0.50

APPENDIX IV

HANDSHEET ELASTIC PROPERTIES

ID	Caliper	Grammage	Apparent Density	C_{11}/ρ	C_{66}/ρ	C_{33}/ρ	C_{44}/ρ
	µm	g/m^2	g/cm^3	$(km/s)^2$	$(km/s)^2$	$(km/s)^2$	$(km/s)^2$
C-U/L	242	123.1	0.510	3.96	1.35	0.049	0.101
	239	121.3	0.508	3.93	1.35	0.049	0.099
	228	118.1	0.517	4.02	1.37	0.052	0.108
	205	103.1	0.503	3.29	1.13	0.031	0.087
	233	115.1	0.494	3.35	1.13	0.035	0.080
	248	123.8	0.500	3.37	1.15	0.036	0.081
	261	125.9	0.482	3.37	1.14	0.035	0.081
Avg.	237	118.6	0.502	3.61	1.23	0.041	0.091
S.D.	17	7.7	0.012	0.34	0.12	0.008	0.012
C.I.	13	5.7	0.009	0.25	0.09	0.006	0.009
C-U/N	257	127.1	0.494	3.37		0.045	0.085
	255	127.0	0.498	3.62		0.049	0.091
	232	118.1	0.510	3.27		0.053	0.093
	255	119.4	0.468	3.22	1.12	0.044	0.089
	250	117.7	0.470	3.21	1.12	0.044	0.086
	253	118.3	0.467	3.59	1.23	0.043	0.090
	267	124.2	0.465	3.56	1.23	0.045	0.094
Avg.	253	121.7	0.482	3.41	1.17	0.046	0.090
S.D.	11	4.3	0.018	0.18	0.06	0.003	0.003
C.I.	8	3.2	0.013	0.13	0.06	0.003	0.003

ID	Caliper	Grammage	Apparent Density	C_{11}/ρ	C_{66}/ρ	C_{33}/ρ	C_{44}/ρ
	µm	g/m^2	g/cm^3	$(km/s)^2$	$(km/s)^2$	$(km/s)^2$	$(km/s)^2$
C-F/N	280	141.3	0.505	4.42	1.53	0.052	0.100
	274	139.0	0.507	4.48	1.54	0.054	0.103
	338	161.8	0.479	3.88	1.30	0.040	0.093
	303	160.1	0.528	4.57	1.59	0.059	0.121
	325	161.4	0.497	4.40	1.50	0.050	0.112
	343	166.5	0.485	3.87	1.34	0.043	0.100
	346	168.3	0.486	3.70	1.28	0.043	0.093
	333	166.4	0.500	3.93	1.35	0.042	0.095
	311	153.9	0.495	4.44	1.52	0.055	0.112
	342	173.3	0.506	4.55	1.58	0.062	0.125
	299	149.0	0.498	4.36	1.49	0.057	0.115
Avg.	318	158.3	0.499	4.24	1.46	0.051	0.106
S.D.	26	11.2	0.013	0.32	0.11	0.007	0.011
C.I.	15	6.6	0.008	0.19	0.07	0.004	0.007
C-U/H	197	129.8	0.659	6.49	2.32	0.142	0.240
	189	126.0	0.665	6.54	2.35	0.141	0.207
	193	134.4	0.695	6.16	2.23	0.130	0.232
	205	144.0	0.701	6.34	2.30	0.128	0.241
	202	142.4	0.705	6.33	2.28	0.128	0.241
	146	104.8	0.716	6.16	2.25	0.117	0.212
Avg.	189	130.2	0.690	6.34	2.29	0.131	0.229
S.D.	22	14.3	0.023	0.16	0.05	0.009	0.015
C.I.	17	11.4	0.019	0.13	0.04	0.007	0.012
C-F/H	277	173.7	0.627	6.23	2.22	0.131	0.199
	287	179.5	0.626	6.31	2.27	0.134	0.222
	234	163.2	0.696	6.63	2.40	0.129	0.221
	221	158.5	0.716	6.60	2.36	0.136	0.213
	240	168.1	0.701	6.51	2.38	0.122	0.219
Avg.	252	168.6	0.673	6.46	2.33	0.130	0.215
S.D.	28	8.3	0.043	0.18	0.08	0.006	0.009
C.I.	25	7.3	0.038	0.15	0.07	0.005	0.008

ID	Caliper	Grammage	Apparent Density	C_{11}/ρ	C_{66}/ρ	C_{33}/ρ	C_{44}/ρ
	μm	g/m^2	g/cm^3	$(km/s)^2$	$(km/s)^2$	$(km/s)^2$	$(km/s)^2$
B-3/N	185	129.4	0.699	6.55	2.29	0.158	0.216
	203	144.0	0.709	6.11	2.12	0.144	0.242
	188	141.0	0.749	6.32	2.21	0.166	0.273
	186	130.3	0.700	6.16	2.16	0.140	0.212
	190	135.2	0.712	6.53	2.28	0.130	0.233
	183	127.3	0.697	5.80	2.02	0.123	0.208
Avg.	189	134.5	0.711	6.25	2.18	0.144	0.231
S.D.	7	6.8	0.020	0.28	0.10	0.016	0.025
C.I.	6	5.4	0.016	0.23	0.08	0.013	0.020
B-6/N	157	111.7	0.713	5.60	1.98	0.145	0.196
	157	116.1	0.740	6.48	2.30	0.179	0.222
	149	117.5	0.788	6.61	2.31	0.213	0.239
	174	127.2	0.731	6.35	2.24	0.154	0.242
	174	122.1	0.700	6.25	2.15	0.135	0.193
	88	67.1	0.765	6.73	2.34	0.223	0.139
Avg.	150	110.3	0.740	6.34	2.22	0.175	0.205
S.D.	32	21.8	0.033	0.40	0.14	0.036	0.038
C.I.	26	17.5	0.026	0.32	0.11	0.029	0.031
B-12/N	133	97.8	0.737	6.44	2.26	0.184	0.207
	165	117.6	0.713	6.13	2.17	0.135	0.224
	146	111.4	0.761	6.13	2.17	0.180	0.235
	185	122.5	0.663	5.92	2.06	0.147	0.228
	182	134.0	0.734	6.22	2.18	0.150	0.258
	195	128.7	0.660	5.99	2.08	0.108	0.182
Avg.	168	118.7	0.711	6.14	2.15	0.151	0.222
S.D.	24	13.0	0.042	0.18	0.07	0.029	0.026
C.I.	19	10.4	0.033	0.15	0.06	0.023	0.021

ID	Caliper	Grammage	Apparent Density	C_{11}/ρ	C_{66}/ρ	C_{33}/ρ	C_{44}/ρ
	µm	g/m^2	g/cm^3	$(km/s)^2$	$(km/s)^2$	$(km/s)^2$	$(km/s)^2$
B-3/H	212	160.3	0.756	7.44	2.58	0.212	0.275
	192	147.9	0.769	7.74	2.76	0.185	0.257
	159	135.2	0.852	8.60	3.16	0.223	0.285
	154	126.5	0.819	7.99	2.94	0.207	0.274
	176	143.7	0.817	8.02	2.89	0.193	0.279
	174	146.7	0.845	8.11	2.93	0.202	0.285
Avg.	178	143.4	0.810	7.98	2.88	0.203	0.276
S.D.	21	11.6	0.039	0.39	0.19	0.014	0.010
C.I.	17	9.3	0.031	0.31	0.16	0.011	0.008
B-6/H	145	122.3	0.845	8.44	3.02	0.225	0.238
	163	137.5	0.844	8.21	2.98	0.248	0.297
	166	141.0	0.848	8.29	2.97	0.243	0.289
	157	128.4	0.818	8.36	3.01	0.206	0.310
	177	145.7	0.822	7.91	2.91	0.202	0.321
	176	146.1	0.829	8.07	2.98	0.212	0.314
Avg.	164	136.8	0.834	8.21	2.98	0.223	0.295
S.D.	12	9.6	0.013	0.20	0.04	0.020	0.030
C.I.	10	7.7	0.010	0.16	0.03	0.016	0.024
B-12/H	163	131.2	0.806	7.74	2.79	0.221	0.276
	177	146.1	0.825	7.96	2.80	0.222	0.298
	162	134.4	0.832	7.97	2.82	0.230	0.272
	154	131.2	0.851	8.24	3.05	0.217	0.338
	168	139.4	0.830	8.28	3.02	0.196	0.278
	150	125.5	0.835	8.29	3.06	0.203	0.269
Avg.	162	134.6	0.830	8.08	2.92	0.215	0.289
S.D.	10	7.2	0.015	0.22	0.13	0.013	0.026
C.I.	8	5.8	0.012	0.18	0.11	0.010	0.021

ID	Caliper	Grammage	Apparent Density	C_{11}/ρ	C_{66}/ρ	C_{33}/ρ	C_{44}/ρ
	µm	g/m^2	g/cm^3	$(km/s)^2$	$(km/s)^2$	$(km/s)^2$	$(km/s)^2$
R-1/N	186	139.1	0.750	7.16	2.60	0.069	0.146
	221	155.4	0.702	6.76	2.43	0.058	0.125
	248	151.6	0.613	5.15	1.84	0.049	0.115
	253	162.7	0.643	5.79	2.10	0.064	0.145
	215	142.0	0.659	6.04	2.12	0.072	0.136
	215	146.6	0.682	6.46	2.27	0.077	0.152
Avg.	223	149.6	0.675	6.23	2.23	0.065	0.137
S.D.	25	8.8	0.048	0.72	0.27	0.010	0.014
C.I.	20	7.0	0.038	0.58	0.21	0.008	0.011
R-2/N	166	130.5	0.786	7.98	2.95	0.076	0.160
	189	147.1	0.780	8.02	2.95	0.062	0.142
	185	145.3	0.787	7.71	2.85	0.073	0.166
	247	151.0	0.612	5.34	1.90	0.053	0.123
	209	139.9	0.669	6.09	2.15	0.072	0.152
	226	151.6	0.672	6.35	2.26	0.076	0.158
Avg.	204	144.2	0.718	6.92	2.51	0.069	0.150
S.D.	30	8.0	0.076	1.14	0.46	0.009	0.016
C.I.	24	6.4	0.061	0.91	0.37	0.007	0.012
R-3/N	153	127.0	0.829	9.27	3.39	0.075	0.144
	153	116.8	0.763	8.35	3.05	0.094	0.150
	160	114.7	0.718	7.25	2.66	0.061	0.126
	171	133.3	0.781	8.79	3.26	0.073	0.139
	198	140.6	0.711	7.08	2.56	0.069	0.147
	191	135.5	0.708	6.89	2.51	0.079	0.155
	202	140.8	0.698	6.52	2.37	0.078	0.151
Avg.	175	129.8	0.744	7.74	2.83	0.076	0.145
S.D.	21	10.7	0.049	1.06	0.40	0.010	0.010
C.I.	16	7.9	0.036	0.78	0.30	0.007	0.007
R-6/N	196	145.9	0.745	6.47	2.34	0.086	0.172
	187	145.6	0.777	7.12	2.60	0.073	0.150
	190	139.8	0.737	6.49	2.31	0.068	0.159
Avg.	191	143.8	0.753	6.69	2.42	0.076	0.160
S.D.	5	3.4	0.021	0.37	0.16	0.009	0.011
C.I.	5	3.9	0.024	0.42	0.18	0.010	0.013

ID	Caliper	Grammage	Apparent Density	C_{11}/ρ	C_{66}/ρ	C_{33}/ρ	C_{44}/ρ
	µm	g/m^2	g/cm^3	$(km/s)^2$	$(km/s)^2$	$(km/s)^2$	$(km/s)^2$
R-12/N	187	147.3	0.787	8.24	3.06	0.100	0.185
	217	154.2	0.710	6.94	2.50	0.082	0.171
	218	144.2	0.660	6.10	2.19	0.066	0.149
	182	147.0	0.805	7.75	2.80	0.097	0.189
	153	121.8	0.795	6.79	2.44	0.086	0.171
	187	141.0	0.755	6.87	2.44	0.078	0.158
Avg.	191	142.6	0.752	7.12	2.57	0.085	0.171
S.D.	24	11.1	0.057	0.76	0.31	0.013	0.015
C.I.	19	8.9	0.045	0.61	0.25	0.010	0.012
R-1/H	223	170.6	0.764	7.98	2.87	0.147	0.246
	208	161.8	0.777	8.34	2.98	0.154	0.263
	202	163.0	0.807	8.44	3.08	0.157	0.279
	173	139.0	0.803	9.26	3.38	0.156	0.234
	174	139.6	0.800	8.75	3.30	0.153	0.273
	204	157.3	0.772	8.02	3.05	0.159	0.237
Avg.	197	155.2	0.787	8.47	3.11	0.154	0.255
S.D.	20	13.1	0.018	0.48	0.19	0.004	0.019
C.I.	16	10.4	0.015	0.39	0.16	0.003	0.015
R-2/H	210	159.9	0.763	8.11	2.91	0.142	0.246
	209	158.1	0.755	7.90	2.87	0.135	0.249
	194	158.2	0.815	8.83	3.24	0.148	0.248
	189	152.6	0.809	9.33	3.45	0.162	0.256
	178	142.2	0.800	9.21	3.35	0.150	0.239
	210	159.7	0.761	8.33	3.05	0.150	0.268
Avg.	198	155.1	0.784	8.62	3.15	0.148	0.251
S.D.	13	6.9	0.027	0.59	0.24	0.009	0.010
C.I.	11	5.5	0.022	0.47	0.19	0.007	0.008

ID	Caliper	Grammage	Apparent Density	C_{11}/ρ	C_{66}/ρ	C_{33}/ρ	C_{44}/ρ
	µm	g/m^2	g/cm^3	$(km/s)^2$	$(km/s)^2$	$(km/s)^2$	$(km/s)^2$
R-3/H	187	153.4	0.822	9.25	3.44	0.142	0.244
	205	161.2	0.787	8.24	3.06	0.162	0.269
	211	163.7	0.776	7.81	2.90	0.155	0.243
	202	158.1	0.783	8.50	3.16	0.152	0.247
	188	145.5	0.775	8.97	3.28	0.147	0.256
	192	149.4	0.777	8.81	3.20	0.147	0.237
Avg.	198	155.2	0.787	8.60	3.17	0.151	0.249
S.D.	10	7.0	0.018	0.52	0.18	0.007	0.011
C.I.	8	5.6	0.014	0.42	0.15	0.005	0.009
R-6/H	161	154.2	0.955	9.89	3.72	0.158	0.254
	179	156.9	0.878	8.72	3.23	0.141	0.231
	177	156.9	0.885	8.89	3.21	0.141	0.233
Avg.	172	156.0	0.906	9.17	3.39	0.147	0.239
S.D.	10	1.6	0.043	0.63	0.29	0.009	0.013
C.I.	11	1.8	0.048	0.72	0.33	0.011	0.014
R-12/H	196	160.4	0.818	8.85	3.20	0.157	0.221
	180	154.6	0.856	9.75	3.63	0.163	0.233
	200	167.9	0.838	8.85	3.30	0.164	0.224
	186	148.4	0.796	8.99	3.31	0.154	0.248
	183	151.2	0.828	9.61	3.59	0.157	0.275
	182	155.7	0.856	9.49	3.46	0.163	0.318
Avg.	188	156.4	0.832	9.26	3.42	0.160	0.253
S.D.	8	7.0	0.023	0.41	0.17	0.004	0.037
C.I.	7	5.6	0.019	0.32	0.14	0.004	0.030
P-3H/L	142	117.3	0.829	8.70	3.03	0.236	0.200
	137	111.9	0.818	8.81	3.10	0.230	0.210
	139	117.4	0.843	8.77	3.15	0.230	0.183
Avg.	139	115.5	0.830	8.76	3.09	0.232	0.198
S.D.	2	3.2	0.013	0.05	0.06	0.004	0.014
C.I.	3	3.6	0.014	0.06	0.07	0.004	0.016

ID	Caliper	Grammage	Apparent Density	C_{11}/ρ	C_{66}/ρ	C_{33}/ρ	C_{44}/ρ
	µm	g/m^2	g/cm^3	$(km/s)^2$	$(km/s)^2$	$(km/s)^2$	$(km/s)^2$
P-6H/L	135	119.8	0.885	10.01	3.47	0.263	0.208
	130	116.9	0.899	9.53	3.45	0.255	0.182
	136	117.8	0.864	9.95	3.55	0.255	0.163
Avg.	134	118.2	0.883	9.83	3.49	0.258	0.184
S.D.	3	1.5	0.018	0.26	0.05	0.005	0.022
C.I.	4	1.7	0.020	0.30	0.06	0.005	0.025
P-12H/L	124	114.3	0.921	10.26	3.71	0.261	0.178
	118	108.1	0.919	10.96	3.90	0.253	0.151
	120	109.5	0.910	10.88	3.85	0.248	0.152
Avg.	121	110.6	0.917	10.70	3.82	0.254	0.161
S.D.	3	3.2	0.006	0.39	0.10	0.007	0.015
C.I.	4	3.7	0.007	0.44	0.11	0.008	0.017
P-24H/L	112	106.8	0.952	10.58	3.88	0.236	0.126
	108	101.5	0.939	10.66	3.84	0.226	0.139
	118	108.1	0.917	10.56	3.80	0.233	0.136
Avg.	113	105.5	0.936	10.60	3.84	0.232	0.134
S.D.	5	3.5	0.017	0.05	0.04	0.005	0.007
C.I.	6	4.0	0.020	0.06	0.05	0.006	0.008
P-3H/N	154	126.5	0.822	8.96	3.19	0.226	0.260
	144	117.1	0.812	9.06	3.21	0.228	0.236
	152	125.1	0.826	9.05	3.22	0.230	0.284
Avg.	150	122.9	0.820	9.02	3.21	0.228	0.260
S.D.	5	5.0	0.007	0.06	0.02	0.002	0.024
C.I.	6	5.7	0.008	0.06	0.02	0.002	0.027
P-6H/N	137	123.3	0.903	9.96	3.51	0.255	0.322
	138	127.5	0.921	10.06	3.59	0.272	0.284
	131	118.1	0.903	9.91	3.59	0.258	0.232
Avg.	135	123.0	0.909	9.98	3.57	0.262	0.279
S.D.	4	4.7	0.011	0.08	0.05	0.009	0.045
C.I.	4	5.3	0.012	0.09	0.05	0.010	0.051

ID	Caliper	Grammage	Apparent Density	C_{11}/ρ	C_{66}/ρ	C_{33}/ρ	C_{44}/ρ
	μm	g/m^2	g/cm^3	$(km/s)^2$	$(km/s)^2$	$(km/s)^2$	$(km/s)^2$
P-12H/N	119	119.8	1.008	11.02	3.94	0.260	0.209
	120	120.7	1.009	10.91	4.05	0.251	0.236
	114	116.0	1.017	11.02	4.01	0.244	0.182
Avg.	118	118.8	1.011	10.98	4.00	0.252	0.209
S.D.	3	2.5	0.005	0.06	0.05	0.008	0.027
C.I.	3	2.9	0.005	0.07	0.06	0.009	0.031
P-24H/N	103	112.7	1.100	11.61	4.32	0.197	0.157
	106	117.1	1.106	11.56	4.22	0.194	0.185
	104	116.1	1.115	11.46	4.33	0.186	0.213
Avg.	104	115.3	1.107	11.54	4.29	0.192	0.185
S.D.	2	2.3	0.008	0.07	0.06	0.006	0.028
C.I.	2	2.6	0.009	0.08	0.07	0.006	0.031
P-3H/H	137	127.8	0.935	10.10	3.72	0.287	0.209
	130	122.2	0.937	10.35	3.80	0.252	0.195
	134	126.5	0.947	10.38	3.82	0.253	0.209
Avg.	134	125.5	0.940	10.28	3.78	0.264	0.204
S.D.	3	2.9	0.006	0.16	0.05	0.020	0.008
C.I.	4	3.3	0.007	0.18	0.06	0.022	0.009
P-6H/H	114	118.7	1.044	11.26	4.20	0.233	0.238
	116	119.6	1.030	11.27	4.13	0.236	0.240
	118	120.6	1.024	11.85	4.17	0.234	0.210
Avg.	116	119.6	1.033	11.46	4.17	0.234	0.229
S.D.	2	0.9	0.010	0.34	0.04	0.001	0.017
C.I.	2	1.1	0.012	0.38	0.04	0.002	0.019
P-12H/H	109	121.3	1.115	12.03	4.41	0.218	0.183
	111	122.5	1.109	11.90	4.39	0.217	0.193
	105	120.3	1.140	12.11	4.31	0.211	0.179
Avg.	108	121.4	1.121	12.01	4.37	0.215	0.185
S.D.	3	1.1	0.017	0.11	0.06	0.004	0.007
C.I.	3	1.3	0.019	0.12	0.06	0.004	0.008

ID	Caliper	Grammage	Apparent Density	C_{11}/ρ	C_{66}/ρ	C_{33}/ρ	C_{44}/ρ
	μm	g/m^2	g/cm^3	$(km/s)^2$	$(km/s)^2$	$(km/s)^2$	$(km/s)^2$
P-24H/H	97	114.7	1.188	12.11	4.47	0.179	0.152
	99	116.4	1.173	11.68	4.43	0.182	0.167
	93	110.8	1.197	12.57	4.53	0.162	0.142
Avg.	96	114.0	1.186	12.12	4.48	0.174	0.154
S.D.	3	2.9	0.012	0.44	0.05	0.010	0.013
C.I.	4	3.2	0.013	0.50	0.05	0.012	0.015
P-3L/L	158	119.2	0.754	7.96	2.74	0.164	0.199
	164	120.8	0.734	7.74	2.72	0.156	0.213
	156	117.5	0.753	7.98	2.86	0.160	0.220
Avg.	160	119.1	0.747	7.89	2.77	0.160	0.210
S.D.	4	1.6	0.011	0.13	0.07	0.004	0.011
C.I.	5	1.8	0.012	0.15	0.08	0.005	0.012
P-6L/L	155	128.8	0.831	9.20	3.25	0.202	0.230
	147	126.0	0.856	9.16	3.26	0.243	0.259
	143	123.6	0.863	9.23	3.26	0.230	0.219
Avg.	148	126.1	0.850	9.20	3.26	0.225	0.236
S.D.	6	2.6	0.017	0.04	0.01	0.021	0.021
C.I.	7	2.9	0.019	0.04	0.01	0.024	0.024
P-12L/L	125	117.6	0.938	10.06	3.57	0.240	0.255
	125	117.9	0.940	10.20	3.58	0.235	0.246
	126	118.9	0.945	10.18	3.62	0.235	0.218
Avg.	126	118.1	0.941	10.15	3.59	0.237	0.240
S.D.	0	0.7	0.004	0.07	0.02	0.003	0.019
C.I.	0	0.8	0.004	0.08	0.03	0.003	0.022
P-24L/L	103	105.1	1.019	10.34	3.77	0.216	0.200
	101	105.0	1.037	10.51	3.84	0.208	0.175
	100	102.8	1.027	10.74	3.83	0.204	0.231
Avg.	101	104.3	1.028	10.53	3.81	0.210	0.202
S.D.	2	1.3	0.009	0.20	0.03	0.006	0.028
C.I.	2	1.5	0.010	0.23	0.04	0.007	0.032

ID	Caliper	Grammage	Apparent Density	C_{11}/ρ	C_{66}/ρ	C_{33}/ρ	C_{44}/ρ
	µm	g/m^2	g/cm^3	$(km/s)^2$	$(km/s)^2$	$(km/s)^2$	$(km/s)^2$
P-3L/N	162	122.5	0.758	8.03	2.86	0.186	0.244
	156	121.1	0.774	8.24	2.84	0.182	0.237
	154	121.4	0.789	8.21	2.87	0.187	0.226
Avg.	157	121.6	0.774	8.16	2.86	0.185	0.235
S.D.	4	0.7	0.016	0.11	0.02	0.003	0.009
C.I.	4	0.8	0.018	0.13	0.02	0.003	0.010
P-6L/N	132	114.6	0.866	9.49	3.37	0.230	0.213
	133	114.8	0.862	9.60	3.39	0.228	0.208
	131	114.4	0.871	9.53	3.43	0.227	0.262
Avg.	132	114.6	0.867	9.54	3.40	0.228	0.228
S.D.	1	0.2	0.005	0.06	0.03	0.001	0.030
C.I.	1	0.2	0.005	0.07	0.04	0.002	0.034
P-12L/N	122	115.4	0.945	10.49	3.74	0.228	0.186
	122	116.5	0.954	10.36	3.71	0.225	0.218
	121	115.4	0.952	10.49	3.82	0.235	0.232
Avg.	122	115.7	0.950	10.45	3.76	0.229	0.212
S.D.	1	0.7	0.004	0.07	0.06	0.005	0.024
C.I.	1	0.7	0.005	0.08	0.07	0.006	0.027
P-24L/N	117	123.1	1.055	11.20	4.05	0.214	0.187
	115	122.9	1.065	11.18	4.00	0.213	0.181
	121	127.1	1.054	10.96	4.05	0.218	0.195
Avg.	118	124.4	1.058	11.11	4.03	0.215	0.188
S.D.	3	2.4	0.006	0.13	0.03	0.002	0.007
C.I.	3	2.7	0.007	0.15	0.03	0.003	0.008
P-3L/H	137	122.5	0.896	9.32	3.38	0.285	0.280
	138	123.1	0.890	9.46	3.52	0.259	0.282
	145	129.6	0.896	9.40	3.42	0.263	0.289
Avg.	140	125.1	0.894	9.39	3.44	0.269	0.284
S.D.	4	3.9	0.003	0.07	0.07	0.014	0.005
C.I.	5	4.5	0.004	0.08	0.08	0.016	0.005

ID	Caliper	Grammage	Apparent Density	C_{11}/ρ	C_{66}/ρ	C_{33}/ρ	C_{44}/ρ
	µm	g/m^2	g/cm^3	$(km/s)^2$	$(km/s)^2$	$(km/s)^2$	$(km/s)^2$
P-6L/H	126	122.7	0.974	10.74	3.92	0.264	0.200
	126	123.2	0.979	10.51	3.86	0.258	0.173
	125	121.6	0.974	11.05	3.98	0.257	0.220
Avg.	126	122.5	0.976	10.77	3.92	0.260	0.198
S.D.	1	0.8	0.003	0.27	0.06	0.004	0.024
C.I.	1	0.9	0.003	0.30	0.07	0.004	0.027
P-12L/H	116	117.4	1.013	10.99	3.99	0.250	0.168
	121	122.2	1.009	11.22	4.20	0.253	0.217
	121	121.8	1.004	11.38	4.17	0.251	0.222
Avg.	119	120.5	1.009	11.20	4.12	0.251	0.202
S.D.	3	2.7	0.005	0.20	0.11	0.001	0.030
C.I.	3	3.0	0.005	0.22	0.13	0.001	0.034
P-24L/H	111	120.9	1.085	11.43	4.34	0.234	0.170
	116	124.5	1.071	11.34	4.22	0.237	0.176
	114	122.8	1.080	11.66	4.37	0.232	0.165
Avg.	114	122.7	1.079	11.48	4.31	0.234	0.170
S.D.	2	1.8	0.007	0.17	0.08	0.003	0.005
C.I.	3	2.0	0.008	0.19	0.09	0.003	0.006

APPENDIX V

FIBER LENGHT AND FINES CONTENT

Group ID	Weight Weighted Average Fiber Length mm	Weight Weighted Fines Content %
C-U/L	2.98	1.87
C-U/N	2.85	2.88
C-U/H	2.92	5.71
C-F/N	3.04	2.04
C-F/H	2.98	3.79
B-3/N	3.14	2.63
B-6/N	2.91	2.75
B-12/N	2.99	2.64
B-3/H	2.90	5.56
B-6/H	2.81	7.51
B-12/H	2.78	6.67
R-1/N	3.03	2.15
R-2/N	3.15	2.23
R-3/N	2.71	3.13
R-12/N	3.00	2.33
R-1/H	3.12	4.16
R-2/H	3.09	4.51
R-3/H	2.80	5.97
R-12/H	2.88	5.86
P-3H/L	3.05	2.31
P-6H/L	3.02	2.31
P-12H/L	3.03	3.03
P-24H/L	2.96	3.92
P-3H/H	3.17	4.33
P-6H/H	3.06	5.54
P-12H/H	3.04	5.26
P-24H/H	2.84	7.31
P-3H/N	3.04	3.25
P-6H/N	2.99	4.02
P-12H/N	2.98	5.12
P-24H/N	2.82	7.12
P-3L/L	3.22	1.75
P-6L/L	2.99	2.05
P-12L/L	3.15	1.95
P-24L/L	3.14	2.86
P-3L/H	2.97	5.18
P-6L/H	3.14	4.44
P-12L/H	2.98	5.01
P-24L/H	3.12	5.27
P-3L/N	3.16	2.57
P-6L/N	2.93	3.39
P-12L/N	2.97	4.03
P-24L/N	2.99	5.18

APPENDIX VI

PLOTS OF PHYSICAL PROPERTY DATA

Physical Property Plots

Tensile Index vs. Apparent Density
Zero–span Tensile Index vs. Apparent Density
Bonding Index vs. Apparent Density
Compressive Index vs. Apparent Density
Internal Tear Resistance vs Apparent Density

Tensile Index vs. Refining Events
Zero–span Tensile Index vs. Refining Events
Bonding Index vs. Refining Events
Compressive Index vs. Refining Events
Internal Tear Resistance vs Refining Events

Nomenclature of Legends

DD - T/F

DD - Device

C - Control
BR - Bending Refiner
RR - Roll Refiner
PM - PFI Mill

T - Treatment

U - Untreated
F - Treated by Formette Dynamique
N - Normal (i.e. BR and RR)
L - Low Load (i.e. PM)
H - High Load (i.e. PM)

F - Fines Content

L - Low
N - Normal
H - High

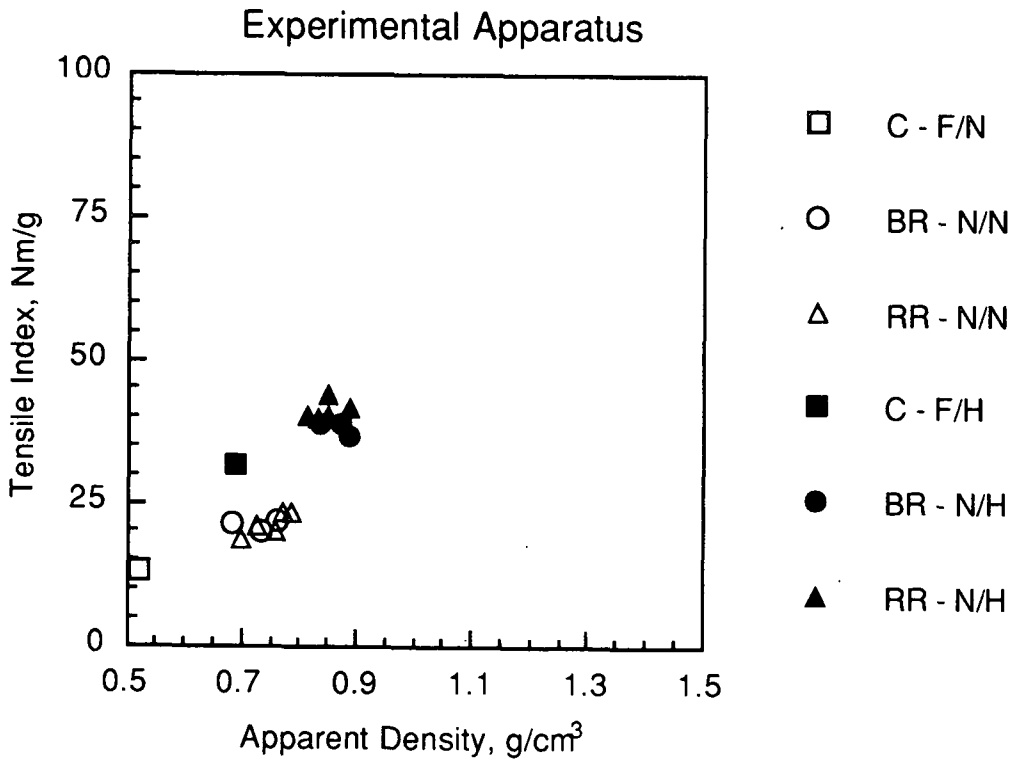

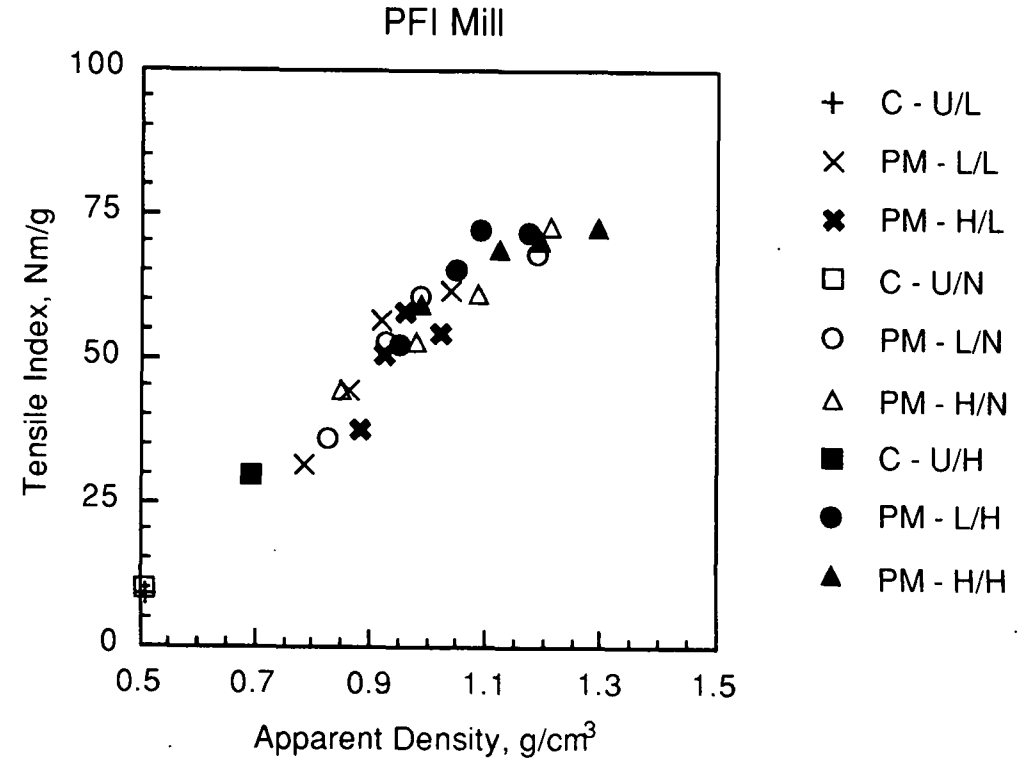

Tensile Index versus Apparent Density. The range of confidence intervals (95%) for tensile index are 0.8 to 5.2 Nm/g and for apparent density are 0.008 to 0.07 g/cm^3.

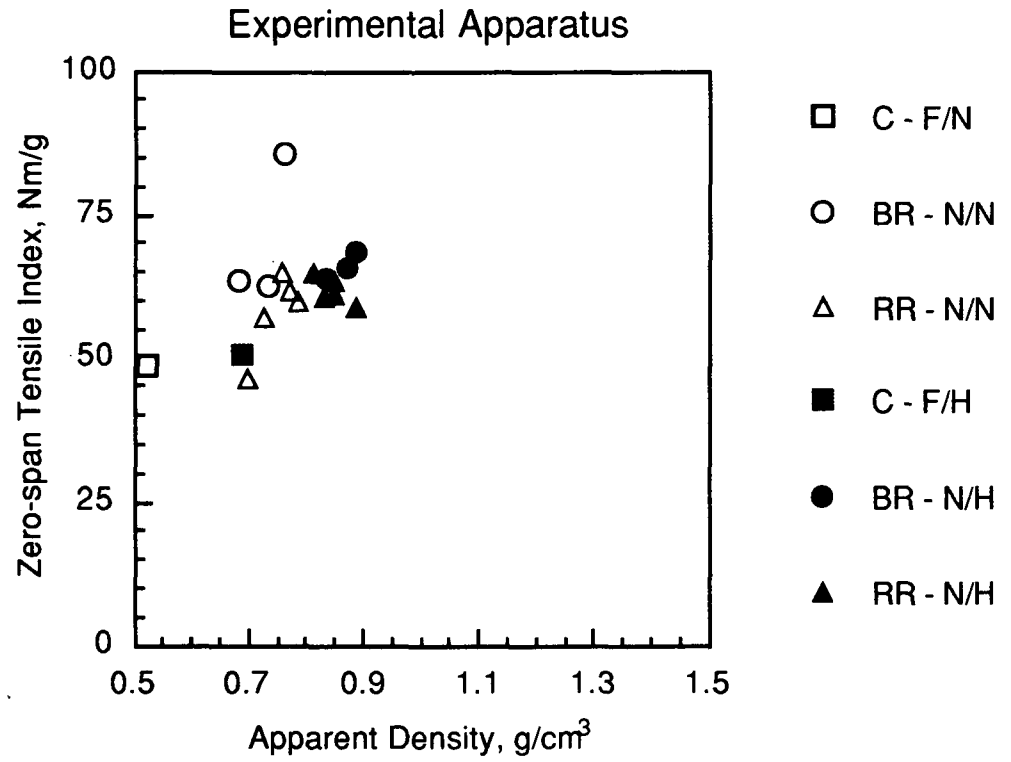

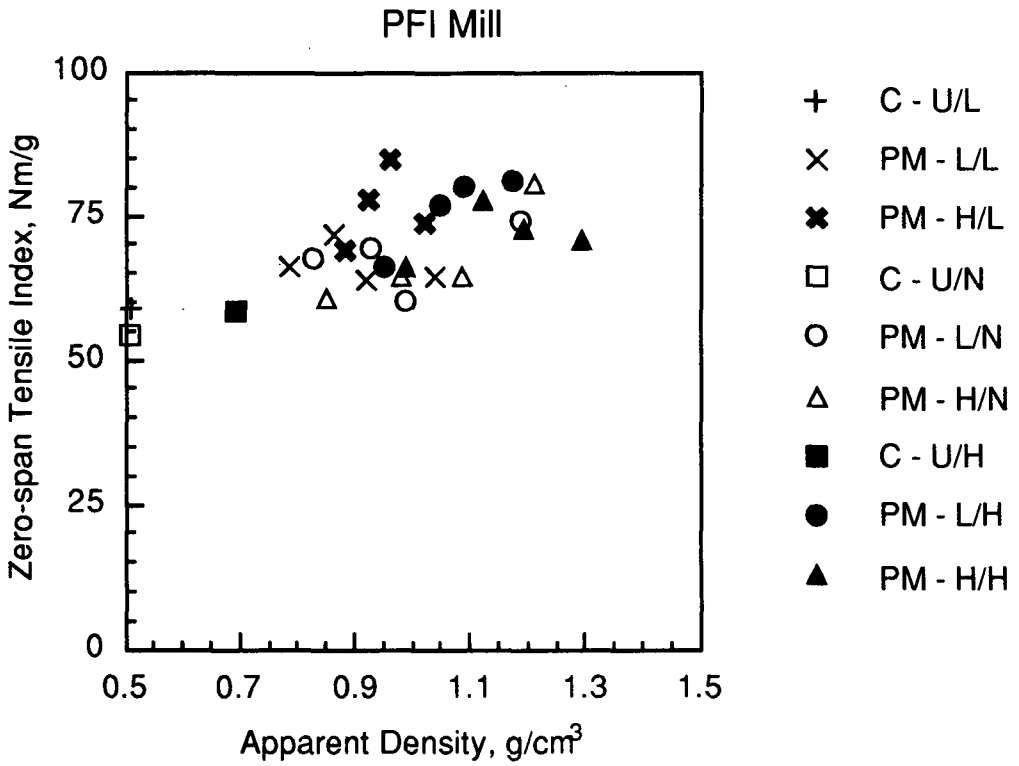

Zero-span Tensile Index versus Apparent Density. The range of confidence intervals (95%) for tensile index are 2.1 to 24.7 Nm/g and for apparent density are 0.008 to 0.07 g/cm^3.

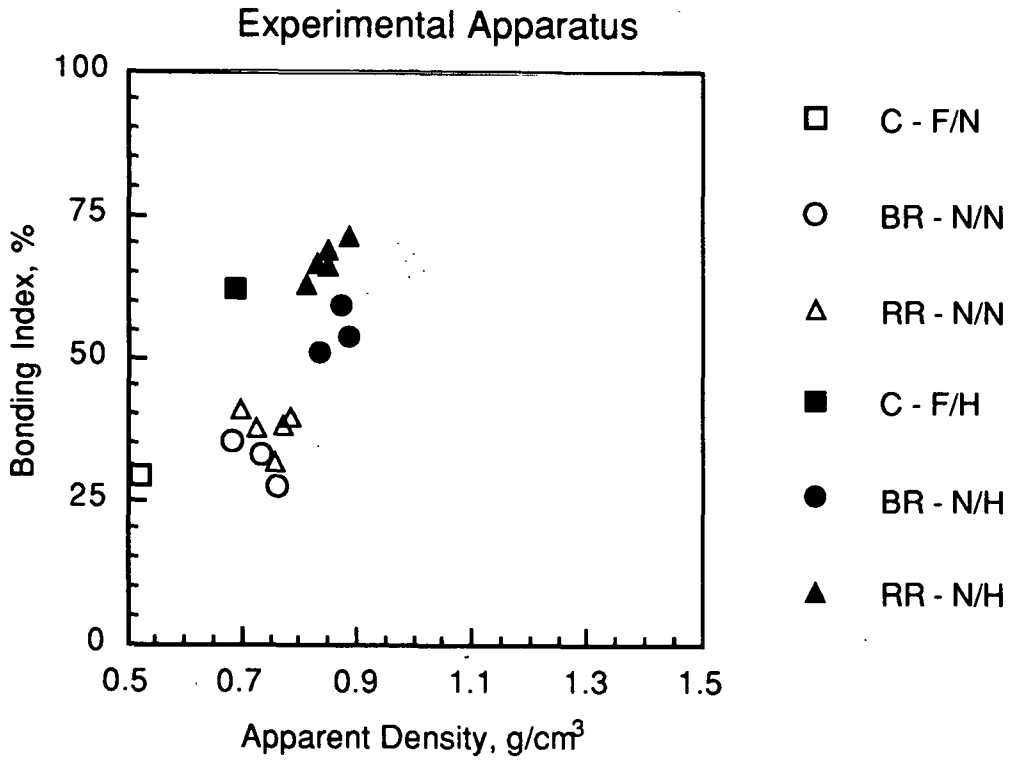

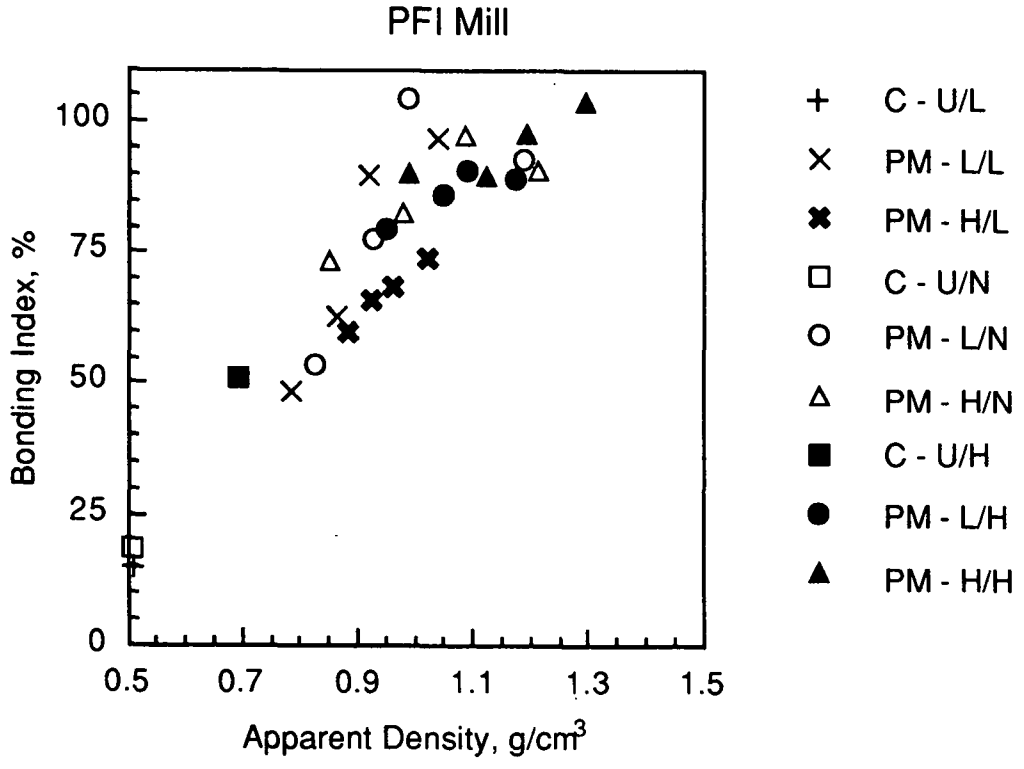

Bonding Index versus Apparent Density. The range of confidence intervals (95%) for bonding index are 1 to 27% and for apparent density are 0.008 to 0.07 g/cm^3.

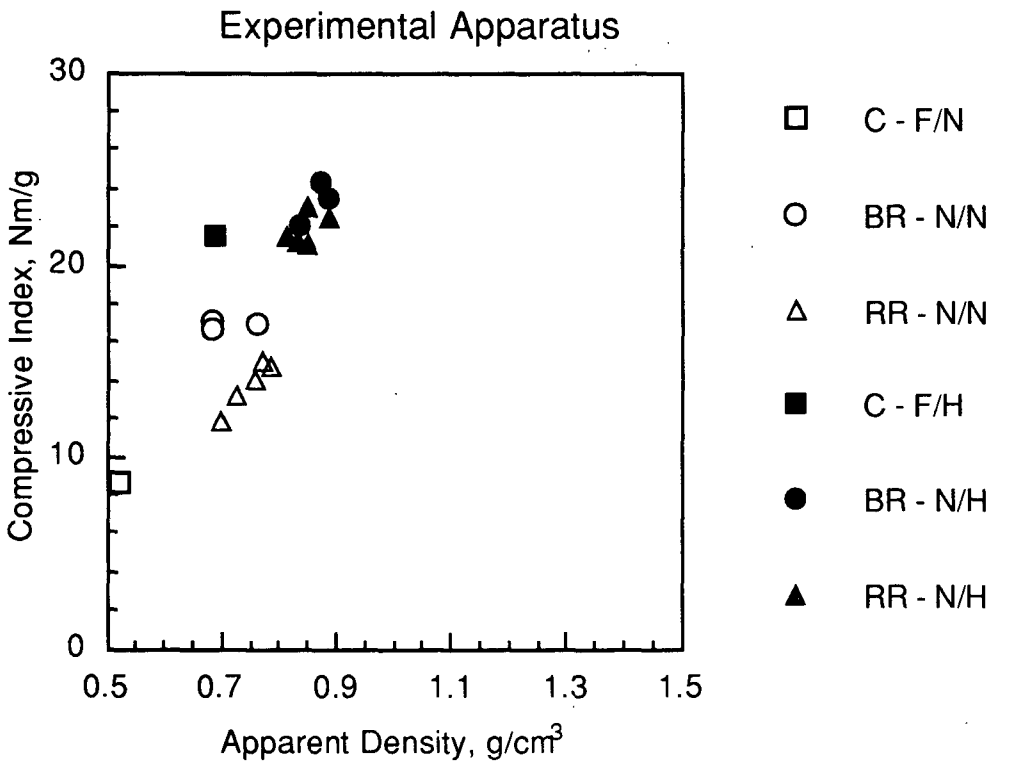

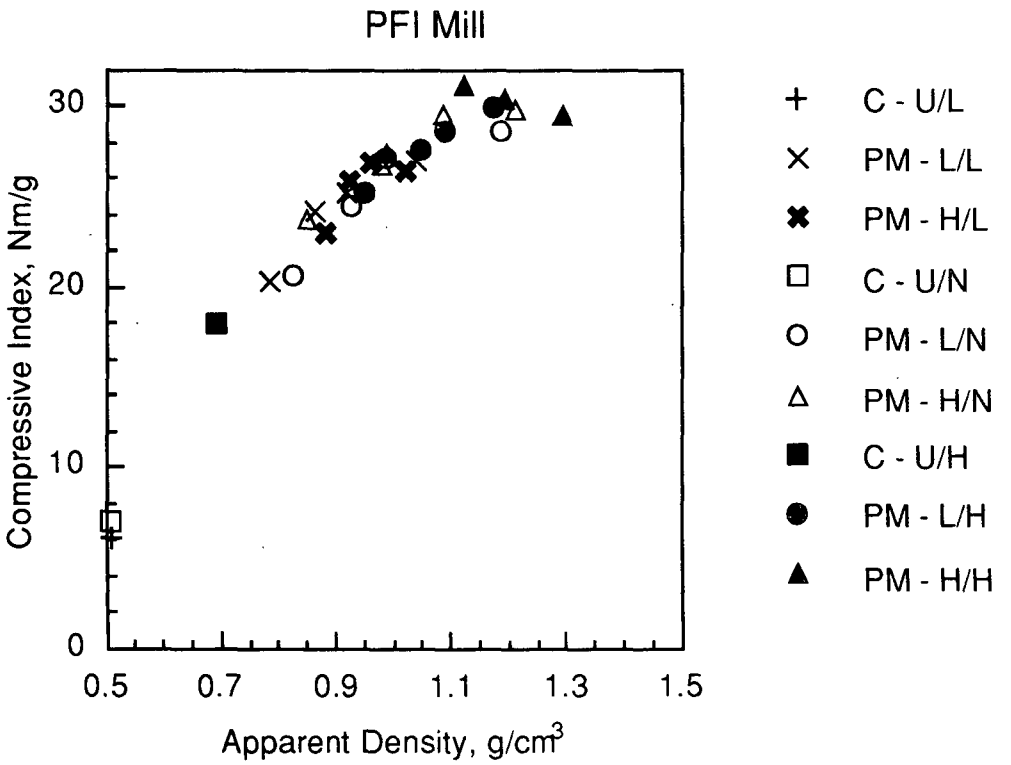

Compressive versus Apparent Density. The range of confidence intervals (95%) for compressive index are not available and for apparent density are 0.008 to 0.07 g/cm^3.

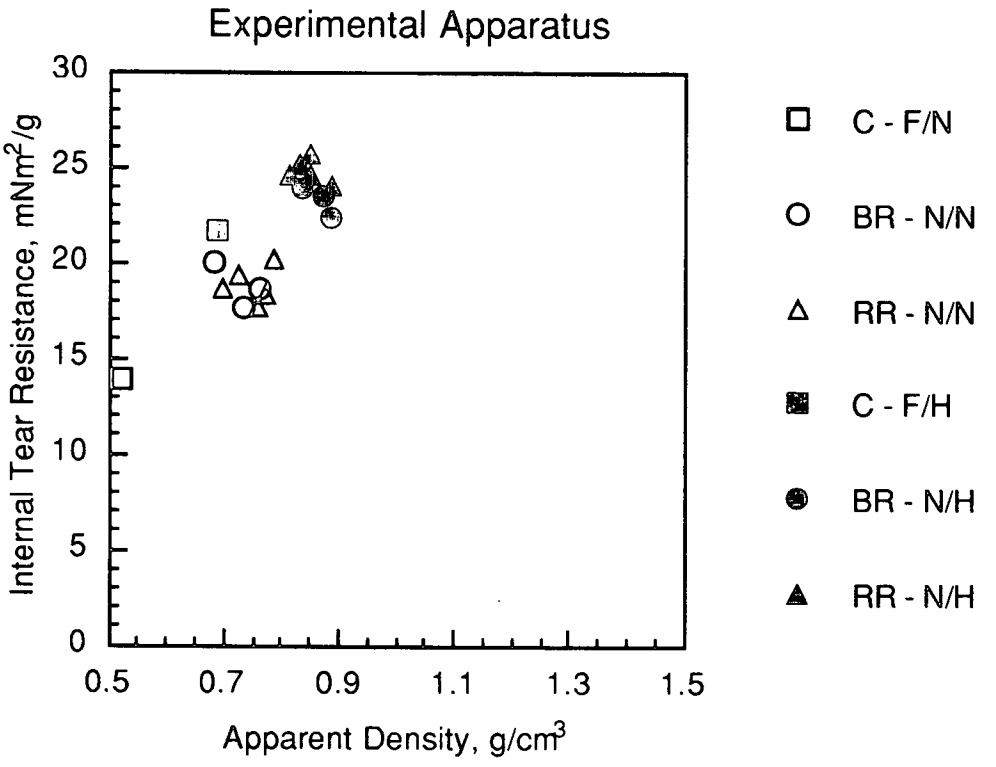

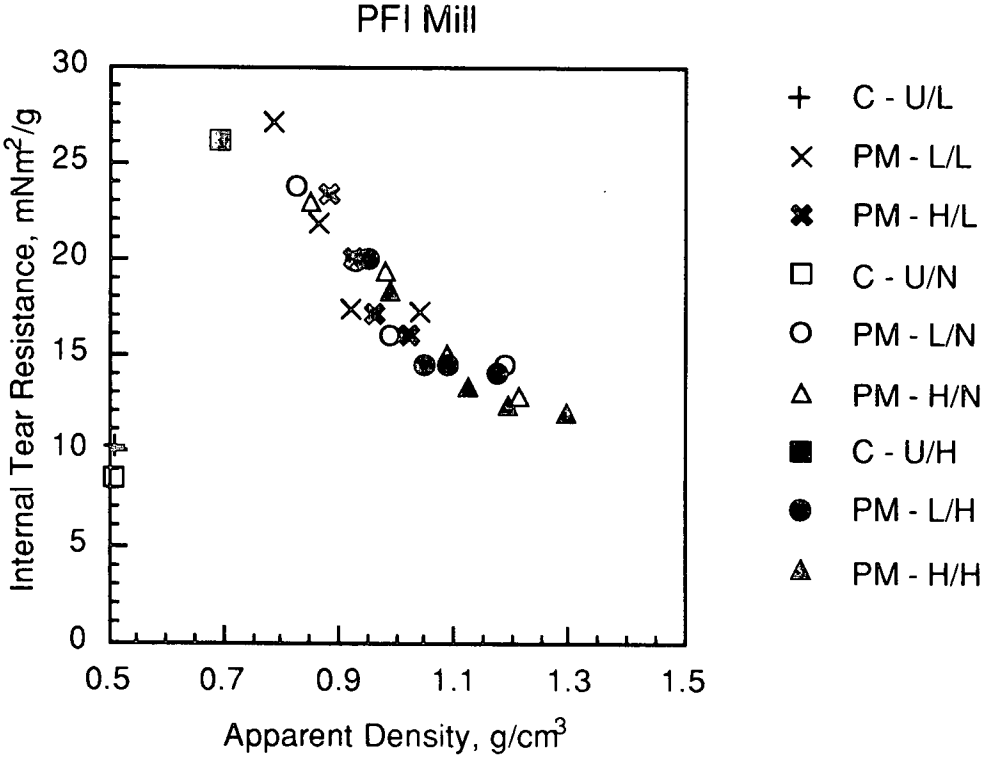

Internal Tear Resistance versus Apparent Density. The range of confidence intervals (95%) for tear resistance are 0.24 to 3.8 mNm^2/g and for apparent density are 0.008 to 0.07 g/cm^3.

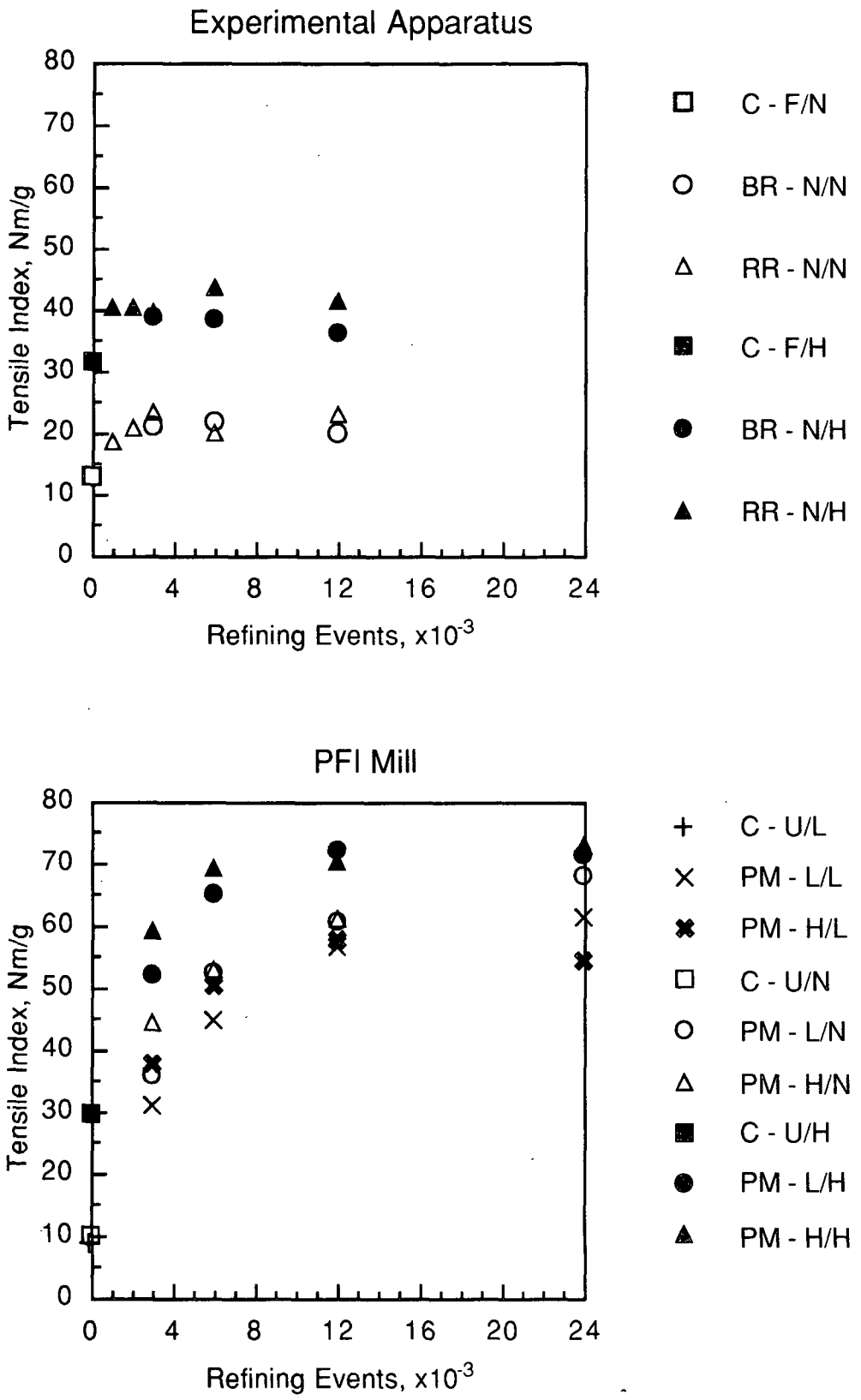

Tensile Index versus Refining Events. The range of confidence intervals (95%) for tensile are 0.8 to 5.2 Nm/g.

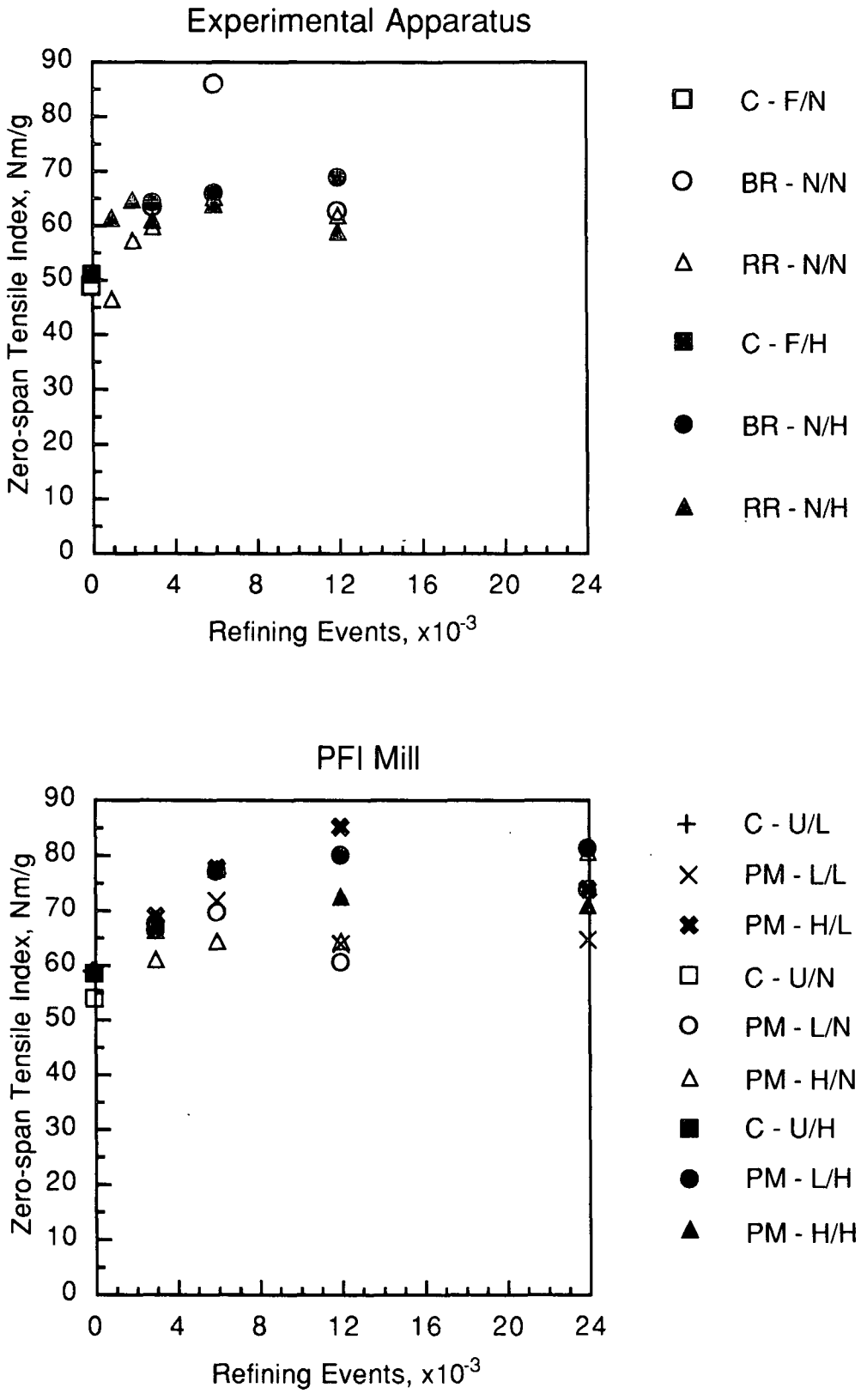

Zero-span Tensile Index versus Refining Events. The range of confidence intervals (95%) for tensile are 2.1 to 24.7 Nm/g.

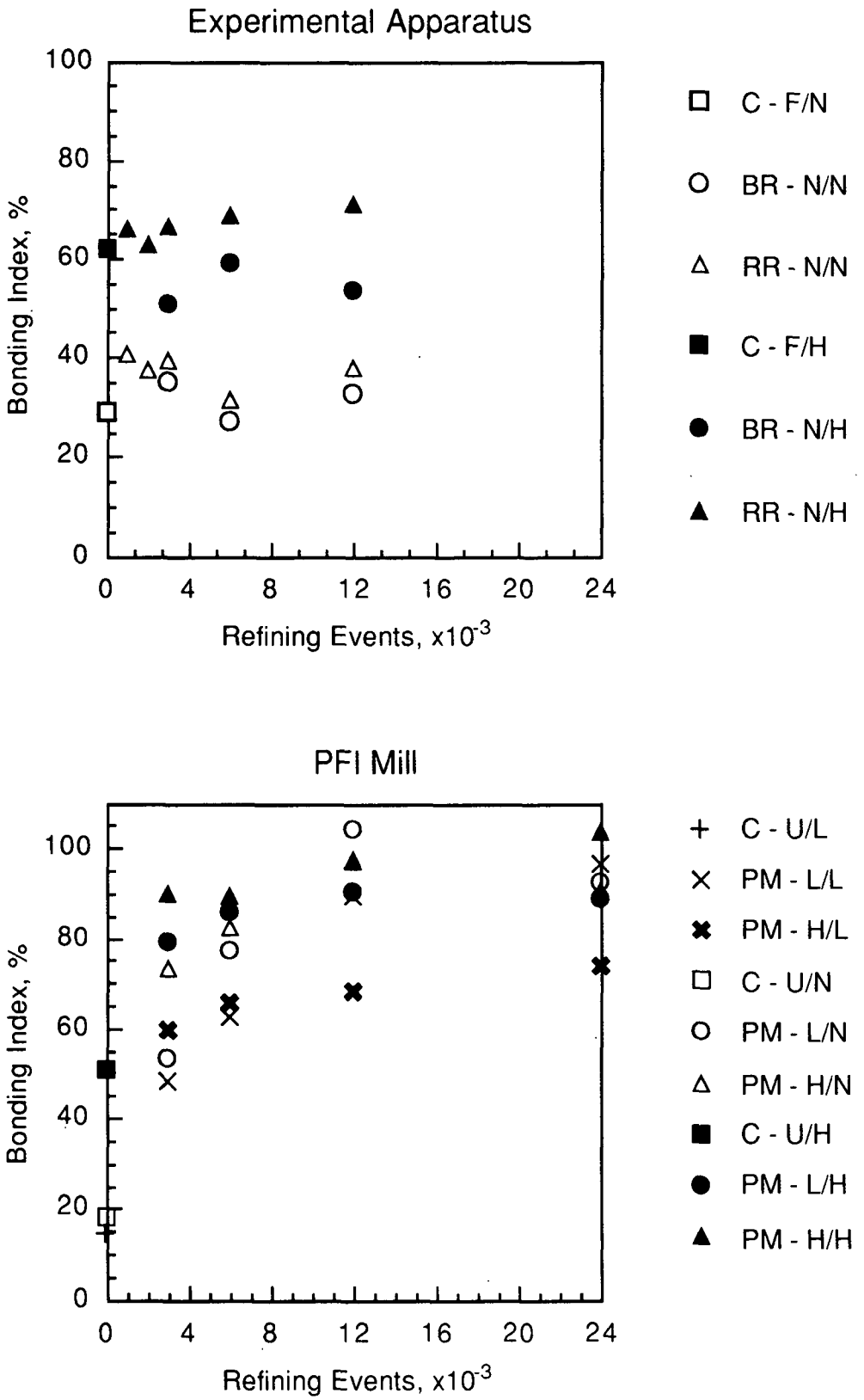

Bonding Index versus Refining Events. The range of confidence intervals (95%) for tensile are 1 to 27%.

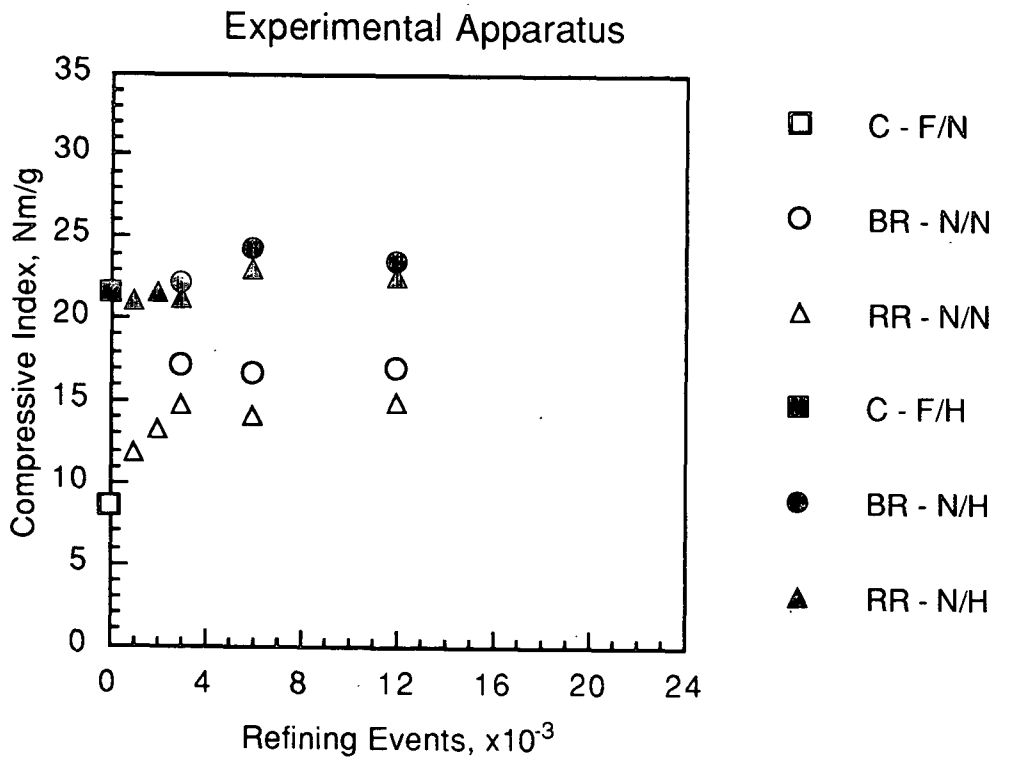

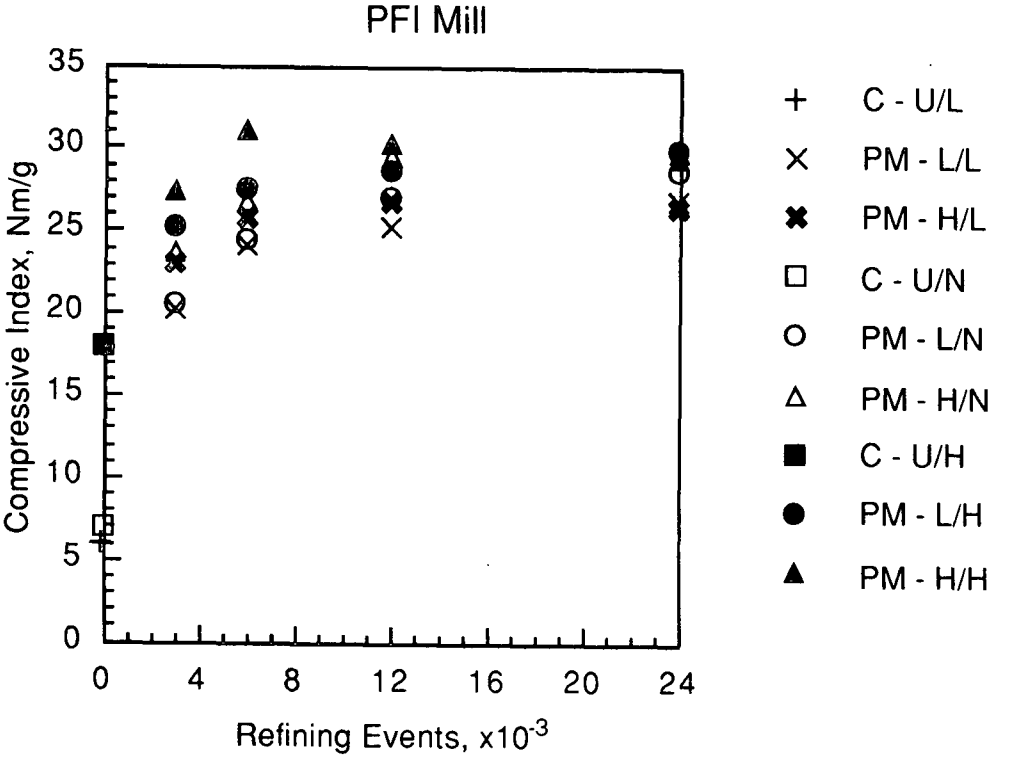

Compressive Index versus Refining Events. The range of confidence intervals (95%) for tensile are not available.

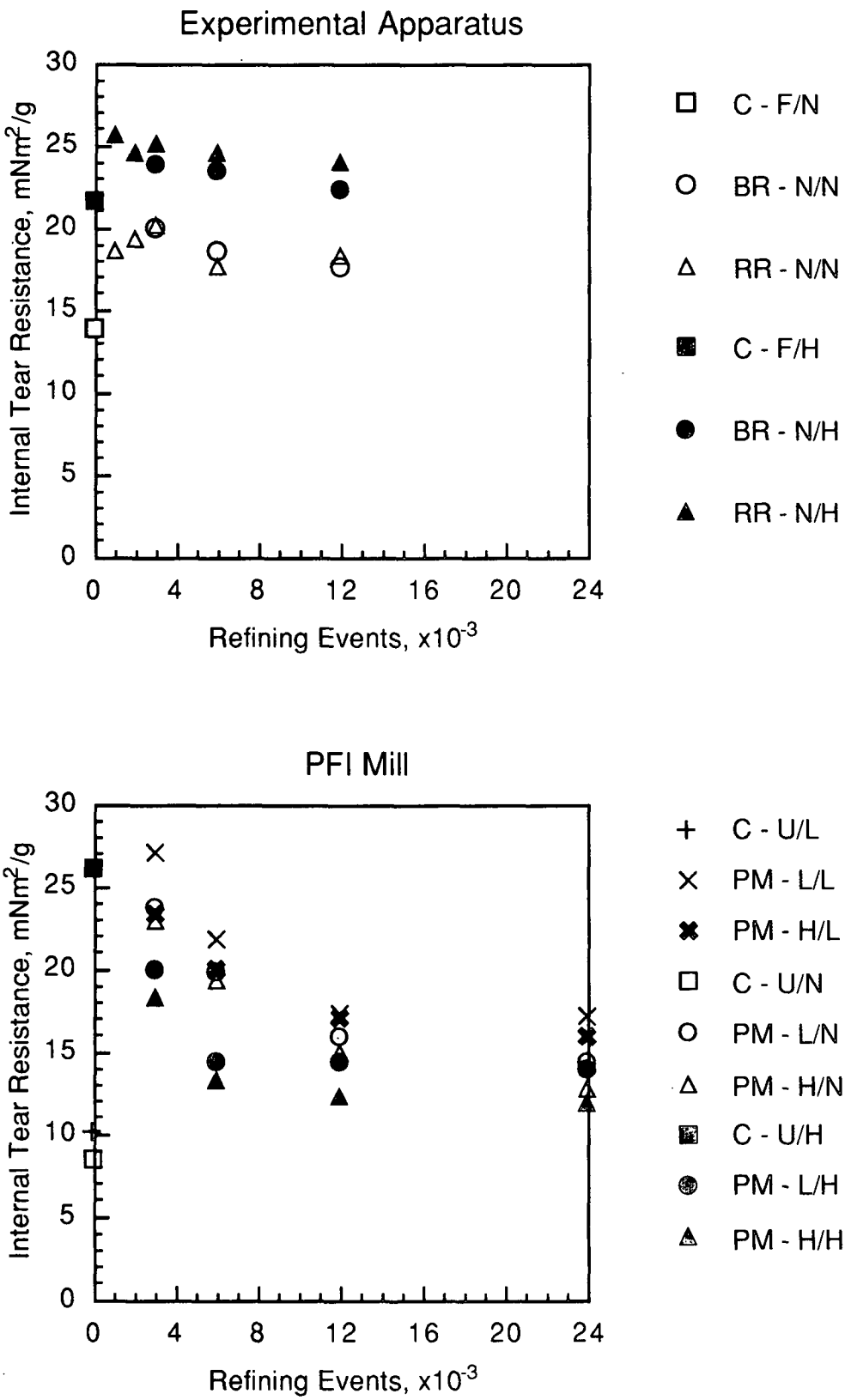

Internal Tear Resistance versus Refining Events. The range of confidence intervals (95%) for tensile are 0.24 to 3.8 mN^2/g.

APPENDIX VII

PLOTS OF ULTRASONIC PROPERTY DATA

Ultrasonic Property Plots

C_{11}/ρ vs. Apparent Density
C_{66}/ρ vs. Apparent Density
C_{33}/ρ vs. Apparent Density
C_{44}/ρ vs. Apparent Density

C_{11}/ρ vs. Refining Events
C_{66}/ρ vs. Refining Events
C_{33}/ρ vs. Refining Events
C_{44}/ρ vs. Refining Events

Nomenclature of Legends

DD - T/F

DD - Device

- C - Control
- BR - Bending Refiner
- RR - Roll Refiner
- PM - PFI Mill

T - Treatment

- U - Untreated
- F - Treated by Formette Dynamique
- N - Normal (i.e. BR and RR)
- L - Low Load (i.e. PM)
- H - High Load (i.e. PM)

F - Fines Content

- L - Low
- N - Normal
- H - High

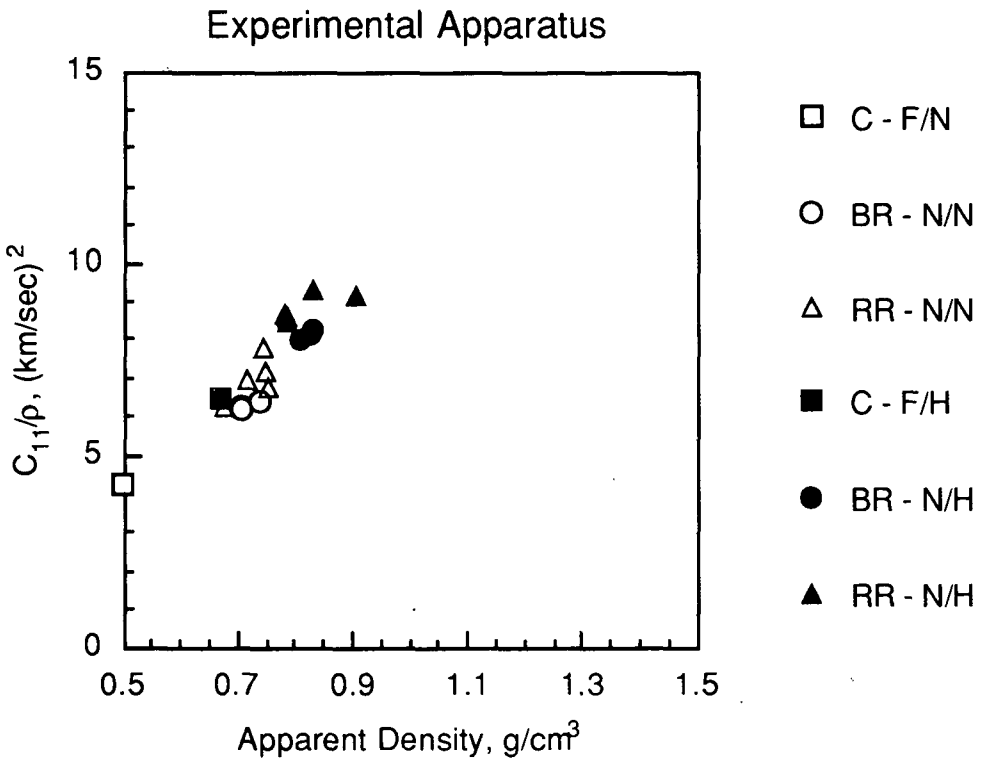

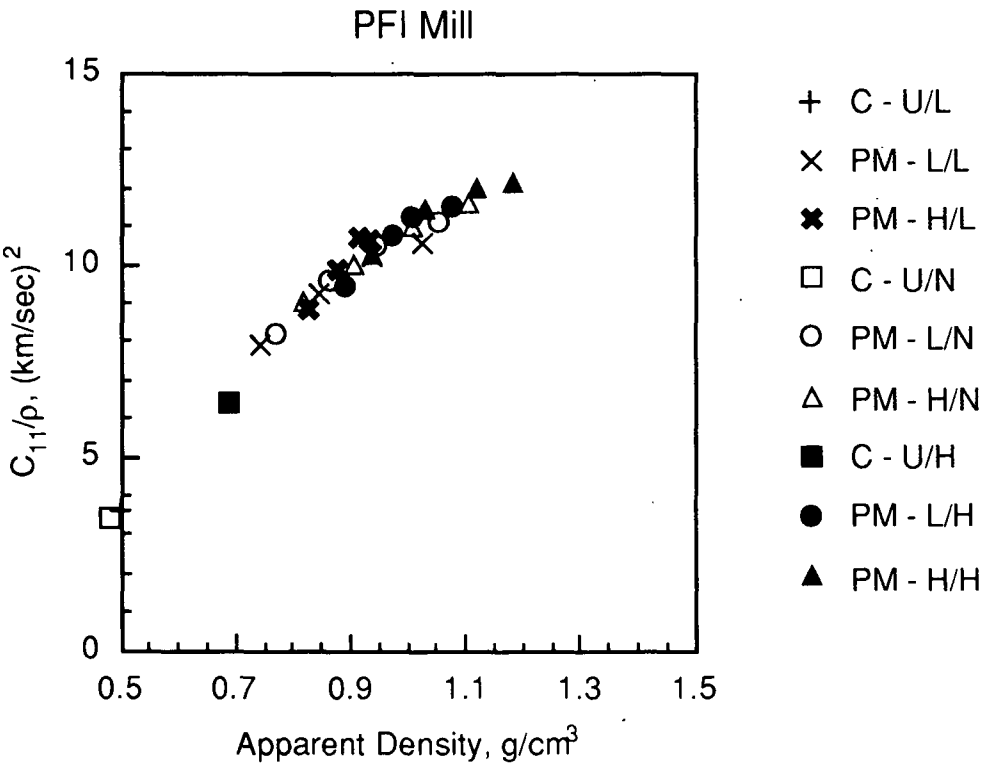

C_{11}/ρ versus Apparent Density. The range of confidence intervals (95%) for C_{11}/ρ are 0.04 to 0.91 $(km/s)^2$ and for apparent density are 0.008 to 0.07 g/cm^3.

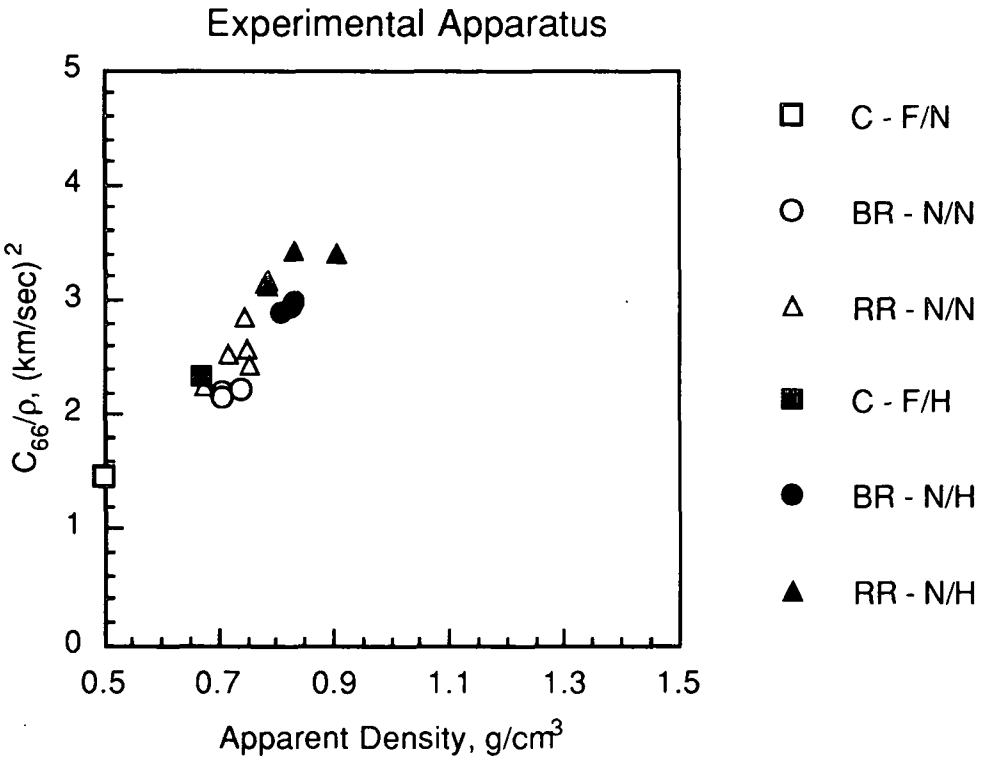

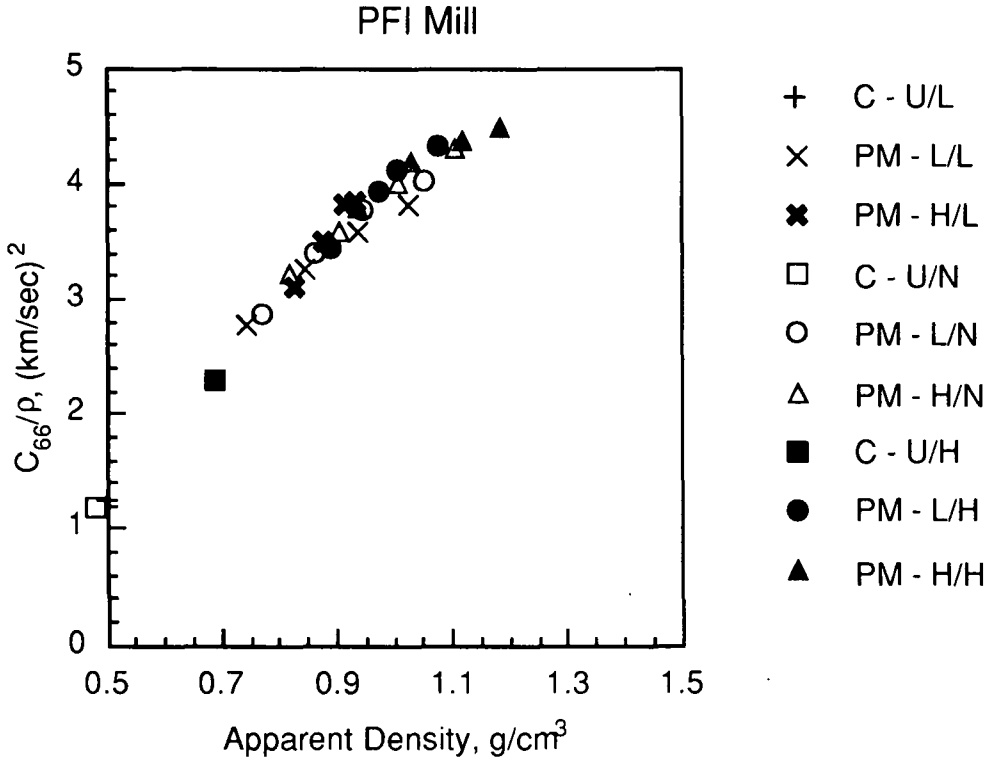

C_{66}/ρ versus Apparent Density. The range of confidence intervals (95%) for C_{66}/ρ are 0.2 to 3.7 $(km/s)^2$ and for apparent density are 0.008 to 0.07 g/cm^3.

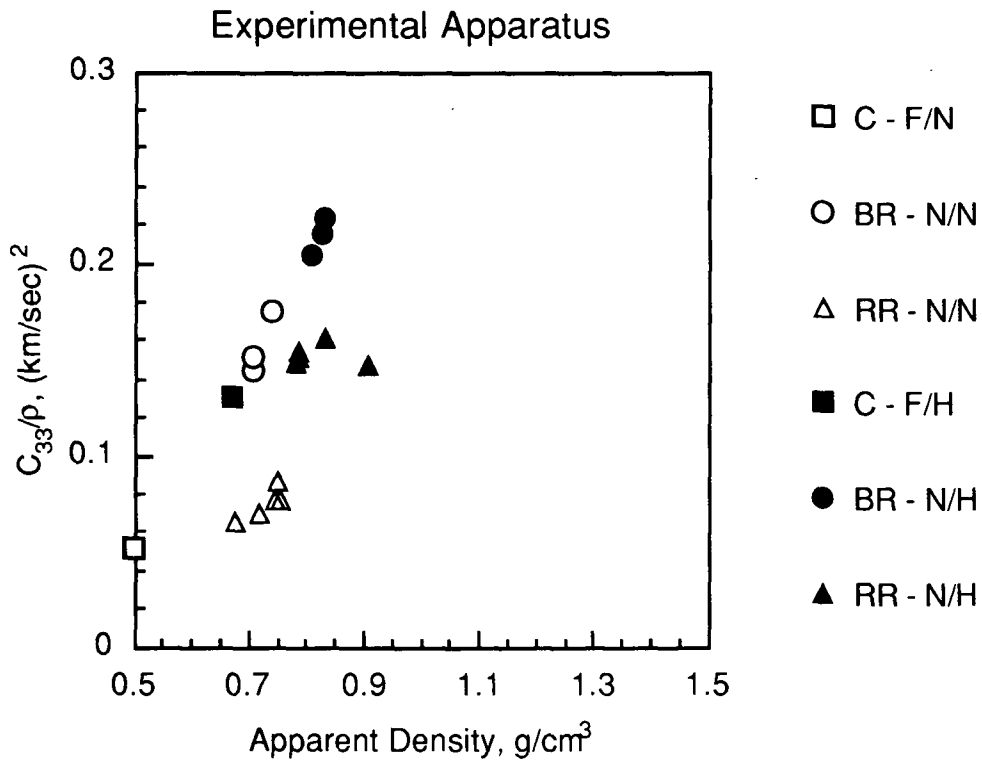

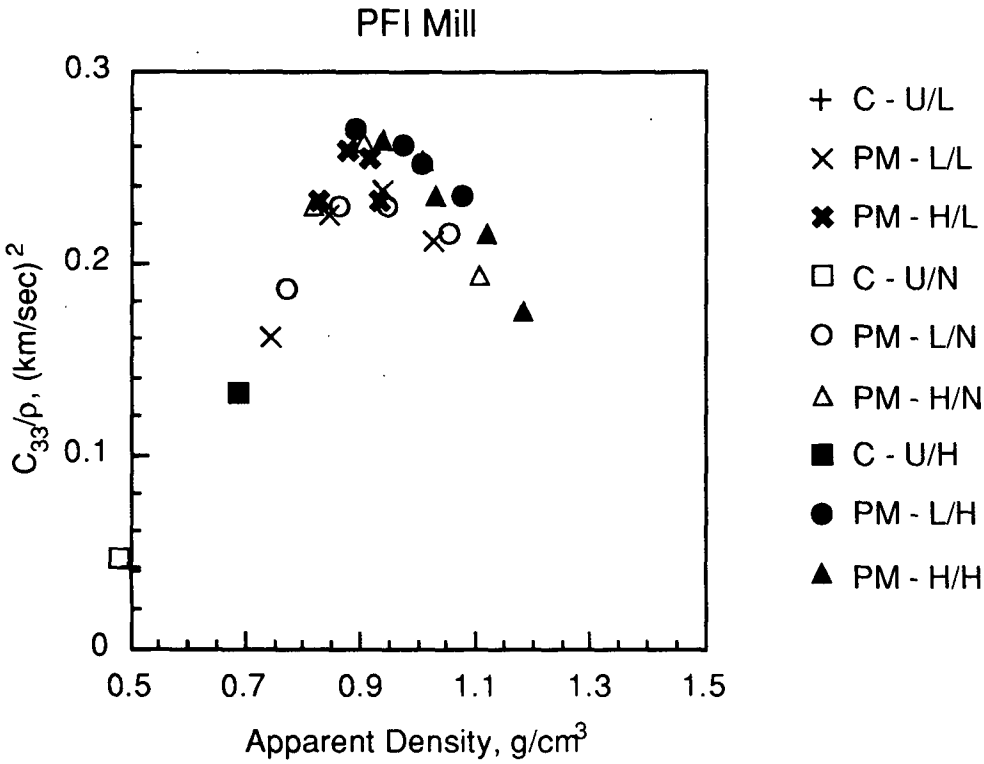

<u>C_{33}/ρ versus Apparent Density</u>. The range of confidence intervals (95%) for C_{33}/ρ are 0.001 to 0.029 $(km/s)^2$ and for apparent density are 0.008 to 0.07 g/cm^3.

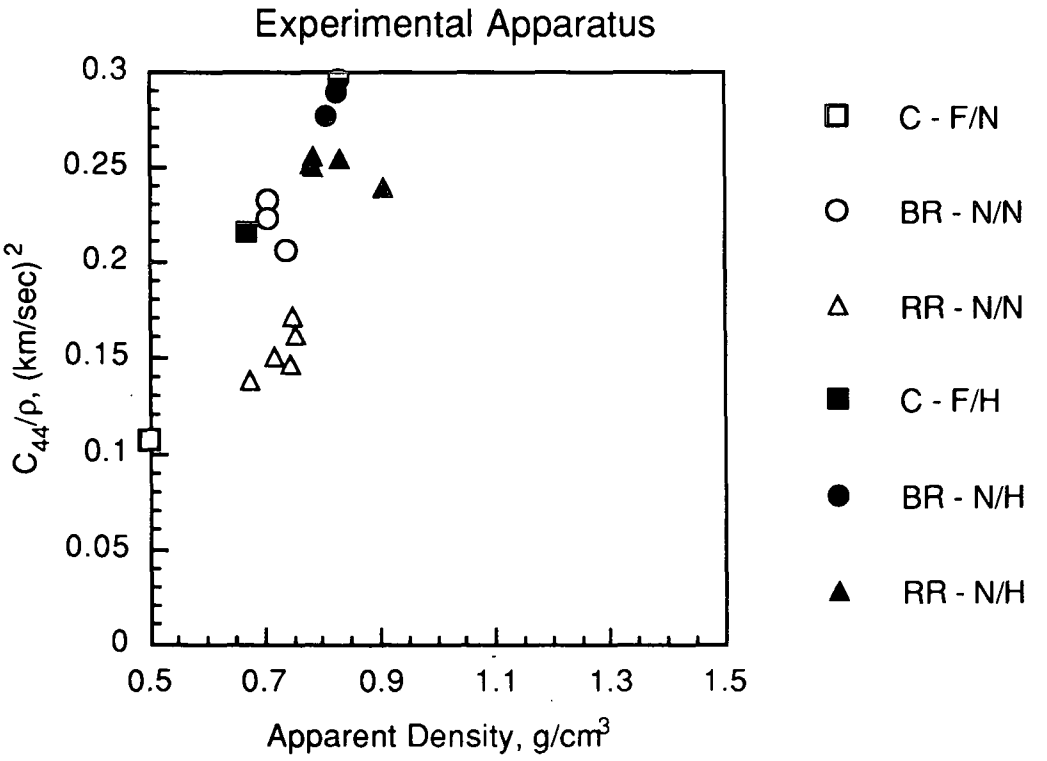

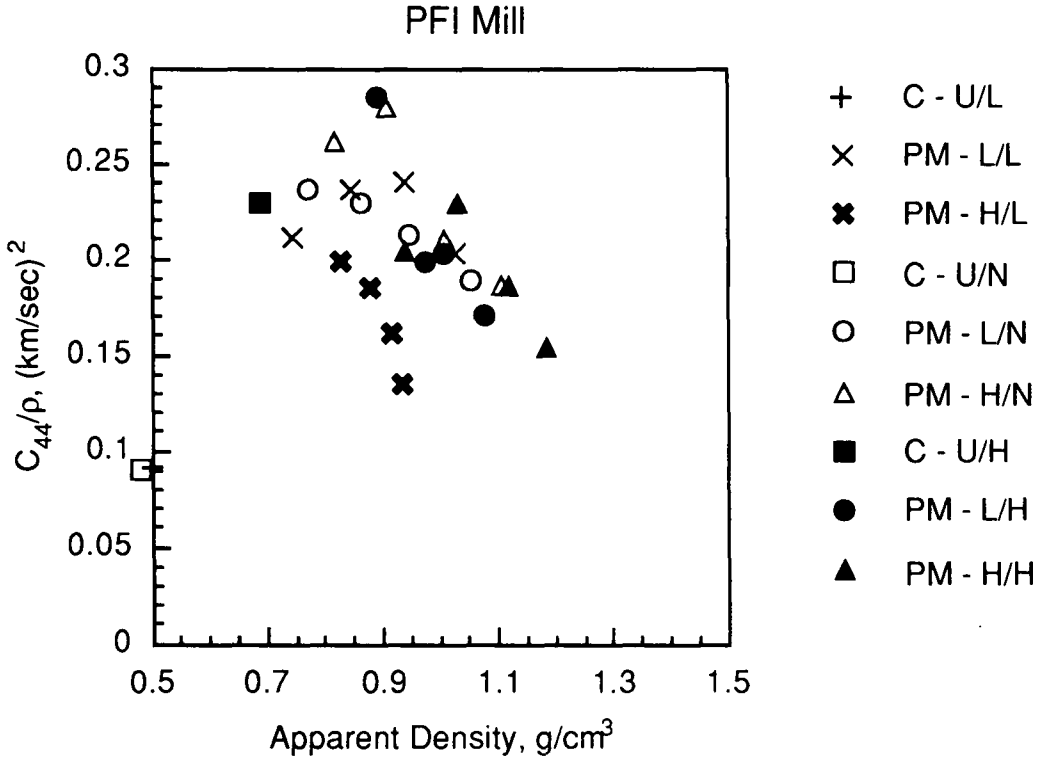

C_{44}/ρ versus Apparent Density. The range of confidence intervals (95%) for C_{44}/ρ are 0.003 to 0.051 $(km/s)^2$ and for apparent density are 0.008 to 0.07 g/cm^3.

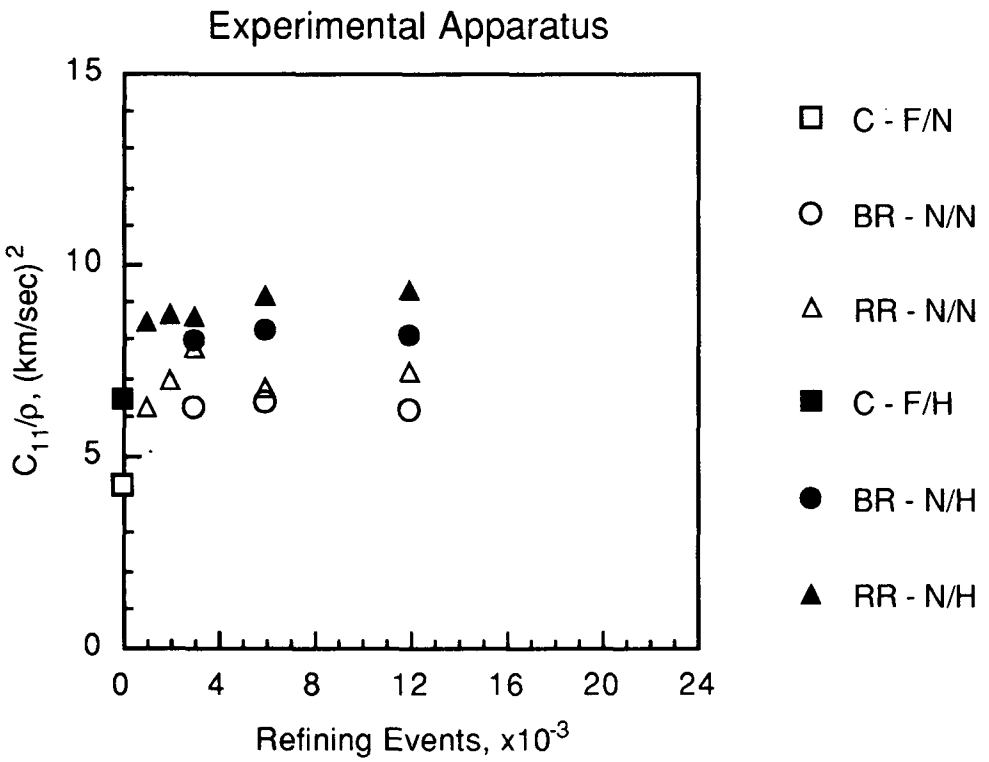

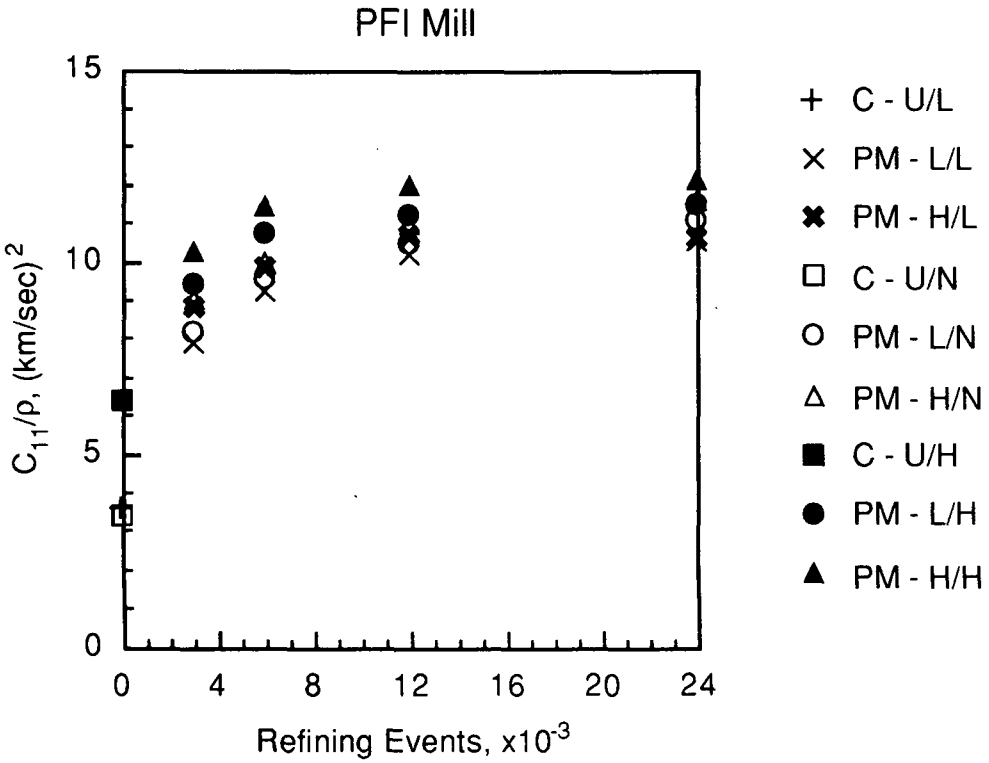

C_{11}/ρ versus Refining Events. The range of confidence intervals (95%) for C_{11}/ρ are 0.04 to 0.91 km/s.

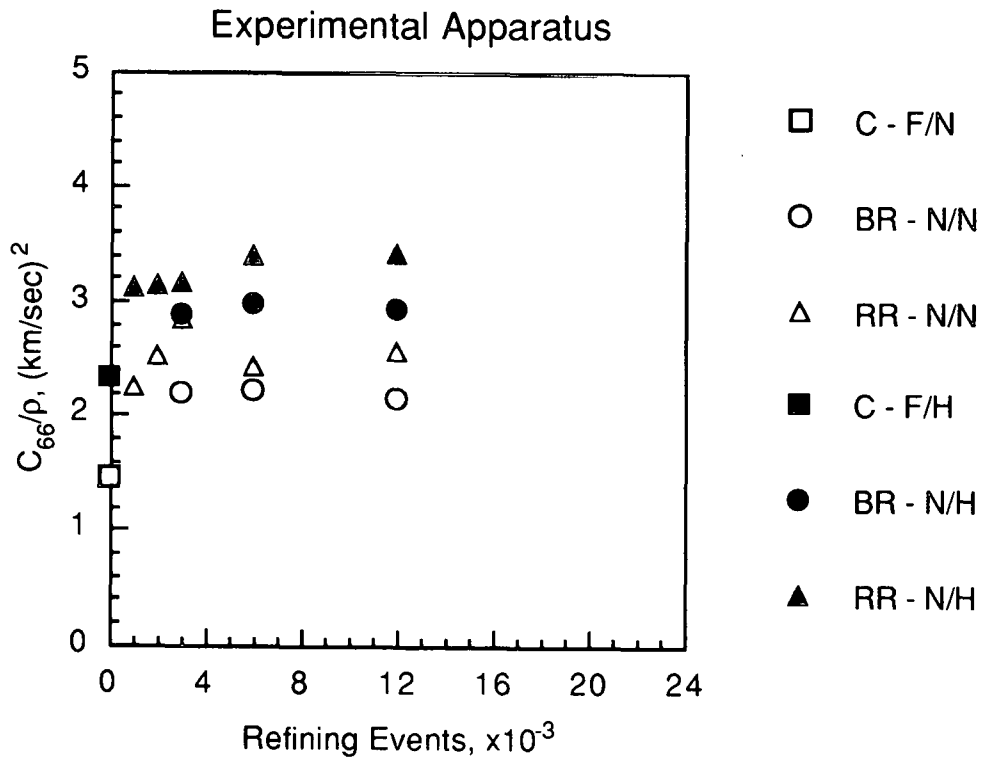

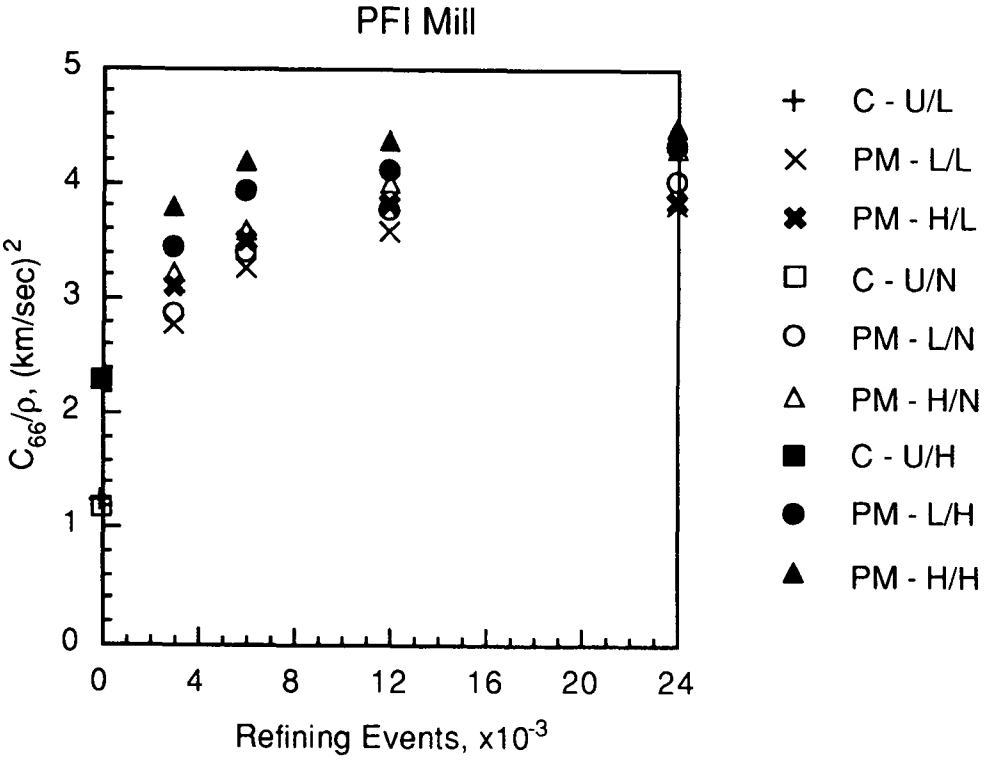

C_{66}/ρ versus Refining Events. The range of confidence intervals (95%) for C_{66}/ρ are 0.02 to 0.37 km/s.

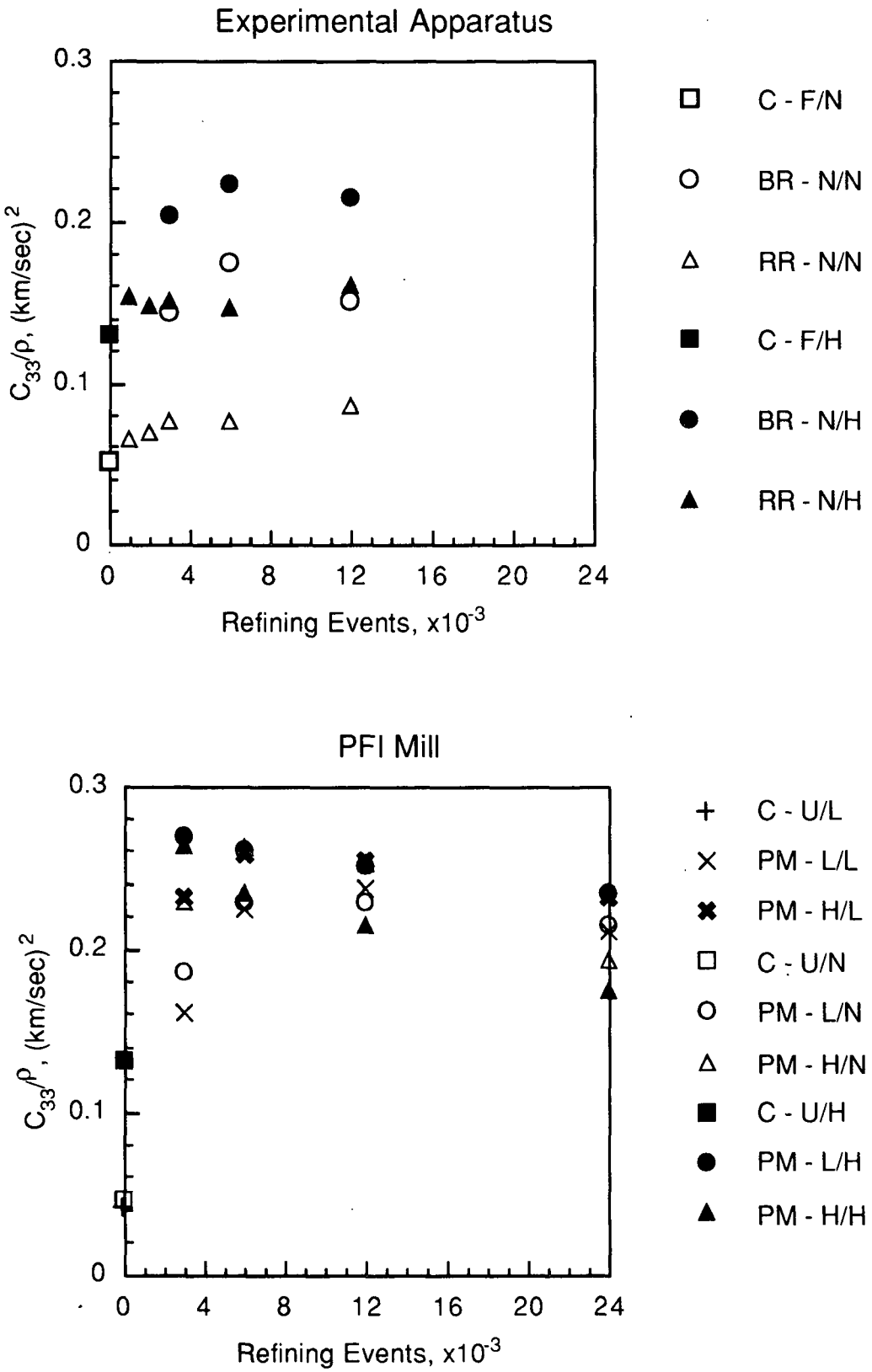

C_{33}/ρ versus Refining Events. The range of confidence intervals (95%) for C_{33}/ρ are 0.001 to 0.029 km/s.

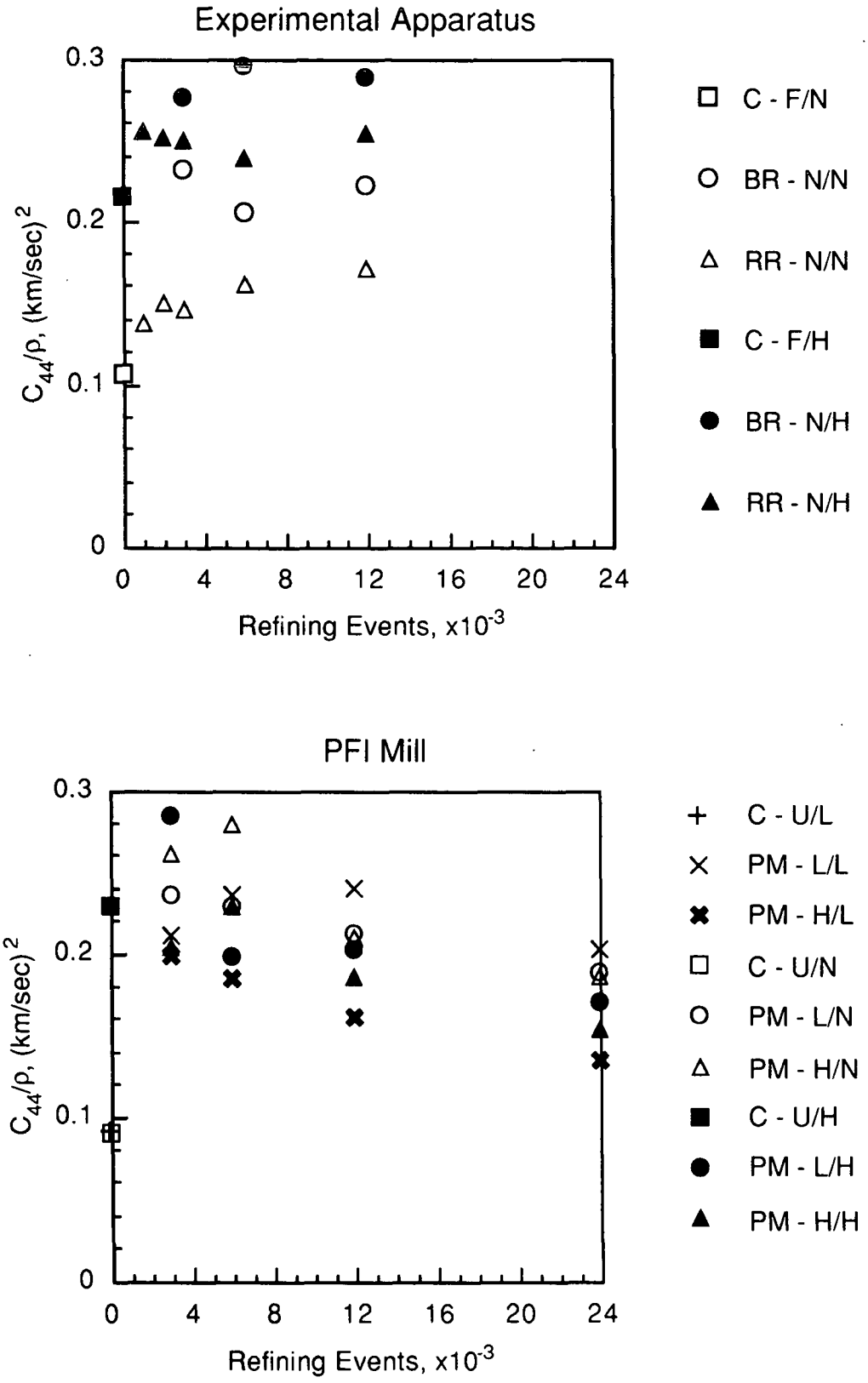

C_{44}/ρ versus Refining Events. The range of confidence intervals (95%) for C_{44}/ρ are 0.003 to 0.051 km/s.